KU LEUVEN

ARENBERG DOCTORAL SCHOOL
Faculty of Science

Beyond semi-classical black holes

Vasil Dimitrov

Supervisors:
Prof. dr. N. Bobev
Prof. dr. B. Vercnocke

Dissertation presented in partial fulfillment of the requirements for the degree of Doctor of Science (PhD): Physics

August 2023

Beyond semi-classical black holes

Vasil DIMITROV

Examination committee:
Prof. dr. T. Li, chair
Prof. dr. N. Bobev, supervisor
Prof. dr. B. Vercnocke, supervisor
Prof. dr. R. Raabe
Prof. dr. W. De Roeck
Prof. dr. T. Van Riet
Prof. dr. T. Hertog
Prof. dr. D. Turton
(Southampton)
Prof. dr. A. Gnecchi
(Padova)

Dissertation presented in partial fulfillment of the requirements for the degree of Doctor of Science (PhD): Physics

August 2023

© 2023 KU Leuven – Faculty of Science
Uitgegeven in eigen beheer, Vasil Dimitrov, Celestijnenlaan 200d - box 2415, B-3001 Leuven (Belgium)

Alle rechten voorbehouden. Niets uit deze uitgave mag worden vermenigvuldigd en/of openbaar gemaakt worden door middel van druk, fotokopie, microfilm, elektronisch of op welke andere wijze ook zonder voorafgaande schriftelijke toestemming van de uitgever.

All rights reserved. No part of the publication may be reproduced in any form by print, photoprint, microfilm, electronic or any other means without written permission from the publisher.

Abstract

Black holes are the inevitable endpoints of gravitational collapse of matter with sufficient mass. They are ubiquitous in our own Universe. Hawking famously showed that black holes carry entropy proportional to their horizon area, meaning that they hold a large number of microscopic states. To do so, he relied on a semi-classical approximation, where he assumed that quantum fields fluctuate around a fixed classical black hole background. In this thesis, we use the methods of string theory to go beyond the semi-classical approximation in two distinct ways.

First, we assume the fuzzball viewpoint, which considers the microscopic states as compact and horizonless bound states of branes. In the supergravity regime some of these microstates manifest themselves as microstate geometries: smooth solitonic solutions to Einstein's equations. We show qualitatively that, while a single microstate geometry returns information in finite proper time as an echo, a quantum superposition of microstate geometries has the tendency to smear and spread these echoes and drastically reduce their amplitude. Our results imply that observing any deviation from the classical black hole behavior is exponentially suppressed and, thus, very difficult to detect using low energy observables, such as gravitational waves.

Second, we consider a certain supersymmetric asymptotically Anti-de Sitter black hole in 5 dimensions, composed of a backreacted set of N M5-branes. We re-derive known results for its semi-classical features. We proceed and include higher derivative corrections to the 5-dimensional supergravity theory that hosts the black hole and we fix the coefficients of these corrections, via our knowledge of its M-theory embedding. In the corrected effective theory of gravity we recover the usual semi-classical entropy and, additionally, we find subleading corrections. As the black hole is in asymptotically Anti-de Sitter space, the holographic conjecture postulates that it should be dual to an ensemble of supersymmetric states in a lower dimensional superconformal field theory. Using quantum field theory methods, one can show that the degeneracy

of states in this ensemble scale as N^3 at leading order and as N at subleading order. We show that the coefficients of the gravitational subleading term and the quantum field theoretic subleading term precisely match. As such, we perform a highly non-trivial test of the holographic conjecture beyond leading order.

Beknopte samenvatting

Zwarte gaten zijn de onvermijdelijke gevolgen van de gravitationele ineenstorting van objecten met voldoende massa. Ze zijn alomtegenwoordig in ons eigen universum. Hawking bewees dat zwarte gaten entropie bezitten, evenredig met de oppervlakte van hun horizon, wat betekent dat ze een groot aantal microscopische toestanden moeten bevatten. Hiertoe vertrouwde hij op de semi-klassieke benadering, waarbij hij aannam dat kwantumvelden fluctueren rond een vaste, klassieke achtergrond die een zwart gat omschrijft. In dit proefschrift gebruiken we methoden uit de snaartheorie om verder te gaan dan deze semi-klassieke benadering op twee verschillende manieren.

Ten eerste gaan we uit van het fuzzball-standpunt, dat de microscopische toestanden beschouwt als compacte, gebonden toestanden van branen zonder horizon. In het regime van superzwaartekracht manifesteren sommige van deze toestanden zich als microtoestandgeometrieën (microstate geometries): gladde, solitonische oplossingen van de Einstein vergelijkingen. We laten kwalitatief zien dat, terwijl een enkele microstate geometry informatie als een echo terugstuurt in een eindige eigentijd, een kwantumsuperpositie van microstate geometries geneigd is deze echo's uit te smeren en hun amplitude drastisch te verminderen. Onze resultaten suggereren dat elke afwijking van het klassieke gedrag van zwarte gaten exponentieel wordt gedempt, en dus zeer moeilijk te detecteren is met behulp van waarneembare objecten met lage energie, zoals zwaartekrachtgolven.

Ten tweede beschouwen we een zeker supersymmetrisch, asymptotisch Anti-de Sitter zwart gat in 5 dimensies, samengesteld uit een teruggekoppeld stel van N M5-branen. We herberekenen enkele bekende resultaten voor zijn semi-klassieke kenmerken. Daarna gaan we verder en voegen we hogere afgeleide correcties toe aan de 5-dimensionale supergravitatietheorie waarin het zwarte gat leeft, en we bepalen de coëfficiënten van deze correcties via onze kennis van de inbedding in M-theorie. In de gecorrigeerde effectieve gravitatietheorie vinden we de gebruikelijke semi-klassieke entropie terug en vinden we bovendien hogere orde correcties. Aangezien het zwarte gat zich in asymptotisch Anti-de

Sitter-ruimte bevindt, postuleert het holografisch principe dat het duaal zou moeten zijn aan een ensemble van supersymmetrische toestanden in een lager-dimensionale superconforme veldentheorie. Met behulp van methoden uit de kwantumveldentheorie kan men aantonen dat de ontaardheid van toestanden in dit ensemble schaalt als N^3 in de eerste orde en als N in de volgende orde. We bewijzen dat de coëfficiënten van de hogere orde term voor de gravitatietheorie en de kwantumveldentheorie precies overeenkomen. Zo voeren we een zeer niet-triviale test uit van de holografische hypothese voorbij de eerste orde.

Acknowledgements

To begin with, I would like to thank my supervisory committee for taking the time to read through this text and for participating in my defense. Your questions, suggestions and criticisms were immensely valuable. Thank you, Tjonnie Li, Riccardo Raabe, Wojciech De Roek, Thomas Van Riet, Thomas Hertog, and, of course, the external members: Alessandra Gnecchi and David Turton. I would also like to use the opportunity to thank the Arenberg Doctoral School for supporting me during the first year of my PhD and FWO for giving me further independence to pursue my academic interests in the remaining four years. Anneleen and Filip, given my infamous organization skills and adherence to regulations and deadlines, without our help at critical times I could not have completed this work. Thank you for your patience and for making ITF the lively and fun place that it is.

A huge thank you goes to my initial supervisor Bert Vercnocke. You opened wide your office door and the doors of high energy physics, for me to walk in. To my first collaborators: Daniel and Vincent, it is hard to express how much I look up to both of you as people and researchers. Thank you for the numerous times you calmed me down when I was storming in your offices proclaiming that I have "just solved the Universe", only to find an impatient error in my reasoning. The lessons you thought me during my initial steps as a researcher will stay with me forever.

To my current supervisor Nikolay Bobev, I think the only proper way to express my gratitude is through the following story. I was deep into the valley of mid-PhD desperation after spending several months not being able to reproduce results from an old supergravity paper by your own supervisor. I prepared 30-40 pages of notes with failed attempts, braced myself for being schooled on my inadequacy, and walked into your office. The only thing I could muster to say was something in the lines of: "This PhD is going nowhere". You took a pause, completely ignoring my stack of papers, and said: "I know". I swallowed whatever was left of my pride and prepared for the worst verdict.

But then you said: “Look, things might not be going great now, but I am willing to adopt you”. And adopt me you did, scientifically for sure and, in many cases, guided me to sensible “real-life” decisions. Since then, I have been on a quest to absorb as much as I can from your deep knowledge of quantum field theories and holography, your pragmatic no-ego approach to physics, and your way of effortlessly orchestrating the projects we worked on. Благодаря ти за всичко: физика, академична подкрепа, критичност и Варненска непринуденост. Не 3в1, а куатро. Not to mention your bottomless artillery of memes and jokes that our skype chats are littered with. But for that I want to also bring in the second set of collaborators that made this PhD special.

Annelien, thank you for introducing the much needed blitzkrieg approach to our M5 papers, I learned a great deal from you. And Val, you have always been there, ready to share your loaded bank of knowledge and give invaluable advice on “how to physics”. From giving talks, to writing application letters, and everything in between. Thank you both for making our work so enjoyable.

Thank you also to all other past and current members of the ITF that made the 6th floor of 200D a second home: Thomas^2, Toine, Jesse, Pieter, Gerben, Kwinten, Natasha, Brandon, Pieter-Jan, Marina, Junho, Vincent, Xuao, and my delightful office mates Joel and Sébastien. I am grateful to have formed lasting friendships with colleagues across Europe at the Solvay Doctoral School. Thank you Evita, Koen, Vincent, Yixuan, Carlos, Dora, Damian, Johannes, Tomas, Vladimir, and everyone else who made the beginning of this PhD a strong cocktail of great emotions and were always there throughout the journey.

Благодаря на цялата компания: Пемби, Демби, Стемби, Ремби, Лемби, набора, Боги и приятели: Вики, Мони, Марти, Калин, Криси, Цани, Иво, Рали, Калин Колев (Хюго), Гери, че сте винаги на линия в България или извън, накъдето и да повее някои от нас. To my “Belgium” friends: Salvatore, Thomas, Laura, Eryk, Vika and Martina, thank you for all the late night conversations, the dancing and the crazy experiences.

Към, майка, татко и Дара, искам да ви благодаря, че сте винаги зад мен каквото и решение да взема и, че семейство Димитрови е точно тази смесица от обич, подкрепа и щипка хаос. Никога не се променяйте.

Finally, to Nadia. You are my soulmate and my best friend. You brought sanity and clarity to the most critical parts of this, sometimes bumpy, PhD ride. In the past three and half years, you have been my inspiration and my partner in crime in countless adventures. I don’t know much about life, the Universe and everything else, despite you always saying: “Нали си физик, измисли го”, but I do know that I want to discover every wonder of life, together, with you.

Contents

Abstract i

Beknopte samenvatting iii

Contents vii

List of Publications xi

List of Abbreviations xiv

List of Figures xv

1 Introduction 1
- 1.1 Motivation . . . 1
- 1.2 Background . . . 4
  - 1.2.1 Black holes in general relativity . . . 4
  - 1.2.2 Black holes in semi-classical gravity . . . 8
  - 1.2.3 A primer on strings and branes . . . 12
  - 1.2.4 Black holes in String Theory . . . 15
  - 1.2.5 A primer on AdS/CFT . . . 17
  - 1.2.6 The fuzzball proposal . . . 19
- 1.3 Can gravitational waves detect black hole microstructure? . . . 21
- 1.4 Subleading corrections to the Bekenstein-Hawking entropy . . . 23

2 Black hole microstate correlators via Hybrid WKB 31
- 2.1 BTZ black holes and wormholes . . . 33
  - 2.1.1 The BTZ black hole . . . 34
  - 2.1.2 Wormholes with BTZ asymptotics . . . 34
  - 2.1.3 The scalar wave equation . . . 39
- 2.2 The hybrid WKB approximation . . . 41
  - 2.2.1 Method outline . . . 42

2.2.2 The BTZ black hole 44
2.2.3 The extremal wormhole 46
2.2.4 Position-space propagator 49
2.3 Connecting BTZ to flat space 51
2.3.1 Scalar probe in BMPV solution and the decoupling limit 51
2.3.2 Scalar quasinormal modes in BMPV 57
2.3.3 Scalar (quasi)normal modes in BMPV wormhole 59
2.3.4 Interpretation 62
2.4 Relation to echo literature in flat space 64
2.4.1 Waves in flat space 64
2.4.2 Waves in AdS 67
2.4.3 Comparison to hybrid WKB 70
2.5 Discussion 71
2.5.1 Where are the quantum corrections? 71
2.5.2 Does a typical black hole microstate have echoes? 77

3 Black hole microstate correlators via real-time holography 83
3.1 BTZ wormhole and wave equation 85
3.1.1 The non-rotating BTZ black hole 85
3.1.2 The non-rotating wormhole 85
3.1.3 The scalar wave equation 87
3.2 Correlators via real time holography 88
3.2.1 Correlators of the BTZ black hole 88
3.2.2 Correlators of the Solodukhin wormhole 96
3.2.3 Feynman correlator of a wormhole transition 101
3.3 Retarded wormhole correlator via hybrid WKB 107
3.3.1 Calculation of the WKB propagator 107
3.3.2 Hybrid WKB vs. real time holography 113
3.4 Position-space correlators 115
3.4.1 Black hole correlator 115
3.4.2 Three ways to the wormhole correlator 117
3.4.3 Wormhole transition Feynman correlator 123

4 Wrapped M5-branes at leading order in large-N 127
4.1 7d gauged supergravity from 11d 129
4.2 Dimensional reduction to 5d $\mathcal{N} = 2$ minimal gauged supergravity 133
4.3 Thermodynamics of the 5d black hole 136
4.3.1 CCLP solution 136
4.3.2 Thermodynamic properties CCLP 139
4.3.3 Thermodynamics in the supersymmetric and BPS limits of CCLP 143
4.4 Holography and the superconformal index 148
4.4.1 Anomalies and the index on the second sheet 148

4.4.2 More general black holes? . . . 150
4.5 Discussion . . . 154

5 Wrapped M5-branes including subleading large-N effects 157
5.1 The Euclidean CCLP solution . . . 159
5.2 HD corrections and the on-shell action . . . 162
5.3 Wald entropy . . . 165
5.4 Discussion . . . 166

6 Conclusion 168

A Appendix 173
A.1 Schwinger-Keldysh formalism in field theory . . . 173
A.2 Skenderis-van Rees real time holography . . . 176
A.2.1 Correlators of empty AdS . . . 180
A.3 Details on the dimensional reduction from 7d to 5d . . . 186
A.3.1 Reducing the action . . . 186
A.3.2 Reducing the BPS equations . . . 188
A.4 Details on the analysis of the 5d CCLP solution . . . 191
A.4.1 Derivation of the Euclidean 5d action . . . 191
A.4.2 Near-horizon Lorentzian geometry . . . 192
A.4.3 Asymptotic Lorentzian geometry . . . 193
A.4.4 Potentials: $(\Omega_1, \Omega_2, \beta, \Phi)$ . . . 196
A.4.5 Charges: (J_1, J_2, Q), via boundary integrals . . . 198
A.4.6 Euclidean on-shell action . . . 198
A.4.7 Charges: (E, J_1, J_2), via holographic renormalization . . . 200
A.4.8 Killing spinor and frame in suitable coordinates . . . 200
A.5 Conventions . . . 202

Bibliography 205

List of Publications

This thesis is based on the following publications:

(i) Dimitrov, V., Lemmens, T., Mayerson, D. R., Min, V. S., and Vercnocke, B. Gravitational Waves, Holography, and Black Hole Microstates

(ii) Dimitrov, V., Mayerson, D. R., and Min, V. Real-time holography and hybrid WKB for BTZ wormholes. *JHEP 06* (2022), 076

(iii) Bobev, N., Dimitrov, V., and Vekemans, A. Wrapped M5-branes and AdS_5 black holes. *JHEP 05* (2023), 012

(iv) Bobev, N., Dimitrov, V., Reys, V., and Vekemans, A. Higher-Derivative Corrections and AdS_5 Black Holes

The author contributed to all conceptual discussions related to the above papers and contributed in equal parts with the rest of the co-authors to the calculations presented there and to drafting the final publications. The above publications form the basis of chapters 2, 3, 4 and 5, with minimal stylistic modifications to fit them into a thesis, rather than a journal article format.

The calculations in (iii) and (iv) were too involved to be performed "by hand" or by using standard symbolic algebra software such as bare bone `Mathematica`. For this reason the author developed a general `Mathematica` package `SolutionsX` that can be found at `https://github.com/waskou/SolutionsX`. It extends the capabilities of the already established tensor algebra package `xAct` to make working with supergravity solutions faster and more convenient. `SolutionsX` was solely developed by and is currently maintained by the author.

Throughout the thesis the pronoun "we" is used. First, to signify the equal part contribution of all co-authors of the publications, that make up the body of this thesis, and, second, to invite you, *the reader*, in rediscovering the wonders that lie *beyond semi-classical black holes*.

List of Abbreviations

AdS Anti-de Sitter. xvi, xviii, 3, 4, 17, 18, 23, 24, 32–34, 37, 39, 41, 53, 54, 56, 57, 59, 62, 64, 67–70, 78, 127, 149, 157, 170, 177–183, 185

BMPV Breckenridge-Mayers-Peet-Vafa. 16, 20, 22, 51–54, 57, 59, 60, 62, 63, 76, 78

BPS Bogomol'nyi-Prasad-Sommerfield. 16, 17, 26, 28, 129, 132, 135, 137, 143–147, 150–152, 155, 157, 160, 166, 187, 188

BTZ Bañados-Teitelboim-Zanelli. xv, xvi, 22, 32–42, 44, 45, 47, 49–53, 55, 58–61, 63, 68, 71, 73–77, 84–88, 91, 96, 98, 101, 107, 109–111, 113, 115, 118

CCLP Chong-Cvetič-Lü-Pope. 28–30, 129, 136, 138–140, 142, 143, 145, 148–150, 155, 158–160, 162, 163, 165–167, 170, 191, 196, 199, 200

CFT conformal field theory. 3, 4, 17, 18, 20, 23, 24, 31–33, 41, 42, 63, 69, 76–78, 127, 157, 170, 179

ECO exotic compact object. xvi, 65–71

GR general relativity. 2, 4, 5, 7, 8, 11, 12, 19, 168

GW gravitational wave. 21, 22, 32, 33

HD higher derivative. 25, 26, 30, 166, 170, 171

IR infrared. 20, 98, 143, 178, 182, 196

KK Kaluza-Klein. 14, 24, 26, 170

NS-NS Neveu-Schwarz-Neveu-Schwarz. 14

QFT quantum field theory. 2, 3, 8, 9, 12, 19, 127, 151, 154, 156, 157, 164, 173, 174

QNM quazi-normal modes. 22, 33, 37, 48, 66, 67, 69

R-R Ramond-Ramond. 14

SCFT superconformal field theory. 17, 23, 26, 28, 127–129, 138, 148–151, 153–158, 161–164, 166

SYM super Yang-Mills. 17, 18

UV ultraviolet. 10, 12, 15, 20, 23–26, 28, 29, 90, 91, 99, 108, 110, 163, 169, 170, 178, 182, 183

VEV vacuum expectation value. 13

WKB Wentzel-Kramers-Brillouin. 32, 33, 37, 41–48, 50, 68, 70, 71, 83, 84, 107, 109, 111, 113, 114, 168, 169

YM Yang-Mills. 17, 18

List of Figures

2.1 Conformal diagram of the extended non-rotating BTZ black hole. The two asymptotically AdS_3 regions are near the lines $r = \pm\infty$. The singularity is at $r = 0$. The dashed lines are lines of constant time and radius. 35

2.2 Conformal diagrams of the Lorentzian non-rotating wormhole in terms of r (left) and r_* (right) coordinates. In the r coordinate we see that the wormhole is created by a left and a right BTZ wedge glued together (the blue solid line) slightly outside of the BTZ horizon. The r_* coordinate, which ranges continuously in $[-L_\lambda/2, L_\lambda/2]$, makes the causal structure more apparent: the glued surfaces $r = \pm r_+$ (on the left) both coincide with the surface $r_* = 0$ (on the right). The gluing is smooth and a radial light-ray (yellow) can explore the entire wormhole by bouncing infinitely many times between the two boundaries. 38

2.3 The wormhole potential $V(x)$, plotted for three different values of λ, and $R = r_+ = \omega = 1$, $k = 0$. The dotted line is the black hole potential $V_{\text{asymp}}(x - 1/\lambda^2)$ for $\lambda^{-2} = 100$, showing graphically the validity of the approximation (2.46). 47

2.4 A schematic depiction of how the BTZ black hole is connected to flat space. In the decoupling limit $\epsilon \to 0$, the flat space region is decoupled from the BTZ region; when $1 \gg \epsilon > 0$, the flat space region is (weakly) coupled to the BTZ region through the intermediate neck region, which allows the scalar field to "leak" out of the BTZ region. 52

2.5 (a) A schematic plot of the radial potential of a rotating black hole with flat asymptotics. Asymptotic infinity is at $x \to \infty$, the horizon at $x \to -\infty$, and the bump is associated with the light-ring; (b) A schematic plot of the radial potential of a rotating ECO with flat asymptotics. Asymptotic infinity is at $x \to \infty$, and at large negative x_0 we put a wall which has arbitrarily complicated behaviour captured by the function $R(\omega, x_0)$. . . . 65
2.6 (a) A schematic plot of the radial potential for a non-rotating black hole with AdS asymptotics. The boundary is at $x \to \infty$, the horizon at $x \to -\infty$. The bump is, similarily to flat space, associated with the light-ring; (b) A schematic plot of the radial potential of a non-rotating ECO with AdS asymptotics. The boundary is at $x \to \infty$, and at large negative x_0 we put a wall which has arbitrarily complicated behaviour captured by the function $R(\omega, x_0)$. 68
2.7 Rough sketch of correlator in a single wormhole geometry $|\lambda\rangle$, and in a typical state $|\psi\rangle$, which is a random superposition over many such wormhole geometries 79

3.1 The non-rotating BTZ black hole: Lorentzian signature (left) and Euclidean signature (right). The Euclidean black hole has periodic time $\tau \sim \tau + \beta$, where $\beta = 1/T$. 86
3.2 The thermal Schwinger-Keldysh contour in CFT_2 (left) and the mixed-signature bulk spacetime, corresponding to it (right). On the boundary contour (left), the grey dots signify gluing between an Euclidean and a Lorentzian segment and the red dots at $(-T, \pm\beta/2)$ are identified and also glued. On the bulk contour (right) the fields are glued at fixed time slices extending all the way into the bulk until the horizon at $r = r_+$ is reached. 89
3.3 The contours $\mathcal{U}, \mathcal{L}, \mathbb{R}$ in the complex ω-plane. The crosses in the upper (resp. lower) half plane are the poles of f^+ (resp. f^-); each vertical line and its reflection across the y-axis corresponds to the poles of $f^\pm$ at fixed k. The circles are the poles of A_{ij} (i.e. the poles of $n(\omega)$), which we discuss in section 3.4.1. 92

3.4 The pure-state Schwinger-Keldysh contour in CFT_2 (left) and the mixed-signature bulk spacetime, corresponding to it (right). On the boundary contour (left) the grey dots signify gluing between an Euclidean and a Lorentzian segment and the red dots are identified and also glued. On the bulk contour (right) the fields are glued on a fixed time slices extending all the way into the bulk. The blue line is the suface $r_* = 0$. On this mixed-signature diagram we have included only the right side of the wormhole, but the reader should envision that the left side is glued to the blue line as in figure 2.2. 97
3.5 The contours $\mathcal{F}, \overline{\mathcal{F}}, \mathcal{W}^>, \mathcal{W}^<$ in the complex ω-plane. The crosses on the real line are the poles of $\tilde{f}$. 100
3.6 The in-out Schwinger-Keldysh contour appropriate for a transition between wormhole states. On the segments γ_a and γ_1 the state is $|\lambda\rangle$. Then at Lorentzian time $t = t_0$ a state-changing operator is suddenly applied (red bullet on the diagram) that changes the state to $|\lambda'\rangle$. This new state then forms that background on the segments γ_2 and γ_b. While, in principle, we can consider a "heavy" state-changing operator in the actual calculation, for technical convenience, we use a "light" state-changing operator and work to first order in $\delta\lambda = \lambda' - \lambda$. . . . 102
3.7 The potential $V(x)$ plotted as a function of x with for $\mu = 1, k = 1, \omega = 2, r_\lambda = 1$, and $\lambda = \{10^{-1}, 10^{-2}, 10^{-3}\}$. As λ decreases, the width of the potential becomes larger and larger. The black hole potential is also depicted, shifted to line up with the $\lambda = 10^{-3}$ graph for $x > 0$. 109
3.8 A plot of $(2/\pi)\,|(\eta - \Theta) \mod \pi|$ as a function of ω. We take $R = r_+ = 1$, and $\lambda = 10^{-20}$ ($L_\lambda \approx 94.88$). The blue, red, and green lines respectively correspond to $k = 0, 5, 10$. The mismatch starts out maximally at $\pi/2$ (see (3.99)) but asymptotes (quickly) to zero (see (3.100)). 114
3.9 The black hole correlator $G^R_{\mathrm{BH}}(\Delta t, \Delta\varphi = 0.1)$ as given in (3.110). We take $R = r_+ = 1$ and $\epsilon = 10^{-10}$. The correlator decays exponentially for $t > 0$; note that each subsequent (small) peak at $t > 0$ come from the contribution of an "image" $m > 0$. The "double-peak" structure (apparent from the close-up on the right) is typical for $\Delta\varphi \neq 0$. 117

3.10 The wormhole correlator $G^R_{\text{WH}}(\Delta t, \Delta\varphi = 0.1)$ as given in (3.118). We take $R = r_+ = 1$, $\lambda = 2 \cdot 10^{-20}$ and $\epsilon = 10^{-1}$, and evaluate each of the four sums in (3.118) up to $n_{max} = 500, k_{max} = 50$. The red line is the computed value and the blue line is a smoothed out average. We can clearly see the first recurrence or "echo", which occur at $\Delta t \approx 2nL_\lambda \approx 186.98n$. 121
3.11 The altered wormhole correlator $G^R_{\widetilde{\text{WH}}_{(\text{low})}}(\Delta t, \Delta\varphi = 0.1)$ as given in (3.128). We take $R = r_+ = 1$, $\epsilon = 10^{-10}$, and $L_\lambda = 100$. We see the clear onset of the first echo at $\Delta t = 2L_\lambda$. 124
3.12 The altered, off-diagonal wormhole correlator $G^F_{\widetilde{\text{WH}}_{(\text{low}),\lambda\to\lambda'}}(\Delta t, \Delta\varphi = 0.1)$ (in red) from (3.133) together with the diagonal correlator $G^F_{\widetilde{\text{WH}}_{(\text{low}),\lambda\to\lambda}}(\Delta t, \Delta\varphi = 0.1)$ (in blue, dashed) (which is (3.133) with $\delta L_\lambda = 0$). We take $R = r_+ = 1$, $\epsilon = 10^{-10}$, $L_\lambda = 100$ and $\delta L_\lambda = 5$. 126

A.1 General Keldysh contour given by (A.1) 174
A.2 Empty AdS_3 with a radial light ray (depicted in yellow). The light ray appears discontinuous on the diagram because we have suppressed the angle φ: after reaching the center of AdS the light ray continues propagating in the antipodal part of the spacetime, reflects from the antipodal point on the boundary and re-emerges at $r = 0$ after time πR. 181

Chapter 1

Introduction

Ту парт. Съмтайм уин,
съмтайм люн.

Hristo Stoichkov

1.1 Motivation

Relaxing on the surface of planet Earth (as humans often do) seems like a pretty innocent activity. In reality there are intricate forces at play that allow you to do that. To begin with, Earth, with its entirety of $\sim 5.9 \times 10^{24}$ kg of mass, packed into a ball of radius $\sim 6.3 \times 10^{6}$ m, gravitationally pulls down on you. Yet, you don't make a huge dent on the surface of Earth to find yourself at the boiling hot core. This is because the outer layer of atoms in your shoes contains electrons as does the outer layer of the surface you are standing on. Quantum mechanics then creates an overall repulsive force between these two sets of electrons due to Pauli's exclusion principle. This repulsive force exactly balances out the pull of gravity. Thus, a bunch of point-like electrons, each of tiny mass $\sim 9.1 \times 10^{-31}$ kg, is able to counteract the influence of a huge and hugely massive object like Earth.

This disparity shows that gravity is immensely weaker compared to electromagnetism. In fact, out of the four fundamental interactions known to science: strong, electromagnetism, weak and gravity, gravity is by far the weakest one. The first three interactions are modelled by the formalism of quantum field

theory (QFT), while gravity is modelled by Einstein's theory of general relativity (GR). These two mathematical frameworks are both wildly successful, when experimentally tested in their respective regimes of validity, and profoundly different in nature. QFT, as the name suggests, is a quantum theory, while GR is classical theory. The established techniques to quantize a classical theory fail spectacularly when applied to GR — we say the GR is non-renormalizable. Apriory, it may sound like human hubris to desire an explanation of everything in the Universe withing a single mathematical framework — a theory of everything. Indeed, due to the happy coincidence of the weakness of gravity, it can safely be ignored when studying quantum interactions in the laboratory. Conversely, due to another happy coincidence, that large bodies in the Universe are usually electrically neutral and that the weak and strong force are short-ranged, the effects of the three quantum interactions can be safely ignored when studying large and heavy object, such as deriving the motions of the planets around the sun, or making a flight plan for a brand new spaceship.

This begs the question: do we really need a theory of quantum gravity? Are there physical systems out there that are simultaneously very small (aka quantum mechanical) and very massive (aka gravitational), in other words, regions of high energy density? Indeed there are. Immediately after the Big Bang the Universe was such a physical system. In the current cosmological era, gravity has an interesting mechanism to hide its shortcomings: try to cram enough matter in a fixed region of space and a black hole will form. The region will be shielded by an *event horizon* — a one-way surface that prevents anything (including light) from escaping, rendering the inside impossible to study (unless you are willing to jump in yourself, against the recommendation of this author and the majority of the physics community). To fully describe black holes, and the origin of the universe, one needs a unified theory of quantum gravity.

Despite lacking such a theory, physicists have been able to make progress. Most notably through the work of Hawking [133], who builded up on previous work of Bekenstein [34], and showed, using a semi-classical approximation, that black holes cary entropy proportional to their horizon area

$$S_{\mathrm{BH}} = \frac{k_B c^3}{G\hbar}\frac{\mathcal{A}}{4}\,, \tag{1.1}$$

where $\mathcal{A}$ is the horizon area, k_B is Boltzman's constant, c is the speed of light, G is Newton's constant of gravitation and $\hbar$ is Planck's constant. The mere appearance of these constants show that black holes are *statistical* (k_B), *relativistic* (c), *quantum* ($\hbar$) , and *gravitational* (G) objects. The status quo in the field is analogous to the status quo in thermodynamics at the end of 19th century before the advent of statistical mechanics. Some *macroscopic* properties of black holes and the relations between them are well established, but what is

lacking is a precise *microscopic* account of the degrees of freedom that manifest these macroscopic properties. For the case of thermodynamics the microscopic ingredients turned out to be atoms and figuring this non-trivial fact out was a major breakthrough for theoretical physics.

Figuring out conclusively the microscopic degrees of freedom that make up the black hole entropy will likely lead to an equally important paradigm shift in our understanding of the world. String theory is an example of a quantum gravity theory that is capable of accounting for the black entropy via its microscopic ingredients: string and branes. It posits that if you were to zoom in sufficiently close to an elementary particle, instead of a point-like object, you will find a tiny vibrating string. Following the implications of this proposition, while demanding quantum mechanical consistency, is a very restrictive theoretical process and it leads to several important predictions: (1) the strings propagate in 10 dimensions, instead of the usual four, (2) a new symmetry of nature, called *supersymmetry*, arises at sufficiently high energies, (3) there exist non-perturbative extended objects, called D-branes, on which open strings end, (4) in the mass spectra of closed strings one necessarily finds a spin-2 quantum field that mediates gravity. Thus, string theory is a consistent quantum theory that "hands quantum gravity on a plate". As we clearly perceive a four-dimensional Universe, it must be that the other six dimensions are curled up and small. Also, since we clearly don't find supersymmetric partners to the known elementary particles in our colliders, it must be that supersymmetry is broken at some high energy scale.

One resounding success of string theory is the recovery of the Bekenstein-Hawking entropy formula for a certain class of supersymmetric black holes from the microscopic dynamics of D-branes [198]. To sketch the idea, there are two regimes in which one can study a collection of D-branes. At weak coupling the dynamics of the branes can be studied using ordinary quantum statistical methods and an entropy can be obtained. At strong coupling the collection of branes backreacts to form a black hole, whose entropy can be computed from the horizon area as in (1.1). The two results agree. Another, remarkable discovery of string theory is the AdS/CFT duality: a conjectured equivalence between an ordinary QFT in $(d-1)$-dimensions and a gravity theory on a negatively curved spacetime in d-dimensions times a $(10-d)$-dimensional compact space. Even though AdS/CFT was first argued to be true using string theory tools, it can be studied independently of string theory. As such it posits a novel way for a quantum completion of gravity: via an intricate way to relate its degrees of freedom to those of a lower dimensional QFT.

In this thesis, we are interested in studying the quantum properties of black holes within the frameworks of string theory and its low energy limit: supergravity. In chapters 2 and 3 we entertain the fuzzball proposal: an idea that the microstates

of the black hole (counted at weak coupling) grow into large smooth horizonless bound states of branes at strong coupling (some of which can be geometrically described within supergravity as microstate geometries). In this setup we ask the question of whether a low-energy observer, such as a gravitational wave laboratory, is capable of distinguishing between a superposition of such microstate geometries and an ordinary black hole as described by GR. In chapters 4 and 5 we position ourselves in a certain realization of AdS/CFT and we push the semi-classical approximation further and find quantum corrections to the Bekenstein-Hawking entropy (1.1). Using our results, we are able to test the AdS/CFT duality beyond leading order.

1.2 Background

In this section we build up in a semi-pedagogical manner the necessary background to follow the calculations that we present in subsequent chapters. We introduce the main ideas behind black hole thermodynamics, black hole microstate counting and the AdS/CFT duality. A more detailed introduction to the work of this author and his collaborators, that constitutes the main body of this thesis, can be found in sections 1.3 and 1.4.

1.2.1 Black holes in general relativity

According to general relativity (GR) a *black object* is a configuration of classical fields (metric, gauge fields, scalar fields, spinor fields) — functions on a D-dimensional spacetime[1], which exhibits the following defining features

(i) a curvature singularity: a space-codimension n ($n \leq D-1$) surface where the Kretchmann scalar grow infinitely large,

(ii) an event horizon: a space-codimension one surface which surrounds the singularity and divides space in two regions: inside and outside, with the property that any object (including a photon) that crosses the event horizon from the outside has its worldline inevitably meet the singularity in finite proper time.

If the event horizon has topology S^{D-2}, we call this black object a *black hole*. In $D > 4$ spacetime dimensions more exotic horizon topologies are allowed. For example, in $D = 5$ one can have an event horizon $S^2 \times S^1$ shielding a black ring

[1] In this thesis we will always consider $D-1$ space dimension and one time dimension

[113]. In GR a metric configuration is called *stationary* if it admits a Killing vector that is asymptotically timelike. Then the metric can always be recast in the form

$$\mathrm{d}s^2 = -\lambda(\mathrm{d}t - \omega_i(y)\,\mathrm{d}y^i)^2 + \lambda^{-1}h_{ij}(y)\,\mathrm{d}y^i\,\mathrm{d}y^j\ , \tag{1.2}$$

where t is the time coordinate, y^i with $i = 1, 2, \ldots, D-1$ are the spatial coordinates and h_{ij} is the spatial metric. In those coordinates the Killing vector reads explicitly $K = \partial/\partial t$, $\lambda = g_{\mu\nu}K^\mu K^\nu$ and ω_i are the so-called *twist parameters*. The presence of non-vanishing twist parameters, that cannot be gauged away via a coordinate transformation, indicates that the spacetime is *rotational*, meaning that the radial infall of geodesics is superimposed with curving. Penrose showed that, under very mild assumptions, a stationary black hole is the natural endpoint of dynamical gravitational collapse of matter with sufficient mass [175]. If we can gauge away the twist parameters to zero the spacetime configuration is called *static*.

As a prototypical example (of astrophysical importance) consider the Kerr-Newman black hole with flat 4d spacetime asymptotics. It solves the equations of motion of Einstein-Maxwell theory in 4d with action

$$I = \frac{1}{16\pi G_4}\int \mathrm{d}^4x\,\sqrt{-g}(R - F_{\mu\nu}F^{\mu\nu})\,, \tag{1.3}$$

where G_4 is the 4d Newton constant and the fundamental fields of the theory are: the metric $g_{\mu\nu}$, with Ricci scalar R, and a one-form A, with field strength $F = \mathrm{d}A$. In coordinates covering the outside region the field configurations take the form

$$\begin{aligned}\mathrm{d}s^2 = &-\frac{\Delta - a^2\sin^2\theta}{\Sigma}\,\mathrm{d}t^2 - 2a\frac{r^2+a^2-\Delta}{\Sigma}\sin^2\theta\,\mathrm{d}t\,\mathrm{d}\phi\\ &+\frac{(r^2+a^2)^2 - \Delta a^2\sin^2\theta}{\Sigma}\sin^2\theta\,\mathrm{d}\phi^2 + \frac{\Sigma}{\Delta}\,\mathrm{d}r^2 + \Sigma\,\mathrm{d}\theta^2\ ,\\ A = &-\frac{Qr}{\Sigma}\big(\mathrm{d}t - a\sin^2\theta\,\mathrm{d}\phi\big) + \alpha\,\mathrm{d}t\ ,\end{aligned} \tag{1.4}$$

where we have defined the functions

$$\Sigma = r^2 + a^2\cos^2\theta\,, \quad \Delta = r^2 - 2mr + a^2 + q^2\,. \tag{1.5}$$

Here, the coordinates (t, r, θ, ϕ) have the following ranges and identifications

$$t \in \mathbb{R}\,, \quad m + \sqrt{m^2 - a^2 - q^2} < r\,, \quad 0 < \theta < \pi\,, \quad \phi \sim \phi + 2\pi\,, \tag{1.6}$$

and (a, m, q) are real parameters. The α term in A is a gauge freedom that we explain in detail below. We will use this specific example to define various physical quantities of interest, but the reader should keep in mind that the concepts explained below can be extended to all black objects in GR.

Conserved charges From the metric (1.4) one can identify the Killing vectors

$$K_{(t)} = \frac{\partial}{\partial t}\,, \quad K_{(\phi)} = \frac{\partial}{\partial \phi}\,, \tag{1.7}$$

which generate time translation and azimuthal rotation symmetries, respectively. In addition, there is a U(1) gauge symmetry mediated by the one-form A. Via Noether's theorem the presence of continuous symmetries results in the existence of conserved charges, calculated at infinity as

$$\begin{aligned} &\text{mass:} && M = -\frac{1}{8\pi G_4}\int_{S^2_\infty} \star \mathrm{d}K_{(t)} = m\,, \\ &\text{angular momentum:} && J = \frac{1}{16\pi G_4}\int_{S^2_\infty} \star \mathrm{d}K_{(\phi)} = am\,, \\ &\text{electric charge:} && Q = \frac{1}{4\pi G_4}\int_{S^2_\infty} \star \mathrm{d}A = q\,, \end{aligned} \tag{1.8}$$

where the overall coefficients have been fixed, relative to the flat space limit of the respective definitions, see [204]. Due to the electro-magnetic duality in 4d one can have a more general Kerr-Newman black hole with magnetic charge $P \propto \int_{S^2_\infty} \mathrm{d}A$. Here we suppress this charge for the sake of brevity.

Horizons and their associated geometric quantities At the zeroes of Δ, given by

$$r_\pm = m \pm \sqrt{m^2 - a^2 - q^2}\,, \tag{1.9}$$

the metric (1.4) diverges. Careful treatment shows that these are merely coordinate singularities and, in fact, the spacetime is perfectly smooth there. The surfaces $r = r_\pm$ are called *outer* and *inner* horizons, respectively. In comparison, the surface $\Sigma = 0$ defines an honest curvature singularity. We define and evaluate the angular velocity measured with respect to a non-rotating frame at infinity

$$\text{angular velocity:} \qquad \Omega = \left.\frac{\mathrm{d}\phi}{\mathrm{d}t}\right|_{r\to r_+} - \left.\frac{\mathrm{d}\phi}{\mathrm{d}t}\right|_{r\to\infty} = \frac{a}{r_+^2 + a^2}\,. \tag{1.10}$$

It has the physical interpretation that a small test object dropped towards the black hole, ends up circumnavigating it at angular velocity Ω, right before falling in. Then, one can see that the Killing vector

$$V = \frac{\partial}{\partial t} + \Omega \frac{\partial}{\partial \phi} \tag{1.11}$$

becomes null at $r = r_+$, meaning that the outer horizon is indeed an *event horizon*: a null hypersurface that has a Killing vector normal to it. We also define and evaluate the surface gravity as

$$\text{surface gravity:} \qquad \kappa = \sqrt{-\frac{1}{2}\nabla^\mu V^\nu \nabla_\mu V_\nu}\bigg|_{r\to r_+} = \frac{r_+ - r_-}{2(r_+^2 + a^2)}\,. \tag{1.12}$$

It has the physical interpretation that an astronaut should apply thrust from their jetpack with proper acceleration κ to remain still on the event horizon and avoid falling in. Using the Killing vector V we can also define and evaluate the electrostatic potential

$$\text{electrostatic potential:} \quad \Phi \;= V^\mu A_\mu\Big|_{r\to r_+} - V^\mu A_\mu\Big|_{r\to\infty} = \frac{q r_+}{r_+^2 + a^2}\,. \tag{1.13}$$

Demanding finiteness of $A^\mu A_\mu$ on the event horizon fixes the gauge choice as

$$\alpha = -\Phi\,. \tag{1.14}$$

Note that Φ itself is independent of the gauge choice. Finally, we define and evaluate the event horizon area

$$\text{area:} \quad \mathcal{A} \;= \int_{S^2_{r_+}} \text{volume of event horizon surface} = 4\pi\big(r_+^2 + a^2\big)\,. \tag{1.15}$$

Analogous horizon quantities can also be defined on the inner horizon, however their physical interpretation is more subtle, see [103, 104, 139]. Combining everything so far one can verify the validity of the *Smarr relation*

$$M = \frac{\kappa\mathcal{A}}{4\pi} + 2\Omega J + \Phi Q\,, \tag{1.16}$$

for the case of the Kerr-Newmann solution. Similar Smarr relations hold for all black objects and they can be derived formally without referring to a particular solution [31].

Black hole laws In the 70's a set of laws, regarding stationary black holes and their perturbations were established, within the framework of GR, that bear striking resemblance with the laws of thermodynamics [31]. Here, we state them without proof:

Zeroth law. The surface gravity is constant over the event horizon.

First law. If a stationary black hole of mass M, angular momentum J and electric charge Q is perturbed so that it settles to another stationary black hole of mass $M + \mathrm{d}M$, angular momentum $J + \mathrm{d}J$ and electric charge $Q + \mathrm{d}Q$, then

$$\mathrm{d}M = \frac{\kappa}{8\pi}\,\mathrm{d}\mathcal{A} + \Omega\,\mathrm{d}J + \Phi\,\mathrm{d}Q\ . \tag{1.17}$$

Second law. In any physical process the area of the horizon does not decrease

$$\Delta\mathcal{A} \geq 0\,. \tag{1.18}$$

Third law. No physical process exists that allows one to perturb a black hole with finite surface gravity to a black hole with zero surface gravity in a finite number of adiabatic steps.

In the concrete example of the Kerr-Newman black hole, one can establish the validity of the first law by considering the operator $\mathrm{d} = \mathrm{d}a\,\partial_a + \mathrm{d}m\,\partial_m + \mathrm{d}q\,\partial_q$ and act on the expressions provided above. Pushing this analogy with thermodynamics, black holes appear to behave as thermodynamic systems with entropy proportional to the horizon area and temperature proportional to the surface gravity. This poses a problem for the GR description of black holes, as, within the same framework, one can establish various *no-hair theorems*, see [167] and references within. For the Kerr-Newman black hole the no-hair theorem states that the black hole is fully characterized using only the asymptotic charges (M, Q, J) and no microstructure deviating from (1.4) is allowed. To rephrase, it states that the black hole has only one microstate corresponding to the macroscopic parameters (M, Q, J). If that is true, then how can it carry an entropy?

1.2.2 Black holes in semi-classical gravity

In '73 Bekenstein constructed a thought experiment that argues, assuming general validity of the second law of thermodynamics, that black holes must posses entropy [34]. Hawking was not convinced and set up a calculation aiming to prove him wrong. Noting that the spacetime curvature in the vicinity of the horizon $r = r_+$ can be arbitrarily small for a large black hole, he coupled quantum field theory (QFT) to that weakly curved background (the weak curvature is essential, since it is well known that naive coupling of QFT to an arbitrarily curved dynamical spacetime, leads to a non-renormalizable theory). Much to his surprise, he discovered that, due to pair production, the black hole radiates like a thermodynamical black body with characteristic temperature

$\kappa/2\pi$, and further that it carries entropy $S = \mathcal{A}/4$, where the area is measured in Plank units [133]. Here, we will establish there results, using the Euclidean methods, developed in [122]. To set the stage we first discuss QFT at finite temperature.

QFT at finite temperature Consider a QFT that admits commuting operators (H, J, Q) which generate time translations, rotations along a selected axis, and gauge transformations, respectively. The corresponding grand-canonical partition function is

$$\mathcal{Z}(\beta, \Omega, \Phi) = \mathrm{Tr}\, e^{-\beta H + \beta\Omega J + \beta\Phi Q}\,, \tag{1.19}$$

where $(\beta = 1/T, \Omega, \Phi)$, with T being the temperature, are considered as generalized chemical potentials for the respective conserved quantities and the grand-canonical ensemble is the one that keeps these potentials fixed. In this background the average of any operator $\mathcal{O}$ is given by $\langle\mathcal{O}\rangle_{\beta,\Omega,\Phi} = \mathcal{Z}^{-1}\mathrm{Tr}\, e^{-\beta H+\beta\Omega J+\beta\Phi Q}\mathcal{O}$ and the Green's function is defined as

$$G_{\beta,\Omega,\Phi}(t, \phi, x) = \mathcal{Z}^{-1}\mathrm{Tr}\, e^{-\beta H+\beta\Omega J+\beta\Phi Q}\mathcal{O}(t, \phi, x)\mathcal{O}(0, 0, 0)\,, \tag{1.20}$$

where ϕ is the azimuthal angle circling the selected axis, and x denote the remaining coordinates. In the Heisenberg picture the evolution of an operator is given by

$$\mathcal{O}(t + \Delta t, \phi + \Delta\phi, x) = e^{\mathrm{i}\Delta t H + \mathrm{i}\Delta\phi J}\mathcal{O}(t, \phi, x)e^{-\mathrm{i}\Delta t H - \mathrm{i}\Delta\phi J}\,. \tag{1.21}$$

Analytically continuing the intervals Δt and $\Delta\phi$ to imaginary values as $\Delta t = \mathrm{i}\beta$ and $\Delta\phi = -\mathrm{i}\beta\Omega$ we obtain

$$\mathcal{O}(t + \mathrm{i}\beta, \phi - \mathrm{i}\beta\Omega, x) = e^{-\beta H+\beta\Omega J}\mathcal{O}(t, \phi, x)e^{\beta H-\beta\Omega J}\,. \tag{1.22}$$

Then the Green's function can be rewritten as

$$\begin{aligned} G_{\beta,\Omega,\Phi}(t, \phi, x) &= \mathcal{Z}^{-1}\mathrm{Tr}\, e^{\beta\Phi Q}\mathcal{O}(t + \mathrm{i}\beta, \phi - \mathrm{i}\beta\Omega, x)e^{-\beta H+\beta\Omega J}\mathcal{O}(0, 0, 0) \\ &= \mathcal{Z}^{-1}\mathrm{Tr}\, e^{-\beta H+\beta\Omega J+\beta\Phi Q}e^{-\beta\Phi Q}\mathcal{O}(0, 0, 0)e^{\beta\Phi Q}\mathcal{O}(t + \mathrm{i}\beta, \phi - \mathrm{i}\beta\Omega, x) \\ &= (-1)^F e^{\beta\Phi q}\mathcal{Z}^{-1}\mathrm{Tr}\, e^{-\beta H+\beta\Omega J+\beta\Phi Q}\mathcal{O}(t + \mathrm{i}\beta, \phi - \mathrm{i}\beta\Omega, x)\mathcal{O}(0, 0, 0) \\ &= (-1)^F e^{\beta\Phi q}G_{\beta,\Omega,\Phi}(t + \mathrm{i}\beta, \phi - \mathrm{i}\beta\Omega, x)\,. \end{aligned} \tag{1.23}$$

Above, the first equality comes from substituting (1.22) into (1.20), the second equality comes from the cyclicity of the trace, and in the third equality we have picked up two phases: one containing the U(1) charge q of the operator $\mathcal{O}$,

and one due to exchanging the two operators, with $F = 0$ if $\mathcal{O}$ is bosonic and $F = 1$ if $\mathcal{O}$ is fermionic. We have shown that (up to phases) thermal correlation functions in the bath (β, Ω, Φ) have *imaginary* periodicities

$$(t, \phi) \sim (t + \mathrm{i}\beta, \phi - \mathrm{i}\beta\Omega)\,. \tag{1.24}$$

This motivates us to Wick rotate time as

$$t \to -\mathrm{i}\tau \tag{1.25}$$

and study Euclidean theories with periodic Euclidean time $\tau \sim \tau + \beta$ to gain understanding of thermal system in Lorentzian time.

Black holes in Euclidean signature The analogy of the black hole laws and the laws of thermodynamics, together with the equivalence of thermal physics and periodic Euclidean time physics prompts us to study black holes in Euclidean signature. We already saw that the Lorentzian solution is completely regular on the surface $r = r_+$. For the naively Wick rotated solution this is not the case (there is a conical singularity and a shrinking S^2), *unless* one makes the identifications

$$(\tau, \phi) = (\tau + c_1, \phi + \mathrm{i}c_2)\,, \tag{1.26}$$

where the constants c_1 and c_2 are determined from the Euclidean geometry near $r = r_+$ to be

$$c_1 = \frac{2\pi}{\kappa}\,, \quad c_2 = \frac{2\pi}{\kappa}\Omega\,. \tag{1.27}$$

Back in the Lorentzian picture we see that the black hole is indeed a thermal system with temperature $T = \kappa/2\pi$. One way to obtain the entropy of this thermal system is to first calculate the Euclidean on-shell action I_E . In the path integral formalism the grand canonical partition function, in the semi-classical approximation is $\mathcal{Z} \approx e^{-I_E}$, and out of it using the standard rules of statistical mechanics the entropy can be extracted. Naively computing the Euclidean on-shell action one obtains ultraviolet (UV) divergences, due to the infinite volume of spacetime. The correct procedure, established in [122], is to evaluate the following Euclidean action

$$I_E = -\frac{1}{16\pi G_4}\int_{\text{cigar}} \mathrm{d}^4x\,\sqrt{g}(R - F_{\mu\nu}F^{\mu\nu}) - \frac{1}{8\pi G_4}\int_{S^2_{r_0}} \mathrm{d}^3x\,\sqrt{h}(K - K_0)\,, \tag{1.28}$$

where K is the extrinsic curvature on a surface $r = r_0$, with $r_0 \gg r_+$, and K_0 is a certain counterterm, which in flat space asymptotics is equal to the extrinsic

curvature on the same surface $r = r_0$, of the Kerr-Newman black hole with $m = 0$ (this is nothing but flat space written in non-conventional coordinates). The "cigar" geometry is what one gets after imposing the identifications (1.26). Evaluating the above one obtains

$$I_E = \frac{2\pi(r_+^2 + a^2)}{r_+ - r_-}\left(m - \frac{q^2 r_+}{r_+^2 + a^2}\right) = \frac{\beta}{2}(M - \Phi Q)\,, \tag{1.29}$$

where the first equality is the direct answer in terms of the black hole parameters and the second equality is a clever rewriting of this answer in terms of the already established black hole charges and potentials. Back in the Lorentzian picture, semi-classically, the Euclidean on-shell action has the interpretation of minus the logarithm of the grand-canonical partition function

$$I_E = -\log \mathcal{Z}(\beta, \Omega, \Phi) + \dots\,, \tag{1.30}$$

where the $\dots$ are corrections beyond the semi-classical approximation. In statistical physics the Legendre transform of $\log \mathcal{Z}(\beta, \Omega, \Phi)$ spells out the logarithm of the microcanonical partition function — or the entropy. Thus the semi-classical entropy of the black hole is

$$S = -I_E + \beta(M - \Omega J - \Phi Q) + \dots\,, \tag{1.31}$$

and should be viewed as a function of the conjugate variables (M, J, Q). Using the expression for I_E one can rewrite the entropy as

$$S = \frac{\beta}{2}M - \beta\Omega J - \frac{\beta}{2}\Phi Q + \dots = \frac{\mathcal{A}}{4} + \dots\,, \tag{1.32}$$

where in the last equality we have identified via the Smarr relation (1.16) that the middle expression coincides with $1/4$ the horizon area. Restoring the suppressed physical constants, we summarize the seminal works of Bekenstein and Hawking: the temperature and entropy of a black hole with horizon area $\mathcal{A}$ and surface gravity κ are

$$T = \frac{\hbar}{c k_B}\frac{\kappa}{2\pi}\,, \quad S = k_B \frac{\mathcal{A}}{4 l_P^2} + \dots\,, \quad l_P^2 = \frac{G\hbar}{c^3}\,, \tag{1.33}$$

where k_B is Boltzmann's constant, c is the speed of light, l_P is Plank's length, which is made out of Newton's gravitational constant G, Plank's constant $\hbar$ and the speed of light c. We carefully treated the example of the Kerr-Newman black hole, however, the above formulas can be established for any black object in semi-classical gravity. We remind the reader of the assumptions that go in this derivation:

(1) The background is fixed to be a classical solution of a GR + matter theory,

(2) Light QFT fields are minimally coupled to this background, and their backreaction is ignored.

A fully honest quantum gravity calculation should challenge both of these assumptions. It is well known that GR is not a UV complete theory, thus UV physics will bring corrections to the background and the dynamics in the Wilsonian sense. Even then, a quantum gravity theory should not distinguish between a fixed background and quantum physics coupled to it, rather the background and its fluctuations should be manifestly described by the same quantum theory. Still, the semi-classical approximation captures the correct physics to leading order in $1/l_P$ and corrections (the $\dots$ in the above formulas) are subleading. Understanding them better is the focus of chapters 4 and 5 of this thesis. Finally, we note that the considerations of Bekenstein and Hawking do not address the singularity in any way. A quantum gravity theory should resolve the singularity, in addition to explaining the statistical origin of the black hole entropy. In the next section we explore what string theory, an example of a UV complete quantum gravity theory, has to say about black holes and their microstructure.

1.2.3 A primer on strings and branes

String theory is a quantum theory of extended object (strings and branes) that have tension. Here we give a lightening review of string theory ingredients relevant to black hole physics. For a comprehensive read on string theory consult [178, 179, 129, 32].

The bosonic string First, consider a classical bosonic string propagating in flat space with metric $\eta_{\mu\nu}$. As it moves it sweeps out a surface, called *worldsheet*, which we parametrize by two coordinates: $\tau \in \mathbb{R}$ and $0 < \sigma < \pi$. We denote the worldsheet metric by h_{ab}, with $a, b = 1, 2$ the worldsheet indices. The classical action of the bosonic string is

$$S = -\frac{1}{4\pi\alpha'} \int \mathrm{d}\tau \, \mathrm{d}\sigma \, \sqrt{-h} h^{ab} \partial_a X^\mu \partial_b X^\nu \eta_{\mu\nu} \,, \tag{1.34}$$

where the tension is given by

$$T = \frac{1}{2\pi\alpha'} \,, \quad \alpha' = l_s^2 \,, \tag{1.35}$$

with l_s being the characteristic length scale of the string. X^μ with $\mu = 1, 2, \dots, D$ is a collection of bosonic fields which live on the worldsheet and have

interpretation as spacetime coordinates on the D-dimensional *target space*. In order to have a well defined variation of this action the boundary terms should vanish. Thus, we should impose one among the following boundary conditions:

$$\begin{aligned} &\text{closed string:} && X^\mu(\tau,\sigma) = X^\mu(\tau,\sigma+\pi)\,, \\ &\text{Neumann open string:} && \partial_\sigma X^\mu(\sigma=0) = \partial_\sigma X^\mu(\sigma=\pi) = 0\,, \\ &\text{Dirichlet open string} && X^\mu(\sigma=0) = \text{const}\,, \quad X^\mu(\sigma=\pi) = \text{const}\,. \end{aligned} \tag{1.36}$$

Clearly, when an open string has Neumann boundary conditions there is no momentum transfer from the endpoints. In contrast, for Dirichlet boundary conditions, the string is assumed to end at hypersurfaces, called *D-branes*, which become dynamical objects due to the momentum transfer. Quantizing the classical bosonic string can be performed in various ways (lightcone quantization, covariant quantization, BRST quantization) all leading to the same conclusions. First, there is a Weyl anomaly on the worldsheet that must be set to zero. One way to do so is to fix the number of spacetime dimensions to the *critical dimension*: $D = 26$. Second, the mass spectrum is given by

$$\begin{aligned} M^2_{\text{closed}} &= \frac{2}{\alpha'}\Big(N + \widetilde{N} - 2\Big)\,, \\ M^2_{\text{Neumann}} &= \frac{1}{\alpha'}(N-1)\,, \\ M^2_{\text{Dirichlet}} &= \left(\frac{l}{2\pi\alpha'}\right)^2 + \frac{1}{\alpha'}(N-1)\,, \end{aligned} \tag{1.37}$$

where l is the length of the string stretched between two D-branes, N and $\widetilde{N}$ are roughly speaking number operators for the left and right moving modes. First, we observe that when $N = \widetilde{N} = 0$, the theory contains imaginary mass states called *tachyonic*. This is pathological and should not be permitted. Second, $N = \widetilde{N} = 1$ gives the massless sector of the theory. From the closed string we obtain a general two-tensor that can be split into: a symmetric graviton $g_{\mu\nu}$, an antisymmetric two-form $B_{\mu\nu}$, and a trace-part scalar ϕ, called *dilaton*. From the Neumann open string we obtain a U(1) gauge field A_μ. Finally, from the Dirichlet open string we obtain: A_m with $m = 1, 2, \ldots, p$ — a gauge field living on the Dp-brane and $(25-p)$ scalars that encode the spacetime fluctuations of the brane.

As strings propagate the can merge and split where the strength of this interaction is controlled by the *string coupling*, which is dynamically determined from the theory as the vacuum expectation value (VEV) of the dilaton

$$g_s = \left\langle e^{\phi} \right\rangle\,. \tag{1.38}$$

The tension of a Dp-brane can be shown to scale as

$$T_p \sim \frac{1}{g_s l_s^{p+1}}\,, \tag{1.39}$$

thus Dp-branes are non-perturbative object predicted by the theory.

The superstring Including fermions on the worldsheet in a supersymmetric fashion modifies the above analysis by: (1) changing the critical dimension to $D = 10$, (2) removing the tachyonic states from the spectrum, (3) allowing for five distinct types of supersymmetric string theories: I, IIA, IIB, $E_8 \times E_8$ and SO(32), (4) by introducing additional spacetime fields to the massless bosonic sector. For example, in the type II theories the massless bosonic sector is

$$\begin{aligned} &\text{IIA}: \quad G_{\mu\nu}\,, B_{\mu\nu}\,, \phi \quad C_{\mu}^{(1)}\,, C_{\mu\nu\rho}^{(3)}\,, \\ &\text{IIB}: \quad G_{\mu\nu}\,, B_{\mu\nu}\,, \phi \quad C^{(0)}\,, C_{\mu\nu}^{(2)}\,, C_{\mu\nu\rho\sigma}^{(4)}\,, \end{aligned} \tag{1.40}$$

where the $C^{(p)}$ are antisymmetric gauge fields that make up the Ramond-Ramond (R-R) sector, the rest of the bosonic fields make up the Neveu-Schwarz-Neveu-Schwarz (NS-NS) sector, and the fermions (that we have omitted) make up the R-NS and NS-R sectors. Fields in the R-R sector couple electrically to D$(p-1)$-branes and charge them. Similarly, $B_{\mu\nu}$ couples to the *fundamental string* F1. Due to the Hodge duality $\star C^{(p+1)} = C^{(7-p)}$, the theories also contain "magnetic" D$(6-p)$-branes. The magnetic duals of F1 are the so called NS5-branes. Finally, strings can also carry momentum waves P, which are dual to Kaluza-Klein (KK) monopoles. In summary, in the NS-NS and R-R sectors of type II string theories we have the following extended objects

$$\begin{aligned} &\text{IIA}: \quad \text{P}, \text{F1}, \text{NS5}, \text{KK} \quad \text{D0}, \text{D2}, \text{D4}, \text{D6}, \text{D8}, \\ &\text{IIB}: \quad \text{P}, \text{F1}, \text{NS5}, \text{KK} \quad \text{D(-1)}, \text{D1}, \text{D3}, \text{D5}, \text{D7}, \text{D9}, \end{aligned} \tag{1.41}$$

where D(-1)-branes are D-instantons and D9-branes are spacetime filling branes. Importantly, we note that even though we deduced the existence of dynamical extended objects using perturbative string theory, these object preserve 1/2 of the maximal supersymmetry of the theory and, thus, they continue to exist at all values of g_s.

The five string theories are all related by various dualities. For example T-duality relates string theories compactified on a small circle of radius R to string theories compactified on a large circle of radius $1/R$, while S-duality relates perturbative string theories at weak coupling g_s to non-perturbative ones are

strong coupling $1/g_s$

$$\begin{aligned} &[\text{IIA}]_R \overset{T}{\longleftrightarrow} [\text{IIB}]_{1/R}\,, \qquad [E_8\times E_8]_R \overset{T}{\longleftrightarrow} [\text{SO}(32)]_{1/R}\,,\\ &[\text{IIB}]_{g_s} \overset{S}{\longleftrightarrow} [\text{IIB}]_{1/g_s}\,, \qquad [\text{SO}(32)]_{g_s} \overset{S}{\longleftrightarrow} [\text{I}]_{1/g_s}\,,\\ &[\text{IIA}]_{1/g_s} \overset{S}{\longleftrightarrow} [\text{M}]_{g_s}\,, \qquad [E_8\times E_8]_{1/g_s} \overset{S}{\longleftrightarrow} [\text{M}]_{g_s}\,. \end{aligned} \tag{1.42}$$

The new entry above is the mysterious M-theory, which is in fact 11-dimensional. Its perturbative spectrum contains M2 and M5 branes and it has no fundamental strings. Compactifying M-theory on a small circle (or line) of size $R_{11} = g_s l_s$ one obtains IIA (or $E_8 \times E_8$) with string couping g_s. Although there is no fundamental understanding of M-theory, it is known that its low energy limit is the celebrated unique 11-dimensional supergravity. In fact, the low energy limit of all string theories corresponds to a particular supergravity theory in the same dimension, and supergravity theories in different dimensions are related via chains of dimensional reductions and uplifts. Thus, even though by themselves supergravity theories are not UV complete, they originate from a UV complete theory. Furthermore, *black brane* solutions of supergravity theories are nothing but stacks of the non-perturbative D-branes of string theory or M-branes of M-theory. For a comprehensive read on supergravity theories in various dimensions and their black brane solutions consult [117]. In the next section we describe one of the most celebrated results in string theory: namely, the successful microscopic account of the entropy of a certain class of supersymmetric black holes.

1.2.4 Black holes in String Theory

In this section we review the famous Strominger-Vafa [198] examination of the D1-D5-P brane system, that at strong coupling describes a black hole in 5d, whose entropy can be accounted for from the brane dynamics that can be safely studied at weak coupling. Due to the supersymmetry protection the statistical physics in the two regimes remains the same.

Positioning ourselves in IIB, consider a configuration of N_5 D5-branes wrapping compact coordinates $x_1, \ldots, x_5$ with periods $R_1, \ldots, R_5$, N_1 D1-branes wrapping x_1 and N_P momentum modes along x_1. In the low energy limit the branes

backreact to a spacetime with metric

$$\begin{aligned} \mathrm{d}s^2 = H_1^{1/2} H_5^{1/2} \Big[& H_1^{-1} H_5^{-1} \Big(-H_P^{-1}\, \mathrm{d}t^2 + H_P \big(\mathrm{d}x_1 - \big(H_P^{-1} - 1 \big)\, \mathrm{d}t \big)^2 \Big) \\ & + H_5^{-1} \big(\mathrm{d}{x_2}^2 + \cdots + \mathrm{d}{x_5}^2 \big) + \mathrm{d}{x_6}^2 + \ldots \mathrm{d}{x_9}^2 \Big] \,, \end{aligned} \tag{1.43}$$

where H_1, H_5 and H_P are harmonic function given by

$$H_1 = 1 + \frac{Q_1}{r^2} \,, \quad H_5 = 1 + \frac{Q_5}{r^2} \,, \quad H_P = 1 + \frac{Q_P}{r^2} \,, \tag{1.44}$$

with $r = \sqrt{x_6^2 + \cdots + x_9^2}$ being the radial distance in the non-compact part of the spacetime, and the charges are given by

$$Q_1 = \frac{N_1 g_s \alpha'^3}{R_2 R_3 R_4 R_5} \,, \quad Q_5 = N_5 g_s \alpha' \,, \quad Q_P = \frac{N_P g_s \alpha'^4}{R_1^2 R_2 R_3 R_4 R_5} \,. \tag{1.45}$$

Note that while we have only spelled out the metric, the above brane configuration gives a $\frac{1}{8}$-Bogomol'nyi-Prasad-Sommerfield (BPS) solution of IIB supergravity. Namely, all the bosonic fields take a known profile, while all the fermionic fields are set to zero. Furthermore, the fermions obey equations of the type

$$\delta_\epsilon(\text{fermion}) = 0 \,, \tag{1.46}$$

where ϵ is a spinor parameter of the supersymmetry transformation. The notation *fraction*-BPS means that ϵ has this *fraction* of its maximal number of components being independent. Upon dimensional reduction on the compact directions the metric becomes

$$\mathrm{d}s_5^2 = (H_1 H_5 H_P)^{-2/3}\, \mathrm{d}t^2 + (H_1 H_5 H_P)^{1/3} \big(\mathrm{d}r^2 + r^2\, \mathrm{d}\Omega_3^2 \big) \,. \tag{1.47}$$

This is the metric of a zero-temperature, finite-entropy 5d black hole, first written down in [69], thus referred to as Breckenridge-Mayers-Peet-Vafa (BMPV) black hole. From the geometry one calculates the horizon area $\mathcal{A} = 2\pi^2 \sqrt{Q_1 Q_5 Q_P}$. Using the relation between the 5d and 10d Newton constant $(2\pi)^5 G_5 = G_{10}/(R_1 R_2 R_3 R_4 R_5)$, via the Bekenstein-Hawking formula, the entropy reads

$$S = \frac{\mathcal{A}}{4G_5} = 2\pi \sqrt{N_1 N_5 N_P} \,. \tag{1.48}$$

For this supergravity analysis to be trustworthy one needs to suppress both string loops and α' corrections, which imposes:

$$g_s \to 0 \text{ at fixed } Q\text{'s} \,, \quad Q\text{'s} \gg \alpha' \implies g_s N_1, g_s N_5, g_s^2 N_P \gg 1 \,, \tag{1.49}$$

where the compactification radii are taken to be of the order of l_s.

Next, we turn our attention to this brane system at weak coupling. The degeneracy of the brane system is equivalent to the number of $\frac{1}{8}$-BPS states of the worldvolume theory. Taking $R_2, R_3, R_4, R_5 \ll R_1$, the relevant worldvolume theory is a 2d superconformal field theory (SCFT) on $\mathbb{R} \times S^1$ consisting of right movers in the ground state, contributing central charge $c = 6N_1N_5$, and left movers that carry N_P momentum modes. Thus, the degeneracy, as given by the Cardy formula, reads $d(c, N_P) = \exp\left(2\pi\sqrt{cN_P/6}\right)$. Then the entropy of the brane dynamics is

$$S = \log d(c, N_P) = 2\pi\sqrt{N_1N_5N_P}\,, \tag{1.50}$$

in exact agreement with the black hole entropy. This match might come as a surprise as the regime of validity of the D-brane perturbation theory, where the counting makes sense is precisely the opposite of the regime of validity of the supergravity picture:

$$g_sN_1, g_sN_5, g_s^2N_P \ll 1\,. \tag{1.51}$$

The match is explained by the fact that supersymmetry protects the degeneracy as we tune the system between the two regimes.

1.2.5 A primer on AdS/CFT

In this section we make a detour of our main black hole story to introduce the AdS/CFT correspondence, which plays a crucial role in our understanding of black hole physics and quantum gravity in general. This section is based on the excellent reviews [190, 108]. Consider a stack of N coincident Dp-branes. At weak coupling we have open strings stretching between the branes whose dynamics is that of a conformal field theory (CFT), more specifically an SU(N) super Yang-Mills (SYM) theory with Yang-Mills (YM) coupling $g_{YM}^2 \sim g_s\alpha'^{(p-3)/2}$. They also interact with the long range forces mediated by the closed strings in the vicinity of the stack and the strength of this interaction is controlled by Newton's constant $G_{10} \sim g_s^2\alpha'^4$. At strong coupling and low energy the system is well approximated by a supergravity black p-brane in whose metric a harmonic function of the type

$$H = 1 + g_{YM}^2N\alpha'^2\left(\frac{r}{\alpha'}\right)^{p-7} \tag{1.52}$$

makes appearance. Now take the following limit

$$\alpha' \to 0\,, \quad \frac{r}{\alpha'} = \text{fixed}\,, \quad g_{YM}^2 = \text{fixed}\,. \tag{1.53}$$

At weak coupling the worldvolume dynamics of the open string is kept non-trivial but decoupled from the closed strings dynamics. At strong coupling it has the effect of "dropping the one" from the harmonic function. It is easy to see on concrete examples that "dropping the one" is equivalent to zooming to the hear-horizon geometry of the zero-temperature black p-brane, which is $\mathrm{AdS}_{p+2}\times S^{8-p}$. Thus, the dynamics of closed strings propagating near the horizon is decoupled from the dynamics of the closed strings propagating asymptotically. This is the so called *decoupling limit*. In this analysis we have omitted the the behavior of the dilaton $e^{\phi}=H^{(3-p)/4}$. We see that the case $p=3$ is special as the dilaton is constant and regular at the horizon. Indeed the original AdS/CFT conjecture, due to Maldacena [156], comes from studying D3-branes. In its strongest form the conjecture postulates an equivalence between

$$\text{IIB string theory on } \mathrm{AdS}_5\times S^5 \iff \text{4d } \mathcal{N}=4 \text{ SU}(N) \text{ SYM}\,, \tag{1.54}$$

where $\mathcal{N}$ denotes the number of conserved supercharges, the YM coupling on the field theory side is $g_{YM}^2=g_s$, and the scale of the AdS_5 (and the S^5) on the string theory side is $L=\left(4\pi g_s N\alpha'^2\right)^{1/4}$. By strongest form we mean that the duality is supposed to hold at any value of N and g_s. This statement is hard to study (and prove), but we can gain understanding by further taking the *'t Hooft limit*

$$N\to\infty\,,\quad \lambda=g_{YM}^2N=\text{fixed}\,, \tag{1.55}$$

where λ is called the *'t Hooft coupling*. It corresponds to

$$g_s\sim\frac{1}{N}\,,\quad \frac{L}{l_P^{(10)}}\sim N^{1/4}\,,\quad \frac{L}{l_s}\sim\lambda^{1/4}\,, \tag{1.56}$$

where $l_P^{(10)}\sim G_{10}^{1/8}\sim(g_s\alpha'^2)^{1/4}$ is the 10-dimensional Plank length and $l_s=\sqrt{\alpha'}$ is the string length. Namely, in the 't Hooft limit the "size" of spacetime is large compared to the Plank length, meaning that we are dealing with classical IIB string theory and the $1/N$ expansion on the field theory side corresponds to perturbative string loop expansion in g_s on the gravity side. After the 't Hooft limit, we can further take $\lambda\to\infty$. Then the "size" of spacetime is additionally large compared to the string length and we are dealing with IIB supergravity, where the the $1/\sqrt{\lambda}$ expansion on the field theory side corresponds to α' expansion in the supergravity. The double limit: $N\to\infty$ followed by $\lambda\to\infty$, is the weakest form of the AdS/CFT conjecture, but it gives most control over the calculations, thus most checks of the duality have been performed in this regime. To conclude we point out some important features and implications of the AdS/CFT proposal:

(i) It suggest that a d-dimensional QFT *without gravity* is equivalent to string theory on AdS_{d+1} times a compact space. Being a duality across dimensions it is a realization of the *holographic principle* [201, 199],

(ii) The word "equivalence" in practice means that the partition functions on both sides match as well as all correlations functions, computed in two very different ways, see [108] for more details on how this work,

(iii) It is a weak/strong duality in the sense that the regime in which the gravity side is weakly coupled $\lambda \gg 1$ is precisely the opposite to the regime in which one can rely on perturbation theory on the QFT side $\lambda \ll 1$.

We presented the duality to some level in detail in the case of D3-branes, but it can be extended to many more concrete examples, see [8] and references within.

1.2.6 The fuzzball proposal

Returning to the main story, we note that while the Strominger-Vafa calculation provides a beautiful statistical account for the black hole entropy, it does so in the regime of weak coupling. Thus, it leaves open the question of how is the GR singularity resolved in string theory. One might expect that when $g_s N$ is dialed to strong coupling the characteristic size of the brane system decreases below the characteristic horizon scale and all the microstates of Strominger-Vafa end up crunched to some unknown Plank scale physics that resolves the singularity. Instead, the *fuzzball proposal* [162, 192], posits that at strong coupling the quantum corrections extend beyond the horizon scale and each microstate becomes a large, horizonless, singularity-free bound state of branes, that has the same asymptotic charges as the macroscopic black hole. Surprisingly, even at low energy — aka the supergravity regime, one is able to find a large number of solitonic (horizonless and smooth) solutions, called *microstate geometries*, that have the same asymptotic charges as the original black hole [162, 163, 50, 49, 189]. One might object to the existence of such gravitational solitons, based on classical GR *no-solitons* and *no-hair* theorems, see [124] and references within. However, a closer inspection reveals that these theorems have a number of hidden assumptions: no extra dimensions, no Chern-Simons terms, no fluxes, no orbifold singularities, and no ambipolar metrics. All of these ingredients are intricately employed in constructing explicit gravitational solitons and avoiding the theorems. The most well studied family of such gravitational solitons is the so called *superstrata* [39, 37, 38]. Without going in depth about their construction, we summarize the main features of these geometries:

(i) They are built in the framework of 6d supergravity, viewed as a compactification of IIB on $S^1 \times \mathcal{M}$, where $\mathcal{M} = T^4$ or $\mathcal{M} = K3$ and the S^1 is parametrically larger then the rest of the compact space,

(ii) They can have either $\mathrm{AdS}_3 \times S^3$ or $S^1 \times \mathbb{R}^{1,4}$ asymptotics. In the second case, compactifying further on S^1, one obtains a smooth (up to orbifold singularities, that can be resolved in string theory) 5d geometry, which has the same asymptotic charges and supersymmetries as the BMPV black hole,

(iii) They interpolate between the above asymptotics in the UV and the deep infrared (IR) region — a deformation of $\mathrm{AdS}_3 \times S^3$. These deformations can be viewed as a backreacted coherent gas of *supergravitons* on the undeformed $\mathrm{AdS}_3 \times S^3$,

(iv) In the deep IR, they use flux to support a large bubble connecting two Gibbons-Hawking centers, and support waves on this bubble. Tuning the metric parameters they can be made to *scale*, meaning that the characteristic size of the IR structure can be brought arbitrarily close to the would be horizon scale of the corresponding 6d black string (or 5d black hole),

(v) The scaling feature means that, although these geometries are perfectly smooth (in string theory) and horizonless, they are arbitrarily good black hole mimickers from the perspective of an asymptotic observer — namely they exhibit the characteristic large redshifts of a black hole, and only return a signal after a parametrically large timescale,

(vi) The AdS_3 'near-structure' region has a very well studied CFT_2 dual — in particular each geometry can be precisely matched to a particular *heavy* CFT operator turned on.

Although the existence of these solitonic solutions is firmly proven, more work is needed before they (and similar constructions) are established as the true black hole microstates in the gravity regime in light of the Strominger-Vafa calculation. Active research undergoes in two main directions: (1) the number of such solutions in supergravity scales as $\sim \sqrt{N_1 N_5} N_P^{1/4}$, which is parametrically smaller compared to the entropy (1.48) [188]. It might be that a broader family of supergravity solutions can be found that fully accounts the BMPV black hole entropy, or it might be that supergravity can only capture the above-mention fraction of microstates and the full machinery of string theory is needed to describe the rest, see also [165]. (2) Superstrata are supposed microstates of a zero-temperature (or *extremal*) black hole. A generalization to finite-temperature black hole microstates is needed to describe astrophysical

black holes and model the mechanism of Hawking radiation within the fuzzball paradigm, see [35] for early efforts in that direction. If both these issues are fully resolved the fuzzball proposal offers the following compelling scenario to avoid formation of singularities in the process of gravitational collapse. As matter of entropy S is crunched down to almost horizon scale, at some point in the collapse, before a singularity has formed, the system undergoes a quantum tunneling process: with very small probability $\sim e^{-S}$ it can tunnel into one of the geometries, but the number of geometries is correspondingly large $\sim e^{S}$, resulting into transition with probability ~ 1 into *at least one* of them [45]. Subsequently, the system might continue to traverse the phase space of smooth horizonless geometries by undergoing further tunneling [93]. See also [136] for a discussion of how this idea might lead to observable effects, such as gravitational wave outbursts.

1.3 Can gravitational waves detect black hole microstructure?

We saw in section 1.2.6 that the fuzzball proposal offers a geometric description of a portion of the microstates of certain supersymmetric and extremal black holes as smooth horizonless scaling geometries. In the absence of a full description of the geometric phase space we consider a toy model that (1) captures the main qualitative features of the existing string theory models, (2) provides a playground to study a full ensemble of microstates, (3) describes the microstates of both extremal and non-extremal black holes. Having all these benefits comes at the price that we require negative energy to source the family of geometries under consideration. The motivation for using this rather crude toy model is to extract generic features of observables that an asymptotic astrophysical laboratory has access to — aiming to see if it is at all viable to detect string theory inspired horizon-scale modifications via classical low-energy experiments, such as detections of gravitational waves (GW).

The toy model We consider a Solodukhin wormhole [195] (see also [105]) as a toy model of the more complicated superstrata microstate geometries. Instead of the supergraviton gas deformation of the 'near-structure' $\mathrm{AdS}_3 \times S^3$ we impose 'by hand' gluing the AdS_3 throat to another AdS_3 throat, such that a traversable wormhole is formed. On the boundary of the second AdS_3 we put reflecting boundary conditions such that a signal thrown in is returned after traveling twice through the effective wormhole length, which is controlled by a parameter λ that appears in the metric. By making λ sufficiently small this

geometry mimics the 3d Bañados-Teitelboim-Zanelli (BTZ) black hole times S^3 arbitrarily well away from the gluing point, much like scaling geometries do. Finally, we couple this 'near-structure' region to 5d flat space and study an ensemble of e^S such geometries with λ-parameters picked from the window $\lambda_{min} < \lambda < \lambda_{max}$, where S is the entropy of the 5d BMPV black hole.

The probe As a probe we minimally couple a scalar field to this background (without letting it backreact) and study two-point functions of the types $\langle HLLH \rangle$ or $\langle HLLH' \rangle$, where H and H' are *heavy* operators creating geometries with parameters λ and λ', respectively and L is the *light* scalar field probe[2]. The rationale here is that a scalar field probe models the trace of a GW probe, without the complications arising from considering a tensor probe.

Results Due to the simplicity of our model we are able to analytically solve the scalar wave equation exactly, then couple the solution perturbatively to flat space and establish four main results:

(1) The two-point function $\langle HLLH \rangle$ closely mimics the two-point function calculated in [41] for a superstratum geometry using the more sophisticated *hybrid-WKB* approximation: namely there is an initial falloff of the correlator, followed by a sequence of *echoes* (the correlator spikes up to $\sim$ its initial amplitude), separated by a timescale determined by real part of the lowest quazi-normal mode (QNM) frequency ω:

$$t_{\text{echo}} \sim (\text{Re}\,\omega)^{-1}\,, \tag{1.57}$$

and we observe a decay timescale, due to modes leaking out at infinity, of the order

$$t_{\text{decay}} \sim (\text{Im}\,\omega)^{-1} \sim t_{\text{echo}}^{-2l-3}\,, \tag{1.58}$$

where l is the S^3 wave number.

(2) We explain how to relate the QNM frequencies of such a λ-geometry to the *reflectivity coefficient* — a more familiar phenomenological approach to impose 'by hand' partially or fully reflective boundary conditions on an otherwise completely absorbing horizon,

(3) We show that after averaging the two-point function over λ-geometries in the microcanonical ensemble echoes get washed away: the correlator

[2]The terms "heavy" and "light" come from the dual CFT description and refer to states created by operators of parametrically large scaling dimension Δ and operators of scaling dimension $\Delta \sim 1$, respectively.

amplitude decreases drastically and is exponentially ($\sim e^{-S}$) suppressed. Further, we observe the expected by unitarity resurgence of the correlator at very long time scales $\sim e^{e^S}$,

(4) We show that an *off-diagonal* correlator of the type $\langle HLLH' \rangle$ gets a further suppression and spreading of its echoes, meaning that if the observation happens at timescales larger than the characteristic tunneling timescale, echoes are even harder to be observed.

Results (1)-(3) are established in chapter 2, while chapter 3 re-establishes result (1) using the formalism of real-time holography and uses the same formalism to establish result (4).

1.4 Subleading corrections to the Bekenstein-Hawking entropy

In this section we clarify the nature of the corrections to the semi-classical Bekenstein-Hawking entropy — the ... in (1.33). To get calculational millage, instead of Kerr-Newmann, we consider supersymmetry preserving asymptotically AdS black hole arsing from stacks of branes. For concreteness, we take M-branes, as the analysis is somewhat simpler compared to D-branes. Fundamentally, the AdS/CFT duality is a statement of the equivalence of the partition functions

$$\mathcal{Z}_{\rm M} \text{ on } {\rm AdS}_d \times \mathcal{M}_{11-d} = \mathcal{Z}_{\rm SCFT} \text{ on } \mathbb{R} \times S^{d-2} \ , \tag{1.59}$$

where $\mathcal{Z}_{\rm M}$ is the partition function of the M-branes, which can partially wrap a compact manifold and backreact at strong coupling to produce an asymptotically ${\rm AdS}_d$ factor and a compact manifold $\mathcal{M}_{11-d}$. We embed the supersymmetry preserving black hole in this ${\rm AdS}_d$ factor and its degeneracy of states can be counted either by directly computing $\mathcal{Z}_{\rm M}$ or by considering an ensemble of states in the dual SCFT that preserve the same amount of supercharges. The UV parameters of this setup are N — an integer capturing the "overall number of branes", and possibly some invariant data of the internal space $\mathcal{M}_{11-d}$, which we collectively denote by z. Many preliminary test of the duality have been performed by independently computing the two sides at leading order in large-N, see [211] for a review. By a precision test of AdS/CFT, we mean a verification that the duality continues to hold beyond leading order. If we consider D-branes, there is an additional UV parameter g_s, and on top of the large-N expansion one should also perform a large-λ expansion, as described in section 1.2.5. Below, we sketch the ingredients that generically appear in calculating the two sides of (1.59). Then, we describe a particular M-branes

realization of the AdS/CFT duality that is the focus of this work and, finally, we quote our results.

Gravity side In the absence of a fundamental M-theory formulation we view the d-dimensional supergravity, obtained from dimensional reduction on $\mathcal{M}_{11-d}$, as its effective theory at low energies

$$e^{-1}\mathcal{L}^{(0)}(g_{\mu\nu},\phi)=\frac{1}{16\pi G_d}\left(R+\frac{(d-1)(d-2)}{L^2}\right)+e^{-1}\mathcal{L}^{(0)}_{\text{matter}}(\phi)\,, \tag{1.60}$$

where L is the AdS_d scale. Excluding some very special cases, the scale of $\mathcal{M}_{11-d}$ is of the same order. Thus, the matter fields, collectively denoted by ϕ, include an infinite tower of KK modes. The prescription to calculate the partition function of this effective theory is: (1) sum over all the classical saddles α of the Euclidean theory that smoothly fill in the bulk and have the same set of prescribed boundary conditions — captured by a set of dimensionless thermodynamic potentials φ, (2) include quantum correction coming from all loops of all fields on top of the saddles. Schematically, we have

$$\mathcal{Z}^{(0)}_{\text{AdS}_d}=\sum_{\alpha}e^{-I^{(0)}_{\alpha}}\mathcal{Z}^{\alpha}_{(0),\text{loops}}\,, \tag{1.61}$$

where $I^{(0)}_{\alpha}$ is the Euclidean on-shell action evaluated on the saddle α

$$I^{(0)}_{\alpha}(\varphi)=f_{\alpha}(\varphi)\frac{L^{d-2}}{G_d}\,. \tag{1.62}$$

Here $f_{\alpha}(\varphi)$ is a function of the dimensionless thermodynamic potentials and the factor L^{d-2}/G_d is a dimensionless parameter build up from the two scales in the problem. Let the saddle $\alpha=0$ be the Wick rotation of the Lorentzian black hole in question and let it be a dominant saddle. On general grounds, one can argue that one-loop effects contribute a log term to $\log\mathcal{Z}_{\text{AdS}_d}$, while higher loops contribute subdominant terms, see [187] and references therein. Overall, one obtains a result of the type

$$-\log\mathcal{Z}^{(0)}_{\text{AdS}_d}=f_0(\varphi)\frac{L^{d-2}}{G_d}+g_0(\varphi)\log\left(\frac{L^{d-2}}{G_d}\right)+\dots\,, \tag{1.63}$$

where $g_0(\varphi)$ is some other function of the thermodynamic potentials and the $\dots$ capture subleading effects coming from subleading saddles, subdominant KK modes and higher loops. At this point we note that, from a Wilsonian standpoint, the theory specified by $\mathcal{L}^{(0)}$ is an effective theory, where all the UV degrees of freedom have been integrated out. We can systematically start integrating out less and less of the UV physics by considering higher derivative

(HD) corrections to $\mathcal{L}^{(0)}$. To obey parity the first such correction includes all compatible four derivative (shorthanded to 4∂) terms. Apart from bringing some 4∂ terms to our effective theory, the bare couplings G_d and L get renormalized and the new effective Lagrangian is of the type

$$e^{-1}\mathcal{L}^{(1)}(g_{\mu\nu},\phi) = \frac{1}{16\pi G_d^{(1)}}\left(R + \frac{(d-1)(d-2)}{L_{(1)}^2}\right) + c_1^{(1)}R^2 + c_2^{(1)}R_{\mu\nu}R^{\mu\nu} + c_3^{(1)}R_{\mu\nu\rho\sigma}R^{\mu\nu\rho\sigma} + e^{-1}\mathcal{L}^{(1)}_{\text{rest}}(g_{\mu\nu},\phi)\,, \tag{1.64}$$

where $c_i^{(1)}$ are some coefficients of mass dimension $4-d$, which are considered small in the sense

$$L^{d-4}c_i^{(1)} \ll L^{d-2}/G_d\,. \tag{1.65}$$

Here the renormalized couplings $G_d^{(1)}$ and $L_{(1)}$ receive corrections of the order $L^{d-4}c_i^{(1)}$, and $\mathcal{L}^{(1)}_{\text{rest}}$ involves all other compatible non-pure-gravity terms up to 4∂, possibly introducing more couplings in the list $c_i^{(1)}$. Schematically, the partition function receives the following corrections

$$\begin{aligned} -\log \mathcal{Z}^{(1)}_{\text{AdS}_d} &= f_0(\varphi)\frac{L_{(1)}^{d-2}}{G_d^{(1)}} + h_0^i(\varphi)L^{d-4}c_i^{(1)} + g_0(\varphi)\log\left(\frac{L_{(1)}^{d-2}}{G_d^{(1)}}\right) + \dots \\ &= f_0(\varphi)\frac{L^{d-2}}{G_d} + \widetilde{h}_0^i(\varphi)L^{d-4}c_i^{(1)} + g_0(\varphi)\log\left(\frac{L^{d-2}}{G_d}\right) + \dots \end{aligned} \tag{1.66}$$

where the second equality comes from expanding $L_{(1)}^{d-2}/G_d^{(1)}$ to order $L^{d-4}c_i^{(1)}$, and now the $\dots$ also include subleading terms coming from expanding $\log\left(L_{(1)}^{d-2}/G_d^{(1)}\right)$. In principle, we can keep going and introduce all compatible 6∂ corrections, 8∂ corrections and so on. However, at some point, new HD corrections will start competing with the $\dots$ above. It is very hard to distinguish which of these subleading effects comes first and this should be analyzed on a case by case basis. The UV completion of this effective theory has parameters N and z and we consider N to be large, so we must have relations of the type

$$\frac{L^{d-2}}{G_d} = u(z)N^{\alpha_1}\,, \quad L^{d-4}c_i^{(1)} = v_i(z)N^{\alpha_2}\,, \quad \alpha_2 < \alpha_1\,, \tag{1.67}$$

Thus, the gravitational result for the partition function, corrected up to 4∂, is

$$-\log \mathcal{Z}^{(1)}_{\text{AdS}_d} = F(\varphi,z)N^{\alpha_1} + H(\varphi,z)N^{\alpha_2} + G(\varphi,z)\log(N) + O(N^{-1})\,, \tag{1.68}$$

where we have assumed that $\alpha_2 > 0$. Otherwise it will appear to order $O(N^{-1})$, where, as a reminder, we have a complicated interplay between KK modes, subdominant saddles, higher loops and HD corrections of one-loop effects. Now we can perform the Legendre transform of the corrected $-\log \mathcal{Z}_{\text{AdS}_d}$, as in section 1.2.2, and obtain the Bekenstein-Hawking entropy, together with its subleading in large-N behavior, as a function of the charges Q conjugate to the potentials φ. The challenge is, of course, to find the functional dependence of $\mathcal{Z}_{\text{AdS}_d}$ from the potentials, to determine the powers of N, and *crucially* to fix the coefficients $c_i^{(1)}$ in terms of the UV parameters z.

Field theory side Even though the field theory side is at strong coupling, calculations are usually in better control when there is supersymmetry. We have a SCFT with gauge group of rank N on $\mathbb{R} \times S^{d-2}$, where d is the dimension of the dual AdS. Let there be a preserved supercharge $\mathcal{Q}$, that satisfies the algebra

$$\left\{\mathcal{Q}, \mathcal{Q}^\dagger\right\} = H - \nu \cdot Q \,, \tag{1.69}$$

where H is the Hamiltonian, Q is a set of commuting with $\mathcal{Q}$ charges, associated with rotations of the S^{d-2}, the R-symmetry and possibly flavour symmetries, and ν are theory dependent coefficients. The finite temperature grand-canonical partition function is given by

$$\text{Tr}\, e^{-\beta H + \beta \Phi \cdot Q} \,, \tag{1.70}$$

where Φ are fugacities for Q. Note that turning temperature on usually breaks the conformal symmetry. Since we are counting states dual to a supersymmetric zero-temperature black hole, we are really interested in BPS states (ones annihilated by $\mathcal{Q}$) that are in the ground state with energy $E = \nu \cdot Q$. Then the partition function of interest is

$$\mathcal{Z}_{\text{SCFT}} = \text{Tr}|_{\mathcal{Q}=0}\, e^{\varphi \cdot Q} \,, \tag{1.71}$$

where we have defined the relevant BPS fugacities $\varphi = \beta(\Phi - \nu)$. Here $\beta \to \infty$, due to zero-temperature, but this is accompanied by $\Phi \to \nu$, due to supersymmetry, such that φ remains finite. Unfortunately, this ground state partition function is usually unaccessible due to the strong coupling. However, a related object, called the *supersymmetric index*

$$\mathcal{I}_{\text{SCFT}} = \text{Tr}|_{\mathcal{Q}=0}\, (-1)^F e^{\varphi \cdot Q} \,, \tag{1.72}$$

where $F = 0$ for bosonic states and $F = -1$ for fermionic states, often times can be computed using *supersymmetric localization* even at strong coupling, see

[102] for a concise review. The argument goes as follows: since Q commutes with $\mathcal{Q}$, the index can equivalently be written as

$$\mathcal{I}_{\text{SCFT}} = \text{Tr}\,(-1)^F e^{-\beta\{\mathcal{Q},\mathcal{Q}^\dagger\}} e^{\varphi\cdot Q}\,. \tag{1.73}$$

This follows from the fact that states with $\mathcal{Q} \neq 0$ come in pairs: a bosonic and a fermionic state of the same energy, and their contribution is cancelled by the factor $(-1)^F$. In particular, this implies that the index is independent of the parameter β and it counts the degeneracy of the ground state, weighted with a minus for fermionic states. The last expression can be viewed as a path integral on $S^1 \times S^{d-2}$ with periodic boundary conditions for *both* bosons and fermions along the S^1. This type of path integral can, in many favorable cases, be localized to an ordinary multidimensional matrix integral, and, in even more favorable circumstances, evaluated exactly to an analytic function of φ, N and the SCFT couplings, which one should relate to the UV parameters z. When the situation is not so favorable, the matrix integral can be approximated at large-N using established techniques, such as as saddle point approximation or Bethe ansatz, see for example [128, 6]. Of course, a valid objection is that $\mathcal{I} \neq \mathcal{Z}$, namely counting fermionic states with a minus can result into large cancellations between ground state bosons and ground state fermions. However, it turns out that for some theories $(-1)^F = 1$ and we are guaranteed that no cancellations occur [211]. When large cancellations are indeed present, it was recently discovered that analytically continuing the fugacities φ to complex values and introducing phases in the index mildens the cancellations [86, 72]. In those cases one can also show [59] that

$$\mathcal{Z}_{\text{SCFT}} = e^{-\mathcal{F}} \mathcal{I}_{\text{SCFT}}\,, \tag{1.74}$$

where $\mathcal{F}$ is the *supersymmetric Casimir energy*, whose large-N behavior can be obtained from the anomalies of the theory. Overall, using supersymmetric field theory techniques one can obtain a large-N expansion for $-\log \mathcal{Z}_{\text{SCFT}}$ and compare to the gravitational answer. Of course, care must be taken to ensure that the meaning of the dimensionless gravitational potentials φ coincides with the meaning of the field theory fugacities φ.

The concrete setup studied in this thesis In chapters 4 and 5 we develop the general story outlined above for the specific case of N M5-branes wrapping a Riemann surface $\Sigma_{\mathfrak{g}}$, of genus $\mathfrak{g}$, residing inside a Calabi-Yau (CY) three-fold. Locally, the CY three-fold can be viewed as a two line bundles fibered on the Riemann surface

$$\mathcal{L}_1 \oplus \mathcal{L}_2 \to \Sigma_{\mathfrak{g}}\,. \tag{1.75}$$

The UV degrees of freedom are N and the the sum and the difference of the first Chern numbers (also known as the degrees) of the two line bundles. We parametrize this more conventiantly by the integer $\mathfrak{g}$ and the rational number z as

$$\deg(\mathcal{L}_1) + \deg(\mathcal{L}_2) = \chi(\Sigma_\mathfrak{g}) = 2\mathfrak{g} - 2\,, \quad \frac{\deg(\mathcal{L}_1) - \deg(\mathcal{L}_2)}{\chi(\Sigma_\mathfrak{g})} = z\,, \tag{1.76}$$

where $\chi(\Sigma_\mathfrak{g})$ is the Euler characteristic of the Riemann surface.

At strong coupling and low energies this brane configuration backreacts to $\mathrm{AdS}_5 \times \Sigma_\mathfrak{g} \times S^4$, and inside the AdS_5 we embed the Chong-Cvetič-Lü-Pope (CCLP) black hole [98, 99] which has two angular momenta J_1 and J_2 corresponding to the two Cartan isometries $\mathrm{U}(1) \times \mathrm{U}(1) \subset \mathrm{SO}(4) \subset \mathrm{SO}(2,4)$ of the AdS_5 and one electric charge Q corresponding to one of the Cartan isometries $\mathrm{U}(1) \subset \mathrm{SO}(5)$ of the S^4.

At weak coupling the 6d worldvolume theory can be compactified on $\Sigma_\mathfrak{g}$ resulting in a particular non-Lagrangian 4d $\mathcal{N} = 1$ SCFT of class $\mathcal{S}$, which has a $\mathrm{U}(1)_R$ R-symmetry [18, 19]. The partition function on the field theory side at finite temeperature is given by

$$\mathrm{Tr}\, e^{-\beta H + \beta\Omega_1 J_1 + \beta\Omega_2 J_2 + \beta\Phi Q}\,, \tag{1.77}$$

where Q is the generator of the R-symmetry. The BPS states of this theory are enumerated by

$$\mathcal{Z}_{\mathrm{SCFT}} = \mathrm{Tr}\, e^{-\beta\left\{\mathcal{Q},\mathcal{Q}^\dagger\right\} + \omega_1\left(J_1 + \frac{Q}{2}\right) + \omega_2\left(J_2 + \frac{Q}{2}\right) - \frac{Q}{2}(\omega_1 + \omega_2 - 2\varphi)}\,, \tag{1.78}$$

where we have used the supersymmetry algebra

$$\left\{\mathcal{Q}, \mathcal{Q}^\dagger\right\} = H - J_1 - J_2 - \frac{3}{2}Q\,, \tag{1.79}$$

and we have defined the BPS fugacities $\omega_1 = \beta(\Omega_1 - 1)$, $\omega_2 = \beta(\Omega_1 - 1)$ and $\varphi = \beta(\Phi - 3/2)$. Supersymmetry imposes the relation

$$\omega_1 + \omega_2 - 2\varphi = 2\pi i n_0\,, \quad n_0 \in \mathbb{Z}\,. \tag{1.80}$$

Insisting on real fugactiries one must fix $n_0 = 0$. Then the field theory partition function has slow growth of states and cannot capture the the corresponding large growth of states of the dual black hole. Allowing the fugactities to be complex, using the charge assignement of the operators to deduce that $e^{\pi i n_0 Q} = (-1)^F$ for odd n_0. Then one can show that the partition function is given by

$$\mathcal{Z}_{\mathrm{SCFT}} = e^{-\mathcal{F}}\mathcal{I}_{\mathrm{SCFT}}\,, \quad \mathcal{I}_{\mathrm{SCFT}} = \mathrm{Tr}|_{\mathcal{Q}=0}\,(-1)^F e^{\omega_1\left(J_1 + \frac{Q}{2}\right) + \omega_2\left(J_2 + \frac{Q}{2}\right)}\,, \tag{1.81}$$

where $\mathcal{F}$ is the supersymmetric Casimir energy and $\mathcal{I}_{\rm SCFT}$ is the superconformal index, defined as a path integral on $S^1 \times S^3$. Due to the theory being non-Lagrangian, one cannot directly use localization to evaluate $\mathcal{I}_{\rm SCFT}$. However, taking a certain Cardy-like limit, where size$(S^3) \gg$ size(S^1), one can compactify the 4d field theory on S^1 and obtain the large-N scaling from the effective 3d theory (it reduces to a computation of contact terms and zero modes alone) [86]. The large-N behaviour of the log of the so defined partition function is entirely controlled by anomalies and reads

$$\begin{aligned}\log \mathcal{Z}_{\rm SCFT} = &\frac{\varphi^3}{6\,\omega_1\omega_2}\mathrm{Tr}\,R^3 - \frac{\varphi(\omega_1^2+\omega_2^2-4\pi^2)}{24\,\omega_1\omega_2}\mathrm{Tr}\,R \\ &+ \log|G| + O\left(e^{-\frac{\text{size}(S^3)}{\text{size}(S^1)}}\right),\end{aligned} \tag{1.82}$$

where $\mathrm{Tr}\,R^3$ and $\mathrm{Tr}\,R$ are the cubic and linear 't Hooft anomalies for the R-symmetry and $|G|$ is the rank of some one-form symmetry that might be present in the theory. The 't Hooft anomalies can be related to the UV parameters of the theory [19, 16] as

$$\begin{aligned}\mathrm{Tr}\,R^3 &= \frac{2(\mathfrak{g}-1)}{27z^2}\left[9z^2-1+(3z^2+1)^{\frac{3}{2}}\right]N^3 \\ &\quad - \frac{\mathfrak{g}-1}{9z^2}\left[(\sqrt{3z^2+1}-1)(2+3z^2)-3z^2\right]N+\dots\,, \\ \mathrm{Tr}\,R &= \frac{\mathfrak{g}-1}{3}\left[4-\sqrt{3z^2+1}\right]N+\dots\,.\end{aligned} \tag{1.83}$$

We see that, at large-N, the expression for the partition function indeed follows the general form (1.68), except that this analysis does not capture the log term in (1.68). Note that the $\log|G|$ term in (1.82) scales as $O(N^0)$, and the exponentially supressed corrections are of more subleading order.

Results Within the setup outlined above we establish the following results:

(1) We recover known results for the Euclidean on-shell action of the CCLP black hole, while illuminating a previously overlooked detail involving a particular finite counterterm that can be added in the process of holographic renormalization,

(2) We show explicitly how the CCLP black hole can be embedded into 11d supergravity and how the UV parameters make appearence. The chain of dimensional reductions involves passing thorugh a consistent truncation of

7d gauged supergravity before ariving to 5d minimal supergravity, which hosts the CCLP black hole. In particular, we show how the spinor variation equations of this 7d theory reduce to the spinor variation equaitons of the 5d theory,

(3) We include HD corrections, up to 4∂, to the 5d minimal supergravity, as outlined in the first paragraph of this section, and precisely recover the first two lines of (1.82) via a gravitational computation,

(4) We perform the (constrained) Legendre transform of the corrected partition function and obtain the first subleading correction to the Bekenstein-Hawking entropy of the CCLP black hole.

Results (1) and (2) are established in chapter 4, while results (2) and (4) are established in chapter 5. As such, we perform a highly non-trivial test of the holographic duality beyond leading order in large-N, and reliably describe the first subleading corrections to the black hole entropy formula in the M5-brane setup outlined here.

Chapter 2

Black hole microstate correlators via Hybrid WKB

Gravitational wave echoes in the late ringdown signal have been at the heart of searches for quantum structure near black hole horizons since the work of [78, 79] and the claim that they were observed in the first LIGO run [3], see [81, 101, 160, 71, 180, 208, 209, 153].

For echoes to appear in the late-time ringdown signal, one needs a change in the absorbing boundary conditions of the wave equation at the location of the event horizon. Echoes follow naturally from waves being temporarily trapped in the cavity that forms between the light-ring and the reflective structure, while the quasinormal frequencies of the structure are determined by the inverse travel time in that cavity and the behaviour near the light ring. Potentially detectable effects extend beyond echoes, and include tidal effects such as tidal deformabilities, tidal heating and inspiral resonances. We refer to the reviews [75, 83] for more references.

The scattering of scalar waves, including the appearance of echoes, was studied in certain microstate geometries in gravity and their holographically dual CFT state in the early days of the fuzzball proposal over 15 years ago [126, 127, 125, 143, 77]; trapping, the slow decay and quasinormal frequencies were discussed in [100, 92, 115, 114, 145, 91]. This was recently extended to more intricate "superstratum" solutions in [41, 36].

However, all of the solutions in question are smooth, classical geometries and thus correspond to coherent states. Scattering of waves off a *typical* microstate

of a black hole may behave quite differently; studying this would require methods that go beyond classical geometries. Quantum effects might well wash out the geometric structure near the location of the horizon, leading to corrections to the semi-classical gravitational observables that are exponentially suppressed in the entropy as $e^{-S_{\rm BH}/2}$ [25, 22, 23]. This would make a typical microstate all but indistinguishable from the black hole [181]; see for example the construction of operators for asymptotically Anti-de Sitter black holes in [170, 173, 172, 171, 174, 28, 107]. This cast doubt on whether gravitational waves can actually successfully probe and capture information on the particular black hole microstate or fuzzball describing an astrophysical black hole.

Here provide a step towards making these statements and questions quantitative. We revisit the scattering of scalar waves, and focus on how a classical, asymptotic observer would interact with the microstates of the black hole offered to us by string theory. Such string theory microstates are best understood through the notion of holography; the degrees of freedom of the near-horizon region of black hole spacetimes are described by a spacetime that is asymptotically Anti-de Sitter (AdS), which is holographically dual to a conformal field theory (CFT) living on its boundary. At present, it is not possible to look into this for four-dimensional Kerr black holes, as the microstates of that system have not been mapped out in detail (although see [40, 43, 134] for recent work in this direction). Therefore, we keep our focus on arguably the most studied black hole in string theory: the five-dimensional asymptotically flat three-charge black hole. Near the horizon, the fibration of one of the internal dimensions over five-dimensional spacetime leads to an $\mathrm{AdS}_3 \times S^3$ region, dual to the two-dimensional D1-D5 orbifold CFT. This near-horizon limit, obtained after a specific decoupling limit, is described by the three-dimensional BTZ black hole; so it is more appropriate to speak of the BTZ $\times S^3$ decoupling region.

For concreteness, we consider the scattering of massless scalar fields as a first step towards richer probes such as GWs [1]. To highlight the relation between asymptotically flat observables and the CFT data, we wil consider a massless scalar field coming in from (flat) infinity in a five-dimensional three-charge black hole background, and descending into the decoupling region. We will describe how the asymptotic behavior is related to the holographically dual field theory. This link between holography in the BTZ decoupling limit and flat space has been pointed out before by using matched asymptotic expansions between the decoupling region and the asymptotically flat region [126, 127, 125, 143, 77], and very recently using a *hybrid WKB method* for microstates that do not have a separable wave equation outside the decoupling region [41, 36, 46].

[1] Note that in scalar-tensor theories, dilaton-gravity theories and, more generally, supergravities arising from string theory GW perturbations indeed have a massless scalar field component

We expand on those ideas in a controlled toy-model setup. It is known that the quasinormal modes (QNMs) of the scalar wave equation in the BTZ region are identical to the poles of the frequency space retarded two-point correlator in the two-dimensional CFT [57, 196]. Therefore, most of our attention will go to discussing the solutions of the wave equation in the decoupling limit, which can be posed as a Schrödinger problem, and relating these solutions to the two-point correlator. For reasons of computation, we chose not to do this in a specific microstate solution. We study instead a rotating variation of the asymptotically AdS wormhole solution introduced by Solodukhin in [195], whose four-dimensional variation by Damour and Solodukhin had one of the first discussions of GW echoes [105, 71]. The benefit of this simple solution is that we have one controllable parameter λ which determines the position of the throat and hence the deviation from a black hole, while we still capture some of the main features expected from classical microstate geometries in $\mathrm{AdS}_3 \times S^3$.

The rest of this chapter is roughly divided into two parts.

In the first part, we focus on the string theoretic calculation of the approximate propagator for the extremal BTZ wormhole and discussing its coupling to flat space. In section 2.1, we review the BTZ black hole and introduce its corresponding Solodukhin-type wormholes as asymptotically AdS_3 spacetimes. Then, in section 3.3, we use the hybrid WKB method of [41] to calculate the correlator and quasinormal modes of the extremal rotating wormhole. We show how this correlator in asymptotically AdS_3 spacetime actually captures flat space physics by explicitly showing their link using a matched asymptotic expansion in section 2.3.

In the second part, we discuss the link between AdS and flat space gravitational wave physics, as well as the feasability of observing echoes in gravitational wave signals. Section 2.4 reviews the language of flat space gravitational wave (echoes) and makes the link with AdS correlator physics explicit. Finally, in section 2.5 we discuss the location of the microstructure in relation to the black hole horizon, and our averaging procedure that indicates the echo signal is heavily damped in a typical microstate background.

2.1 BTZ black holes and wormholes

Here, we introduce the asymptotically AdS_3 geometries that we will use extensively in the rest of the chapter. First, we review the BTZ black hole. Then, we consider asymptotically BTZ wormholes which are taken and generalized from [195]; we also extend this wormhole to the extremally rotating limit which will allow us to connect to the five-dimensional microstates discussed later in

this chapter. Along the way, we discuss a few basic properties of the wormholes that we will need later on.

2.1.1 The BTZ black hole

Our starting point is the BTZ black hole [27, 26] with metric:

$$\begin{aligned} \mathrm{d}s^2 &= -X(r)\,\mathrm{d}t^2 + \frac{\mathrm{d}r^2}{Y(r)} + r^2(\mathrm{d}\varphi + N_\varphi(r)\,\mathrm{d}t)^2 \\ X(r) = Y(r) &= \frac{(r^2 - r_+^2)(r^2 - r_-^2)}{R^2 r^2}, \quad N_\varphi(r) = -\frac{r_+ r_-}{R r^2}, \end{aligned} \tag{2.1}$$

where R is the AdS radius, the coordinate ranges and identifications are $t \in (-\infty, \infty)$, $r \in [r_+, \infty)$, $\varphi \sim \varphi + 2\pi$, and $r_\pm$ label the outer and inner horizons. One can use Kruskal coordinates in the standard way to maximally extend the spacetime, obtaining two outside (left and right) regions which each have a separate asymptotic AdS_3 region — this can be interpreted as two entangled black holes connected by a non-traversible Einstein-Rosen bridge [154]; see also figure 2.1. The asymptotic mass and angular momentum of the black hole, in units where $8G_3 = 1$, are

$$M = \frac{r_+^2 + r_-^2}{R^2}, \qquad J = \frac{2 r_+ r_-}{R}, \tag{2.2}$$

while the temperature and the entropy of the black hole are given by

$$T = \frac{r_+^2 - r_-^2}{2\pi R^2 r_+}, \qquad S = 4\pi r_+. \tag{2.3}$$

In the holographically dual CFT_2, the black hole corresponds to a thermal state with the same temperature. There are two special cases of interest:

- $r_- = 0$ ($J = 0$): the non-rotating, static BTZ black hole (see figure 2.1).
- $r_+ = r_-$ ($J = MR$): the extremal BTZ black hole.

2.1.2 Wormholes with BTZ asymptotics

By changing the metric factor $X(r)$ in (3.1), we can alter the BTZ geometry to be a Solodukhin wormhole. For the extremal case, we will also need to change $Y(r)$. We will discuss the two cases described earlier: the non-extremal non-rotating wormhole ($r_- = 0$) and extremal rotating wormhole ($r_+ = r_-$).

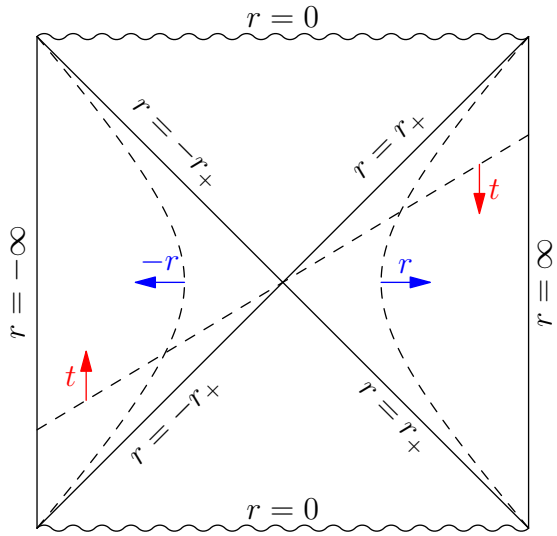


Figure 2.1: Conformal diagram of the extended non-rotating BTZ black hole. The two asymptotically AdS_3 regions are near the lines $r = \pm\infty$. The singularity is at $r = 0$. The dashed lines are lines of constant time and radius.

The non-rotating Solodukhin wormhole

It is straightforward to modify the non-rotating BTZ metric (3.1) with $r_- = 0$ into a wormhole as proposed originally by Solodukhin [195]:

$$\begin{aligned} \mathrm{d}s^2 &= -X(r)\,\mathrm{d}t^2 + \frac{\mathrm{d}r^2}{Y(r)} + r^2\,\mathrm{d}\varphi^2\ , \\ X(r) &= \frac{r^2 - r_\lambda^2}{R^2}\,, \quad Y(r) = \frac{r^2 - r_+^2}{R^2}\,, \quad r_\lambda^2 \equiv r_+^2(1-\lambda^2)\,, \end{aligned} \tag{2.4}$$

where now the radial coordinate ranges between $r \in (-\infty, -r_+] \cup [r_+, \infty)$. This is a one-parameter family of modifications parametrized by the small dimensionless parameter $\lambda > 0$. Just as in the original wormhole of [195], when $r \gg r_+$ the metric looks almost like that of the original black hole since λ is small. However, the global structure of spacetime is very different: there is no longer a horizon at $r = r_+$ since $X(r_+) > 0$. Rather, at this position, we smoothly glue a second copy of this spacetime (with $r < -r_+$), thus creating a traversable wormhole. See section 3.1.3 for more details on how the two copies are "glued" together in practice. We discuss the physical significance of the

parameter λ and its relation to quantum corrections to the corresponding BTZ black hole in section 2.5.1.

The stress energy tensor that supports this geometry is given by:

$$T_{\mu\nu} = R_{\mu\nu} - \frac{1}{2}Rg_{\mu\nu} + \Lambda g_{\mu\nu} = \lambda^2 \begin{pmatrix} 0 & 0 & 0 \\ 0 & -\dfrac{r_+^2}{\rho^2(\rho^2+\lambda^2 r_+^2)} & 0 \\ 0 & 0 & \dfrac{(1-\lambda^2)r_+^4(\rho^2+r_+^2)}{R^2(\rho^2+\lambda^2 r_+^2)^2} \end{pmatrix},$$

where we have defined $\rho^2 \equiv r^2 - r_+^2$. As can be expected, the wormhole is no longer a vacuum AdS_3 solution to Einstein gravity (in contrast to the BTZ metric), but rather requires the presence of exotic matter with negative pressure. We can also calculate the stress tensor in the holographically dual boundary CFT_2, following the standard prescription [24, 191]:

$$2\pi T_{\mu\nu}^{\text{holo}} = \pi \frac{r_+^2}{R^2} \begin{pmatrix} 1 & 0 \\ 0 & R^2(1-2\lambda^2) \end{pmatrix}. \tag{2.5}$$

From this we see that the holographic stress tensor has $O(\lambda^2)$ corrections compared to the corresponding (BTZ) black hole.

The parameter λ determines the length of the wormhole. To see this, we can define the tortoise coordinate $r_*(r)$ for $r > r_+$ as:

$$\begin{aligned} r_*^{(r>r_+)}(r) &= \int_{r_+}^{r} \mathrm{d}r' \, \frac{1}{\sqrt{X(r')Y(r')}} \\ &= \frac{R^2}{r_+\sqrt{1-\lambda^2}} \left[K\left(\frac{1}{1-\lambda^2}\right) - F\left(\arcsin\left(\frac{r}{r_+}\right); \frac{1}{1-\lambda^2}\right)\right], \end{aligned} \tag{2.6}$$

where $K(\cdot)$ is a complete elliptic integral of the first kind and $F(\cdot;\cdot)$ is an elliptic integral of the first kind. The tortoise coordinate can then be extended over the entire wormhole spacetime as:

$$r_*(r) = \theta(r-r_+) r_*^{(r>r_+)}(r) - \theta(-r-r_+) r_*^{(r>r_+)}(-r), \tag{2.7}$$

where $\theta(\cdot)$ is a Heaviside function. The tortoise coordinate ranges continuously in $[-L_\lambda/2, L_\lambda/2]$, where the asymptotic AdS_3 boundary $r \to +\infty$ is at $L_\lambda/2$, with:

$$\begin{aligned} L_\lambda &= 2\frac{R^2}{r_+\sqrt{1-\lambda^2}} \left[K\left(\frac{1}{1-\lambda^2}\right) + iK\left(-\frac{\lambda^2}{1-\lambda^2}\right)\right] \\ &= \frac{R^2}{r_+} \log\frac{16}{\lambda^2} + O(\lambda^2)\,. \end{aligned} \tag{2.8}$$

We call L_λ the wormhole throat length. It corresponds to the travel time from one AdS boundary to the boundary on the other side, as measured by an observer at the asymptotic boundary of AdS (either one). For that reason, it was dubbed the 'optical length' in [195].

The finiteness of the range of the tortoise coordinate distinguishes the wormhole from the black hole (for which the corresponding tortoise coordinate goes to $r_* \to -\infty$ at the horizon). In figure 2.2 we give conformal diagrams of the non-rotating wormhole using, resp., r and r_* as radial coordinates.

The QNMs of this non-rotating wormhole were determined by a WKB method in [195]; we will focus on the extremal rotating limit from now on.

The extremal Solodukhin wormhole

As we are interested in modelling extremally rotating BTZ black holes in string theory, we can also construct a wormhole based on the extremal BTZ black hole with $r_- = r_+$:

$$\begin{aligned} \mathrm{d}s^2 &= -X(r)\,\mathrm{d}t^2 + \frac{\mathrm{d}r^2}{Y(r)} + r^2\left(\mathrm{d}\varphi - \frac{r_+^2}{Rr^2}\,\mathrm{d}t\right)^2 \\ X(r) &= \frac{(r^2-r_\lambda^2)^2}{R^2r^2}\,, \quad Y(r) = \frac{(r^2-r_\lambda^2)(r^2-r_+^2)}{R^2r^2}\,, \quad r_\lambda^2 \equiv r_+^2(1-\lambda^2)\,. \end{aligned} \tag{2.9}$$

We chose to construct the extremal wormhole in such a way that the gluing point $r = r_+$ is a *simple* zero of $Y(r)$.[2] The discussion of the extremal wormhole proceeds very similarly to the above discussion for the non-rotating wormhole; in particular, the wormhole throat at $r = r_+$ is glued to a second copy of the spacetime with $r < -r_+$.

[2]This is a choice; other constructions are also possible. We made this choice since when $r = r_+$ is a simple zero of $Y(r)$, it is somewhat easier to integrate the tortoise coordinate expression.

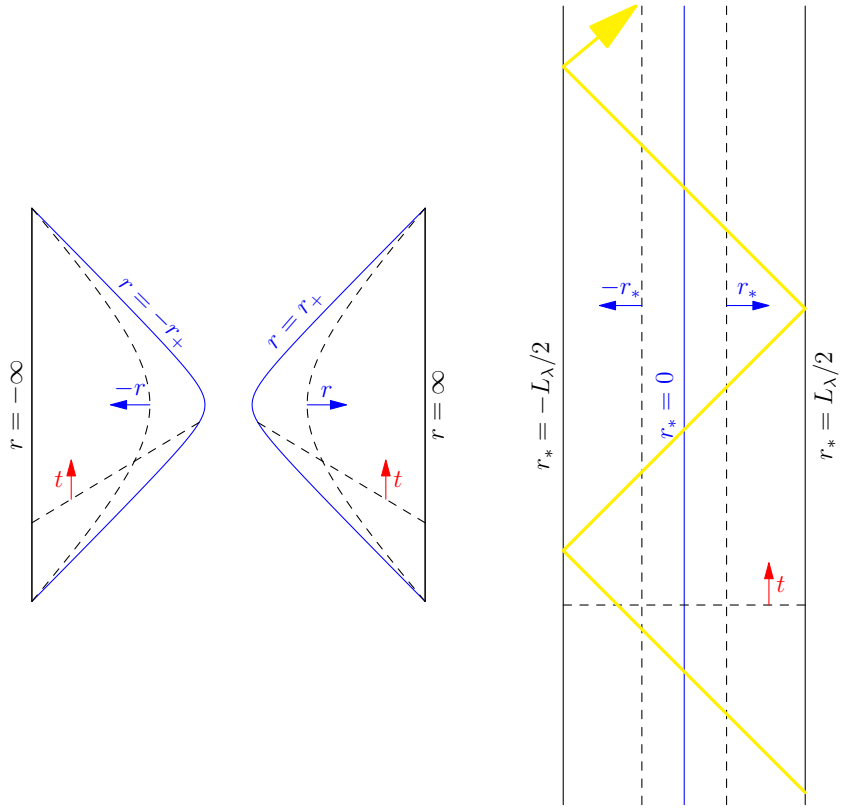


Figure 2.2: Conformal diagrams of the Lorentzian non-rotating wormhole in terms of r (left) and r_* (right) coordinates. In the r coordinate we see that the wormhole is created by a left and a right BTZ wedge glued together (the blue solid line) slightly outside of the BTZ horizon. The r_* coordinate, which ranges continuously in $[-L_\lambda/2, L_\lambda/2]$, makes the causal structure more apparent: the glued surfaces $r = \pm r_+$ (on the left) both coincide with the surface $r_* = 0$ (on the right). The gluing is smooth and a radial light-ray (yellow) can explore the entire wormhole by bouncing infinitely many times between the two boundaries.

The wormhole throat length is qualitatively different in the extremal limit. To see this, once again define the tortoise coordinate:

$$r_*^{(r>r_+)}(r) = \int_{r_+}^{r} dr' \frac{1}{\sqrt{X(r')Y(r')}} \tag{2.10}$$

$$= \left(\frac{R^2}{r_+}\frac{1}{\lambda^2} + \mathcal{O}(\lambda^0, \log\lambda)\right)$$

$$+ \frac{R^2}{r_+^2 - r_\lambda^2}\left(r\sqrt{\frac{r^2 - r_+^2}{r^2 - r_\lambda^2}} - r_+ E\left(\sin^{-1}\frac{r}{r_\lambda}, \frac{r_\lambda^2}{r_+^2}\right)\right),$$

where $E(\cdot,\cdot)$ is the elliptic integral of the second kind. The asymptotic AdS_3 boundary is located at $r_* = L_\lambda/2$ with:

$$L_\lambda = 2\frac{R^2}{r_+}\frac{1}{\lambda^2} + \mathcal{O}(\lambda^0, \log\lambda). \tag{2.11}$$

Since the time coordinate t corresponds to the asymptotic time of the D1-D5-P black hole metric (see section 2.3), the throat length L_λ is now a measure of the travel time from the AdS boundary to other boundary, both as measured by an observer at the AdS boundary, and an observer in the asymptotically flat spacetime of the D1-D5-P black hole.

The throat length is polynomially dependent on (the inverse of) λ, as opposed to the logarithmic dependence for the non-rotating wormhole (2.8). This behavior is typical for redshifts associated to extremal black hole horizons. When $\lambda^2 \ll (r - r_+)/r_+ \ll 1$, we can write the approximate inverse relation:

$$r(r_*) \approx \frac{R^2}{4}\frac{1}{L_\lambda/2 - r_*}\left(1 + \sqrt{1 + 16\frac{r_+^2(r_* - L_\lambda/2)^2}{R^4}}\right), \tag{2.12}$$

From here we see that for $r - r_+ \sim \mathcal{O}(\lambda^0)$, we must also have $r_* \sim \mathcal{O}(L_\lambda) \sim \mathcal{O}(\lambda^{-2})$. From (2.10), we can also see that $r_* \sim \mathcal{O}(\lambda^0)$ when $r - r_+ \sim \mathcal{O}(\lambda^6)$.

2.1.3 The scalar wave equation

We will be considering a probe scalar Φ on the BTZ metric background (3.1) or the wormhole metrics (3.4) and (2.9), with general equation of motion:

$$\nabla^2\Phi = m^2\Phi. \tag{2.13}$$

We can solve this by a separation of variables:

$$\Phi(t, r, \varphi) = e^{-i\omega t + ik\varphi}\Phi_r(r), \tag{2.14}$$

where the radial function $\Phi_r(r)$ must satisfy the differential equation:

$$\begin{aligned}\Phi_r'' + \left(\frac{1}{r} + \frac{X'}{2X} + \frac{Y'}{2Y}\right)\Phi_r' \\ + \left(\frac{\omega^2}{XY} - \frac{k^2}{r^2 Y} - \frac{m^2}{Y} + kN_\varphi\frac{2\omega + kN_\varphi}{XY}\right)\Phi_r = 0.\end{aligned} \tag{2.15}$$

Relating wormhole to BTZ solutions and matching conditions We will be interested in finding the scalar wave solutions to (3.8) in both the black hole and wormhole metrics. For the BTZ black hole, the solutions to (3.8) are explicitly known. Here, we will discuss how the solutions to the corresponding wormhole are related to these black hole solutions.

Let us work in the non-rotating asymptotically AdS_3 wormhole given by (3.4) for definitiveness. We work with the wormhole tortoise coordinate $r_*^{\rm WH}(r)$ introduced in (2.6), which can be expanded over the entire wormhole as in (2.7). Note that $r_*^{\rm WH}=0$ indicates the center of the wormhole throat or the "gluing point". The corresponding (non-rotating) black hole (3.1) has tortoise coordinate:

$$r_*^{\rm BH}(r)=\frac{R^2}{2r_+}\log\left(\frac{r-r_+}{r+r_+}\right)+\frac{L_\lambda}{2}, \tag{2.16}$$

where we have used the constant of integration to set $r_*^{\rm BH}(r\to\infty)=r_*^{\rm WH}(r\to\infty)=L_\lambda/2+\mathcal{O}(\lambda^2)$, with the throat length defined in (2.8).

Now, the radial scalar wave equation (3.8) can be rewritten using $\Phi_r(r)=h(r)\phi(r_*)$, with $h(r)=\sqrt{R/r}$, as:

$$\partial_{r_*}^2\phi(r_*)-V(r_*)\phi(r_*)=0, \tag{2.17}$$

for both the black hole and wormhole geometries (using the respective tortoise coordinate for each). Now, we can easily see that on one side of the wormhole, $V^{\rm WH}(r_*^{\rm WH}(r))=V^{\rm BH}(r_*^{\rm BH}(r))+\mathcal{O}(\lambda^2)$, so that over the entire wormhole:

$$V^{\rm WH}(r_*^{\rm WH})=\theta(r_*^{\rm WH})V^{\rm BH}\left(r_*^{\rm BH}=r_*^{\rm WH}\right)+(r_*^{\rm WH}\to -r_*^{\rm WH})+\mathcal{O}(\lambda^2). \tag{2.18}$$

Thus, the general solution $\phi^{\rm BH}(r)$ to the black hole radial equation (2.17) are also the general solutions (to $\mathcal{O}(\lambda^2)$) to the wormhole radial equation, so $\phi^{\rm WH}(r)=\phi^{\rm BH}(r)$ on the right side of the wormhole, and $\phi^{\rm WH}(-r)=\phi^{\rm BH}(r)$ on the other side. Additionally, the general solution of the wormhole radial equation (and its first derivative) must be continuous at the wormhole throat radius r_t. From (2.18), we see that the wormhole throat $(r_*^{\rm WH})_t=0$ is at $(r_*^{\rm BH})_t=0$, which translates in the coordinate r as (keeping the leading order difference with r_+):

$$r_t^{(\text{non-rot})}=r_+\left(1+\frac{\lambda^2}{8}\right)+\mathcal{O}(\lambda^4). \tag{2.19}$$

The full solution to the scalar wave equation thus must satisfy:

$$\phi^{\rm WH}(r_t)=\phi^{\rm WH}(-r_t),\qquad \partial_r\phi^{\rm WH}(r_t)=\partial_r\phi^{\rm WH}(-r_t). \tag{2.20}$$

For the extremal wormhole (2.9) and its corresponding extremal black hole (3.1), a similar calculation can be done. This is a bit trickier as the extremal

black hole tortoise coordinate cannot be exactly inverted to give $r(r_*)$. However, since only an approximate relation to $\mathcal{O}(\lambda^2)$ is needed, we can still find:

$$r_t^{(\text{ext})} = r_+ \left(1 + \frac{\lambda^2}{4}\right). \tag{2.21}$$

Tortoise and other global wormhole coordinates The tortoise coordinate r_* has a physical interpretation as measuring the travel time of a light ray. Thus, its finite range (see (2.8) and (2.11)) for the wormhole indicates that the entire wormhole geometry is accessible by null geodesics in a finite (coordinate) time t. For example, a light ray can travel radially from the right boundary, through the wormhole, reflect on the left boundary and return to the original point in a time $2L_\lambda$. See also figure 2.2. Thus, we can view the wormhole as a rudimentary toy model of a smooth, horizonless black hole microstate; the left side of the wormhole, including the asymptotic AdS boundary (where we assume reflecting boundary conditions), acts as a "cap" which reflects any infalling matter back out in finite (but long) time, controlled by the wormhole length L_λ.

The tortoise coordinate r_* is not the unique coordinate for which the wormhole potential takes the symmetric form (2.18). In section 3.3, to facilitate the hybrid WKB analysis, we will introduce a coordinate x, which is also globally defined over the entire wormhole and in which the radial equation also takes the Schrödinger form (2.17) with a symmetric potential such as (2.18). The coordinate x moreover will be chosen to have an infinite range and satisfy $\lim_{x\to\infty} V(x) = 1$; this requires a different choice for the function $h(r)$ than what we choose above.

2.2 The hybrid WKB approximation

We discussed the equation of motion for a probe scalar field Φ in the asymptotically AdS_3 spacetimes of the BTZ black hole and wormholes in section 3.1.3. Any such bulk AdS_3 scalar field will be holographically dual to a scalar operator $\mathcal{O}$ on the two-dimensional CFT that lives on the "boundary" (at spatial infinity) of AdS_3 [8, 191]. In this section, we will calculate the two-point correlation function of this holographic scalar operator $\mathcal{O}$.

Below, we will introduce a radial coordinate x for which the AdS_3 boundary is at $x \to \infty$. Solutions of the bulk AdS_3 scalar field Φ behave near the boundary in these coordinates as (we suppress angular φ dependence for simplicity):

$$\Phi(t, x) \approx e^{-it\omega} \left(\beta(\omega) e^{\mu x} + \alpha(\omega) e^{-\mu x}\right). \tag{2.22}$$

This asymptotic expansion of Φ can be used to calculate correlation functions of the holographically dual scalar operator $\mathcal{O}$ in the boundary CFT. In particular, we will be interested in the retarded two-point correlator $G^R(t) \equiv \theta(t)\langle[\mathcal{O}(t), \mathcal{O}(0)]\rangle$, which for a linearized analysis of the scalar field is related to the ratio of coefficients of the asymptotic expansion of the bulk field Φ as [191, 41]:

$$\mathcal{R}(\omega) \equiv -i \int dt e^{-it\omega} G^R(t) = \frac{\alpha(\omega)}{\beta(\omega)}. \tag{2.23}$$

In order to calculate the holographic correlator (2.23) in the extremal wormhole toy model, we will use the hybrid WKB technique developed by [41]. First, we will give a brief overview of the method in section 2.2.1 and the main steps in applying it to the systems at hand. Then we will review the calculation of the free scalar correlator in the extremal BTZ black hole background in section 2.2.2, and then redo the calculation for the the extremal BTZ wormhole in section 2.2.3. Finally, we give some brief remarks on the expectations for the free scalar position-space propagator $G^R(t)$ in section 3.4.2.

2.2.1 Method outline

The hybrid WKB approximation works in a number of steps. First, we apply the traditional WKB method to find an approximate solution to the wave equation. In order to proceed with finding the WKB approximation to the propagator, one needs to analyze the asymptotic structure of the approximate solution around the boundary. However, this is generally a hard task, because the WKB solution is not written in a basis that is conducive to asymptotic analysis. This is where the second step of the hybrid WKB technique is employed. One finds a new potential that asymptotically approaches the original potential and for which the wave equation can be solved exactly. Then the WKB solution is matched with the asymptotic solution, which allows one to efficiently analyze the asymptotic structure of the approximate solutions to the wave equation and ultimately extract the propagator.

Practically speaking, we will divide the method into three parts, which we will now discuss.

Setting up the radial equation and potential

We wish to split the radial part of the scalar as:

$$\Phi_r(r) = h(r)\phi(r)\,, \tag{2.24}$$

and we perform a coordinate transformation $r \to x(r)$ to write the radial wave equation (3.8) for ϕ in the Schrödinger form:

$$\frac{\partial^2}{\partial x^2}\phi(x) - V(x)\phi(x) = 0\,. \tag{2.25}$$

The absence of a term proportional to $\partial_x \phi$ leads to the condition:

$$h(r) = \frac{1}{\left(r^2 X(r) Y(r) \left(\frac{\partial x(r)}{\partial r}\right)^2\right)^{1/4}}\,. \tag{2.26}$$

We are still free to choose $x(r)$, which will affect the form of the potential $V(x)$. To align with the analysis in [41], we choose $x(r)$ such that the potential approaches a particular constant in the UV:

$$\lim_{x\to\infty} V(x) = 1 + m^2 R^2 \equiv \mu^2\,. \tag{2.27}$$

where we have defined the dimensionless parameter μ. This can be achieved by fixing the function $x(r)$ such that:

$$h(r) = \frac{R}{r}\,. \tag{2.28}$$

The following condition needs to be met in order for the WKB approximation to be valid

$$\left|(V(x))^{-\frac{3}{2}}\,\frac{\partial V(x)}{\partial x}\right| \ll 1\,. \tag{2.29}$$

This quantity should be evaluated away from the turning points, defined by $V(x_{\rm turn}) = 0$, where the left side diverges.

Asymptotic solutions

For large x, the potential asymptotes to a potential $V_{\rm asymp}(x)$:

$$V(x) \sim V_{\rm asymp}(x), \tag{2.30}$$

that we will make precise below. The solutions to the wave equation (3.67) with this potential $V_{\rm asymp}(x)$ are given by $\phi_{\rm asymp}(x)$ with the following structure

$$\phi_{\rm asymp}(x) = c_1 \phi^{\rm grow}_{\rm asymp}(x) + c_2 \phi^{\rm dec}_{\rm asymp}(x)\,, \tag{2.31}$$

where in the UV we have defined the two linearly independent solutions as those that behave at large x as:[3]

$$\begin{aligned}\phi^{\rm grow}_{\rm asymp}(x) &= e^{\mu x}\,(1+\dots)\,,\\ \phi^{\rm dec}_{\rm asymp}(x) &= e^{-\mu x}\,(1+\dots)\,,\end{aligned} \tag{2.32}$$

where the omitted terms are subleading in x at large x. When μ is an integer, there are also pieces proportional to x in the UV expansion; we will assume μ not to be an integer and analytically continue the final result to integer μ. Both $\phi^{\rm grow}_{\rm asymp}$ and $\phi^{\rm dec}_{\rm asymp}$ are real functions of x (for real r_+, k, ω, μ, R).

Calculation of the WKB propagator

Now we have all ingredients to evaluate the propagator that follows from the hybrid WKB technique. According to [41], the propagator is given by

$$\mathcal{R} = \left(\mathcal{A} + \frac{\sqrt{3}}{2}\right) e^{-2I_+} - \frac{\phi^{\rm grow}_{\rm asymp}(x_+)}{\phi^{\rm dec}_{\rm asymp}(x_+)}\,. \tag{2.33}$$

where

$$I_+ = -\mu x_+ + \int_{x_+}^{\infty} \left(\sqrt{|V(z)|} - \mu\right) dz\,, \tag{2.34}$$

and the turning points $x_\pm$ are defined such that $V(x_\pm) = 0$. The expression for $\mathcal{A}$ depends on the number of turning points. For a single turning point, we have

$$\mathcal{A} = \frac{i}{2}\text{sign}(\omega)\,. \tag{2.35}$$

For two turning points x_- and x_+, we have

$$\mathcal{A} = \frac{1}{2}\tan(\Theta)\,, \qquad \Theta = \int_{x_-}^{x_+} \sqrt{|V(z)|}dz\,. \tag{2.36}$$

This will be the formula we will need to evaluate to find the wormhole propagator. The general expression for $\mathcal{A}$ for more than two turning points can be found in an appendix of [41].

2.2.2 The BTZ black hole

It is useful to first review the hybrid WKB calculation applied to the extremal BTZ black hole itself.

[3]Note that the full radial function Φ_r in (3.7) is still given by $\Phi_r(r) = \phi(x)R/r$.

Setting up the radial equation and potential

We choose the radial coordinate:

$$x^{\rm BH}(r) = \frac{1}{2}\log\frac{r^2-r_+^2}{r_+^2} - \frac{1}{2}\frac{r_+^2}{r^2-r_+^2}, \tag{2.37}$$

such that the black hole potential is

$$V^{\rm BH}(x^{\rm BH}(r_*)) = \frac{(r^2-r_+^2)^2}{r^8}(2r^2r_+^2-3r_+^4+r^4\mu^2)+\frac{R^2}{r^2}(k^2-R^2\omega^2)-\frac{R^2r_+^2}{r^4}2k(k-R\omega), \tag{2.38}$$

for which indeed $V(x\to\infty)=\mu^2$. It is plotted along with the wormhole potential in figure 2.3.

Asymptotic solutions

The explicit analytic solutions $\phi^{\rm dec}_{\rm asymp}(x,)\phi^{\rm grow}_{\rm asymp}(x)$ for the extremal BTZ black hole are known in terms of Whittaker M,W functions (see (2.78)), however, we do not actually need their expressions. Remarkably, as we will show below, we can use the WKB method to find an approximation for the wormhole propagator in terms of the black hole one without using the form of the explicit solutions $\phi_{\rm asymp}$.

Calculation of the WKB propagator

The BTZ potential has only one turning point, so one finds

$$\mathcal{R}^{\rm BH} \approx \left(\frac{i}{2}{\rm sign}(\omega)+\frac{\sqrt{3}}{2}\right)e^{-2I_+} - \frac{\phi^{\rm grow}_{\rm asymp}(x_+)}{\phi^{\rm dec}_{\rm asymp}(x_+)}\,. \tag{2.39}$$

As noted earlier, the exact solutions $\phi^{\rm grow,dec}_{\rm asymp}$ are real and so is I_+. This allows us to write

$$\begin{aligned}{\rm Re}\left(\mathcal{R}^{\rm BH}\right) &\approx \frac{\sqrt{3}}{2}e^{-2I_+} - \frac{\phi^{\rm grow}_{\rm asymp}(x_+)}{\phi^{\rm dec}_{\rm asymp}(x_+)}\,,\\ {\rm Im}\left(\mathcal{R}^{\rm BH}\right) &\approx \frac{1}{2}{\rm sign}(\omega)e^{-2I_+}\,.\end{aligned} \tag{2.40}$$

This will be useful when we calculate the WKB approximation for the wormhole propagator later on. Note that using the solutions $\phi_{\rm asymp}$ one can compute the extremal BTZ propagator; this was done in [41].

2.2.3 The extremal wormhole

We can now apply the method above to find the approximate propagator in the Solodukhin extremal wormhole metric (2.9).

Setting up the radial equation and potential

We choose to work with the following coordinate:

$$x(r) = \frac{r_\lambda^2}{r_+^2 - r_\lambda^2}\sqrt{\frac{r^2 - r_+^2}{r^2 - r_\lambda^2}} + \log\left(\sqrt{\frac{r^2 - r_\lambda^2}{r_\lambda^2}} + \sqrt{\frac{r^2 - r_+^2}{r_\lambda^2}}\right) - \frac{1}{\sqrt{3}}\frac{1}{\lambda^2}\,, \quad (2.41)$$

for which $h(r)$ satisfies (3.70) and $x(r_t) = O(\log\lambda)$ (where r_t is the matching radius given by (2.21)); the range of x coordinate is $-\infty$ to ∞ and spans the whole wormhole. The potential in this x coordinate is:

$$V(x(r), \lambda) = V^{\rm BH}(x) + \mathcal{O}(\lambda^2), \quad (2.42)$$

with $V^{\rm BH}(x)$ given in (2.38) such that again $V(x \to \infty) = \mu^2$. At the wormhole throat $x = 0$:

$$V(x = 0) = -\frac{R^2}{r_+^2}(k - R\omega)^2 + \mathcal{O}(\lambda^2). \quad (2.43)$$

To check that the condition (3.75) is satisfied, we note that away from the turning point of the potential, $r - r_+ \ll r_+$ (see also the discussion below, around (2.50)). Expanding (3.75) to second order in $r - r_+$, we get:

$$\left|(V(x))^{-\frac{3}{2}}\frac{\partial V(x)}{\partial x}\right| = \left|\frac{(R\omega - 3k)}{(R\omega - k)^2}\left(\frac{6(r - r_+)}{R}\lambda^2 + \frac{8(r - r_+)^2}{Rr_+}\right)\right|. \quad (2.44)$$

The condition that this is much smaller than unity gives us the condition:

$$(R\omega - k)^2 \gg 12|k|\lambda^2\left(\frac{r - r_+}{R}\right) = 24|k|\frac{R}{L_\lambda}\left(\frac{r - r_+}{r_+}\right), \quad (2.45)$$

so we need $(R\omega - k)$ to be sufficiently large so that the WKB approximation is valid.

Asymptotic solutions

Because $x^{\rm BH}(r_t) = -1/\lambda^2 + \mathcal{O}(\log\lambda)$ (whereas for the wormhole, $x(r_t) = \mathcal{O}(\log\lambda)$), we can conclude that the wormhole potential is well approximated

by two copies of the shifted asymptotic black hole potential:

$$V(x,\lambda) = \theta(x) V_{\text{asymp}}\left(x - \frac{1}{\lambda^2}\right) + (x \to -x) + \mathcal{O}(\log\lambda). \tag{2.46}$$

This is, of course, the analogous relation in the x coordinate for the extremal wormhole to (2.18). We have plotted an example of this potential in figure 2.3.

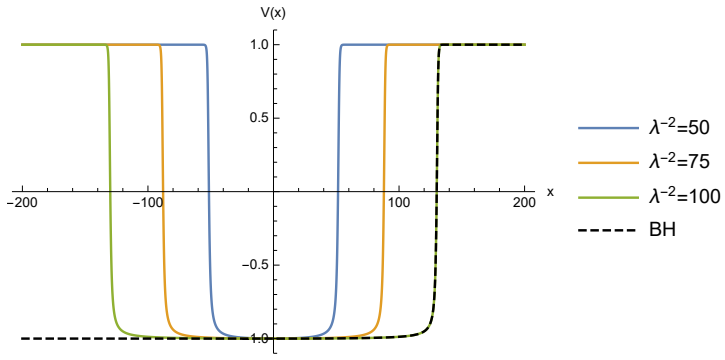


Figure 2.3: The wormhole potential $V(x)$, plotted for three different values of λ, and $R = r_+ = \omega = 1$, $k = 0$. The dotted line is the black hole potential $V_{\text{asymp}}(x - 1/\lambda^2)$ for $\lambda^{-2} = 100$, showing graphically the validity of the approximation (2.46).

Calculation of the WKB propagator

The wormhole potential is essentially two copies of the black hole potential, leading to two turning points, so $\mathcal{A}$ will differ with respect to the BTZ propagator (3.87). However, due to (3.79) we can see that $I_+^{\text{wormhole}} = I_+^{\text{BH}} + \mathcal{O}(\lambda^2)$, and thus we can write

$$\mathcal{R}^{\text{WH}} \approx \text{Re}\left(\mathcal{R}^{\text{BH}}\right) + 2\,\text{sign}(\omega)\,\mathcal{A}\,\text{Im}\left(\mathcal{R}^{\text{BH}}\right)\,, \tag{2.47}$$

where $\approx$ now denotes both inaccuracy due to the WKB approximation and corrections of order λ^2. Thus, as anticipated, we do not need the explicit form of ϕ_{asymp} to be able to write down our wormhole propagator as a function of the black hole one.

To get a rough approximation for Θ, we can use the change of integration variables to the tortoise coordinate r_* defined by (2.10):

$$\Theta = \int_{x_-}^{x_+} \sqrt{|V(x)|}dx = \int_{r_*(x_-)}^{r_*(x_+)} \sqrt{|V(x(r(r_*)))|}\frac{dx}{dr}\frac{dr}{dr_*}dr_*\,. \tag{2.48}$$

For $\lambda \ll 1$, this integral is dominated by a flat potential in the wormhole throat. To see this, note that

$$\lim_{r\to r_+} \sqrt{|V(x(r(r_*)))|}\frac{dx}{dr}\frac{dr}{dr_*} = \left|\omega - \frac{k}{R}\right| , \tag{2.49}$$

and further that (for $x_+ > x > 0$, that is on the right side of the wormhole $r > r_+$):

$$\frac{d}{dx}\left(\sqrt{|V(x(r(r_*)))|}\frac{dx}{dr}\frac{dr}{dr_*}\right) \approx \frac{8|k|}{Rr_+^2}(r-r_+)^2 . \tag{2.50}$$

From the discussion of the extremal wormhole tortoise coordinate around (2.10) and (2.12), we know that as long as $r_* \lesssim L_\lambda/2$, we have $r - r_+ \ll r_+$ and so (2.50) implies the potential remains very flat; thus, we can approximate (2.48) very well by

$$\Theta \approx \left|\omega - \frac{k}{R}\right| L_\lambda. \tag{2.51}$$

Note that $R\omega - k$ needs to sufficiently large for the WKB approximation to be valid, see (2.45). The approximate value (2.51) is indeed what we would expect intuitively from a potential that is very similar to that of a square well (see figure 2.3) with a depth of (2.49) and a length of L_λ. The normal modes of the wormhole are the poles of $\tan\Theta$, which are then (approximately):

$$\omega_n = \frac{k}{R} + \left(n + \frac{1}{2}\right)\frac{\pi}{L_\lambda}. \tag{2.52}$$

The spacing between modes is to leading order:

$$\Delta\omega_n \equiv \omega_{n+1} - \omega_n = \frac{\pi}{L_\lambda}, \tag{2.53}$$

In this rough approximation, the propagator is then given by:

$$\mathcal{R}^{\mathrm{WH}} \approx \mathrm{Re}\left(\mathcal{R}^{\mathrm{BH}}\right) + \tan\left(\left|\omega - \frac{k}{R}\right| L_\lambda\right) \mathrm{Im}\left(\mathcal{R}^{\mathrm{BH}}\right) , \tag{2.54}$$

We restrict to the result for the QNMs to leading order in λ, as this is enough to for our purposes in the next sections. At next-to-leading order, the modes are no longer evenly spaced, as discussed for the non-rotating wormhole in [195]. We will briefly discuss the position-space propagator that follows from (2.54) below in section 3.4.2.

It is interesting to compare our (rough) result (2.51) with the analysis of [41], where the scalar correlator was calculated in the complicated $(1, 0, n)$ superstratum metric [37, 38] (which, in the decoupling limit, asymptotes to

AdS_3 as does extremal BTZ). In particular, we can compare their result for Θ in the microstate cap regime when the scalar mode frequency is high enough (see [41], eq. (5.3)). The general structure they find for Θ and thus for the correlator matches our result qualitatively very well: the dominant piece in Θ is linear in ω and proportional to the microstate throat length L_{micro} (with $L_{micro} \sim R_y b^2/a^2$, using the parameters in [41]). As they also find, this piece is responsible for echoes in the position space correlator at a time of order $\sim L_{micro}$ and integer multiplies of this (see [41], figure 13). Thus, our very simple Solodukhin wormhole toy model captures this feature of the complicated superstratum geometry very well.

2.2.4 Position-space propagator

We can use a few simple arguments to understand the general structure of the position-space propagator that follows from the frequency space result (2.54). Note that in [41], the position-space propagator is discussed at length.

Consider the distributional identity:

$$\tan x = \sum_{n=1}^{\infty} 2(-1)^{n-1} \sin(2nx), \tag{2.55}$$

and its Fourier transform:

$$\begin{aligned} \mathcal{F}(t) &\equiv \frac{1}{2\pi} \int d\omega e^{-i\omega t} \tan \omega L_\lambda \\ &= i \sum_{n=1}^{\infty} (-1)^{n-1} \left(\delta(t + 2nL_\lambda) - \delta(t - 2nL_\lambda)\right). \end{aligned} \tag{2.56}$$

Then, using the convolution theorem for Fourier transforms on the retarded propagator (2.54):

$$G^R_{\mathrm{WH}}(\Delta t, \Delta\varphi) \approx G^0(\Delta t, \Delta\varphi) + (G^1 * \mathcal{F})(\Delta t, \Delta\varphi), \tag{2.57}$$

$$G^0(\Delta x) \equiv -\frac{\theta(\Delta t)}{2\pi^2} \sum_k e^{ik\Delta\varphi} \int d\omega e^{-i\omega\Delta t} \mathrm{Re}(\mathcal{R}^{\mathrm{BH}}), \tag{2.58}$$

$$G^1(\Delta x) \equiv -\frac{\theta(\Delta t)}{2\pi^2} \sum_k e^{ik\Delta\varphi} \int d\omega e^{-i\omega\Delta t} \mathrm{Im}(\mathcal{R}^{\mathrm{BH}}), \tag{2.59}$$

so that $G^R_{\rm BH}(\Delta t, \Delta\varphi) = G^0(\Delta t, \Delta\varphi) + iG^1(\Delta t, \Delta\varphi)$, and the convolution gives:

$$(G^1 * \mathcal{F})(\Delta t, \Delta\varphi) = i\sum_{n=1}^{\infty}(-1)^{n-1}\int dt' G^1(\Delta t - t', \Delta\varphi)\left(\delta(t' + 2nL_\lambda) - \delta(t' - 2nL_\lambda)\right)$$

$$= i\sum_{n=1}^{\infty}(-1)^{n-1}\left(G^1(\Delta t + 2nL_\lambda) - G^1(\Delta t - 2nL_\lambda)\right), \tag{2.60}$$

so that we have the relation:

$$G^R_{\rm WH}(\Delta t, \Delta\varphi) \approx G^0(\Delta t, \Delta\varphi) + i\sum_{n\in\mathbb{Z}}(-1)^n \mathrm{sgn}(n) G^1(\Delta t - 2nL_\lambda), \tag{2.61}$$

where we define the $n = 0$ term of the sum to be $G^1(\Delta t)$ — although note that the Fourier transform of the tan, as naively calculated above, does not contain this $n = 0$ term. It is important to realize that (2.61) is merely a schematic expression: we did not treat the integration over ω carefully (by closing its contour and picking up appropriate residues of poles), and moreover the expression (2.54) we obtained using the hybrid WKB method is only approximately valid.[4] In the next chapter, we will use real time holography and carefully obtain a precise expression for an analogous correlator in the non-rotating BTZ background. Despite its shortcomings, (2.61) captures the most important behavior: one can clearly see the appearance of "echoes" in the propagator: recurrences at periodic intervals $2L_\lambda$ of the correlator. Thus, at early times $0 < \Delta t \ll 2L_\lambda$, the propagator will mimic the BTZ propagator and decay exponentially; only at a time $\Delta t \sim 2L_\lambda$ will the propagator start to differ qualitatively from the black hole one due to the appearance of the first echo.[5] We show this behaviour in figure 2.7a.

Even though the scalar two-point function in a single wormhole geometry has clear echoes, if we take such wormholes seriously as (toy models for) black hole microstates, a typical microstate will be a superposition of many such geometries. Then generically one expects the echo behaviour of such a typical state to be exponentially suppressed (in the black hole entropy). We discuss this in more detail in section 2.5.2.

[4] In particular, it will have apparent poles in the complex frequency plane with non-zero imaginary part. However, the correct full propagator in frequency space will necessarily only have poles on the real axis, as the geometry only admits normal modes and no quasi-normal modes.

[5] For the extremal BTZ black hole, after the initial exponential falloff, the correlator transitions to a polynomial falloff due to the contribution of scattering events with period 2π, originating from the compactness of the φ coordinate, known as "images". See [41] for detailed discussion.

2.3 Connecting BTZ to flat space

In the previous section, we calculated the two-point correlation function of a probe scalar field in the extremal BTZ black hole spacetime (3.1), as well as its extremal Solodukhin wormhole counterpart (2.9). We saw how the wormhole gave rise to normal modes ω_n given by (2.52) in frequency space with spacing $\Delta\omega_n = \pi/L_\lambda$ (with the wormhole throat length L_λ given by (2.11) for the extremal wormhole) so that the position space correlator correspondingly has echoes, as discussed in section 3.4.2 .

In this section, we discuss how these asymptotic AdS_3 correlators can be related to (5D) flat space gravitational waves (as modeled by a scalar probe). This relation is given by the well-known decoupling limit of the five-dimensional asymptotically BMPV black hole [69], or more precisely its three-charge generalization [68]. Our focus will be on solving the minimally coupled probe scalar wave equation on this background (and its corresponding Solodukhin wormhole), relating the (quasi)normal modes of the asymptotically flat five-dimensional black hole (resp. wormhole) to the (quasi)normal modes of the extremal BTZ black hole (resp. extremal wormhole) through the decoupling limit. We will use methods similar to [91, 92] (see also [203, 109] for similar ideas and methods).

As we saw before (in section 2.2.3), the Solodukhin wormhole that corresponds to the extremal BTZ geometry has only normal modes: the eigenfrequencies are real, with an approximate spacing between modes of L_λ^{-1}. We will see here (in section 2.3.3) that by coupling this wormhole to flat space, or said otherwise, by constructing the Solodukhin wormhole corresponding to the BMPV black hole, these normal modes receive a small imaginary part, making them quasinormal modes. This is related to the wave being able to "leak out" into flat infinity; see figure 2.4. The real and imaginary parts of the resulting five-dimensional wormhole quasinormal modes follow the general scaling discussed in [83] for (flat space) compact objects, as we discuss briefly in section 2.3.4. Note that in principle the quasinormal modes are sufficient information to determine the entire analytic structure of the response function, so that they give a complete characterization of the system (see section 2.4).

2.3.1 Scalar probe in BMPV solution and the decoupling limit

In this section, we will first describe the decoupling limit of BMPV, which gives the extremal BTZ black hole in AdS_3. Then, we describe the probe scalar wave equation in this background and solve it in three different regions where explicit analytic solutions are possible.

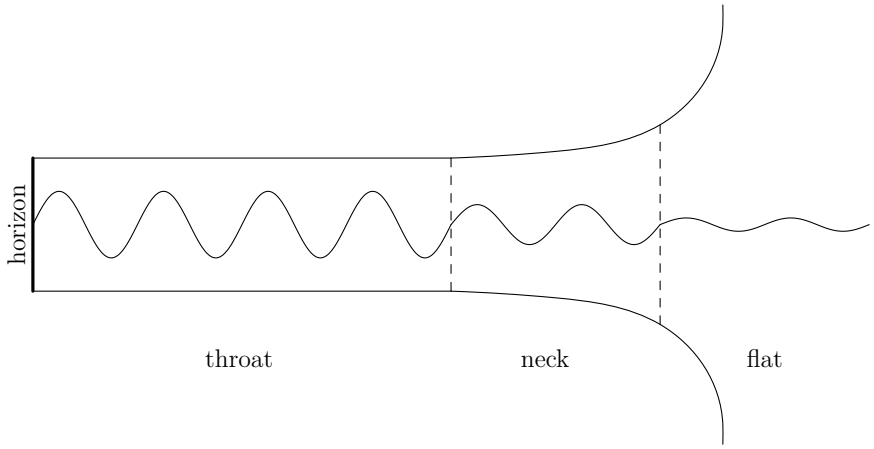


Figure 2.4: A schematic depiction of how the BTZ black hole is connected to flat space. In the decoupling limit $\epsilon \to 0$, the flat space region is decoupled from the BTZ region; when $1 \gg \epsilon > 0$, the flat space region is (weakly) coupled to the BTZ region through the intermediate neck region, which allows the scalar field to "leak" out of the BTZ region.

BMPV and decoupling limit

The three-charge asymptotically flat non-rotating BMPV black hole [68] has as 6D metric:

$$\begin{aligned} \mathrm{d}s^2_{6D} = (H_1 H_5)^{-1/2} \left(-dt^2 + dy^2 + \frac{Q_P}{\rho^2}(dy - dt)^2 \right) \\ + (H_1 H_5)^{1/2}(d\rho^2 + \rho^2 d\Omega_3^2), \end{aligned} \tag{2.62}$$

with:

$$H_1 = 1 + Q_1/\rho^2, \qquad H_5 = 1 + Q_5/\rho^2. \tag{2.63}$$

The y-direction is compact with period $2\pi R_y$; $d\Omega_3^2$ is the volume form on the unit radius S^3 sphere. Thus, this solution can be seen as a six-dimensional black string, or after reduction along the compact y direction, a 5D black hole. Note that the (finite size) horizon is at $\rho = 0$.

This black hole can be uplifted to a full 10D type IIB supergravity solution [150], where then the parameters Q_1, Q_5 can be seen as the D1- and D5-brane charges of the solution, where both wrap the y direction and the D5-branes also wrap the compact M_4; Q_P is the momentum travelling along the y-direction. These charges are related to the quantized number of branes N_1, N_5 and quanta

of momentum N_P as:

$$Q_1 = c_1 \frac{\alpha'^3}{V_4} N_1, \qquad Q_5 = c_5 \alpha' N_5, \qquad Q_P = c_P \frac{\alpha'^4}{V_4 R_y^2} N_P, \tag{2.64}$$

where $\alpha' = l_s^2$ is the string length squared and $V_4 = vol(M_4)$. The c_I are factors which contain numerical factors as well as powers of the string coupling g_s, which will not enter in our discussion (see for example [155]).

In the (near-)decoupling limit of this metric, we realize that we can decouple excitations near the horizon and those very far away from the black hole. Concretely, we take $\alpha' = R_y^2 \epsilon^2$ for a dimensionless parameter ϵ which is sent to zero in the strict decoupling limit [8, 150]. (This limit is sometimes called the "large R_y limit" [150, 91], as we are taking R_y to be much larger than the string scale.) We further take $\rho \sim \epsilon^2$ so that ρ/α' remains fixed. Note that we must have $V_4 \sim \alpha'^2 \sim R_y^4 \epsilon^4$. The charges scale as: $Q_1, Q_5 \sim R_y^2 \epsilon^2$ and $Q_P \sim R_y^4 \epsilon^4$. The resulting metric in the $\epsilon \to 0$ limit is given by taking the initial asymptotically flat metric (2.62) and "dropping the 1's" in the functions $H_{1,5}$, we get:

$$ds^2_{BTZ\times S^3} = \frac{\rho^2}{R^2}\left(-dt^2 + dy^2 + \frac{Q_P}{\rho^2}(dt-dy)^2\right) + \frac{R^2}{\rho^2}d\rho^2 + R^2 d\Omega_3^2. \tag{2.65}$$

The metric (2.65) is the direct product of an S^3 with constant radius $R = (Q_1 Q_5)^{1/4}$ and an AdS_3 factor with the same radius — the extremal rotating BTZ black hole with mass, angular momentum and horizon radius:

$$M = J = 2Q_P/R^2, \qquad r_+ = \sqrt{Q_P}. \tag{2.66}$$

To compare with the BTZ metric in (3.1), take $\rho^2 = r^2 - r_+^2$ and $\varphi = y/R$.[6]

If we had considered the region $\rho \sim \epsilon^0$ instead, the leading order metric would have been pure 6D flat space (more precisely: $\mathbb{R}^{4,1} \times S^1(y)$):

$$ds^2_{\text{6D,flat}} = -dt^2 + dy^2 + d\rho^2 + \rho^2 d\Omega_3^2. \tag{2.67}$$

True to its name, the decoupling limit $\epsilon \to 0$ thus decouples excitations in the asymptotically flat region (2.67) from the near-horizon AdS_3 region (2.65). In the near-decoupling limit, when $\epsilon > 0$ (but still $\epsilon \ll 1$), the asymptotic flat region (2.67) is weakly coupled to the AdS region (2.65); this results in excitations in the AdS region being able to weakly "leak out" into the flat space region; see figure 2.4. This is precisely the effect we will see when we calculate the quasinormal modes of the BMPV black hole (2.62).

[6] Note that the periodicity of y is different compared to what would be expected from this coordinate transformation.

Three regions in the decoupling limit As we mentioned above, in the AdS region we have $\rho \sim \epsilon^2$ or $\rho/R \ll 1$, whereas in the asymptotic flat region $\rho \sim \epsilon^0$ or $\rho/R \gg 1$. However, (in analogy with [91, 92]) we will instead introduce a second small, dimensionless parameter $\sigma \ll 1$ by hand, so that the AdS region of the decoupling limit is given by:

$$0 \leq \frac{\rho}{R} \leq \sigma, \tag{2.68}$$

whereas the flat space region is given by:

$$\frac{\rho}{R} \geq \frac{1}{\sigma}. \tag{2.69}$$

These regions obviously *do not* overlap, and so we cannot match a solution from AdS directly to flat space. To match solutions between the AdS and the flat region, we will need to pass through the so-called "neck" region, which is defined as:

$$\sigma \leq \frac{\rho}{R} \leq \frac{1}{\sigma}. \tag{2.70}$$

Solving the scalar wave equation

We will consider the minimally coupled probe scalar wave equation:

$$\nabla_6^2 \Phi = 0, \tag{2.71}$$

on the full BMPV metric background (2.62). We use the separation ansatz:[7]

$$\Phi(t, \rho, y, \Omega_3) = \exp\left(-i\omega t + i\tilde{m} y + i m_1 \phi_1 + i m_2 \phi_2\right) \Theta(\theta) g(\rho), \tag{2.72}$$

Note that we can write $\tilde{m} = m/R_y$ with m, m_1, m_2 integers. We will be looking for $\omega \sim 1/R_y$, which corresponds to large wavelength, low energy modes in the decoupling limit. Note that if $\mathrm{Im}(\omega) < 0$, the mode is exponentially decaying. The angular function is a solution to:

$$\Theta'' + 2\cot 2\theta\, \Theta' - \left(m_1^2 \csc^2\theta + m_2^2 \sec^2\theta\right)\Theta = -\Lambda\, \Theta, \tag{2.73}$$

with $\Lambda = \ell(\ell+2)$ and ℓ an integer.

Radial equation It is convenient to use the dimensionless radial coordinate $\chi = R_y^2/\rho^2$ to get the radial scalar wave equation in the form:

$$\chi^2 g''(\chi) + V(\chi) g(\chi) = 0, \tag{2.74}$$

[7] For definitiveness, we use the (flat) three-sphere metric $d\Omega_3^2 = d\theta^2 + \sin^2\theta d\phi_1^2 + \cos^2\theta d\phi_2^2$, where θ ranges between 0 and $\pi/2$, and $\phi_{1,2}$ are periodic with period 2π.

with potential:

$$4V(\chi) = \frac{R_y^2}{\chi}\left[\omega^2 - \tilde{m}^2\right] + \left[1-\nu^2\right] + \frac{\chi}{R_y^2}\left[\kappa(\omega^2-\tilde{m}^2)\right] + \frac{\chi^2}{R_y^4}\left[\Xi^2(\omega-\tilde{m})^2\right], \tag{2.75}$$

where we have defined:

$$\begin{aligned}
\nu^2 &= (\ell+1)^2 - (Q_1+Q_5)(\omega^2-\tilde{m}^2) - Q_P(\omega-\tilde{m})^2 = (\ell+1)^2 + \mathcal{O}(\epsilon^2),\\
\kappa &= R^4 + (\epsilon^6)(Q_1+Q_5)Q_P\frac{(\omega-\tilde{m})^2}{\omega^2-\tilde{m}^2} = R^4(1+\mathcal{O}(\epsilon^2)),\\
\Xi &= R^2 Q_P^{1/2}.
\end{aligned} \tag{2.76}$$

Note that $\kappa, \Xi \sim \epsilon^4$.

Solutions in three regions Now, we solve the radial wave equation (2.74) in the three regions in the three regions (2.68), (2.69), and (2.70) separately (note that $\chi^2\partial_\chi^2 \sim (\epsilon\,\sigma)^0$):

- In the AdS region (2.68), for which we implement the strict decoupling limit $\rho \sim \epsilon\,\sigma$ so that $\chi \sim (\epsilon\,\sigma)^{-2}$; the potential (2.75) reduces to:

$$4V(\chi) = \left(\left[1-\nu^2\right] + \frac{\chi}{R_y^2}\left[(\kappa(\omega^2-\tilde{m}^2)\right] + \frac{\chi^2}{R_y^4}\left[\Xi^2(\omega-\tilde{m})^2\right]\right). \tag{2.77}$$

  This is precisely the radial potential of a scalar field in the 3D extremal BTZ metric (3.1), where the scalar has the 3D mass $m^2 = \nu^2 - 1$ and the effective extremal BTZ parameters R, r_+ are given by $R = \kappa^{1/4}, r_+ = \Xi/\kappa^{1/2}$. The solutions to the wave equation with the potential (2.77) are given by Whittaker W, M functions (which could also be expanded in terms of hypergeometric functions):

$$\begin{aligned}
g(\chi) =& c_1^A\, M\left(i\frac{\kappa}{4\Xi}(\omega+\tilde{m}), \frac{\nu}{2}, -i\chi\frac{\Xi}{R_y^2}(\omega-\tilde{m})\right)\\
&+ c_2^A\, W\left(i\frac{\kappa}{4\Xi}(\omega+\tilde{m}), \frac{\nu}{2}, -i\chi\frac{\Xi}{R_y^2}(\omega-\tilde{m})\right),
\end{aligned} \tag{2.78}$$

- In the flat region, we have $\rho \sim \epsilon/\sigma$ so that $\chi \sim \sigma^2/\epsilon^2$, we find:

$$4V(\chi) = \left(\left[1-\nu^2\right] + (\frac{R_y^2}{\chi} \left[\omega^2 - m^2\right] \right) + \mathcal{O}(\epsilon^2\sigma^2), \tag{2.79}$$

  The solutions to the wave equation with this potential are given by Bessel functions:

$$g(\rho) = \frac{1}{\rho} \left(c_1^F I_{-\nu}(i\sqrt{\omega^2 - m^2}\rho) + c_2^F I_\nu(i\sqrt{\omega^2 - m^2}\rho) \right). \tag{2.80}$$

  The I_ν are the modified Bessel functions of the first kind.[8]

- Finally, in the neck region, $\rho \sim \epsilon\, \sigma^0$ so that $\chi \sim \epsilon^{-2}\sigma^0$, we have:

$$4V(\chi) = \left(\left[1-\nu^2\right] \right) + \mathcal{O}(\epsilon^2\sigma^0), \tag{2.81}$$

  The solution to the wave equation with this potential is given by a polynomial:

$$g(\rho) = c_1^N \rho^{\nu-1} + c_2^N \rho^{-\nu-1}. \tag{2.82}$$

Matching solutions across the neck To obtain a full solution for the scalar wave, we must glue the different solutions together inside the neck region. We need to match the AdS region solutions $g(\rho)|_{\text{AdS}}$ and the neck solution $g(\rho)|_{\text{neck}}$ at a fiducial radius ρ_A inside the neck, $g(\rho_A)|_{\text{AdS}} = g(\rho_A)|_{\text{neck}}$ and $g'(\rho_A)|_{\text{AdS}} = g'(\rho_A)|_{\text{neck}}$. Similarly, we match the flat space solution to the neck solution at a different fiducial radius ρ_F.

The AdS solutions for large ρ (approaching the neck region), as well as the flat solutions for small ρ, both are of the form (2.82). We can define the following ratio of coefficients in the neck region:

$$\Upsilon_{(\text{region})} \equiv \frac{c_1^{(\text{region})}}{c_2^{(\text{region})}}, \tag{2.83}$$

where (region) is either flat or AdS, and the subscript 1 (resp. 2) denotes the coefficient of the $\rho^{\nu-1}$ (resp. $\rho^{-\nu-1}$) piece (just as in (2.82)).

In general, matching the solutions will be complicated and depend on the matching points ρ_A, ρ_F. However, it turns out that to $\mathcal{O}(\epsilon^2)$, the matching does not depend on ρ_A, ρ_F and is precisely equivalent to simply setting the coefficients $c_i^{(\text{region})}$ equal, which (apart from an overall normalization factor) amounts to the physical condition that the ratios defined above are equal:

$$\Upsilon_{\text{AdS}} = \Upsilon_{\text{flat}} \left(1 + \mathcal{O}(\epsilon^2)\right). \tag{2.84}$$

[8] We do not need to be careful with using Bessel functions of the first *and* second kind since ν is not an integer at $\mathcal{O}(\epsilon^2)$. Thus, I_ν and $I_{-\nu}$ will not be linearly dependent.

Quasinormal mode conditions To find a solution to the scalar wave equation everywhere in the BMPV spacetime, we need to solve the wave equation separately in the flat space and AdS regions and match these solutions across the neck region using (2.84). We will focus on finding the quasinormal modes, which are special solutions to the wave equation where the following two conditions are imposed:

- In the asymptotic flat region, we must demand that there are *no incoming waves from spatial (flat) infinity*: as $\rho \to \infty$, the coeficient of $\exp\left(i\rho\sqrt{\omega^2 - \tilde{m}^2}\right)$ must vanish in the flat space solution.
- In the AdS region, we must demand that there are *no outgoing waves at the horizon*: as $\rho \to 0$, the coefficient of $\exp\left(-i\omega/\rho^2\right)$ must vanish in the AdS solution.

The flat and AdS solutions both have two integration constants each, of which one is fixed by an overall normalization of the wave. The remaining two constants are fixed by the two conditions above. Then, the ratios Υ are given by:

$$\Upsilon_{\text{AdS}} = \frac{(-i\Xi(\omega - \tilde{m}))^{-\nu}\Gamma(\nu)\Gamma\left(\left(\frac{1}{4}(2 - 2\nu - i\frac{\kappa}{\Xi}(\omega + \tilde{m}))\right)\right)}{\Gamma(-\nu)\Gamma\left(\left(\frac{1}{4}(2 + 2\nu - i\frac{\kappa}{\Xi}(\omega + \tilde{m}))\right)\right)}, \tag{2.85}$$

$$\Upsilon_{\text{flat}} = \frac{4^{-\nu}e^{-2i\pi\nu}\nu(\tilde{m}^2 - \omega^2)^{\nu}\Gamma(-\nu)}{\Gamma(1 + \nu)}. \tag{2.86}$$

Thus, the matching condition (2.84) imposes non-trivial constraints on the parameters of the solution, and in particular will only have solutions for particular, quantized value $\omega(\tilde{m}, \ell)$ — the quasinormal modes of the BMPV black hole.

2.3.2 Scalar quasinormal modes in BMPV

As derived in the previous subsection, the condition to have a quasinormal mode scalar solution in the full BMPV black hole is (2.84) such that $\Upsilon_{\text{AdS}} = \Upsilon_{\text{flat}}$ with the ratios given by (2.85)-(2.86). We will now solve this equation to find the quasinormal modes $\omega(\tilde{m}, \ell)$ of the BMPV black hole.

Leading order(s): BTZ quasinormal modes

First, remembering that $\Xi \sim \epsilon^4$ and $\nu = (\ell+1) + \mathcal{O}(\epsilon^2)$, we can see that solutions to (2.84) must be given by $\omega = \tilde{\omega}_n + \delta\tilde{\omega}_n$, where $\tilde{\omega}_n$ is a solution to $\Upsilon_{\text{AdS}}(\tilde{\omega}_n) = 0$, and $\delta\tilde{\omega}_n \sim \mathcal{O}(\epsilon^{4l})$.[9]

Demanding $\Upsilon_{\text{AdS}}(\tilde{\omega}_n) = 0$ can only be achieved by frequencies $\tilde{\omega}_n$ that cause the Γ function in the denominator to have a pole:

$$\tilde{\omega}_n = -\tilde{m} - i4\frac{\Xi}{\kappa}\left(n + \frac{\nu+1}{2}\right) = -\tilde{m} - i4\frac{\sqrt{Q_P}}{R^2}\left(n + 1 + \frac{\ell}{2}\right) + \mathcal{O}(\epsilon^2), \quad (2.87)$$

for $n \geq 0$ integer. At $\mathcal{O}(\epsilon^0)$, these are precisely the quasinormal modes of extremal BTZ with $M = J = 2Q_P/R^2$ and (3D) scalar mass $m_{\text{3D}}^2 = \ell(\ell+2)$ [94, 95] (as should be expected in the strict decoupling limit $\epsilon \to 0$). Using (2.64), we can see that these are indeed low-energy excitations with $\tilde{\omega}_n \sim R_y^{-1}$.

The expression (2.87) are *exact* zeros of Υ_{AdS}, which means the $\mathcal{O}(\epsilon^2)$ and higher order parts of this expression are the correct first corrections to the BTZ quasinormal modes due to the small but non-zero coupling ϵ to flat space; these remain the only ϵ corrections until the subleading corrections from Υ_{flat} contribute as well, which is when we must solve for $\delta\tilde{\omega}_n$.

Subleading corrections from flat space

Since the quasinormal modes (2.87) satisfy $\Upsilon_{\text{AdS}}(\tilde{\omega}_n) = 0$, the correction $\delta\tilde{\omega}_n$ that is necessary to solve (2.84) must be:

$$\Upsilon_{\text{AdS}}(\tilde{\omega}_n + \delta\tilde{\omega}_n) = \Upsilon_{\text{flat}}(\tilde{\omega}_n), \quad (2.88)$$

or, solving for $\delta\tilde{\omega}_n$:

$$\delta\tilde{\omega}_n = \frac{\Upsilon_{\text{flat}}(\tilde{\omega}_n)}{\Upsilon'_{\text{AdS}}(\tilde{\omega}_n)}. \quad (2.89)$$

In $\Upsilon'_{\text{AdS}}(\tilde{\omega}_n)$, the derivative must hit the Γ function in the denominator of (2.85) that is responsible for the vanishing of Υ_{AdS}. This gives:

$$\partial_\omega\left(\left[\Gamma\left(\left(\frac{1}{4}(2+2\nu - i\frac{\kappa}{\Xi}(\omega+\tilde{m})\right)\right)\right]^{-1}\right)_{\omega=\tilde{\omega}_n} = -i(-1)^n n!\frac{\kappa}{4\Xi}. \quad (2.90)$$

[9] One could be worried about $\ell = 0$, as then naively $\tilde{\omega}_n$ and $\delta\tilde{\omega}_n$ would be of the same order. However, a simple calculation shows that the same reasoning holds for $\ell = 0$, and in particular (2.87) and (2.91) are still valid for $\ell = 0$. The reason that the same relations are still valid for $\ell = 0$ is essentially that $\Upsilon'_{\text{AdS}}(\tilde{\omega}_n) \sim \epsilon^{-4\ell-4}$ in (2.89), which means $\delta\tilde{\omega}_n$ in (2.91) is subleading to (2.87), even for $\ell = 0$.

The full expression for the correction (2.89) is then given by:

$$\delta\tilde{\omega}_n = (-1)^{\ell+1}\frac{2^{1-2\ell}}{(\ell!)^3}\binom{\ell+n+1}{\ell+1}\frac{Q_P^{1+\ell/2}R^{2l}}{Q_1+Q_5}\tilde{\omega}_{n,i}^{\ell}(4\tilde{m}^2+\tilde{\omega}_{n,i}^2)^{\ell+1/2} \times (\cos(2\ell+1)\alpha + i\sin(2\ell+1)\alpha)\ , \tag{2.91}$$

where we have written the original solution $\tilde{\omega}_n$ of (2.87) as $\tilde{\omega}_n = -\tilde{m} - i\tilde{\omega}_{n,i}$, and we have defined:

$$\alpha = \tan^{-1}\left(\frac{\tilde{\omega}_{n,i}}{2\tilde{m}}\right). \tag{2.92}$$

The full quasinormal modes of the BMPV black hole are then given by $\tilde{\omega}_n + \delta\tilde{\omega}_n$. The correction $\delta\tilde{\omega}_n$ in (2.91) is clearly a $\mathcal{O}(\epsilon^{4\ell+2})$ correction to $\tilde{\omega}_n$ (analogous to the results in [92]). Both the real and imaginary part of the quasinormal frequencies get a (very) small correction due to the flat space coupling; when $\epsilon \ll 1$, the full BMPV quasinormal modes are thus very well approximated by the BTZ quasinormal modes.

2.3.3 Scalar (quasi)normal modes in BMPV wormhole

Now, we will turn the BMPV black hole into a Solodukhin wormhole by changing the extremal BTZ black hole of the near-horizon (decoupling) geometry into its corresponding Solodukhin wormhole as discussed in section 2.1.2. Note that we will consider the wormhole parameter λ to be much smaller than the decoupling limit parameter ϵ:

$$\lambda \ll \epsilon, \tag{2.93}$$

so that it makes sense to keep only leading pieces in λ while going to higher orders in ϵ, as we do when calculating the quasinormal modes in the flat space geometry. Physically, this also makes sense as one would expect the quantum correction at the horizon (governed by λ) to be much smaller than the non-extremality (controlled by ϵ).

Solutions in the BTZ wormhole

To find the quasinormal modes of the BMPV Solodukhin wormhole, we need to replace the effective decoupling limit extremal BTZ metric in the AdS region by the corresponding extremal wormhole, and solve the scalar wave equation on the wormhole background. The extremal BTZ metric we are considering is given by (3.1) with effective BTZ parameters $R = \kappa^{1/4}$ and $r_+ = r_- = \Xi/\kappa^{1/2}$. (Remember also that the "Schwarzschild" type radial coordinate r used in (3.1) is related to the radial coordinate ρ as $\rho^2 = r^2 - r_+^2$.)

As discussed in section 3.1.3, the general solution $g^{\rm WH}(r)$ to the radial scalar wave equation for the wormhole geometry is given by the corresponding solution to the black hole wave equation, $g^{\rm WH}(r) = g^{\rm BH}(r)$, with the important condition that the wormhole radial solution and its first derivative is continuous at the wormhole throat radius r_t given in (2.21). Moreover, because the wormhole potential is even with respect to the wormhole throat position when written in the tortoise coordinate, $V^{\rm WH}(r_*) = V^{\rm WH}(-r_*)$ (see (2.18)), the normal mode solutions will be either even or odd themselves, which corresponds to the two possible conditions on the BTZ black hole solutions:

$$g_-^{BTZ}(r = r_t) = 0, \qquad \partial_r g_+^{BTZ}(r = r_t) = 0. \tag{2.94}$$

The conditions (2.94) replace the BTZ black hole quasinormal condition that there are no ingoing waves at the horizon. The resulting scalar wave solution, expanded at large ρ (or equivalently r), then gives rise to a new ratio $\Upsilon_{\rm WH}$ (replacing (2.85)), given by:

$$\begin{aligned}\Upsilon_{\rm WH}(\omega) = \Xi^{-\nu} &\frac{(-i(\omega-\tilde{m}))^{-\nu}\Gamma(\nu)\Gamma(1+\nu)\Gamma\left(\frac{1}{4}(2-2\nu-i(M+W))\right)}{\Gamma\left(\frac{1}{4}(2+2\nu-i(M+W))\right)} \\ &\times X_\pm\Bigg[\Gamma(-\nu)\Gamma(1+\nu)X_\pm - (-i(\omega-\tilde{m}))^{i/2(W+M)}\Gamma\left(\frac{1}{4}(2-2\nu-i(M+W))\right) \\ &\times\Gamma\left(\frac{1}{4}(2+2\nu-i(M+W))\right)\Bigg]^{-1},\end{aligned} \tag{2.95}$$

$$\begin{aligned}X_\pm = \left(\frac{\Xi}{\kappa}\right)^{i/2(W+M)} &\Bigg(\mp e^{\frac{-2i(W-M)}{\lambda^2}}\left(\frac{\lambda^2}{2}\right)^{i(W+M)/2} \\ &- ie^{-i/2\pi\nu}(W-M)^{i/2(M+W)}\frac{\Gamma\left(\frac{1}{4}(2+2\nu-i(M+W))\right)}{\Gamma\left(\frac{1}{4}(2+2\nu+i(M+W))\right)}\Bigg),\end{aligned} \tag{2.96}$$

$$M = \frac{\kappa}{\Xi}\tilde{m}, \qquad W = \frac{\kappa}{\Xi}\omega, \tag{2.97}$$

where X_- (resp. X_+) corresponds to the odd (resp. even) modes.

Leading order(s): wormhole normal modes

To find the quasinormal modes of the BMPV wormhole, we now have to solve the altered version of (2.84):

$$\Upsilon_{\rm WH}(\omega) = \Upsilon_{\rm flat}(\omega)\left(1 + \mathcal{O}(\epsilon^2)\right), \tag{2.98}$$

with $\Upsilon_{\rm WH}(\omega)$ given by (2.95) and $\Upsilon_{\rm flat}(\omega)$ still given by (2.86). A similar scaling analysis as equation (2.88) for (2.98) applies, and in particular the leading order solutions to (2.98) are given by $\Upsilon_{\rm WH}(\omega_n) = 0$. This is equivalent to demanding $X_\pm = 0$.[10]

This transcendental equation cannot be analytically solved in general. In the large ω limit, we find the approximate solutions:

$$\omega_n = \tilde{m} + \left(n + \ell + \frac{1}{2}\right)\frac{\pi}{L_\lambda} + \mathcal{O}(L_\lambda^{-2}, \tilde{m}L_\lambda^{-1}\log L_\lambda), \tag{2.99}$$

where we used (2.11), where n is an integer (to $\mathcal{O}(\epsilon^2)$); when n is even (resp. odd), the normal mode corresponds to an even (resp. odd) mode obtained by $X_+ = 0$ (resp. $X_- = 0$). These high frequency normal modes (up to the $\mathcal{O}(\tilde{m}L_\lambda^{-1}\log L_\lambda)$ term) agree with what we found before in (2.52) with the substitution[11] $k \to mR/R_y = \tilde{m}R$.

We can also solve (2.98) in a low-frequency limit $\omega - \tilde{m} \sim L_\lambda^{-1}$:

$$\omega_n = \tilde{m} + \left(n + \frac{\ell}{2}\right)\frac{\pi}{L_\lambda} + \mathcal{O}(\tilde{m}L_\lambda^{-1}), \tag{2.100}$$

where n even (resp. odd) corresponds to the odd (resp. even) mode obtained by $X_- = 0$ (resp. $X_+ = 0$).

Subleading corrections from flat space

Now, we can calculate the corrections to the modes due to the coupling to flat space. We need to calculate $\Upsilon'_{\rm AdS}(\omega_n)$; this derivative must hit the $X_\pm$ in the numerator. Even though we do not have an analytic expression for the modes ω_n, we can still simplify the resulting derivative and write the expression for the correction $\delta\omega_n$ explicitly in terms of ω_n. The leading real and imaginary

[10] Although the quasinormal modes $\tilde{\omega}_n$ in (2.87) of the BTZ black hole also satisfy $\Upsilon_{\rm WH} = 0$, these will not correspond to actual (quasi)normal modes of the wormhole, as a complete analysis of the allowed solutions in the wormhole would reveal.

[11] This substitution is necessary since y in (2.65) is periodic with $2\pi R_y$ and φ is periodic with 2π.

parts of $\delta\omega_n$ are then:

$$\begin{aligned}\delta\omega_n &= \frac{\Upsilon_{\text{flat}}(\omega_n)}{\Upsilon'_{\text{WH}}(\omega_n)} \\ &= -\frac{1}{L_\lambda}\left(R^{2\ell+2}Q_P^{(1+\ell)/2}\right)\frac{(\omega_n^2-\tilde{m}^2)^\ell(\omega_n-\tilde{m})^{\ell+1}}{2^{2\ell+1}\ell!^3(\ell+1)!}\left|\Gamma\left(1+\frac{\ell}{2}+\frac{i}{4}(M+W_n)\right)\right|^2 \\ &\times e^{\pi/4(M+W_n)}\left(\frac{1}{Q_1+Q_5}+i\frac{\pi}{2}\frac{\omega_n^2-\tilde{m}^2}{\ell+1}\right). \qquad (2.101)\end{aligned}$$

The real part is a correction to the quasinormal frequency at order $\mathcal{O}(\epsilon^{4\ell+2})$ (as it was for the BMPV black hole frequencies in section 2.3.2) whereas the imaginary part enters at $\mathcal{O}(\epsilon^{4\ell+4})$ (similar to [92]). Of course, the correction to the real part is small compared to the original (real) normal mode ω_n. Note that[12] $\text{Im}(\delta\omega_n) < 0$, as appropriate for a decaying mode.

2.3.4 Interpretation

In this section, we calculated the quasinormal modes for the BMPV black hole, as well as for the Solodukhin wormhole modification of BMPV. For both examples, we solved the wave equation in the near-decoupling limit (with small decoupling parameter ϵ), and found that near-horizon, asymptotic AdS (decoupling) region gives the most important contribution to the quasinormal modes. As we will discuss in the next section 2.4, the quasinormal modes of a system determine the analytic structure of the relevant response function; thus, they capture the physics of the reflection and transmission coefficients as well as the entire correlator.

For the BMPV black hole, the (small) coupling to flat space provides a small correction to both the real and imaginary parts which is subleading in ϵ. For the BMPV wormhole, the key difference is that the wormhole itself has only non-decaying normal modes, and the imaginary part of the full quasinormal mode is thus entirely due to the (small) coupling to flat space. Physically, this coupling to flat space allows the scalar wave to "leak out" at (flat) infinity instead of being trapped in the asymptotically AdS wormhole "box" forever (see figure 2.4). Thus, the "echoes" that a scalar field in the asymptotically flat BMPV black hole will have are determined by the real part of the quasinormal modes and hence by the behaviour of the scalar field in the AdS spacetime. The small coupling to flat space and the resulting small imaginary part of the

[12] Although we do not show it explicitly, we have $\omega \geq \tilde{m}$ for all normal modes of the wormhole.

quasinormal mode simply gives a small attenuation of the echo amplitude over time; this attenuation is directly determined by the travel time down the BTZ throat $2L_\lambda$. So, we can conclude that the relation between the behaviour of the scalar field signal (in position space) in the BMPV black hole and BMPV wormhole is captured by the relation between the BTZ black hole and BTZ wormhole behaviors of the scalar field, and thus by the holographic correlators for those solutions that we studied in section 3.3.

From the CFT perspective, the normal modes of the wormhole correspond to the poles of the scalar two-point correlator. The "leaking" into flat space can be thought of as the result of perturbing the CFT with an irrelevant deformation [13] which changes the UV and thus also perturbes the scalar correlator. As long as the irrelevant deformation is small (as it is here, controlled by $\epsilon \ll 1$), the deformation can be treated perturbatively in the CFT [14].

Note that the imaginary part of the quasinormal frequencies is parametrically small compared to the real part. As we saw above in (2.101), the imaginary part of the quasinormal modes is $\mathcal{O}(\epsilon^{4\ell+4}\lambda^2)$: it is both small due to the small part of the scalar wave escaping to infinity (the ϵ dependence), as well as parametrically small in the wormhole parameter λ.

The resulting system of quasinormal frequencies for the BMPV wormhole is reminiscent of other flat space Solodukhin type wormholes [71, 29]. In particular, we can compare the scaling of real and imaginary parts of the quasinormal modes with the analysis of sec 4.1 in [83] for the quasinormal modes of general wormholes (or other "cavity" potentials) in (4D) flat space. Defining $\hat{\omega}_n = \omega_n - \tilde{m}$, we see that:

$$\hat{\omega}_n \sim \frac{1}{L_\lambda}. \tag{2.102}$$

The real part of the quasinormal mode scales as the inverse "cavity size" (in tortoise coordinates). Moreover, we can also see from (2.101) that the imaginary part scales as:

$$\mathrm{Im}(\delta\omega_n) \sim \frac{1}{L_\lambda}\hat{\omega}^{2\ell+2} \sim \hat{\omega}^{2\ell+3}, \tag{2.103}$$

in precise agreement with the scaling found in eq. (34) of [83]. This scaling of the imaginary part of the mode can be understood as the product of the tunneling amplitude $|\mathcal{A}|^2 \sim \hat{\omega}_n^{2\ell+2}$ of the wave [197] to reach outside the cavity, with the timescale $\Delta t \sim L_\lambda^{-1}$ needed for the wave to travel once through the cavity of length L_λ [83]. Note that the general scaling (2.103) also holds in the asymptotically flat microstate geometries considered in [36]; there, the "cavity size" is determined by the (large) redshift down the microstate throat, $n_1 n_5/j_L$.

2.4 Relation to echo literature in flat space

In this section, we make the connection to wave scattering in flat space. To keep the discussion general, we now consider the Schrödinger problem with source $S(x, \omega)$:

$$\frac{d^2\psi(x)}{dx^2} - V(x)\psi(x) = S(x, \omega)\,, \tag{2.104}$$

where V is a potential and S is a source. This equation can describe, for example, the scattering problem of a gravitational wave in Fourier space (where x is the tortoise coordinate); or it can be used to find quasinormal modes when the source vanishes.

We will recall first how to obtain the solution with a source $S(x)$ in flat space and what the precise relation is to the quasinormal modes and echoes, and then proceed to generalize the discussion to include AdS correlators and quasinormal modes discussed above.

Although we focus on four-dimensional black holes in section 2.4.1, the results apply to general spacetime dimensions d, unless specified otherwise. In different dimensions, the form of the potential may change, but its asymptotic behaviour remains similar.

2.4.1 Waves in flat space

This section is based on the discussion of [160], and follows conventions of [83]. For more details, we refer to those references. For the scattering problem with a rotating black hole in four dimensions, the potential asymptotically approaches a negative constant, and all derivatives are zero at the asymptotic boundaries:

$$\lim_{x\to\infty} V(x) = -\omega^2\,, \qquad \lim_{x\to-\infty} V(x) = -(\omega - \omega_0)^2\,. \tag{2.105}$$

In the above equation, ω is the frequency of the particular mode and ω_0 a constant depending on the spin of the black hole. The potential has a maximum at the position of the light-ring, the location of the unstable photon orbit (for Schwarzschild in usual radial coordinates, this is at $r = 3M$). We give a schematic representation in figure 2.5a; for the detailed form of potentials depending on the spin of the perturbation, see [212, 56].

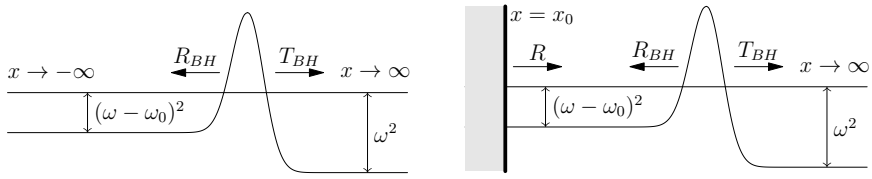


Figure 2.5: (a) A schematic plot of the radial potential of a rotating black hole with flat asymptotics. Asymptotic infinity is at $x \to \infty$, the horizon at $x \to -\infty$, and the bump is associated with the light-ring; (b) A schematic plot of the radial potential of a rotating ECO with flat asymptotics. Asymptotic infinity is at $x \to \infty$, and at large negative x_0 we put a wall which has arbitrarily complicated behaviour captured by the function $R(\omega, x_0)$.

The wave equation has two homogeneous independent solutions, which we can choose to have the following asymptotic behaviour:

$$\begin{aligned} &\text{ingoing at hor.:} \quad \psi_- \sim \begin{cases} e^{-i(\omega-\omega_0)x}\,, \\ A_{\rm in}(\omega)e^{-i\omega x} + A_{\rm out}(\omega)e^{i\omega x}\,, \end{cases} \\ &\text{outgoing at } \infty\text{:} \quad \psi_+ \sim \begin{cases} B_{\rm in}(\omega)e^{-i(\omega-\omega_0)x} + B_{\rm out}(\omega)e^{i(\omega-\omega_0)x}\,, \\ e^{i\omega x}\,, \end{cases} \end{aligned} \tag{2.106}$$

where the top entries are at $x \to -\infty$ and the bottom ones at $x \to \infty$. One can find the transmission and reflection coefficients for waves coming in from infinity and scattering off the potential. It is most convenient for the current discussion to define those coefficients for waves coming from the left, see figure 2.5a,

$$R_{\rm BH}(\omega) = \frac{B_{\rm in}(\omega)}{B_{\rm out}(\omega)}\,, \qquad T_{\rm BH}(\omega) = \frac{1}{B_{\rm out}(\omega)}\,. \tag{2.107}$$

The physical solution to the wave equation is composed only of ingoing waves at the horizon and outgoing waves at infinity

$$\psi_{\rm BH} \sim \begin{cases} e^{-i(\omega-\omega_0)x}, & x \to -\infty \\ e^{i\omega x}, & x \to +\infty. \end{cases} \tag{2.108}$$

The black hole Green's function solves the wave equation with source $S = \delta(x - x')$ and obeys the boundary conditions (2.108):

$$G_{\rm BH}(x, x') = \frac{\psi_+(\max(x, x'))\psi_-(\min(x, x'))}{W(\omega)}, \tag{2.109}$$

where $W(\omega) = \psi_- \psi'_+ - \psi_+ \psi'_-$ is the Wronskian. For this simple second order differential equation, the Wronskian is a constant and can be evaluated at infinity: $W(\omega) = 2i\omega A_{\rm in}(\omega)$. The solution to the full wave equation is then

$$\psi_{\rm BH} = \psi_+ \int_{-\infty}^{x} \frac{S\psi_-}{W} + \psi_- \int_{x}^{\infty} \frac{S\psi_+}{W} \,. \tag{2.110}$$

The frequencies of the QNMs, the solutions for $S = 0$, are determined by the poles of the Green's function, or alternatively: the zeroes of the Wronskian $W(\omega_n) = 0$. Note that these are also precisely the frequencies for which ψ_+ and ψ_- are linearly dependent.

Now imagine that we have an exotic compact object (ECO), whose potential agrees very well with the black hole potential up until some very large negative Schrödinger coordinate $x_0 \ll 0$, which is assumed to be located somewhere in the flat region of the potential, away from any possible light-ring structure. For $x < x_0$ the potential starts to significantly deviate from the black hole potential. One can model this behaviour by putting some generic ω-dependent effective reflective boundary condition at x_0, see figure 2.5b. This changes the boundary condition for a purely outgoing mode at infinity to

$$\psi_{\rm ECO} \sim \begin{cases} e^{-i(\omega-\omega_0)x} + R(\omega, x_0) e^{i(\omega-\omega_0)x}, & x \to x_0 \\ e^{i\omega x}, & x \to \infty, \end{cases} \tag{2.111}$$

where the reflection coefficient $R(\omega, x_0)$ is determined by the details of the ECO model. Note that we follow [76] and have absorbed a factor of $e^{2i\omega x_0}$ into R with respect to [160].

We can write

$$\psi_{\rm ECO} = \psi_{\rm BH} + \psi_{\rm H} \,, \tag{2.112}$$

with $\psi_{\rm H}$ a homogenous solution such that $\psi_{\rm ECO}$ obeys the boundary conditions (2.111). This means that $\psi_{\rm H} = A(\omega, x_0)\psi_+$ for some function A. Following [160], we take a judicious choice of multiplication constant for later comparison with the black hole solution as $A(\omega, x_0) = \mathcal{K}(\omega, x_0) \int_{-\infty}^{\infty} \frac{S\psi_+}{W} dx$:

$$\psi_{\rm H} = \mathcal{K}\psi_+ \int_{-\infty}^{\infty} \frac{S\psi_+}{W}, \tag{2.113}$$

where $\mathcal{K}(\omega, x_0)$ is a constant called the 'transfer function' As $x \to x_0$, we have $\psi_{\rm BH} = \psi_+ \int_{x_0}^{\infty} \frac{S\psi_+}{W}$ and $\psi_{\rm H} = \mathcal{K}\psi_+ \int_{x_0}^{\infty} \frac{S\psi_+}{W}$, so that at large negative x we find

$$\begin{aligned} \psi_{\rm ECO} = &\left(e^{-i(\omega-\omega_0)x} + \mathcal{K}(\omega, x_0)(B_{\rm in}(\omega) e^{-i(\omega-\omega_0)x} + B_{\rm out}(\omega) e^{i(\omega-\omega_0)x}) \right) \\ &\times \int_{x_0}^{\infty} \frac{S\psi_+}{W} dx, \end{aligned} \tag{2.114}$$

Comparing with (2.111) gives:

$$\mathcal{K}(\omega) = \frac{T_{\rm BH}(\omega)R(\omega, x_0)}{1 - R_{\rm BH}(\omega)R(\omega, x_0)}\,. \tag{2.115}$$

At large distances, relevant to a detector, the wave function has the form

$$\psi_{\rm ECO}(\infty) = \psi_{\rm BH}(\infty) + \mathcal{K}(\omega, x_0)e^{i(\omega+(\omega-\omega_0))x}\psi_{\rm BH}(-\infty)\,, \tag{2.116}$$

hence the response of the ECO corresponds to the initial BH response, followed by an additional term that is determined by the reflectivity of the compact object. It is this second term that can be written as a train of echoes following the main signal, from the geometric series expansion:

$$\mathcal{K}(\omega, x_0) = T_{\rm BH}(\omega)R(\omega, x_0)\sum_{n=1}^{\infty}(R_{\rm BH}(\omega)R(\omega, x_0))^{n-1}. \tag{2.117}$$

The ECO QNM frequencies ω_n are the poles of $\mathcal{K}$, or equivalently:

$$1 - R_{\rm BH}(\omega_n)R(\omega_n, x_0) = 0, \tag{2.118}$$

If we consider the simple example of a (possibly partially reflective) ω-independent "brick wall" located at x_0 and assume a slowly varying $R_{\rm BH}(\omega)$, we have

$$R_{\rm BH}(\omega) \approx R_{BH}, \qquad R(\omega, x_0) = Re^{-2i(\omega-\omega_0)x_0}. \tag{2.119}$$

In this case, the asymptotic detector receives the initial signal from the ECO which decays very similarly to the black hole; then, after a time $\Delta t = 2x_0$, a series of echoes follows. The QNM frequencies are approximately

$$\omega_n = \omega_0 + \frac{\pi}{x_0}\left(n + \frac{i}{2\pi}\ln(R_{\rm BH}R)\right) + \mathcal{O}\left(\frac{\pi n/x_0}{R_{\rm BH}(\omega_n)/R'_{\rm BH}(\omega_n)}\right), \tag{2.120}$$

where $n = 0, 1, 2, \ldots$. The relation to Green's function, and in particular how a very similar (early-time) behaviour in the ECO and black hole backgrounds nevertheless is associated with vastly different QNM spectrums, was worked out in [140].

2.4.2 Waves in AdS

Changing the asymptotics from flat space to AdS does not change the Schrödinger form of the wave equation (2.104). We choose $x \to \infty$ to correspond

to the asymptotic AdS boundary and $x \to -\infty$ to the horizon. For scattering problems in black hole backgrounds in AdS, the potential asymptotically approaches a positive constant at the AdS boundary and a negative constant near the horizon:[13]

$$\lim_{x\to\infty} V(x) = \tilde{\mu}^2\,, \qquad \lim_{x\to-\infty} V(x) \to -\omega^2\,, \tag{2.121}$$

and all derivatives are zero at the asymptotic boundary. For simplicity, here we are taking non-rotating black holes (or ECOs) in AdS. Then, the potential asymptotes to the frequency of the mode ω at $x \to -\infty$. The potential for a non-rotating AdS black hole is schematically depicted in figure 2.6a.

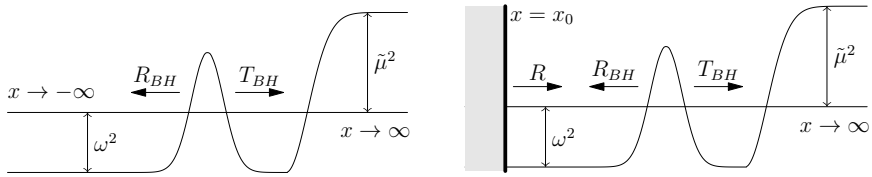


Figure 2.6: (a) A schematic plot of the radial potential for a non-rotating black hole with AdS asymptotics. The boundary is at $x \to \infty$, the horizon at $x \to -\infty$. The bump is, similarily to flat space, associated with the light-ring; (b) A schematic plot of the radial potential of a non-rotating ECO with AdS asymptotics. The boundary is at $x \to \infty$, and at large negative x_0 we put a wall which has arbitrarily complicated behaviour captured by the function $R(\omega, x_0)$.

For easy comparison to [41] we take the two independent solutions to be:

$$\begin{aligned}
\psi^{\text{grow}} &\sim \begin{cases} B_{\text{in}}^{\text{grow}}(\omega)e^{-i\omega x} + B_{\text{out}}^{\text{grow}}(\omega)e^{i\omega x}, & x \to -\infty \\ e^{\tilde{\mu}x}, & x \to \infty, \end{cases} \\
\psi^{\text{dec}} &\sim \begin{cases} B_{\text{in}}^{\text{dec}}(\omega)e^{-i\omega x} + B_{\text{out}}^{\text{dec}}(\omega)e^{i\omega x}, & x \to -\infty \\ e^{-\tilde{\mu}x}, & x \to \infty. \end{cases}
\end{aligned} \tag{2.122}$$

What is important to realize is that, although the boundary conditions (2.122) are analogous to the flat space case (2.106), what is different in AdS is that the $x \to \infty$ boundary conditions imposed in (2.122) immediately imply that $\psi^{\text{dec}}, \psi^{\text{grow}}$ are *real*[14] for all x. In particular, we have:

$$B_{\text{in}}^{\text{grow}} = (B_{\text{out}}^{\text{grow}})^*\,, \qquad B_{\text{in}}^{\text{dec}} = \left(B_{\text{out}}^{\text{dec}}\right)^*. \tag{2.123}$$

[13]For example, we can use a (rescaled) version of the WKB coordinates defined in section 3.3 for the BTZ black hole. Then we have $\tilde{\mu}^2 = (r_+^2/R^4)\mu^2$.

[14]This follows because the real and imaginary parts of the solution must each satisfy the same Schrödinger equation as long as the potential $V(x)$ is real.

For AdS spacetimes, we will not introduce a bulk source $S(x,\omega)$; however, as we will see below, the presence of the growing mode is interpreted as a holographic source on the boundary using the AdS/CFT dictionary. We first discuss the QNMs. The appropriate boundary conditions for black hole QNMs are

$$\psi_{\rm BH}^{\text{non-sourced}} \sim \begin{cases} e^{-i\omega x}, & x \to -\infty \\ e^{-\tilde{\mu} x}, & x \to +\infty. \end{cases} \tag{2.124}$$

From the decaying mode, we can again define reflection and transmission coefficients, for waves coming from the left, see figure 2.6a,

$$R_{\rm BH}(\omega) = \frac{B_{\rm in}^{\rm dec}(\omega)}{B_{\rm out}^{\rm dec}(\omega)}, \qquad T_{\rm BH}(\omega) = \frac{1}{B_{\rm out}^{\rm dec}(\omega)}. \tag{2.125}$$

The frequencies of the black hole QNMs are then precisely given by the poles of $R_{\rm BH}(\omega)$. Note that from (2.123), it follows that:

$$|R_{\rm BH}| = 1, \qquad T_{\rm BH} = |T_{\rm BH}|(R_{\rm BH})^{1/2}, \tag{2.126}$$

A solution at a generic frequency will include the growing mode (see (2.22)):

$$\psi_{\rm BH}^{\rm sourced} = \beta_{\rm BH}(\omega)\psi^{\rm grow} + \alpha_{\rm BH}(\omega)\psi^{\rm dec}, \qquad \beta_{\rm BH} B_{\rm out}^{\rm grow} + \alpha_{\rm BH} B_{\rm out}^{\rm dec} = 0, \tag{2.127}$$

where the condition on the coefficients is there to ensure only ingoing modes at the horizon. The coefficient $\beta_{\rm BH}$ is proportional to the holographic source of the CFT boundary operator, and $\alpha_{\rm BH}$ is proportional to the vacuum expectation value of the boundary operator. The holographic CFT (retarded) two-point function for this boundary scalar operator is then given by:

$$\mathcal{R}_{\rm BH}(\omega) = \frac{\alpha_{\rm BH}(\omega)}{\beta_{\rm BH}(\omega)} = -T_{\rm BH}(\omega) B_{\rm out}^{\rm grow}(\omega)\,. \tag{2.128}$$

If we now take an ECO, generically the solution will instead be (valid for all x):

$$\psi_{\rm ECO}^{\rm sourced} = \beta_{\rm ECO}(\omega)\psi^{\rm grow} + \alpha_{\rm ECO}(\omega)\psi^{\rm dec}. \tag{2.129}$$

Just like in flat space, we can assume that the potential of the ECO is described by the black hole one up until a point $x_0 \ll 0$, deep in the IR, where it starts to deviate significantly. We can again model this as an ω-dependent reflection at large negative x_0, see figure 2.6b. This changes the IR boundary conditions as

$$\psi_{\rm ECO}^{\rm sourced} \sim \begin{cases} e^{-i\omega x} + R(\omega, x_0) e^{i\omega x}, & x \to x_0 \\ \beta_{\rm ECO}(\omega)\psi^{\rm grow} + \alpha_{\rm ECO}(\omega)\psi^{\rm dec}, & x \to \infty. \end{cases} \tag{2.130}$$

Since (2.129) is valid everywhere, the boundary conditions (2.130) give the relation:

$$\frac{\beta_{\rm ECO}(\omega)B^{\rm grow}_{\rm out}(\omega)+\alpha_{\rm ECO}(\omega)B^{\rm dec}_{\rm out}(\omega)}{\beta_{\rm ECO}(\omega)B^{\rm grow}_{\rm in}(\omega)+\alpha_{\rm ECO}(\omega)B^{\rm dec}_{\rm in}(\omega)}=R(\omega,x_0)\,. \tag{2.131}$$

Finally, the two-point function of the ECO is given by

$$\mathcal{R}_{\rm ECO}(\omega)=\frac{\alpha_{\rm ECO}(\omega)}{\beta_{\rm ECO}(\omega)}=\mathcal{R}_{\rm BH}(\omega) + \mathcal{K}(\omega,x_0)[B^{\rm grow}_{\rm in}(\omega)-R_{\rm BH}(\omega)B^{\rm grow}_{\rm out}(\omega)], \tag{2.132}$$

where

$$\mathcal{K}(\omega,x_0)=\frac{T_{\rm BH}(\omega)R(\omega,x_0)}{1-R_{\rm BH}(\omega)R(\omega,x_0)}\,. \tag{2.133}$$

Using (2.123), (2.126), and (2.128), we can further simplify (2.132) to

$$\mathcal{R}_{\rm ECO}(\omega)\;=\mathrm{Re}(\mathcal{R}_{\rm BH}(\omega))+i\left(\frac{1+R_{\rm BH}R}{1-R_{\rm BH}R}\right)\mathrm{Im}(\mathcal{R}_{\rm BH}(\omega)). \tag{2.134}$$

At this point a natural question arises: How do we compare (2.134) to hybrid WKB expression for the propagator (3.89)? We address this question in the next section.

2.4.3 Comparison to hybrid WKB

AdS asymptotics differ from flat asymptotics in that the scalar wave does not "leak" out at infinity. This means that a scalar wave in a spacetime without a horizon (or other absorbing boundary conditions) only admits normal (real) modes instead of quasinormal modes (that have a finite imaginary part). The scalar wave will explore the inner structure of the ECO (which can be arbitrarily complicated, and take arbitrarily long), but will always end up being reflected out.

Since there is no dissipation and we have only normal modes ω_n, we can assume the correlator $\mathcal{R}_{\rm ECO}(\omega)$ is real for real ω. From (2.134) and using (2.126), it is easy to see that this is equivalent to the condition $|R|=1$. It is then convenient to define the black hole phase $e^{i\theta_{\rm BH}}$ and the ECO phase $\theta_{\rm ECO}$ as:

$$R_{\rm BH}\equiv e^{i\theta_{\rm BH}},\qquad R\equiv e^{i\theta_{\rm ECO}}, \tag{2.135}$$

as then (2.134) becomes simply:

$$\mathcal{R}_{\rm ECO}(\omega)\;=\mathrm{Re}(\mathcal{R}_{\rm BH}(\omega))-\cot\left(\frac{\theta_{\rm BH}+\theta_{\rm ECO}}{2}\right)\mathrm{Im}(\mathcal{R}_{\rm BH}(\omega)). \tag{2.136}$$

We can further assume that the potential $V(x)$ has two turning points $x_\pm$ where $V(x_\pm) = 0$ — for example, this is the case for the wormhole we discuss in section 2.2.3,[15] and for the actual microstate geometries discussed in [41]. Then, comparing (2.136) to the propagator (3.89) of the hybrid WKB method propagator as in section 2.2.3 or [41], we arrive at the relation:

$$\theta_{\rm ECO} = \pi - \theta_{\rm BH} + 2\Theta = \pi - \theta_{\rm BH} + 2\int_{x_-}^{x_+} \sqrt{|V(z)|}\,{\rm d}z\,. \tag{2.137}$$

If we model the behaviour of the ECO as a "brick wall" with total reflection at a radius $x = x_0$, we take $R(\omega, x_0) = -e^{-2i\omega x_0}$ so that $\theta_{\rm ECO} = \pi - 2\omega x_0$. Moreover, for the non-rotating Solodukhin wormhole (in analogy with (2.51)), we would have approximately $\Theta \approx \omega L_\lambda$, so that:

$$x_0 = -L_\lambda + \frac{\theta_{\rm BH}}{2\omega}, \tag{2.138}$$

For ω and L_λ large, the second term goes as $\mathcal{O}(\omega^0, L_\lambda^0)$ for the non-rotating BTZ black hole, and so $x_0 \approx -L_\lambda$ is the position at which we would need to put the totally reflective wall in order to model the behaviour of the Solodukhin wormhole.

2.5 Discussion

2.5.1 Where are the quantum corrections?

Here, by using the travel time down a microstate throat [41], we argue that the origin of quantum corrections to the black hole can be interpreted as sitting exponentially close to the horizon, both in terms of the Planck length and in terms of the black hole entropy. Second, we can perform an ensemble average over wormhole geometries that reveals how the echo amplitude generically gets exponentially suppressed in a typical state, and how it follows that the Poincaré recurrence time is doubly-exponential in the entropy.

If we imagine or model a black hole microstate (geometry) as (quantum) corrections around the black hole horizon, one can then wonder *where* these quantum corrections are located with respect to the horizon. Is the geometry

[15] Note that both the wormhole of section 2.2.3 as well as the microstate geometries in [41] have extremally rotating BTZ asymptotics, whereas in section 2.4.2 and 2.4.3 we are only considering non-rotating AdS asymptotics. The hybrid WKB analysis can also be performed for the non-rotating Solodukhin wormhole, with approximate result $\Theta \approx |\omega| L_\lambda$, see next chapter.

made up out of seeming perturbative corrections within a Planck distance from the horizon? For the wormhole toy model (3.4), this would mean that $\lambda \propto \ell_P/L$, with ℓ_P the Planck length. Or, alternatively, are the corrections exponentially suppressed near the horizon, such that $\lambda \propto \exp(-L/\ell_P)$ for some reference length L? We could equivalently formulate this distinction as corrections that are perturbative or non-perturbative in the black hole entropy S. Here, we will first make a connection to recent 4D gravity literature and then answer this question by combining our wormhole analysis with results from recent microstate literature.

Intuition in four-dimensional asymptotically flat space To quantify how compact objects (such as microstate geometries) differ from a black hole, one can define a 'closeness parameter' ε, as suggested in [83]. For example, for a very crude model of a spherically symmetric reflective surface at a location r_0, a natural choice for this parameter is given by $r_0 = r_S(1+\varepsilon)$ with r_S the Schwarzschild radius $r_S = 2M$. One recovers the black hole metric in the limit $\varepsilon \to 0$. For more sophisticated objects than simple reflecting surfaces, one can often still determine a location of r_0 of the "horizon structure" or corrections based on natural criteria, such as a location where the Kretschmann scalar is noticably different, or the radius beyond which most of the mass is concentrated (for boson star configurations), or some other criteria of distance or location. For reference, we can rewrite the definition of the closeness parameter ε for a Schwarzschild black hole as:

$$\varepsilon \approx 1.4 \times 10^{-39} \left(\frac{r_0 - r_S}{\ell_P}\right) \left(\frac{M_\odot}{M}\right) . \tag{2.139}$$

We see that $\varepsilon \sim 10^{-39}$ corresponds to a coordinate distance of a Planck length from the horizon for a solar mass black hole. For our wormholes, the role of closeness parameter is essentially played by λ.

By quantifying models in terms of ε, we can introduce a notion of "distance" of the structure to the event horizon. Other notions of distance can also be considered instead:

- The parameter $\varepsilon = (r_0 - r_S)/r_S$, the relative coordinate distance of the corrections.
- The proper distance Δs of the corrections from the horizon.
- The (minimal) value of the redshift factor $\sqrt{|g_{tt}|}$, at the location of the corrections.
- The travel time Δt as seen by an asymptotic observer of a light ray from, say, the light ring to the location of the corrections.

For simple structures that are being compared to the four-dimensional Schwarzschild metric, we can easily see that these measures are all equivalent, as pointed out in [83]. The proper distance is related to ε as:

$$\Delta s \equiv \int_{r_S}^{r_S(1+\varepsilon)} \sqrt{g_{rr}} dr \approx 2\sqrt{\varepsilon} r_S, \quad \text{or} \quad \varepsilon \approx 2.1 \times 10^{-78} \left(\frac{\Delta s}{\ell_P}\right) \left(\frac{M_\odot}{M}\right). \tag{2.140}$$

The redshift that corresponds to it is

$$\sqrt{|g_{tt}|} \approx \varepsilon^{1/2} \tag{2.141}$$

and the travel time from the light ring ($r = 3r_S/2$) to the structure is

$$\Delta t = M(1 - 2\varepsilon - \log(4\varepsilon^2)) \approx -2M \log \varepsilon. \tag{2.142}$$

However, for a wormhole, or a microstate geometry, some of the above notions may not be related or even well-defined, and so cannot be used to define or determine r_0. First of all, such an object has no interior, and one can only make observations from the outside. This makes it impossible to have a simple notion of coordinate distance r_0 or proper distance from the would-be horizon. Second, microstate geometries are known to have ergosurfaces, aka a surface where an asymptotically timelike Killing vector K becomes null. Past this surface the Killing vector becomes spacelike $K^\mu K_\mu > 0$ and that region of the spacetime defines the ergoregion. When $K = \partial_t$ the ergosurface is equivalently defined as the surface where $g_{tt} = 0$. The ergosurface of microstate geometries and rotating black holes are located at different locations, so keeping minimal redshift $\sqrt{|g_{tt}|}$ as the notion of the location of the structure could easily give the wrong idea.

For such geometries, then, we will use the travel time as measured by an asymptotic observer as a well-defined notion to quantify the deviation from the black hole metric. Such an approach has partly been followed already in [47] where the travel time was directly related to the mass gap (the energy of the lowest excitation in the throat) and is thus directly related to redshift at the 'cap', where the black hole-like throat smoothly ends.

Perturbative or non-perturbative? We follow an approach based on the equivalences mentioned for four-dimensional solutions. In particular, we compare the travel time in wormholes and microstate geometries with the time in the corresponding BTZ metric to travel from the asymptotic boundary to a location r_0 and back. This allows us to determine, in terms of the wormhole or microstate geometry parameters, the fictional radius r_0 where we would naively have to put reflecting boundary conditions in the black hole geometry to mimick the

microstructure — and hence, give an indication of the "location" of quantum corrections to the BTZ geometry as coming from our wormhole or microstate geometries.

There are two caveats we wish to highlight with this approach if one wishes to apply it more generally. First, getting the travel time from a wave equation or geodesic equation is technically possible for a simple, integrable model such as our wormhole geometries, or the separable superstrata solutions considered in [41, 46]. However, a more typical microstate geometry will not have a separable wave equation or geodesic equation. Due to mixing between radial and angular modes, it becomes harder to find or calculate a unique, well-defined infalling travel time. Thus, the location of the would-be radius r_0 one could derive in this setup would be at best an upper bound. The second caveat is that the travel time (for example, as measured by the time between echoes) is only a crude measure of microstructure and might miss other interesting structures in the black hole throat, such as the tidal stresses or curvature effects that have been advocated to play a role at smaller timescales than the travel time, i.e. $t_{\text{tidal}} \ll \Delta t$, see for example [205, 41, 44].

Relating λ to r_0 for wormholes First, we can discuss the Solodukhin wormhole as an example of where we can apply the above reasoning; this was already partly analyzed in [195]. We focus here on the general non-extremal BTZ black hole and its corresponding wormhole for generality, taking $r_+ > r_- \geq 0$.

For a radially infalling null geodesic in the BTZ metric, the travel time from the boundary to a location r_0 and back to the boundary is given by:[16]

$$\Delta t_{\text{BTZ}} = \frac{2R^2}{r_+^2 - r_-^2}\left(r_+ \tanh^{-1}\left(\frac{r_+}{r_0}\right) - r_- \tanh^{-1}\left(\frac{r_-}{r_0}\right)\right). \tag{2.143}$$

When $\varepsilon = \frac{r_0 - r_+}{r_+} \ll 1$, this becomes:

$$\Delta t_{\text{BTZ}} = \frac{r_+ R^2}{r_+^2 - r_-^2} \log\frac{2}{\varepsilon} + O(\varepsilon^0). \tag{2.144}$$

We need to compare this to the travel time in our wormhole toy model. The time it takes for a signal to travel from the boundary through the wormhole and come back to the boundary is (to leading order in λ) twice the throat

[16] Radially infalling means we take $L_\phi = \frac{d\phi}{d\tilde{\lambda}} + N_\phi \frac{dt}{d\tilde{\lambda}} = 0$, where $\tilde{\lambda}$ is an affine parameter along the geodesic. The travel time is then defined as $\Delta t = 2\int_{r_0}^{\infty} \frac{dt}{dr} dr = 2\int X^{-1} dr$. The proper distance from the horizon is defined as $\Delta s = \int_{r_+}^{r_0} X^{-1/2} dr$.

length: $\Delta t_{\rm WH} = 2L_\lambda$. An analogous computation of the travel time for the non-extremal rotating wormhole of sections 2.1.2 and 2.1.2 [17] gives:

$$L_\lambda = \frac{r_+ R^2}{r_+^2 - r_-^2} \log \frac{16}{\lambda^2}. \tag{2.145}$$

Then, equating $\Delta t_{\rm BTZ} = 2L_\lambda$, we find a relation between λ and ε:

$$\varepsilon = \frac{\lambda^4}{128} \ . \tag{2.146}$$

For a more coordinate invariant notion of distance, one can evaluate the proper distance Δs between $r = r_+(1+\varepsilon)$ and the horizon. This quantity is related to ε as

$$\Delta s = \frac{r_+ R}{2} \sqrt{\frac{2\varepsilon}{r_+^2 - r_-^2}} + O(\varepsilon) \ . \tag{2.147}$$

The proper distance to the horizon diverges for an extremal wormhole, so we can only compare λ to the radial location r_0 in the BTZ metric. For the extremal BTZ black hole, we find that the travel time is given by:

$$\Delta t_{\rm BTZ} = \frac{R^2}{2 r_+ \varepsilon} + O(\varepsilon^0) \, . \tag{2.148}$$

This is now no longer logarithmic, but inversely proportional to the (coordinate) distance to the horizon. The travel time in the extremal wormhole is again given by $\Delta t_{\rm WH} = 2L_\lambda$, with $L_\lambda = 2\frac{R^2}{r_+}\frac{1}{\lambda^2}$ from eq. (2.11). Setting $\Delta t_{\rm BTZ} = 2L_\lambda$ again then gives to leading order:

$$\varepsilon = \frac{\lambda^2}{8} \, . \tag{2.149}$$

Therefore, both for the non-extremal and the extremal wormholes, we see that the parameter λ can be interpreted as a measure for the (proper) distance that the wormhole throat sits from the would-be horizon radius.

Relating distance to entropy. As we mentioned above, an important question to ask is: at what distance from the (would-be) horizon should we expect microstructure to arise? For the wormholes we consider, the two most obvious options for the location of the structure (i.e. the wormhole throat) are either perturbative or non-perturbative corrections.

[17] To generalize the non-rotating wormhole metric (3.4) to the rotating, non-extremal case, we can simply change $X(r)$ by taking $r_+ \to r_\lambda$ in the BTZ metric (3.1), while leaving $Y(r)$ and $N_\varphi(r)$ unchanged.

By perturbative corrections, we mean a wormhole parameter λ (and thus distance to the horizon) that scales as $\lambda \sim G_N/r_+$, while non-perturbative is taken to be exponential in the gravitational coupling. Through the Bekenstein-Hawking entropy of the BTZ black hole,

$$S_{\rm BH} = \frac{\pi r_+}{2G_N} \tag{2.150}$$

we can also interpret perturbative corrections as scaling with the black hole entropy as $\lambda_{\rm pert} \propto 1/S_{\rm BH}$, while non-perturbative corrections have $\lambda_{\rm non-pert} \propto \exp(-\alpha S_{\rm BH})$ for some dimensionless constant α.

Using holography, one could also consider the CFT central charge c instead of G_N. By the Brown-Henneaux central charge relation

$$c = \frac{3R}{2G_N} \tag{2.151}$$

we could also have defined perturbative corrections as $\lambda \sim 1/c$, while non-perturbative corrections are $\lambda \sim \exp(-ac)$ for some constant a. These relations are explored in [195]. These two viewpoints are related through the Cardy formula for the CFT entropy, $S_{\rm BH} = 2\pi\sqrt{c\,E/6}$, where $E = (c/6)(r_+/R)^2$ is the energy of the state in the CFT. We will choose to work with the entropy as opposed to the central charge as this interpretation does not necessarily hinge on the existence of a CFT dual.

Extra input from microstate geometries For a wormhole, we cannot directly determine the relation of λ to G_N or the entropy. Instead, we will use an indirect route of comparing our wormhole toy model to black hole microstate geometries. Recently, the travel time for a scalar wave packet in superstrata was considered in [41]. The travel time from the boundary to the cap is determined by the mass gap $E_{\rm gap} = (N_1N_5)^{-1}$ [205, 48, 47], the energy of the lowest energy excitation down the throat of the supersymmetric solution:

$$\Delta t_{\rm microstate} \approx E_{\rm gap}^{-1} R_y = N_1 N_5 R_y\,. \tag{2.152}$$

For our extremal wormhole, we found $\Delta t = 2L_\lambda = \frac{4R^2}{r_+\lambda^2}$. Equating these two travel times, we find

$$\lambda^2 \propto \frac{1}{\sqrt{N_1N_5N_P}} \propto \frac{1}{S_{\rm BH}}\,, \tag{2.153}$$

where we used $R = (Q_1Q_5)^{1/4}$, $r_+ = \sqrt{Q_p}$, $\frac{Q_1Q_5}{Q_P} = \frac{N_1N_5}{N_P}R_y^2$, and the entropy of the BMPV black hole with the same charges of the microstate is $S_{\rm BH} = 2\pi\sqrt{N_1N_5N_P}$.[18]

[18]We used that the $(1,0,n)$ superstratum with parameter $b \gg a$ has nearly-vanishing quantized angular momentum j_L, such that the entropy is given to excellent approximation by $S_{\rm BH} = 2\pi\sqrt{N_1N_5N_P - j_L^2} \approx 2\pi\sqrt{N_1N_5N_P}$, see [135, 41, 37, 38].

Imagine now that we add a small amount of non-extremality to the microstate, for instance by adding a small number of anti-branes down the D1-D5-P throat (or, equivalently, right-movers in the CFT dual to the BTZ solution). The black hole then becomes near-extremal, and the behavior of travel time becomes logarithmic in λ. However, we do not expect such a small change to the superstratum geometry to drastically change the travel time, so we assume it is still proportional to the mass gap $E_{\rm gap}$[19] Then, assuming that at leading order the non-extremality does not alter the relation (2.152), nor the relations between R, r_+ and the charges N_1, N_5, N_P, we find that equating $\Delta t_{\rm microstate} = 2L_\lambda$ (see eq. (2.145)) leads to

$$\log \frac{16}{\lambda^2} \propto \left(1 - \frac{r_-^2}{r_+^2}\right) \sqrt{N_1 N_5 N_P} \propto S \ , \tag{2.154}$$

Hence, we have that:

$$\lambda \propto e^{-\alpha S_{\rm BH}} \tag{2.155}$$

This exponential suppression of λ suggests that the 'closeness parameter' $\varepsilon \propto \lambda^4$ can be interpreted as being sub-planckian, even though the microstate geometry itself is well-behaved in the supergravity limit. However, note that this prefactor $\alpha \sim 1 - r_-^2/r_+^2$, which is in principle small near extremality. One can conjecture that (2.155) still remains valid further away from extremality (with $\alpha \sim \mathcal{O}(1)$); it would be interesting to investigate whether this is indeed the case in future work.

2.5.2 Does a typical black hole microstate have echoes?

Here, we perform an ensemble average over wormhole geometries that reveals how the echo amplitude generically gets exponentially suppressed in a typical state, and how it follows that the Poincaré recurrence time is doubly-exponential in the entropy.

There have been many studies of black hole mimickers giving rise to discernible echo structure in the post-ringdown gravitational wave signal, coming from the partial or complete reflection of the wave around the would-be horizon scale — see for example [78, 79, 81, 82, 29]; there have even been serious attempts to find echoes in existing gravitational wave signals [3, 11, 4, 5, 1, 2].

As we discussed above in section 2.5.1, the (quantum) corrections to the (non-extremal) geometry are expected to be exponentially suppressed as $e^{-\alpha S_{\rm BH}}$, so

[19] Note that $E_{\rm gap}$ is still meant to be the SUSY mass gap, and should not be confused with the mass gap of excitations above the near-extremal solution, which is expected to scale as $e^{-S_{\rm BH}}$. This introduces a new scale that should be decoupled from the travel time itself, as it is related to jumps in energy to *different* microstates, see [42].

one might immediately conclude that such corrections can never be measureable. How, then, could we expect to see these echoes?

The answer is simple: in the echo time, we pick up a logarithm, such that $\Delta t \propto \log \lambda \propto 1/S_{\rm BH}$ and corrections to the travel time are perturbative. Thus, there is a clear difference between geometric corrections and the corrections to observables such as echoes in wave response.

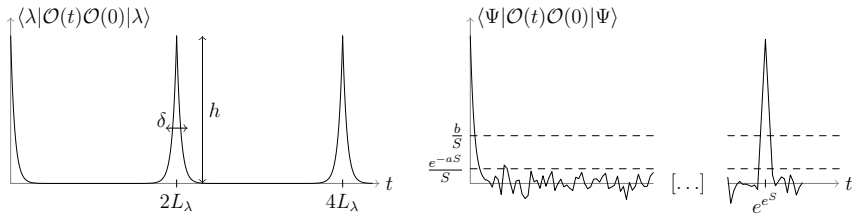
However, if we are to interpret the black hole mimickers (such as the Solodukhin wormhole studied here) as serious candidates or toy models of black hole microstates, then a *typical* black hole microstate would be an arbitrary superposition of such states. One such state, described by one particular value of λ, indeed has large corrections and an observable echo signal. But when forming a typical state by superposition of many such states, one gets exponential suppression of the *amplitude* of subsequent echoes by interference.

As we discussed in sections 2.4.2 and 2.4.3, echoes in an asymptotically AdS spacetime have a direct counterpart in the two-point correlator of the dual holographic CFT, where many results are known that describe in detail the expectation for the behaviour of such correlators. Generically, one expects to find that the behaviour of this correlator in a thermal unitary quantum field theory has the following features [157, 30]:

- at early times, the correlator decays exponential as $\langle \mathcal{O}\mathcal{O}\rangle \sim \exp\left(-2\pi \frac{2\Delta}{\beta} t\right)$ (where Δ is the scaling dimension of the operator $\mathcal{O}$);
- after the initial falloff, there are random fluctuations; these are suppressed by the entropy as $\langle \mathcal{O}\mathcal{O}\rangle \lesssim e^{-S/2}$;
- at very long time scales there is a (Poincaré) resurgence expected, at a time that scales doubly exponential with the entropy.

Can we recreate this behaviour by performing a statistical average of microstates with supergravity duals? For realistic microstates of the BMPV black hole, performing such an averaging is beyond current technology; only certain atypical states have known supergravity duals. However, using the Solodukhin wormhole as a toy model for microstates, we can consider an ensemble of wormholes with different λ parameters, and give some crude estimates for the generic expectations of the correlator in a typical state.

A microcanonical ensemble Denote a single Solodukhin wormhole state as $|\lambda\rangle$ with throat length $L_\lambda = -2r_0 \log \lambda$, and assume that for any two such states we



(a) Single λ geometry (b) Random superposition of λ geometries

Figure 2.7: Rough sketch of correlator in a single wormhole geometry $|\lambda\rangle$, and in a typical state $|\psi\rangle$, which is a random superposition over many such wormhole geometries

have $\langle\lambda'|\lambda\rangle = \delta_{\lambda,\lambda'}$.[20] We will be interested in two-point functions of a (light) scalar operator Φ in these states; we assume Φ is light enough so that it does not deform the (heavy) state $|\lambda\rangle$ much, meaning also $\langle\lambda'|\Phi(t)\Phi(0)|\lambda\rangle \approx 0$. Following the general structure of the two-point functions we have found (see section 3.4.2, especially (2.61)), let us assume here a schematic two-point function of the form:

$$\langle\lambda|\Phi(t)\Phi(0)|\lambda\rangle = G_0(t) + \sum_{n=0}^{\infty} G_1(t - 2nL_\lambda), \tag{2.156}$$

where $G^{\rm BH}(t) = G_0(t) + G_1(t)$ is the corresponding black hole correlator, which peaks at $t = 0$ and then quickly decays (see the bullet points above). The $n > 1$ terms are those that give the "echoes" at late times, starting with the first echo at $t \approx 2L_\lambda$.

Now, we assume the black hole can be described by a microcanonical ensemble of such wormhole states $|\lambda\rangle$ with $\lambda_{min} \leq \lambda \leq \lambda_{max}$ and corresponding throat lengths $L_{\lambda,max}, L_{\lambda,min}$. We assume $\lambda_{min} \ll \lambda_{max} \ll 1$ (and so $r_0 \ll L_{\lambda,max} \ll L_{\lambda,min}$). The number of states that spans this ensemble is $\#(\{|\lambda\rangle\}) = e^S$, where S is the black hole entropy. A generic state in the microcanonical ensemble is given by:

$$|\Psi\rangle = \sum_{\{|\lambda\rangle\}} b_\lambda |\lambda\rangle, \tag{2.157}$$

[20] If the states $|\lambda\rangle$ are more accurately described as coherent states (which would be natural for classical supergravity solutions), then their overlap would be exponentially small but not zero.

where b_λ are randomly selected[21] complex numbers such that $\sum_{\{|\lambda\rangle\}} |b_\lambda|^2 = 1$. This implies that on average $|b_\lambda|^2 \sim e^{-S}$. Then our assumptions imply:

$$\langle\Psi|\Phi(t)\Phi(0)|\Psi\rangle = \sum_{\{|\lambda\rangle\}} |b_\lambda|^2 \left(G_0(t) + \sum_{n=0}^{\infty} G_1(t - 2nL_\lambda) \right) = G^{\rm BH}(t) + \tilde{G}_1^{mc}(t), \tag{2.158}$$

where we have defined $\tilde{G}_1^{mc}(t)$, the deviation from the black hole correlator. We are interested in the behaviour of $\tilde{G}_1^{mc}(t)$ at late times. Let us model G_1 by a simple theta function of height h and width δ, which captures the fact that the correlator $G^{\rm BH}(t)$ is peaked around $t = 0$ and small for late times, see figure 2.7a:

$$G_1(t) = h[\Theta(t - \delta) - \Theta(t + \delta)], \tag{2.159}$$

so that:

$$\tilde{G}_1^{mc}(t) = \sum_{\{|\lambda\rangle\},n>0} |b_\lambda|^2 h \left[\Theta(t - 2nL_\lambda - \delta) - \Theta(t - 2nL_\lambda + \delta)\right] \tag{2.160}$$

$$\approx h e^{-S} \sum_{n>0} (\lambda_{1,n} - \lambda_{0,n}) = h e^{-S} \sum_{n>0} \left(\exp\left(-\frac{t-\delta}{4nr_0} \right) - \exp\left(-\frac{t+\delta}{4nr_0} \right) \right) \tag{2.161}$$

where we have used $|b_\lambda|^2 \sim e^{-S}$ and $\lambda_{1,n}$ (resp. $\lambda_{0,n}$) are the largest (resp. smallest) possible λ for which the theta functions in (2.160) don't vanish. The sum over n has a finite range as we must have that $\lambda_{min} \leq \lambda_{0,n} < \lambda_{1,n} \leq \lambda_{max}$. This gives:

$$\frac{t+\delta}{2L_{\lambda,min}} \leq n \leq \frac{t-\delta}{2L_{\lambda,max}}. \tag{2.162}$$

We now approximate the sum over n in (2.161) by an integral and use $t \gg \delta$ and $L_{\lambda,min/max} \gg r_0$ to find:

$$\tilde{G}_1^{mc}(t) \approx h\delta e^{-S} \left(\frac{e^{-L_{\lambda,max}/(2r_0)}}{L_{\lambda,max}} - \frac{e^{-L_{\lambda,min}/(2r_0)}}{L_{\lambda,min}} \right) \approx h\delta e^{-S} \frac{\lambda_{max}}{L_{\lambda,max}}, \tag{2.163}$$

where we used $L_{\lambda,min} \gg L_{\lambda,max}$ and $\lambda_{max} \gg \lambda_{min}$. Equation (2.163) shows that the correlator is suppressed by e^{-S}, λ_{max} and $L^{-1}_{\lambda,max}$, such that $\tilde{G}_1^{mc}(t)/\tilde{G}_1^{mc}(0) \ll 1$. The conclusion is that the difference of the two-point correlator in the typical state $|\Psi\rangle$ from the black hole correlator is negligibly small.

To determine more precisely the suppression of the correlator in terms of the entropy, one should keep in mind that S and λ_{max} are related in some way

[21] More precisely: chosen with the Haar measure.

that we have yet to specify in our crude model. For example, if the states $\{|\lambda\rangle\}$ differ in λ by some constant spacing $\Delta\lambda$, we find $e^S = \frac{\lambda_{max}-\lambda_{min}}{\Delta\lambda} \approx \frac{\lambda_{max}}{\Delta\lambda}$. The exponential factors in the entropy then cancel and our correlator is only polynomially suppressed in the entropy: $\tilde{G}_1^{mc}(t)/\tilde{G}_1^{mc}(0) \propto b/S$, for some positive constant b. By contrast, if we assume the scaling of λ with the entropy S in equation (2.155), then the suppression is e^{-aS}/S for some positive constant a, see figure 2.7b.

This simple crude calculation in our toy model has shown us the generic expectation for typical black hole microstates: any "echo structure" that might be found in individual, highly non-typical microstates (here, in any single state $|\lambda\rangle$), is generically washed away in a typical state that is a random superposition of these states.

Recurrence time Instead of studying $\tilde{G}_1^{mc}(t)$ at a generic (late) time as we have done above, we can ask the reverse question: at what time t_R do we expect to find $\tilde{G}_1^{mc}(t_R) \approx h$, i.e. having an amplitude peak similar to the original (black hole) peak at $t = 0$. To have such a recurrence at a time t_R, we need that approximately *all* the states in the ensemble, $\lambda_i \in \{|\lambda\rangle\}$, satisfy:

$$t_R - 2n_i L_{\lambda,i} - \delta \leq 0 \leq t_R - 2n_i L_{\lambda,i} + \delta, \tag{2.164}$$

for some collection of integers $\{n_i\}$. This means that, for every pair i, j, we need:

$$\left| n_i \frac{L_{\lambda,i}}{\delta} - n_j \frac{L_{\lambda,j}}{\delta} \right| \leq 1. \tag{2.165}$$

Unless there is a special way the ensemble $\{|\lambda\rangle\}$ is constructed, the λ_i's and thus the L_{λ_i}'s will generically be random; together with $\delta \ll L_{\lambda,max}$ this implies the solution must be (multiples of):

$$n_i \approx \prod_{j\neq i} \frac{L_{\lambda,j}}{\delta}. \tag{2.166}$$

Then:

$$t_R \approx 2n_i L_{\lambda,i} \approx 2\delta \prod_i \frac{L_{\lambda,i}}{\delta}. \tag{2.167}$$

If we take $L_{\lambda,max} = N\delta$ (with $N \gg 1$), then we can give a bound on t_R as:

$$t_R \geq (2\delta) N^{e^S}, \tag{2.168}$$

which gives the expected characteristic doubly exponential behaviour, see figure 2.7b.

To conclude, we have seen that even our very crude toy model of averaging over microstate geometries, the correlator behaviour matches remarkably well with the generic QFT expectations we discussed above:

- At early times, the decay is exactly the same as the one for a black hole, since the $n = 0$ contribution of (2.156) is precisely the black hole correlator, and is independent of the particular heavy state $|\lambda\rangle$).
- After the initial decay, there are "random" fluctuations due to the individual microstate in question, given by (2.163). The smallness of these fluctuations depends on the specifics of the distribution of λ's within the ensemble, and so depends on the details of our toy model.
- For an ensemble of appropriately random $|\lambda\rangle$'s, the recurrence time (2.167) is indeed doubly exponential in the entropy.

Chapter 3

Black hole microstate correlators via real-time holography

In the previous chapter we argued that a Solodukhin wormhole [195] (see also [105]) can be used as a toy model of the more complicated superstrata microstate geometries, as it captures some of its essential features [110]. Such a wormhole connects two asymptotically AdS_3 regions through a wormhole throat (which sits at the would-be horizon scale) and behaves roughly as a "cap" where the boundary conditions on the second AdS_3 boundary reflect back the information. Using this toy model, we obtained a correlator that is qualitatively very similar to the $(1, 0, n)$ superstratum correlator of [41], containing an initial fall-off identical to that of the black hole, and with echoes at times of order the wormhole throat length.

In this chapter, we investigate such scalar correlators in the Solodukhin wormhole toy models in more detail. In particular, we use the Skenderis-van Rees formalism of real-time holography [193, 194] to calculate this correlator exactly. This allows us to compare the exact answer to the hybrid WKB answer, which is the first time such an explicit comparison is made. It also allows us to calculate all possible two-point correlators (Feynman, Wightman, retarded, advanced), as opposed to only the retarded one, as one calculates using the hybrid WKB method.

Note also that [41, 36, 110] (mainly) consider microstates of a supersymmetric

black hole, which has an extremal BTZ throat. In this chapter, we use the non-rotating (non-extremal) BTZ black hole and its corresponding Solodukhin wormhole as the starting point for our calculations. As such, one can view our toy model as a playground to explore basic features of correlators of non-extremal microstate geometries.

The real-time holography formalism has the additional benefit that it in principle allows us to compute correlators in a background that describes *off-diagonal* correlators in the CFT such as $\langle HLLH' \rangle$, where the initial and final heavy states are *different*.[1] These no longer correspond to a scalar correlator in a single geometry, but rather (using the real-time formalism) can be seen to correspond to a *transition* between different (Euclidean) geometries. Such correlators are the first step towards understanding the correlators in a mixed-state given by a density matrix constructed from several heavy states H_i — one would hope that the black hole correlator will be arbitrarily well approximated by such a density matrix correlator using sufficiently many microstate geometry heavy states [41]. We model this transition in the Solodukhin wormhole toy model and compute this off-diagonal correlator for an infinitesimal change in heavy state. To our knowledge, this is the first ever such calculation that explores off-diagonal correlators [2], albeit in a toy model for microstate geometries. Our results suggest that the sharp echoes (of diagonal correlators) will get smoothed out in off-diagonal correlators.

This chapter is organized as follows: In section 3.1 we introduce the BTZ black hole, its corresponding Solodukhin wormhole modification, as well as discuss the scalar wave equations in these backgrounds. In section 3.2, we calculate the scalar correlator using the real-time holography formalism to successively more complicated geometries: the BTZ black hole, its Solodukhin wormhole, and the (infinitesimal) transition between two such wormholes. In section 3.3, we apply hybrid WKB to obtain the (approximate) retarded correlator of the wormhole, and compare it to the exact result obtained in section 3.2.2. In section 3.4, we explicitly calculate the appropriate contour integrals on the momentum-space correlators obtained in section 3.2 to obtain the position-space correlators of BTZ, the wormhole and the transitioning wormhole. The appendices A.1 and A.2 contain a brief overview of the necessary details of the Schwinger-Keldysh real-time correlator formalism in quantum field theory and Skenderis-van Rees real-time holography.

[1] Note that such a scenario can only be of physical relevance if the timescale of observation is much larger that timescale of such a transition, and moreover that the probability of transition between neighboring heavy states is sufficiently high. We will be considering the case where the transition happens between infinitesimally close states.

[2] Although see the discussion in [70] in the large c limit of CFTs

3.1 BTZ wormhole and wave equation

The rest of this chapter we will use the non-rotating BTZ black hole metric and its corresponding Solodukhin-type wormhole [195]. In this section, we will review the BTZ black hole and introduce the wormhole geometry as well as a few of its basic properties. We will also discuss the wave equation of a minimally coupled scalar in these geometries. Note that most of this introductory and review material was also presented in chapter 2, which also included the expressions for the extremal BTZ black hole and corresponding Solodukhin wormhole.

3.1.1 The non-rotating BTZ black hole

The non-rotating BTZ black hole [27, 26] has metric:

$$\begin{aligned} \mathrm{d}s^2 &= -X(r)\,\mathrm{d}t^2 + \frac{\mathrm{d}r^2}{Y(r)} + r^2\,\mathrm{d}\varphi^2\,, \qquad & \begin{cases} r \in [r_+, \infty)\,, \\ t \in (-\infty, \infty)\,, \\ \varphi \sim \varphi + 2\pi\,, \end{cases} \\ X(r) &= Y(r) = \frac{(r^2 - r_+^2)}{R^2}\,, & \end{aligned} \tag{3.1}$$

where R is the AdS radius. These coordinates cover the patch outside the horizon ($r > r_+$). The asymptotic mass of the black hole, in units where $8G_3 = 1$, reads

$$M = \frac{r_+^2}{R^2}\,, \tag{3.2}$$

while the temperature and the entropy of the black hole are given by

$$T = \frac{r_+}{2\pi R^2}\,, \qquad S = 4\pi r_+\,. \tag{3.3}$$

In the holographically dual CFT_2, the black hole corresponds to a thermal state with the same temperature.

3.1.2 The non-rotating wormhole

To modify the non-rotating BTZ metric (3.1) into a wormhole in the style of Solodukhin [195] (see also [105]), we simply alter by hand one of the metric

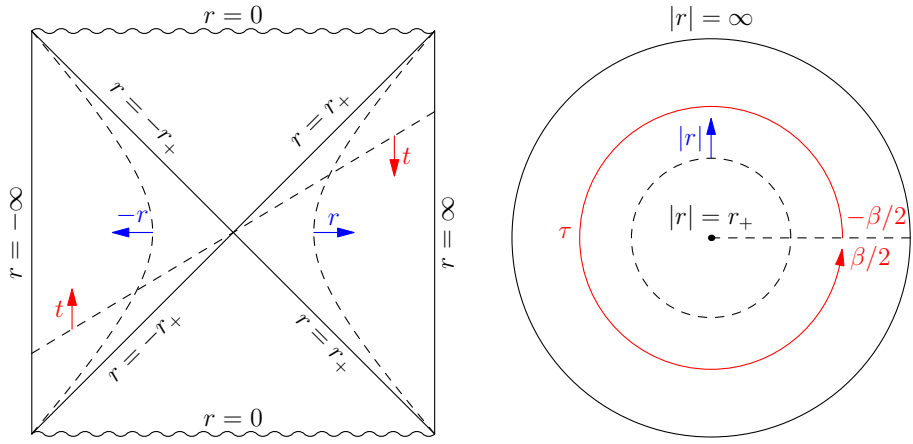


Figure 3.1: The non-rotating BTZ black hole: Lorentzian signature (left) and Euclidean signature (right). The Euclidean black hole has periodic time $\tau \sim \tau + \beta$, where $\beta = 1/T$.

components, giving:

$$\begin{aligned} \mathrm{d}s^2 &= -X(r)\,\mathrm{d}t^2 + \frac{\mathrm{d}r^2}{Y(r)} + r^2\,\mathrm{d}\varphi^2 \ , \\ X(r) &= \frac{r^2 - r_\lambda^2}{R^2}\,, \quad Y(r) = \frac{r^2 - r_+^2}{R^2}\,, \quad r_\lambda^2 \equiv r_+^2(1-\lambda^2)\,, \end{aligned} \tag{3.4}$$

where now the radial coordinate ranges between $r \in (-\infty, -r_+] \cup [r_+, \infty)$. For each value of the (small) dimensionless parameter $\lambda > 0$, this gives us a wormhole geometry. For $r \gg r_+$, the smallness of λ ensures that the metric looks almost like that of the original black hole. However, the global structure of spacetime is drastically altered, as there is no longer a horizon in the spacetime. Instead, we have essentially glued a second copy of this asymptotic flat spacetime (with $r < -r_+$) to the old horizon position, thus creating a traversable wormhole.

In chapter 2, we discussed the stress energy tensor of this geometry and show that it requires the presence of exotic matter, localized roughly where the two throats meet. There, we also compute the holographic stress energy tensor and show that it differs from the one of the corresponding black hole at $\mathcal{O}(\lambda^2)$. Further, in chapter 2 we calculated explicitly the tortoise coordinate of the extended, two-sided geometry, showing that it has a finite range. This allows us to define the effective length L_λ of the wormhole as:

$$L_\lambda \equiv \frac{R^2}{r_+} \log \frac{16}{\lambda^2}\,. \tag{3.5}$$

3.1.3 The scalar wave equation

A minimally coupled scalar field Φ on the BTZ metric background (3.1) or the wormhole metric (3.4) has the general equation of motion:

$$\nabla^2\Phi = m^2\Phi\,. \tag{3.6}$$

We can solve this by a separation of variables:

$$\Phi(t,r,\varphi) = e^{-i\omega t+ik\varphi}\Phi_r(r)\,, \tag{3.7}$$

where the radial function $\Phi_r(r)$ must satisfy the differential equation:

$$\Phi_r'' + \left(\frac{1}{r} + \frac{X'}{2X} + \frac{Y'}{2Y}\right)\Phi_r' + \left(\frac{\omega^2}{XY} - \frac{k^2}{r^2Y} - \frac{m^2}{Y}\right)\Phi_r = 0\,. \tag{3.8}$$

We are interested in finding the scalar wave solutions to (3.8) in both the black hole and wormhole metrics. Note that for the BTZ black hole, the solutions to (3.8) are explicitly known (see (3.16)).

To find the solutions to (3.8) for the wormhole, note that we can introduce appropriate tortoise coordinates r_* in both the black hole and wormhole geometries such that for $\phi = \Phi_r\sqrt{r/R}$, the equation (3.8) becomes:

$$(\partial_{r_*}^2 - V(r_*))\phi(r_*) = 0. \tag{3.9}$$

Further, using the relation between the respective black hole and wormhole tortoise coordinates, one finds:

$$V^{\rm WH}(r_*) = \theta(r_*)V^{\rm BH}(r_*) + (r_* \to -r_*) + \mathcal{O}(\lambda^2), \tag{3.10}$$

so that the wormhole scalar potential is the same as the black hole potential on each side of the wormhole, up to $\mathcal{O}(\lambda^2)$ corrections. This means that the solutions on each side of the wormhole can be taken to be the black hole ones, $\phi^{\rm WH}(r) = \phi^{\rm BH}(r)$ and $\phi^{\rm WH}(-r) = \phi^{\rm BH}(r)$. This must then be supplemented with a continuity condition at the center of the wormhole throat (at $r_* = 0$), which gives

$$\Phi_r(r_t) = \Phi_r(-r_t)\,, \qquad \partial_r\Phi_r(r_t) = \partial_r\Phi_r(-r_t)\,, \tag{3.11}$$

where we have defined the "gluing point" radius:

$$r_t = r_+\left(1 + \frac{\lambda^2}{8}\right) + \mathcal{O}(\lambda^4)\,. \tag{3.12}$$

For more details on this matching, see chapter 2.

3.2 Correlators via real time holography

In this section, we will use the Skenderis-van Rees formalism of real-time holography [194, 193] to calculate various two-point correlation functions (Feynman, Wightman, and retarded) for a minimally coupled scalar field in various geometries of interest: the (non-rotating) BTZ black hole, the (non-rotating) Solodukhin wormhole, and a time-dependent geometry that transitions between two Solodukhin wormholes with different λ.

A brief overview as well as the relevant formulas of real-time holography and its preliminary Schwinger-Keldysh formalism are assembled in appendices A.1 and A.2.

3.2.1 Correlators of the BTZ black hole

Here, we use the real-time formalism to obtain the two-point functions of a minimally coupled scalar field in a non-rotating BTZ background. This was first done in the context of real-time holography in [194] and later expanded and generalized in [206, 66, 67]; earlier works include [196, 137]. The calculation can also be generalized to consider minimally coupled gauge fields in this background [106].

Schwinger-Keldysh contour To find the BTZ two-point correlation function of a minimally coupled scalar field, we start with a thermal Schwinger-Keldysh contour (A.1) with $\sigma_a = \sigma_b = \sigma_c = \beta/2$ and identified endpoints [146, 194]. Then the forward (resp. backward) running Lorentzian segments are interpreted as segments on the left (resp. right) boundary: $\gamma_1 \equiv \gamma_L$ and $\gamma_2 \equiv \gamma_R$; the Euclidean segments are connected to both L and R akin to a Hartle-Hawking state [157, 142]. Thus, the ranges of the complex Keldysh time $\theta = t - i\tau$ are as follows; see figure 3.2 (left):

$$\begin{aligned} \gamma_a &: \quad \theta \in [-T + i\beta/2, -T]\,, \qquad & \gamma_L &: \quad \theta \in [-T, T]\,, \\ \gamma_b &: \quad \theta \in [T, T - i\beta/2]\,, & \gamma_R &: \quad \theta \in [-T - i\beta/2, T - i\beta/2]\,. \end{aligned} \tag{3.13}$$

To construct the bulk dual to this field theory contour, we take the upper half of the thermal circle in Euclidean time, whose time ranges in $\tau \in [-\beta/2, 0]$, and we glue it to the line $t = -T$ in the Lorentzian non-rotating BTZ (see figure 3.1). Similarly, we glue the lower half of the thermal circle, whose time ranges in $\tau \in [0, \beta/2]$, to the line $t = T$; note that $\tau = \pm\beta/2$ are identified. The resulting bulk contour is depicted in figure 3.2 (right). The bulk gluings dictate

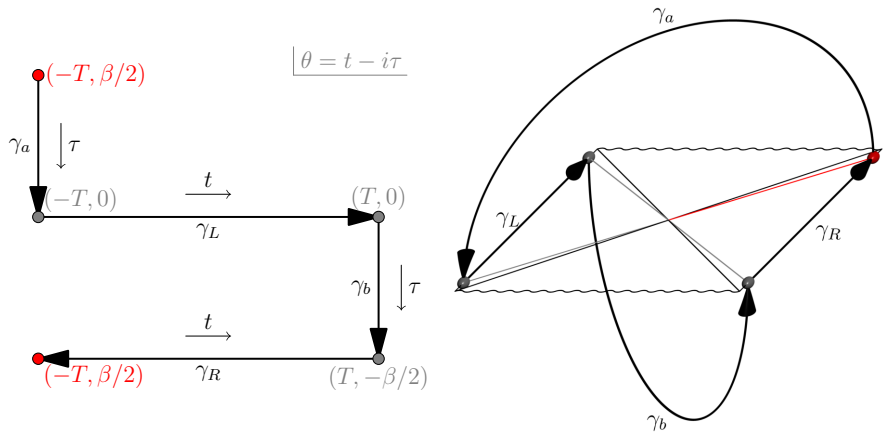


Figure 3.2: The thermal Schwinger-Keldysh contour in CFT_2 (left) and the mixed-signature bulk spacetime, corresponding to it (right). On the boundary contour (left), the grey dots signify gluing between an Euclidean and a Lorentzian segment and the red dots at $(-T, \pm\beta/2)$ are identified and also glued. On the bulk contour (right) the fields are glued at fixed time slices extending all the way into the bulk until the horizon at $r = r_+$ is reached.

the following matching conditions that the piecewise bulk fields must obey:

$$\begin{aligned}
\Phi_a(0,\varphi,|r|) &= \Phi_L(-T,\varphi,-r)\,, & \partial_\tau\Phi_a(0,\varphi,|r|) &= -i\partial_t\Phi_L(-T,\varphi,-r)\,,\\
\Phi_L(T,\varphi,-r) &= \Phi_b(0,\varphi,|r|)\,, & -i\partial_t\Phi_L(T,\varphi,-r) &= \partial_\tau\Phi_b(0,\varphi,|r|)\,,\\
\Phi_b(\beta/2,\varphi,|r|) &= \Phi_R(T,\varphi,r)\,, & \partial_\tau\Phi_b(\beta/2,\varphi,|r|) &= -i\partial_t\Phi_R(T,\varphi,r)\,,\\
\Phi_R(-T,\varphi,r) &= \Phi_a(-\beta/2,\varphi,|r|)\,, & -i\partial_t\Phi_R(-T,\varphi,r) &= \partial_\tau\Phi_a(-\beta/2,\varphi,|r|)\,.
\end{aligned} \tag{3.14}$$

Scalar wave solutions We can use separation of variables as in (3.7) to solve the equations of motion for the minimally coupled scalar on the different pieces of the Schwinger-Keldysh contour:

$$\Phi_i = e^{-i\omega t}e^{ik\varphi}\tilde{s}_i(\omega,k)f(\omega,k,r)\,, \qquad \Phi_I = e^{-\omega\tau}e^{ik\varphi}\tilde{s}_I(\omega,k)f(\omega,k,r)\,, \tag{3.15}$$

with $i = \{L, R\}$ for the Lorentzian segments and $I = \{a, b\}$ for the Euclidean segments. The radial function $f(\omega, k, r)$ is a solution to the radial wave equation (3.8) with the metric functions given in (3.1) with $r_- = 0$; the general solution

is a linear combination of $f^{\pm}$ with:

$$f^{\pm}(\omega,k,r) = \mathcal{N}^{\pm}_{\omega k}\left(1-\frac{r_+^2}{r^2}\right)^{\pm ir_+\overline{\omega}/2} \times \ {}_2F_1\left(\frac{i}{2}\big(\pm r_+\overline{\omega}-\overline{k}\big),\frac{i}{2}\big(\pm r_+\overline{\omega}+\overline{k}\big);1\pm ir_+\overline{\omega};1-\frac{r_+^2}{r^2}\right), \quad (3.16)$$

where we have introduced the rescaled quantities $\overline{k} = Rk/r_+$ and $\overline{\omega} = R^2\omega/r_+^2$. At the horizon, these functions behave as:

$$f^{\pm}(\omega,k,r) \sim (r-r_+)^{\pm\frac{ir_+\overline{\omega}}{2}} \sim e^{\pm i\omega r_*}, \quad (3.17)$$

where r_* is the standard black hole tortoise coordinate, so that f^+ (resp. f^-) is identified with outgoing (resp. ingoing) modes.[3] We choose the normalization constants:

$$\mathcal{N}^{\pm}_{\omega k} = \frac{\Gamma\big(1\pm\frac{i}{2}(r_+\overline{\omega}-\overline{k})\big)\Gamma\big(1\pm\frac{i}{2}(r_+\overline{\omega}+\overline{k})\big)}{\Gamma(1\pm ir_+\overline{\omega})}, \quad (3.18)$$

such that at the UV boundary $r\to\infty$, we have $f^{\pm}\to 1$; the asymptotic expansion is then:

$$f^{\pm}(\omega,k,r) = 1+\frac{r_+^2}{r^2}\alpha(\omega,k)\left(\beta^{\pm}(\omega,k)+\log\frac{r_+^2}{r^2}\right)+\dots, \quad (3.19)$$

$$\alpha(\omega,k) = -\frac{1}{4}\left(r_+^2\overline{\omega}^2-\overline{k}^2\right),$$

$$\beta^{\pm}(\omega,k) = \psi\left(1+\frac{i}{2}\big(\pm r_+\overline{\omega}-\overline{k}\big)\right)+\psi\left(1+\frac{i}{2}\big(\pm r_+\overline{\omega}+\overline{k}\big)\right)\pm\frac{2ir_+\overline{\omega}}{r_+^2\overline{\omega}^2-\overline{k}^2},$$

where $\psi(\cdot)$ is the digamma function and we have given $\beta^{\pm}$ up to constants which do not affect the poles of $\alpha\beta^{\pm}$. These poles of $f^{\pm}$ can be obtained from the poles of the normalization factors (or equivalently from the poles of $\alpha\beta^{\pm}$) and are located at

$$R\omega^{\pm}_{nk+} = k\pm i\frac{2r_+}{R}n, \quad R\omega^{\pm}_{nk-} = -k\pm i\frac{2r_+}{R}n, \quad (3.20)$$

where $n\in\{1,2,3,\dots\}$ and $k\in\mathbb{Z}$. The $\omega^{-}_{nk\pm}$ frequencies with negative imaginary part are the poles corresponding to the ingoing mode f^- and thus

[3]We do not impose ingoing boundary conditions at the horizon so that we are in principle able to compute all correlators; imposing ingoing boundary conditions would mean we are computing the retarded correlator [206, 196, 137].

are the quasi-normal modes of the non-rotating BTZ black hole [80] which are exponentially damped at late times (corresponding to the scalar field leaking into the black hole horizon). Note that the poles of $f^{\pm}$ precisely correspond to the poles of the normalization factors $\mathcal{N}^{\pm}_{\omega k}$ in (3.18).

Finally, we define a more convenient basis of modes as

$$g^{\pm} = \frac{1}{2}(f^{+} \pm f^{-})\,, \tag{3.21}$$

where g^{+} (resp. g^{-}) is the non-normalizable mode (resp. normalizable mode) as it asymptotes to 1 (resp. 0) in the UV ($r \to \infty$).

Constructing bulk fields piecewise Our next task is to construct the piecewise bulk fields. A generic Lorentzian field is expanded as

$$\Phi_i = \sum_k e^{ik\varphi} \int_{\mathcal{C}_i} \mathrm{d}\omega\, e^{-i\omega t}\big(g^{+}\delta_{ij} + g^{-}A_{ij}\big)\tilde{s}_j\,, \tag{3.22}$$

where A_{ij} are arbitrary meromorphic functions of ω and $\mathcal{C}_i$ is an arbitrary contour that avoids the poles of A_{ij} and $g^{\pm}$. Note that (3.22) indeed corresponds to introducing a source s_i on the boundary:

$$\lim_{r\to\pm\infty} \Phi_i = \sum_k e^{ik\varphi} \int_{\mathcal{C}_i} \mathrm{d}\omega\, e^{-i\omega t}\delta_{ij}\tilde{s}_j \equiv s_i\,. \tag{3.23}$$

The real time formalism fixes both $\mathcal{C}_i$ and A_{ij} by the matching conditions. We parametrize the freedom in $\mathcal{C}_i$ as:

$$\begin{aligned}\Phi_i = \sum_k e^{ik\varphi} \Bigg[&\int_{\mathbb{R}} \mathrm{d}\omega\, e^{-i\omega t}\big(g^{+}\delta_{ij} + g^{-}A_{ij}\big)\tilde{s}_j \\ &+ \int_{\mathcal{U}} \mathrm{d}\omega\, e^{-i\omega t} g^{-} U_{ij}\tilde{s}_j + \int_{\mathcal{L}} \mathrm{d}\omega\, e^{-i\omega t} g^{-} L^{-}_{ij}\tilde{s}_j \Bigg]\,.\end{aligned} \tag{3.24}$$

Here $\mathcal{U}$ is a positively oriented contour around the upper-half-plane and $\mathcal{L}$ is a negatively oriented contour around the lower-half-plane, see figure 3.3. The coefficients U_{ij}, L_{ij} thus pick up additional normalizable mode contributions, related to the choice of contour in (3.22).

The Euclidean fields do not have sources as we are interested in the thermal state without extra excitations (see [67] for a more general treatment), so they are composed solely of normalizable modes:

$$\Phi_I = \sum_k e^{ik\varphi} \left[\int_{\mathcal{U}} \mathrm{d}\omega\, e^{-\omega\tau} g^{-} U_{Ij}\tilde{s}_j + \int_{\mathcal{L}} \mathrm{d}\omega\, e^{-\omega\tau} g^{-} L_{Ij}\tilde{s}_j \right]. \tag{3.25}$$

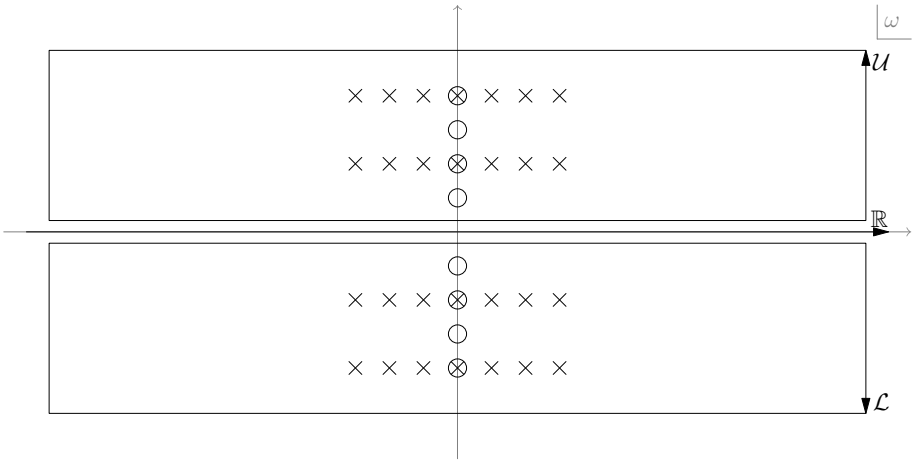


Figure 3.3: The contours $\mathcal{U}, \mathcal{L}, \mathbb{R}$ in the complex ω-plane. The crosses in the upper (resp. lower) half plane are the poles of f^+ (resp. f^-); each vertical line and its reflection across the y-axis corresponds to the poles of $f^\pm$ at fixed k. The circles are the poles of A_{ij} (i.e. the poles of $n(\omega)$), which we discuss in section 3.4.1.

Applying the matching conditions At early times $t \sim -T$ (resp. late times $t \sim T$), the sources all lie in the future (resp. past) so we must close the Feynman integral in the upper (resp. lower) half plane (see also the discussion in appendix A.2.1 and especially around (A.39)), so that:

$$\begin{aligned}
\Phi_i(t \sim -T) &= \sum_k e^{ik\varphi} \Bigg[\int_{\mathcal{U}} \mathrm{d}\omega\, e^{-i\omega t} g^- (\delta_{ij} + A_{ij} + U_{ij}) \tilde{s}_j \\
&\qquad + \int_{\mathcal{L}} \mathrm{d}\omega\, e^{-i\omega t} g^- L_{ij} \tilde{s}_j \Bigg], \\
\Phi_i(t \sim T) &= \sum_k e^{ik\varphi} \Bigg[\int_{\mathcal{U}} \mathrm{d}\omega\, e^{-i\omega t} g^- U_{ij} \tilde{s}_j \\
&\qquad + \int_{\mathcal{L}} \mathrm{d}\omega\, e^{-i\omega t} g^- (-\delta_{ij} + A_{ij} + L_{ij}) \tilde{s}_j \Bigg],
\end{aligned} \tag{3.26}$$

where we have used that:

$$\begin{aligned}\int_{\mathcal{U}} \mathrm{d}\omega\, e^{-i\omega t} g^{+}\delta_{ij}\tilde{s}_j &= \int_{\mathcal{U}} \mathrm{d}\omega\, e^{-i\omega t}\frac{1}{2} f^{+}\delta_{ij}\tilde{s}_j = \int_{\mathcal{U}} \mathrm{d}\omega\, e^{-i\omega t} g^{-}\delta_{ij}\tilde{s}_j\,,\\ \int_{\mathcal{L}} \mathrm{d}\omega\, e^{-i\omega t} g^{+}\delta_{ij}\tilde{s}_j &= \int_{\mathcal{L}} \mathrm{d}\omega\, e^{-i\omega t}\frac{1}{2} f^{-}\delta_{ij}\tilde{s}_j = \int_{\mathcal{L}} \mathrm{d}\omega\, e^{-i\omega t}(-g^{-})\delta_{ij}\tilde{s}_j\,.\end{aligned} \tag{3.27}$$

Since each of the contours picks up independent pole residues (i.e. normalizable modes), the two contour integrals $\mathcal{U}$, $\mathcal{L}$ must be independently matched, giving:

$$\begin{aligned}\mathcal{U}: \quad U_{aj}e^{-i\omega T} &= \delta_{Lj} + A_{Lj} + U_{Lj}\,,\\ U_{bj}e^{i\omega T} &= U_{Lj}\,,\\ U_{bj}e^{i\omega T} &= U_{Rj}e^{\beta\omega/2}\,,\\ U_{aj}e^{-i\omega T} &= (\delta_{Rj} + A_{Rj} + U_{Rj})e^{-\beta\omega/2}\,,\end{aligned} \tag{3.28}$$

$$\begin{aligned}\mathcal{L}: \quad L_{aj}e^{-i\omega T} &= L_{Lj}\,,\\ L_{bj}e^{i\omega T} &= -\delta_{Lj} + A_{Lj} + L_{Lj}\,,\\ L_{bj}e^{i\omega T} &= (-\delta_{Rj} + A_{Rj} + L_{Rj})e^{\beta\omega/2}\,,\\ L_{aj}e^{-i\omega T} &= L_{Rj}e^{-\beta\omega/2}\,.\end{aligned} \tag{3.29}$$

First, we solve for the Lorentzian functions U_{ij}, L_{ij} in terms of A_{ij}:

$$\begin{aligned}U_{Lj} = U_{Rj}e^{\beta\omega/2} &= -(\delta_{Lj} + A_{Lj})\frac{e^{\beta\omega}}{e^{\beta\omega}-1} + (\delta_{Rj} + A_{Rj})\frac{e^{\beta\omega/2}}{e^{\beta\omega}-1}\,,\\ L_{Lj} = L_{Rj}e^{-\beta\omega/2} &= -(\delta_{Lj} - A_{Lj})\frac{1}{e^{\beta\omega}-1} + (\delta_{Rj} - A_{Rj})\frac{e^{\beta\omega/2}}{e^{\beta\omega}-1}\,.\end{aligned} \tag{3.30}$$

Note that no factors of $e^{\pm i\omega T}$ appear in (3.30) (as opposed to (3.29)). Now, regularity at late times of the $\mathcal{U}$ contour integral in (3.26) for $\omega \to i\infty$ forces us to set $U_{ij} = 0$; similarly, regularity of the $\mathcal{L}$ integral at early times imposes $L_{ij} = 0$. These regularity conditions, together with (3.29), now fix all unknown

functions uniquely:

$$
\begin{aligned}
A_{ij} &= 2\begin{pmatrix} -(n+1/2) & \sqrt{n(n+1)} \\ -\sqrt{n(n+1)} & (n+1/2) \end{pmatrix}_{ij}, \qquad n(\omega) = \frac{1}{e^{\beta\omega}-1}\,, \\
U_{aj} &= 2\begin{pmatrix} -n & \sqrt{n(n+1)} \end{pmatrix}_j e^{i\omega T}\,, \qquad U_{bj} = 0\,, \\
L_{aj} &= 0\,, \qquad L_{bj} = 2\begin{pmatrix} -(n+1) & \sqrt{n(n+1)} \end{pmatrix}_j e^{-i\omega T}\,.
\end{aligned}
\tag{3.31}
$$

Note that U_{aj} and L_{bj} indeed have appropriate exponential tails in $\mathbb{R}$, coming from $n(\omega)$, that ensure regularity of the Euclidean fields when $\omega \to \pm\infty$; moreover, the factors of $e^{\pm i\omega T}$ ensure regularity (at all times) for $\omega \to \pm i\infty$.

Extracting the correlators Finally, having solved the bulk fields entirely, we can extract the correlation functions from them. For this, we extract the r_+^2/r^2 term in the expansion of the Lorentzian fields (see appendix A.2):

$$
\phi_i^{(2)} = \frac{1}{2}\sum_k e^{ik\varphi}\int_{\mathbb{R}} \mathrm{d}\omega\, e^{-i\omega t}\big[\alpha\beta^+(\delta_{ij}+A_{ij})\tilde{s}_j + \alpha\beta^-(\delta_{ij}-A_{ij})\tilde{s}_j\big]\,. \tag{3.32}
$$

Then, we use the Fourier transform $s(t,\varphi)$ of $\tilde{s}_j(\omega,k)$ defined in (3.23) and perform functional derivatives with respect to $s_j(t',\varphi')$ to obtain the black hole correlators:

$$
\begin{aligned}
iG^{ij}_{\mathrm{BH}}(x,x') &= \frac{2(-1)^{\delta_{ij}-\delta_{iR}+1}}{i}\,\frac{\delta\phi_i^{(2)}(x)}{\delta s_j(x')}\bigg|_{s_i=0} \\
&= \frac{(-1)^{\delta_{ij}-\delta_{iR}+1}}{4\pi^2 i}\sum_k e^{ik(\varphi-\varphi')}\int_{\mathbb{R}}\mathrm{d}\omega\, e^{-i\omega(t-t')}\big[(\delta_{ij}+A_{ij})\alpha\beta^+ + (\delta_{ij}-A_{ij})\alpha\beta^-\big]\,.
\end{aligned}
\tag{3.33}
$$

Explicitly, we can write:

$$
\begin{aligned}
iG^{LL}_{\rm BH}(x,x') &= \frac{1}{2\pi^2 i}\sum_k e^{ik(\varphi-\varphi')}\int_{\mathbb{R}} \mathrm{d}\omega\, e^{-i\omega(t-t')}\left[-n\alpha\beta^+ + (n+1)\alpha\beta^-\right],\\
iG^{LR}_{\rm BH}(x,x') &= \frac{1}{2\pi^2 i}\sum_k e^{ik(\varphi-\varphi')}\int_{\mathbb{R}} \mathrm{d}\omega\, e^{-i\omega(t-t')}\left[-\sqrt{n(n+1)}\alpha\beta^+ + \sqrt{n(n+1)}\alpha\beta^-\right],\\
iG^{RL}_{\rm BH}(x,x') &= \frac{1}{2\pi^2 i}\sum_k e^{ik(\varphi-\varphi')}\int_{\mathbb{R}} \mathrm{d}\omega\, e^{-i\omega(t-t')}\left[-\sqrt{n(n+1)}\alpha\beta^+ + \sqrt{n(n+1)}\alpha\beta^-\right],\\
iG^{RR}_{\rm BH}(x,x') &= \frac{1}{2\pi^2 i}\sum_k e^{ik(\varphi-\varphi')}\int_{\mathbb{R}} \mathrm{d}\omega\, e^{-i\omega(t-t')}\left[-(n+1)\alpha\beta^+ + n\alpha\beta^-\right].
\end{aligned}
\tag{3.34}
$$

These correlators require a careful interpretation. First, we identify the Feynman correlator as $iG^F_{\rm BH} \equiv iG^{LL}_{\rm BH}$ and the anti-Feynman correlator as $iG^{\overline{F}}_{\rm BH} \equiv iG^{RR}_{\rm BH} = \left[iG^{LL}_{\rm BH}(x,x')\right]^*$. The interpretation of this is that the R-region Feynman correlator behaves as a L-region anti-Feynman correlator, in accordance with the notion that the time in R in the thermofield-double state runs oppositely to the time in L, see figure 3.1. Next, we note that $iG^{LR}_{\rm BH} = iG^{RL}_{\rm BH}$; they are not conjugate and should not be identified with Wightman functions. Instead, these functions measure correlations between the L and R regions as "propagated through" the non-traversable Einstein-Rosen bridge that connects them. As for the Wightman functions, our contour (3.13) cannot produce them explicitly; rather, one would first need to introduce a 'doubled' contour containing also a reverse-L and a reverse-R segments. However, a simple shortcut to find the Wightman functions without this calculation is to use (A.8), which gives them in terms of the Feynman correlators.

We are most interested in the retarded propagator (see section A.1 and in particular (A.10)), which according to (A.9) is given by

$$
\begin{aligned}
iG^R_{\rm BH}(x,x') &= \theta(t-t')[iG^{LL}_{\rm BH}(x,x') - iG^{RR}_{\rm BH}(x,x')]\\
&= \frac{\theta(t-t')}{2\pi^2 i}\sum_k e^{ik(\varphi-\varphi')}\int_{\mathbb{R}} \mathrm{d}\omega\, e^{-i\omega(t-t')}\left[\alpha\beta^+ + \alpha\beta^-\right]\\
&= \frac{\theta(t-t')}{2\pi^2 i}\sum_k e^{ik(\varphi-\varphi')}\int_{\mathcal{L}} \mathrm{d}\omega\, e^{-i\omega(t-t')}\alpha\beta^-,
\end{aligned}
\tag{3.35}
$$

where we used the pole structure of $\alpha\beta^\pm$ to simplify the integral; note that the contour $\mathcal{L}$ simply picks up all of the poles in the complex lower half plane

(see figure 3.3). We will find the explicit expression for this position-space propagator in section 3.4.1.

3.2.2 Correlators of the Solodukhin wormhole

Here, we will apply the real-time holography formalism to the non-rotating Solodukhin wormhole with metric (3.4).

Schwinger-Keldysh contour Since the wormhole is a pure state, we take a pure state (zero temperature) Schwinger-Keldysh contour, similar to that in empty AdS in appendix A.1. This consists of two Euclidean (γ_I, $I = a, b$) and two Lorentzian (γ_i, $i = 1, 2$) segments, whose Keldysh time $\theta = t - i\tau$ runs as

$$\begin{aligned} \gamma_a: &\quad \theta \in [-T + i\infty, -T]\,, \qquad \gamma_1: \quad \theta \in [-T, T]\,, \\ \gamma_b: &\quad \theta \in [-T, -T - i\infty]\,, \qquad \gamma_2: \quad \theta \in [-T, T]\,. \end{aligned} \tag{3.36}$$

To construct the bulk dual to this contour, we follow the same strategy as for empty AdS (see appendix A.2.1). We have two Lorentzian pieces and one Euclidean piece, which is split in two and glued to the the ends of the Lorentzian pieces — see figure 3.4. These gluings dictate the matching conditions that the piecewise bulk fields obey:

$$\begin{aligned} &\Phi_a(0,\varphi,r) = \Phi_1(-T,\varphi,r)\,, \quad \partial_\tau \Phi_a(0,\varphi,r) = -i\partial_t \Phi_1(-T,\varphi,r)\,, \\ &\Phi_1(T,\varphi,r) = \Phi_2(T,\varphi,r)\,, \qquad \partial_t \Phi_1(T,\varphi,r) = \partial_t \Phi_2(T,\varphi,r)\,, \\ &\Phi_b(0,\varphi,r) = \Phi_2(-T,\varphi,r)\,, \quad \partial_\tau \Phi_b(0,\varphi,r) = -i\partial_t \Phi_2(-T,\varphi,r)\,. \end{aligned} \tag{3.37}$$

Scalar wave solutions As discussed in section 3.1.3, the solutions of the scalar wave equation to $\mathcal{O}(\lambda^2)$ on each side of the wormhole are those of the BTZ black hole itself, i.e. the modes $f^\pm$ in (3.16). These need to be supplemented with the continuity condition (3.11) at $r_t = r_+(1 + \lambda^2/8)$. Note that at the gluing point $\pm r_t$, the modes $f^\pm$ behave as:

$$\begin{aligned} &f^+(\omega,k,\pm r_t) = \mathcal{N}^+_{\omega k}\left(\frac{\lambda}{2}\right)^{ir_+\overline{\omega}}\,, \qquad f^-(\omega,k,\pm r_t) = \mathcal{N}^-_{\omega k}\left(\frac{\lambda}{2}\right)^{-ir_+\overline{\omega}}\,, \\ &\partial_r f^+(\omega,k,\pm r_t) = \pm\frac{4i\overline{\omega}}{\lambda^2}\mathcal{N}^+_{\omega k}\left(\frac{\lambda}{2}\right)^{ir_+\overline{\omega}}\,, \quad \partial_r f^-(\omega,k,\pm r_t) = \mp\frac{4i\overline{\omega}}{\lambda^2}\mathcal{N}^-_{\omega k}\left(\frac{\lambda}{2}\right)^{-ir_+\overline{\omega}}\,, \end{aligned} \tag{3.38}$$

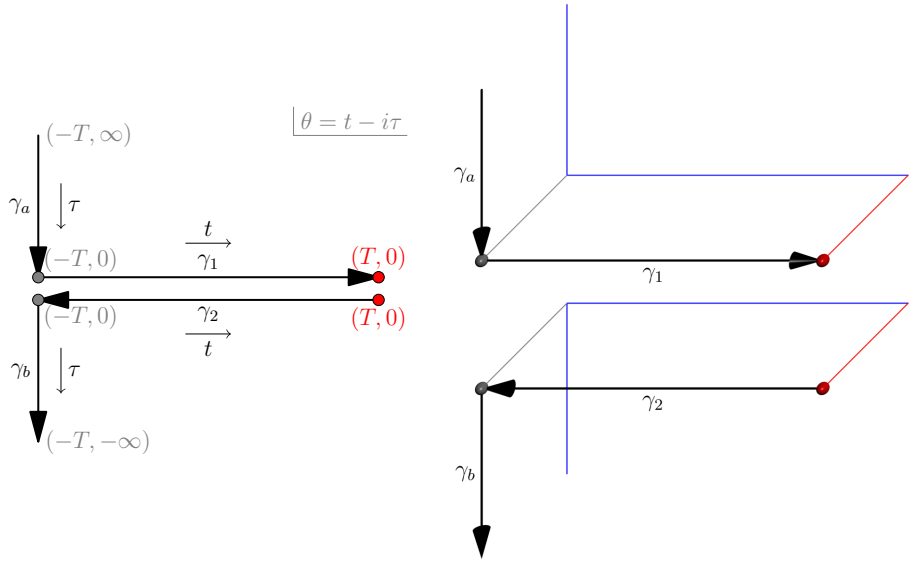


Figure 3.4: The pure-state Schwinger-Keldysh contour in CFT_2 (left) and the mixed-signature bulk spacetime, corresponding to it (right). On the boundary contour (left) the grey dots signify gluing between an Euclidean and a Lorentzian segment and the red dots are identified and also glued. On the bulk contour (right) the fields are glued on a fixed time slices extending all the way into the bulk. The blue line is the suface $r_* = 0$. On this mixed-signature diagram we have included only the right side of the wormhole, but the reader should envision that the left side is glued to the blue line as in figure 2.2.

where we remember that the normalization factors $\mathcal{N}^{\pm}_{\omega k}$ are given by (3.18).

We are interested in the holographic correlators for the CFT that sits on the boundary on one side — say, the right, i.e. $r > r_t$ — of the wormhole. Thus, the holographic sources live here, at $r \to \infty$. It is then natural to impose that there are no sources present on the *other*, i.e. left, boundary at $r \to -\infty$. This means that the only allowed mode must be proportional to $f^+ - f^-$ for $r \leq -r_t$,

which, using (3.38), means the allowed mode for $r > r_t$ is:[4]

$$f^\lambda \equiv \frac{1}{1-\kappa_\lambda^2}(f^+ - \kappa_\lambda^2 f^-)\,, \qquad \kappa_\lambda(\omega,k) \equiv \frac{\mathcal{N}^+_{\omega k}}{\mathcal{N}^-_{\omega k}}\left(\frac{\lambda}{2}\right)^{i\,2r_+\overline{\omega}}\,, \tag{3.39}$$

which has been normalized so that $\lim_{r\to\infty} f^\lambda = 1$. Note that imposing the condition of no sources on the left boundary is the analogue of the IR regularity condition in empty AdS (see appendix A.2.1) that also eliminates one linear combination of the scalar wave solutions.

In principle, we are free to choose different, fixed boundary conditions on the left boundary (including a non-normalizable piece). Alternatively, we could have performed a holographic analysis on the direct product of the CFTs on the right *and* left boundaries, introducing sources on both boundaries. This allows us to also compute the "mixed" left-right correlation functions (similar to the LR and RL correlators of the eternal black hole in (3.34)); the correlators we are calculating here are then simply the "right-right" correlators (where functional derivatives are taken with respect to the right sources and the left sources are set to zero).

While the BTZ black hole modes f^+ (resp. f^-) have poles in the upper (resp. lower) complex ω plane, a careful analysis shows that f^λ does *not* have these (or other) poles with non-zero imaginary part. Instead, f^λ only has poles on the real line, at locations where $\kappa_\lambda = \pm 1$. Explicitly, these normal modes are the solutions to the transcendental equation:

$$\frac{\Gamma\big(1+\frac{i}{2}(r_+\overline{\omega}-\overline{k})\big)\Gamma\big(1+\frac{i}{2}(r_+\overline{\omega}+\overline{k})\big)\Gamma(1-ir_+\overline{\omega})}{\Gamma\big(1-\frac{i}{2}(r_+\overline{\omega}-\overline{k})\big)\Gamma\big(1-\frac{i}{2}(r_+\overline{\omega}+\overline{k})\big)\Gamma(1+ir_+\overline{\omega})}\left(\frac{\lambda}{2}\right)^{i\,2r_+\overline{\omega}} = \pm 1\,. \tag{3.40}$$

This equation cannot be solved analytically in general; however, there are two frequency regimes where the (approximate) solution is simple. First of all, in the "low-frequency" regime:

$$\omega \sim \frac{1}{L_\lambda}\,, \tag{3.41}$$

where we used the wormhole throat length definition (3.5); note that $L_\lambda = R^2/r_+ \log\big(16\lambda^{-2}\big) \gg R, r_+$ (i.e. it is the largest scale in the solution). Then, we have the solutions:

$$\omega_n \approx n\frac{\pi}{L_\lambda}\,, \qquad n \in \mathbb{Z}\,. \tag{3.42}$$

[4]The expression for f^λ on the left side of the wormhole can be inferred from (3.39), (3.38), and the matching conditions (3.11). Note that specifying the wavefunction on (only) the right side uniquely determines the wavefunction on the left side (and vice versa). In particular, the mode (3.39) is well-defined and well-behaved on the right side, and from symmetry it will then also be so on the left side.

Second, in the "high-frequency" regime:[5]

$$\omega \gg \frac{r_+}{R^2}\,, \tag{3.43}$$

or equivalently $\overline{\omega} \gg r_+^{-1}$; note that then automatically $\omega \gg L_\lambda^{-1}$. In this limit, we find:

$$\omega_n \approx \left(n \pm \frac{1}{2}\right)\frac{\pi}{L_\lambda}\,, \qquad n \in \mathbb{Z}\,, \tag{3.44}$$

Curiously, these differ only from the low frequency normal modes (3.42) by a shift of $\pi/(2L_\lambda)$. The intermediate frequency regime must then interpolate between the solutions (3.42) and (3.44). In any case, we can conclude that the modes are (approximately) equally spaced with a spacing inversely proportional to the wormhole length. Note that the wormhole thus only has *normal* modes and no quasinormal modes, as appropriate for a pure state in AdS,[6] such as also empty AdS as discussed in appendix A.2.1.

Constructing bulk fields piecewise Our next task is to construct the piecewise bulk fields; this construction is analogous to the construction of the fields in empty AdS in appendix A.2.1. The Lorentzian fields are expanded as

$$\Phi_i = \sum_k e^{ik\varphi}\int_{\mathcal{C}_i} \mathrm{d}\omega\, e^{-i\omega t} f^\lambda \delta_{ij}\tilde{s}_j\,, \tag{3.45}$$

where in this notation $i, j = \{1, 2\}$ specify whether we are on the forward or the backward Lorentzian bulk piece. This ansatz has the correct UV asymptotics since:

$$\begin{aligned}\lim_{r\to\infty}\Phi_i &= \sum_k e^{ik\varphi}\int_{\mathcal{C}_i} \mathrm{d}\omega\, e^{-i\omega t} f^\lambda \delta_{ij}\tilde{s}_j \equiv s_i\,,\\ \lim_{r\to-\infty}\Phi_i &= \sum_k e^{ik\varphi}\int_{\mathcal{C}_i} \mathrm{d}\omega\, e^{-i\omega t} f^\lambda \delta_{ij}\tilde{s}_j \equiv 0\,.\end{aligned} \tag{3.46}$$

We parametrize the freedom in choosing the contour $\mathcal{C}_i$ by writing (again, precisely analogous to empty AdS in appendix A.2.1):

$$\Phi_i = \sum_k e^{ik\varphi}\left[\int_{\mathcal{F}} \mathrm{d}\omega\, e^{-i\omega t} f^\lambda \delta_{ij}\tilde{s}_j + \int_{\mathcal{W}^<} \mathrm{d}\omega\, e^{-i\omega t} f^\lambda V_{ij}\tilde{s}_j + \int_{\mathcal{W}^>} \mathrm{d}\omega\, e^{-i\omega t} f^\lambda W_{ij}\tilde{s}_j\right]. \tag{3.47}$$

[5] In this limit, we will also always assume $r_+\overline{\omega} \gg \overline{k}$.

[6] Without a horizon and in AdS asymptotics, there is nowhere that the scalar field can "leak" out to, so the amplitude of an eigenfunction cannot decrease. This is in contrast to Damour-Solodukhin wormholes in flat space, which have quasinormal modes (with a very small imaginary part) since the scalar wavefunction can "leak" out to flat infinity [71].

Here, V_{ij} and W_{ij} are arbitrary analytic functions of ω, $\mathcal{F}$ is a Feynman contour, $\mathcal{W}^>$ is a negatively oriented contour around $\mathbb{R}_{>0}$ and $\mathcal{W}^<$ is a positively oriented contour around $\mathbb{R}_{<0}$, see figure 3.5. Note that, as opposed to the black hole field

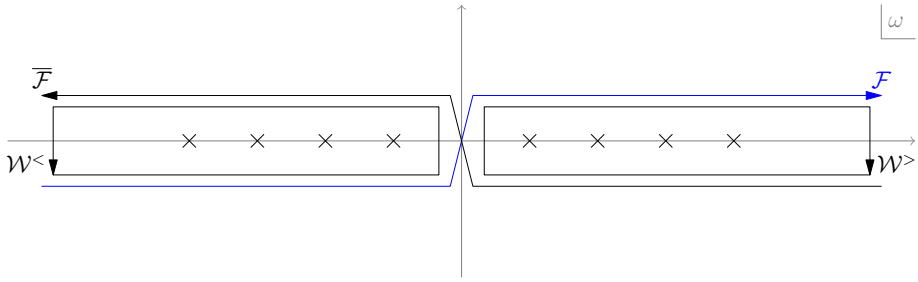


Figure 3.5: The contours $\mathcal{F}, \overline{\mathcal{F}}, \mathcal{W}^>, \mathcal{W}^<$ in the complex ω-plane. The crosses on the real line are the poles of $\tilde{f}$.

ansatz (3.24), we do not include a term with an upper or lower complex plane contour $\mathcal{U}$ or $\mathcal{L}$ as f^λ (and V_{ij} and W_{ij}) have no poles there. The Euclidean fields, since there are no Euclidean sources, are decomposed as

$$\Phi_I = \sum_k e^{ik\varphi} \left[\int_{\mathcal{W}^<} \mathrm{d}\omega\, e^{-\omega\tau} f^\lambda V_{Ij} \tilde{s}_j + \int_{\mathcal{W}^>} \mathrm{d}\omega\, e^{-\omega\tau} f^\lambda W_{Ij} \tilde{s}_j \right]. \tag{3.48}$$

Regularity on γ_a ($\tau < 0$) as $\omega \to +\infty$ further fixes $W_{aj} = 0$, and regularity on γ_b ($\tau > 0$) as $\omega \to -\infty$ fixes $V_{bj} = 0$.

Applying matching conditions The Schwinger-Keldysh contour (3.36), the piecewise bulk fields (3.47) and (3.48), and the matching conditions (3.37) are precisely the same as those of empty AdS discussed in appendix A.2.1 after substituting the AdS scalar mode f with the wormhole mode f^λ used here. Thus, applying and solving the matching conditions proceeds precisely the same way as in appendix A.2.1, and the results are:

$$\begin{aligned} V_{ij} &= \begin{pmatrix} 0 & -1 \\ 0 & -1 \end{pmatrix}, \qquad W_{ij} = \begin{pmatrix} 0 & 0 \\ 1 & -1 \end{pmatrix}, \\ V_{aj} &= \begin{pmatrix} 1 & -1 \end{pmatrix} e^{i\omega T}, \quad W_{bj} = \begin{pmatrix} 1 & -1 \end{pmatrix} e^{i\omega T}. \end{aligned} \tag{3.49}$$

The Euclidean and Lorentzian fields are thus completely determined in terms of the sources $\tilde{s}_i$.

Extracting the correlators Extracting the correlators of the wormhole happens entirely analogous to empty AdS in appendix A.2.1 (again, with the substitution

of the AdS mode f by f^λ). The result for the retarded correlator is then:

$$\begin{aligned} iG^R_{\rm WH}(x,x') &= \frac{\theta(t-t')}{2\pi^2 i}\sum_k e^{ik(\varphi-\varphi')}\int_{\mathcal{F}-\overline{\mathcal{F}}} \mathrm{d}\omega\, e^{-i\omega(t-t')}\alpha\beta^\lambda\,, \\ &= \frac{\theta(t-t')}{2\pi^2 i}\sum_k e^{ik(\varphi-\varphi')}\int_{\mathbb{R}+i\epsilon} \mathrm{d}\omega\, e^{-i\omega(t-t')}\alpha\beta^\lambda\,, \\ &= \frac{\theta(t-t')}{2\pi^2 i}\sum_k e^{ik(\varphi-\varphi')}\int_{\mathcal{W}^>-\mathcal{W}^<} \mathrm{d}\omega\, e^{-i\omega(t-t')}\alpha\beta^\lambda\,, \end{aligned} \tag{3.50}$$

where in the second line we have used the relation $\mathcal{F}-\overline{\mathcal{F}} = \mathbb{R}+i\epsilon$, with $\epsilon>0$ a small, real, and positive parameter, and in the third line we have used that $\theta(t-t')$ forces the contour of $\mathbb{R}+i\epsilon$ to close in the lower half plane, see figure 3.5. Note that

$$\beta^\lambda = \frac{1}{1-\kappa_\lambda^2}\left(\beta^+ - \kappa_\lambda^2\beta^-\right), \tag{3.51}$$

and α is the same as for the BTZ black hole, see (3.19).

3.2.3 Feynman correlator of a wormhole transition

The real-time holography formalism can also be used to calculate "off-diagonal" correlators such as $\langle\lambda'|\mathcal{O}\mathcal{O}|\lambda\rangle$, where we denote the light scalar operator dual to the probe scalar field Φ by $\mathcal{O}$. To calculate such a correlator, one must prepare Euclidean states with wormhole parameter λ, resp. λ' on γ_a, resp. γ_b (using the notation of (3.36)). The Lorentzian piece on $\gamma_{1,2}$ is then in principle completely determined by the boundary conditions obtained by "gluing" the two Euclidean sections to the Lorentzian piece appropriately.

In this way, the Lorentzian piece *must* become time-dependent, as it interpolates between a geometry with wormhole parameter λ at (Lorentzian) time $t=-T$ and a geometry with parameter λ' at $t=+T$. We will model this time-dependence as a "sudden" transition at time $t=t_0$ between the two wormhole states $|\lambda\rangle, |\lambda'\rangle$. We will demand that $|\lambda-\lambda'|\ll\lambda$ so that this procedure can provide a meaningful approximation.[7]

Having set up the problem in this simplified way, we will now show that it is relatively straightforward to obtain the explicit results for the "off-diagonal"

[7]Note that the Solodukhin wormhole does not satisfy the (vacuum) Einstein equations in any case, and that we have never specified explicitly what matter would be necessary to support it. As long as $|\lambda-\lambda'|\ll\lambda$, then the time-dependent Lorentzian "transition" geometry will actually have the same approximate energy-momentum tensor supporting it as the original (time-independent) wormhole.

momentum space correlator to $\mathcal{O}(\lambda - \lambda')$. We will consider (only) the Feynman correlator, as this is the natural one to consider when the (heavy) initial and final states are not the same.

Schwinger-Keldysh contour We take an in-out Schwinger-Keldysh contour consisting of two Euclidean ($\gamma_I,\ I = a, b$) and two Lorentzian ($\gamma_i,\ i = 1, 2$) segments, whose Keldysh time $\theta = t - i\tau$ runs as

$$\begin{aligned} \gamma_a: &\quad \theta \in [-T + i\infty, -T]\,, & \gamma_1: &\quad \theta \in [-T, t_0]\,, \\ \gamma_b: &\quad \theta \in [T, T - i\infty]\,, & \gamma_2: &\quad \theta \in [t_0, T]\,. \end{aligned} \tag{3.52}$$

As mentioned above, we imagine that at time $t = t_0$, there is an instantaneous change in the wormhole state from $|\lambda\rangle$ to $|\lambda'\rangle$. We depict this contour in figure 3.6; note that this contour is set up to calculate the Feynman correlator as mentioned above. The bulk version of this Schwinger-Keldysh contour follows

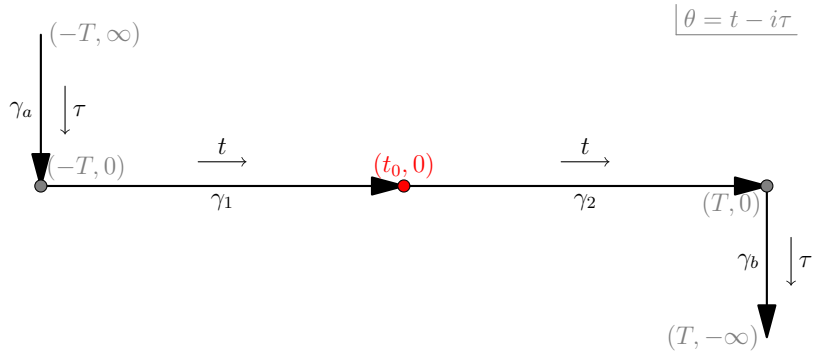


Figure 3.6: The in-out Schwinger-Keldysh contour appropriate for a transition between wormhole states. On the segments γ_a and γ_1 the state is $|\lambda\rangle$. Then at Lorentzian time $t = t_0$ a state-changing operator is suddenly applied (red bullet on the diagram) that changes the state to $|\lambda'\rangle$. This new state then forms that background on the segments γ_2 and γ_b. While, in principle, we can consider a "heavy" state-changing operator in the actual calculation, for technical convenience, we use a "light" state-changing operator and work to first order in $\delta\lambda = \lambda' - \lambda$.

analogously to the bulk versions that we previously considered and essentially fills in the bulk in such a way that the bulk fields obey smoothness conditions (in r) at the two different throat positions. Thus, we have the (temporal) matching

conditions:

$$\begin{aligned}
&\Phi_a(0,\varphi,r) = \Phi_1(-T,\varphi,r)\,, \quad \partial_\tau \Phi_a(0,\varphi,r) = -i\partial_t \Phi_1(-T,\varphi,r)\,,\\
&\Phi_1(t_0,\varphi,r) = \Phi_2(t_0,\varphi,r)\,, \quad \partial_t \Phi_1(t_0,\varphi,r) = \partial_t \Phi_2(t_0,\varphi,r)\,,\\
&\Phi_b(0,\varphi,r) = \Phi_2(T,\varphi,r)\,, \quad \partial_\tau \Phi_b(0,\varphi,r) = -i\partial_t \Phi_2(T,\varphi,r)\,.
\end{aligned} \tag{3.53}$$

These matching equations are valid at all r from the throat position at r_t to infinity; however, note that the throat position is now dependent on the time (i.e. whether $t < t_0$ or $t > t_0$). For $t = t_0$ we can take the lower bound on r as $\min(r_{t,\lambda}, r_{t,\lambda'})$.

Scalar wave solutions We follow the same reasoning as in section 3.2.2. In particular, we choose to only put sources on the right side of the wormhole. Since for $t < t_0$, resp. $t > t_0$, the wormhole geometry is given by the time-independent geometry with wormhole parameter λ, resp. λ', it follows that the scalar solutions are simply f^λ, resp. $f^{\lambda'}$, given by (3.39). Note that these functions have normal mode poles specified by (3.40) with λ, resp. λ'.

Constructing bulk fields piecewise We express the Lorentzian fields as

$$\begin{aligned}
\Phi_1 &= \sum_k e^{ik\varphi}\left[\int_{\mathcal{F}} \mathrm{d}\omega\, e^{-i\omega t} f^\lambda \delta_{1j}\tilde{s}_j + \int_{\mathcal{W}^<} \mathrm{d}\omega\, e^{-i\omega t} f^\lambda V_{1j}\tilde{s}_j + \int_{\mathcal{W}^>} \mathrm{d}\omega\, e^{-i\omega t} f^\lambda W_{1j}\tilde{s}_j\right],\\
\Phi_2 &= \sum_k e^{ik\varphi}\left[\int_{\mathcal{F}} \mathrm{d}\omega\, e^{-i\omega t} f^{\lambda'} \delta_{2j}\tilde{s}_j + \int_{\mathcal{W}^<} \mathrm{d}\omega\, e^{-i\omega t} f^{\lambda'} V_{2j}\tilde{s}_j + \int_{\mathcal{W}^>} \mathrm{d}\omega\, e^{-i\omega t} f^{\lambda'} W_{2j}\tilde{s}_j\right],
\end{aligned} \tag{3.54}$$

where, for convenience, we have split the Lorentzian source into two parts s_1, s_2, where the source $s_1(t,\varphi)$ is defined to vanish for $t \geq t_0$ and the source $s_2(t,\varphi)$ is defined to vanish for $t \leq t_0$. As before, we also express the regulated, sourceless Euclidean fields as

$$\begin{aligned}
\Phi_a &= \sum_k e^{ik\varphi} \int_{\mathcal{W}^<} \mathrm{d}\omega\, e^{-\omega\tau} f^\lambda V_{aj}\tilde{s}_j\,,\\
\Phi_b &= \sum_k e^{ik\varphi} \int_{\mathcal{W}^>} \mathrm{d}\omega\, e^{-\omega\tau} f^{\lambda'} W_{bj}\tilde{s}_j\,.
\end{aligned} \tag{3.55}$$

Near the matching points, the Lorentzian fields behave as (closing the contours appropriately):

$$\begin{aligned}
\Phi_1(t\sim -T) &= \sum_k e^{ik\varphi}\left[\int_{\mathcal{W}^<} \mathrm{d}\omega\, e^{-i\omega t} f^\lambda(\delta_{1j}+V_{1j})\tilde{s}_j + \int_{\mathcal{W}^>} \mathrm{d}\omega\, e^{-i\omega t} f^\lambda W_{1j}\tilde{s}_j\right],\\
\Phi_1(t\sim t_0) &= \sum_k e^{ik\varphi}\left[\int_{\mathcal{W}^<} \mathrm{d}\omega\, e^{-i\omega t} f^\lambda V_{1j}\tilde{s}_j + \int_{\mathcal{W}^>} \mathrm{d}\omega\, e^{-i\omega t} f^\lambda(\delta_{1j}+W_{1j})\tilde{s}_j\right],\\
\Phi_2(t\sim t_0) &= \sum_k e^{ik\varphi}\left[\int_{\mathcal{W}^<} \mathrm{d}\omega\, e^{-i\omega t} f^{\lambda'}(\delta_{2j}+V_{2j})\tilde{s}_j + \int_{\mathcal{W}^>} \mathrm{d}\omega\, e^{-i\omega t} f^{\lambda'} W_{2j}\tilde{s}_j\right],\\
\Phi_2(t\sim T) &= \sum_k e^{ik\varphi}\left[\int_{\mathcal{W}^<} \mathrm{d}\omega\, e^{-i\omega t} f^{\lambda'} V_{2j}\tilde{s}_j + \int_{\mathcal{W}^>} \mathrm{d}\omega\, e^{-i\omega t} f^{\lambda'}(\delta_{2j}+W_{2j})\tilde{s}_j\right].
\end{aligned} \tag{3.56}$$

Applying matching conditions The matching (3.53) conditions at $t=\pm T$ give:

$$W_{1j}=0\,,\qquad V_{2j}=0\,. \tag{3.57}$$

The matching condition (3.53) at $t=t_0$ in principle give a matching of sums over the residus of the *different* poles of f^λ and $f^{\lambda'}$. However, working to first order in $\delta\lambda=\lambda'-\lambda$, we can write:

$$f^{\lambda'} = f^\lambda + \frac{R^2}{r_+}\frac{4i\omega}{\lambda}\frac{\kappa_\lambda^2}{(1-\kappa_\lambda^2)^2}\big(f^+-f^-\big)\delta\lambda + O(\delta\lambda^2)\,. \tag{3.58}$$

Thus, at this order, it follows that the normal mode poles of f^λ and $f^{\lambda'}$ are the same (i.e. the solutions to $\kappa_\lambda^2=1$). We can denote ω_{nk}^+ to be the positive normal mode solutions of (3.40), where $n=1,2,\ldots$ labels successively larger solutions and $k\in\mathbb{Z}$. Similarly, we denote ω_{nk}^- to be the negative solutions of (3.40). Note that the $\mathcal{O}((\delta\lambda)^n)$ term in this expansion goes as $\sim(\omega\,\delta\lambda)^n$, so that the expansion breaks down for sufficiently large ω.

We define the following residues:

$$\begin{aligned}
\oint_{\omega_{nk}^\pm} \mathrm{d}\omega\,\frac{1}{1-\kappa_\lambda^2} &= \pm 2\pi\frac{1}{q_\lambda(\omega_{nk}^\pm,k)}\,,\\
\oint_{\omega_{nk}^\pm} \mathrm{d}\omega\,\frac{1}{(1-\kappa_\lambda^2)^2} &= \pm 2\pi\frac{A_\lambda(\omega_{nk}^\pm,k)}{q_\lambda(\omega_{nk}^\pm,k)}\,,
\end{aligned} \tag{3.59}$$

where the circular integral around ω^+_{nk} (resp. ω^-_{nk}) is defined to have negative (resp. positive) direction to conform with our definition of $\mathcal{W}^{\gtrless}$. The quantity $q_\lambda(\omega,k)$ is given by:

$$q_\lambda(\omega,k) = \frac{R^2}{r_+}\left[4\log\left(\frac{\lambda}{2}\right) + \psi\left(1+\frac{i}{2}(r_+\overline{\omega}-\overline{k})\right) + \psi\left(1-\frac{i}{2}(r_+\overline{\omega}-\overline{k})\right)\right.$$
$$-2\psi(1-ir_+\overline{\omega}) + \psi\left(1+\frac{i}{2}(r_+\overline{\omega}+\overline{k})\right)$$
$$\left.+\psi\left(1-\frac{i}{2}(r_+\overline{\omega}+\overline{k})\right) - 2\psi(1+ir_+\overline{\omega})\right]. \tag{3.60}$$

The quantity $A_\lambda(\omega,k)$ has a similar (but lengthier) expression in terms of polygamma functions.

Using the residues (3.59), the basis functions (to first order in $\delta\lambda$) (3.39) and (3.58), together with the Euclidean matching results (3.57), the behaviour of the fields (3.56) near $t\sim t_0$ can be rewritten as:

$$\Phi_1(t\sim t_0) = 2\pi\sum_k e^{ik\varphi}\left[-\sum_n e^{-i\omega^-_{nk}t}\frac{g^-(\omega^-_{nk},k,r)}{q_\lambda(\omega^-_{nk},k)}V_{1j}(\omega^-_{nk})\tilde{s}_j(\omega^-_{nk},k)\right.$$
$$\left.+\sum_n e^{-i\omega^+_{nk}t}\frac{g^-(\omega^+_{nk},k,r)}{q_\lambda(\omega^+_{nk},k)}\delta_{1j}\tilde{s}_j(\omega^+_{nk},k)\right],$$

$$\Phi_2(t\sim t_0) = 2\pi\sum_k e^{ik\varphi}\Bigg[$$

$$-\sum_n e^{-i\omega^-_{nk}t}\frac{g^-(\omega^-_{nk},k,r)}{q_\lambda(\omega^-_{nk},k)}\left(1+\frac{R^2}{r_+}\frac{4i\omega^-_{nk}}{\lambda}A_\lambda(\omega^-_{nk},k)\delta\lambda\right)\delta_{2j}\tilde{s}_j(\omega^-_{nk},k)$$

$$+\sum_n e^{-i\omega^+_{nk}t}\frac{g^-(\omega^+_{nk},k,r)}{q_\lambda(\omega^+_{nk},k)}\left(1+\frac{R^2}{r_+}\frac{4i\omega^+_{nk}}{\lambda}A_\lambda(\omega^+_{nk},k)\delta\lambda\right)W_{2j}(\omega^+_{nk})\tilde{s}_j(\omega^+_{nk},k)\Bigg], \tag{3.61}$$

where we used the definition (3.21) for g^-. Using these expressions, the matching condition (3.53) can now be performed separately for each of the (linearly independent) residue terms in the sum. This gives us the remaining contour-

correcting functions (to first order in $\delta\lambda$):

$$\begin{aligned} V_{1j}(\omega,k) &= \left(1+\frac{R^2}{r_+}\frac{4i\omega}{\lambda}A_\lambda(\omega,k)\delta\lambda\right)\delta_{2j}\,, \quad \omega<0\,,\\ W_{2j}(\omega,k) &= \left(1-\frac{R^2}{r_+}\frac{4i\omega}{\lambda}A_\lambda(\omega,k)\delta\lambda\right)\delta_{1j}\,, \quad \omega>0\,. \end{aligned} \tag{3.62}$$

Extracting the correlator Without loss of generality, we take one operator insertion to be at time $t<t_0$; then, as we slide the other operator insertion between $t'\in[-T,T]$, we obtain for the Feynman correlator:

$$\begin{aligned} iG^F_{\lambda\to\lambda'}(x,x') &= \theta(t_0-t')iG^{11}(x,x')+\theta(t'-t_0)iG^{12}(x,x')\\ &= \frac{1}{2\pi^2 i}\sum_k e^{ik(\varphi-\varphi')}\left[\theta(t_0-t')\int_{\mathcal{F}}\mathrm{d}\omega\, e^{-i\omega(t-t')}\alpha\beta^\lambda\right.\\ &\left.+\theta(t'-t_0)\int_{\mathcal{W}^<}\mathrm{d}\omega\, e^{-i\omega(t-t')}\alpha\beta^\lambda\left(1+\frac{R^2}{r_+}\frac{4i\omega}{\lambda}A_\lambda\delta\lambda\right)\right]. \end{aligned} \tag{3.63}$$

We can recast this result as

$$\begin{aligned} &iG^F_{\lambda\to\lambda'}(x,x')-iG^F_{\lambda\to\lambda}(x,x')=\\ &+\frac{\theta(t'-t_0)}{2\pi^2 i}\sum_k e^{ik(\varphi-\varphi')}\int_{\mathcal{W}^<}\mathrm{d}\omega\, e^{-i\omega(t-t')}\alpha\beta^\lambda\left(\frac{R^2}{r_+}\frac{4i\omega}{\lambda}A_\lambda\delta\lambda\right)\\ &-\frac{4R^2\theta(t'-t_0)}{\pi r_+}\frac{\delta\lambda}{\lambda}\sum_{n,k}e^{ik(\varphi-\varphi')}\left(e^{-i\omega(t-t')}\alpha(\beta^+-\beta^-)\frac{\omega A_\lambda}{q_\lambda}\right)\Big|_{\omega=\omega^-_{nk}}, \end{aligned} \tag{3.64}$$

where $iG^F_{\lambda\to\lambda}(x,x')$ is the Feynman propagator of a wormhole that retains the same parameter λ throughout the whole Lorentzian (and Euclidean) evolution, i.e. the propagator as follows from (3.50) and section 3.2.2. Note that this expression is in principle only valid where the expansion (3.58) is valid, so (as mentioned above after (3.58)), it cannot be trusted at arbitrary high frequencies. We will discuss the position-space propagator following from (3.64) in section 3.4.3.

3.3 Retarded wormhole correlator via hybrid WKB

In this section we aim to apply the hybrid WKB technique, developed by in [41], to the wormhole toy model.[8] Our goal is to obtain the free scalar retarded correlator for the non-rotating wormhole and compare this WKB result to the real-time holography result we obtained above in (3.50). We will write this retarded propagator as:

$$iG^R(\Delta t, \Delta\varphi) = \frac{\theta(\Delta t)}{2\pi^2 i} \sum_k \int_{\mathbb{R}+i\epsilon} \mathrm{d}\omega \, e^{-i\omega\Delta t + ik\Delta\varphi} \mathcal{R}(\omega, k)\,, \tag{3.65}$$

with $\Delta t = t - t'$ and $\Delta\varphi = \varphi - \varphi'$. The hybrid WKB technique will then give us $\mathcal{R}(\omega, k)$.

The hybrid WKB approximation works in a number of steps. First, we apply the traditional WKB method to find an approximate solution to the wave equation. In order to proceed with finding the WKB approximation to the propagator, one needs to analyze the asymptotic structure of the approximate solution around the boundary. This is generally a hard task as the WKB solution is not written in a basis that is conducive to asymptotic analysis. Thus, in the second step of the method, one finds a new potential that asymptotically approaches the original potential and for which the wave equation can be solved exactly. Then, the WKB solutions can be matched to the asymptotic solutions, which finally allows one to efficiently analyze the asymptotic structure of the approximate solutions to the wave equation and ultimately extract the propagator.

3.3.1 Calculation of the WKB propagator

We will now apply the hybrid WKB method step-by-step to a free scalar in the (non-rotating) wormhole background with metric (3.4).

Setting up the radial equation and potential We wish to split the radial part of the scalar as:

$$\Phi_r(r) = h(r)\phi(r)\,, \tag{3.66}$$

and we perform a coordinate transformation $r \to x(r)$ to write the radial wave equation (3.8) for ϕ in the Schrödinger form:

$$\frac{\partial^2}{\partial x^2}\phi(x) - V(x)\phi(x) = 0\,. \tag{3.67}$$

[8] This method was used in [36] in an asymptotically flat setting; we also used this method in our previous chapter [110] to calculate correlators for the extremal BTZ wormhole.

The absence of a term proportional to $\partial_x \phi$ leads to the condition:

$$h(r) = \frac{1}{\left(r^2 X(r) Y(r) \left(\frac{\partial x(r)}{\partial r}\right)^2\right)^{1/4}} . \tag{3.68}$$

We are still free to choose $x(r)$, which will affect the form of the potential $V(x)$. To align with the analysis in [41], we choose $x(r)$ such that the potential approaches a particular constant in the UV:

$$\lim_{x\to\infty} V(x) = 1 + m^2 R^2 \equiv \mu^2 . \tag{3.69}$$

where we have defined the dimensionless parameter μ. This can be achieved by fixing the function $x(r)$ such that:

$$h(r) = \frac{R}{r} . \tag{3.70}$$

A choice of $x(r)$ that satisfies (3.68) and (3.70) is:

$$x(r) = \log\left(\sqrt{\frac{r^2 - r_\lambda^2}{r_\lambda^2}} + \sqrt{\frac{r^2 - r_+^2}{r_\lambda^2}}\right) - \log\lambda , \tag{3.71}$$

Note that $x(r_+) = 0 + \mathcal{O}(\lambda^2)$.[9] The x coordinate spans the whole wormhole and ranges from $-\infty$ to ∞. The relation between $x(r)$ and r can be inverted to find

$$r^2 = r_\lambda^2 \left(1 + \frac{\lambda^2}{4(1-\lambda^2)^2}(e^{-x} + e^x(1-\lambda^2))^2\right) = r_+^2 \left(1 + \lambda^2 \sinh^2 x\right) + O(\lambda^4) . \tag{3.72}$$

The potential now takes a relatively simple form in terms of the radial coordinate x:

$$V(r(x)) = \mu^2 + \frac{R^2}{r^2}\left(k^2 - m^2 r_\lambda^2 - R^2\omega^2\right) - \frac{r_\lambda^2}{r^4}\left(k^2 R^2 + r_+^2\right) . \tag{3.73}$$

Figure 3.7 is a plot of the potential for different values of λ. The potential approaches μ^2 in the UV and at the throat position[10] $x = 0$ we find:

$$V(x=0) = -\frac{\omega^2 R^4}{r_+^2} + O\left(\lambda^2\right) , \tag{3.74}$$

[9] We could have also chosen e.g. $x(r_t) = 0 + O(\lambda^2)$; this would introduce an extra constant term $-\log 1/2(1+\sqrt{5})$ in (3.71). Such a constant does not change the derivation of the end result (3.90).

[10] We saw above that at the throat position $r = r_+$, we actually have $x = O(\lambda^2)$ instead of $x = 0$; however (3.74) will still be the value of the potential at the throat position to $O(\lambda^2)$.

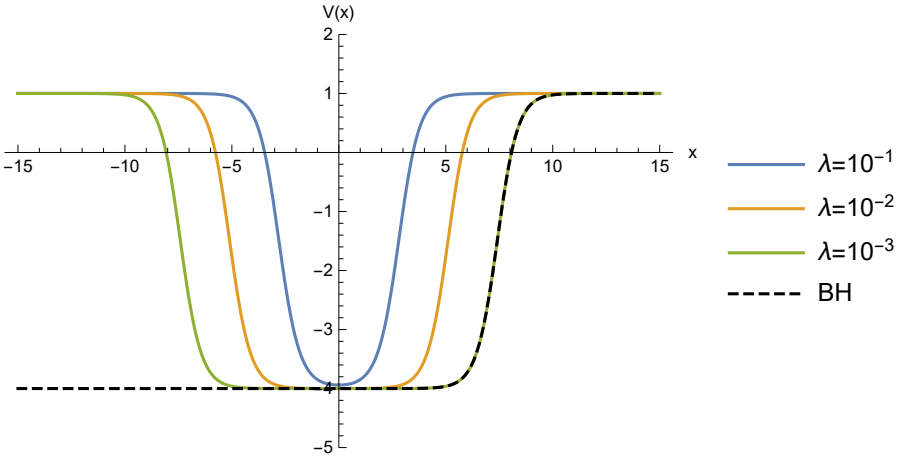


Figure 3.7: The potential $V(x)$ plotted as a function of x with for $\mu = 1, k = 1, \omega = 2, r_\lambda = 1$, and $\lambda = \{10^{-1}, 10^{-2}, 10^{-3}\}$. As λ decreases, the width of the potential becomes larger and larger. The black hole potential is also depicted, shifted to line up with the $\lambda = 10^{-3}$ graph for $x > 0$.

The following condition needs to be met in order for the WKB approximation to be valid

$$\left|(V(x))^{-\frac{3}{2}} \frac{\partial V(x)}{\partial x}\right| \ll 1\,. \tag{3.75}$$

This quantity should be evaluated away from the turning points, defined by $V(x_{\text{turn}}) = 0$, where the left side diverges. Expanding the left hand side of (3.75) for small λ, we find:

$$\left|(V(x))^{-\frac{3}{2}} \frac{\partial V(x)}{\partial x}\right| = \lambda^2 \left|\frac{r_+}{R^6\omega^3}(k^2R^2 + r_+^2(1+\mu^2) + \omega^2R^4)\sinh 2x\right| + \mathcal{O}(\lambda^4)\,. \tag{3.76}$$

The prefactor of λ^2 ensures that (3.75) is satisfied around the throat position (as long as the frequency is sufficiently high (e.g. $\omega R \gg \lambda$).

Asymptotic solutions Applying the same procedure outlined above to the non-rotating BTZ black hole metric (3.1) gives as black hole x coordinate:

$$x^{\text{BH}}(r) = \log\sqrt{\frac{r^2}{r_+^2} - 1}, \tag{3.77}$$

and potential:

$$V_{\rm asymp}(x) = \frac{e^{2x}}{(1+e^{2x})^2}\left(1+\frac{k^2R^2}{r_+^2}-\frac{\omega^2R^4\left(1+e^{-2x}\right)}{r_+^2}+\mu^2\left(1+e^{2x}\right)\right). \tag{3.78}$$

Now, the wormhole potential is well approximated by:

$$V(x) = \theta(x)V_{\rm asymp}(x+\log(\lambda/2)) + (x\to -x) + \mathcal{O}(\lambda^2)\,, \tag{3.79}$$

where the shift in argument by $\log(\lambda/2)$ comes from comparing the wormhole x^{WH} coordinate (3.71) and the black hole x^{BH} coordinate (3.77) at the matching radius $r = r_t = r_+(1+\lambda^2/8)$ (see (3.12)); i.e. we have $x^{WH} = \mathcal{O}(\lambda^2)$ and $x^{BH} = \log(\lambda/2)$. Physically, this shift in (3.79) for the x coordinate arises from the wormhole of length L_λ opening up. The expression (3.79) thus nicely encapsulates that for small λ, we get two copies of the BTZ potential connected by a wormhole of length L_λ.

The exact solutions $\phi_{\rm asymp}(x)$ are the well-known solutions to the BTZ wave equation (3.16), which we repeat here in the x coordinate:

$$\begin{aligned}\phi_{\rm asymp}(x) = &\sum_{\pm} c_\pm \left(1+e^{2x}\right)^{\frac{1}{2}-\frac{ikR}{2r_+}} e^{\pm\frac{i\omega R^2 x}{r_+}}\times\\ &{}_2F_1\left(\frac{1-\mu}{2}-iR\frac{k\mp\omega R}{2r_+},\frac{1+\mu}{2}-iR\frac{k\mp\omega R}{2r_+};1\pm\frac{i\omega R^2}{r_+};-e^{2x}\right).\end{aligned} \tag{3.80}$$

This general solution (3.80) has the structure:

$$\phi_{\rm asymp}(x) = c_1\phi^{\rm grow}_{\rm asymp}(x) + c_2\phi^{\rm dec}_{\rm asymp}(x)\,, \tag{3.81}$$

where in the UV we have defined the two linearly independent solutions as those that behave at large x as:[11]

$$\begin{aligned}\phi^{\rm grow}_{\rm asymp}(x) &= e^{\mu x}\left(1+\dots\right)\\ \phi^{\rm dec}_{\rm asymp}(x) &= e^{-\mu x}\left(1+\dots\right),\end{aligned} \tag{3.82}$$

where the omitted terms are subleading in x at large x. When μ is an integer, there are also pieces proportional to x in the UV expansion; we will assume μ not to be an integer and analytically continue the final result to integer μ (as we are interested in $\mu = 1$). Note that both $\phi^{\rm grow}_{\rm asymp}$ and $\phi^{\rm dec}_{\rm asymp}$ are real functions of x (for real r_+, k, ω, μ, R).

[11] Note that the full radial function Φ_r in (3.7) is still given by $\Phi_r(r) = \phi(x)R/r$.

Calculation of the WKB propagator Now we have all ingredients to evaluate the propagator that follows from the hybrid WKB technique. According to [41] the propagator is given by

$$\mathcal{R}_{\rm WKB} = \left(\mathcal{A} + \frac{\sqrt{3}}{2}\right) e^{-2I_+} - \frac{\phi^{\rm grow}_{\rm asymp}(x_+)}{\phi^{\rm dec}_{\rm asymp}(x_+)}\,. \tag{3.83}$$

where

$$I_+ = -\mu x_+ + \int_{x_+}^{\infty} \left(\sqrt{|V(z)|} - \mu\right) dz\,, \tag{3.84}$$

and the turning points $x_\pm$ are defined such that $V(x_\pm) = 0$. The expression for $\mathcal{A}$ depends on the number of turning points. For a single turning point, we have

$$\mathcal{A} = \text{sign}(\omega)\frac{i}{2}\,. \tag{3.85}$$

For two turning points x_- and x_+, we have

$$\begin{aligned} \mathcal{A} &= \frac{1}{2}\tan(\Theta)\,, \\ \Theta &= \int_{x_-}^{x_+} \sqrt{|V(z)|}dz\,. \end{aligned} \tag{3.86}$$

This will be the formula we will need to evaluate to find the wormhole propagator. The general expression for $\mathcal{A}$ for more than two turning points can be found in an appendix of [41].

It is useful to first apply the WKB approximation to the (non-rotating) BTZ black hole itself. The BTZ potential has only one turning point, so one finds

$$\mathcal{R}^{\rm BH}_{\rm WKB} \approx \left(\frac{i}{2}\text{sign}(\omega) + \frac{\sqrt{3}}{2}\right) e^{-2I_+} - \frac{\phi^{\rm grow}_{\rm asymp}(x_+)}{\phi^{\rm dec}_{\rm asymp}(x_+)}\,. \tag{3.87}$$

As noted earlier, the exact solutions $\phi^{\rm grow,dec}_{\rm asymp}$ are real and so is I_+. This allows us to write

$$\begin{aligned} \text{Re}\left(\mathcal{R}^{\rm BH}_{\rm WKB}\right) &\approx \frac{\sqrt{3}}{2}e^{-2I_+} - \frac{\phi^{\rm grow}_{\rm asymp}(x_+)}{\phi^{\rm dec}_{\rm asymp}(x_+)}\,, \\ \text{Im}\left(\mathcal{R}^{\rm BH}_{\rm WKB}\right) &\approx \frac{1}{2}\text{sign}(\omega)e^{-2I_+}\,. \end{aligned} \tag{3.88}$$

The wormhole potential is essentially two copies of the black hole potential, leading to two turning points, so $\mathcal{A}$ will differ with respect to the BTZ propagator

(3.87). However, due to (3.79) we can see that $I_+^{\text{wormhole}} = I_+^{\text{BH}} + \mathcal{O}(\lambda^2)$, and thus we can write

$$\mathcal{R}_{\text{WKB}}^{\text{WH}} \approx \text{Re}\left(\mathcal{R}^{\text{BH}}\right) + 2\,\text{sign}(\omega)\,\mathcal{A}\,\text{Im}\left(\mathcal{R}^{\text{BH}}\right)\,, \tag{3.89}$$

where $\approx$ now denotes both inaccuracy due to the WKB approximation and corrections of order λ^2. Now, we need to evaluate $\mathcal{A}$ or equivalently Θ:

$$\begin{aligned}\Theta &= \int_{x_-}^{x_+} \sqrt{|V_{\text{asymp}}(z)|}dz + \mathcal{O}(\lambda^2) \\ &= \left|\log\left[e^{-\frac{1}{2}(\pi\mu)}\left(\frac{16\omega^2R^2}{\lambda^2}\right)^{\omega R^2/r_+}\left(-\frac{r_+^2\left(\mu^2+1\right)+2ir_+\mu\omega R^2+k^2R^2-\omega^2R^4}{r_+^2\left(\mu^2+1\right)-2ir_+\mu\omega R^2+k^2R^2-\omega^2R^4}\right)^{i\mu/2}\right.\right. \\ &\left(-2\omega^2\left(k^2R^2-r_+^2\left(\mu^2-1\right)\right)+\left(\frac{r_+^2}{R^2}\left(\mu^2+1\right)+k^2\right)^2+\omega^4R^4\right)^{\frac{\sqrt{r_+^2+k^2R^2}-\omega R^2}{2r_+}} \\ &\left.\left.\left(\omega\left(2\sqrt{r_+^2+k^2R^2}+\omega R^2\right)+\frac{r_+^2}{R^2}\left(\mu^2+1\right)+k^2\right)^{-\frac{\sqrt{r_+^2+k^2R^2}}{r_+}}\right]\right| + \mathcal{O}(\lambda^2)\,.\end{aligned} \tag{3.90}$$

This expression simplifies in the "low-frequency" limit (3.41), $\omega \sim L_\lambda^{-1}$ (where wormhole throat length L_λ is defined in (3.5)), and in the "high-frequency" limit (3.43), $\omega \gg r_+/R^2$. In both cases, the expression that we get is (for $\mu = 1$, and subtracting integer multiples of π):

$$\Theta = |\omega\, L_\lambda|\ . \tag{3.91}$$

We discarded terms of $O(\lambda^2)$ as well as terms of $O(\lambda^0\omega)$ as they will always be subleading. We can understand this expression for Θ as follows: when L_λ becomes very large (λ is exponentially small), the wormhole throat contribution dominates the integral in (3.90). Since the potential is very flat for (almost) the entire wormhole, as can be seen from (3.79) and figure 3.7, we can approximate the integral by:

$$\begin{aligned}\Theta &\approx \sqrt{|V(0)|}\,L_\lambda + \mathcal{O}(\lambda^0) \\ &= |\omega\, L_\lambda| + \mathcal{O}(\lambda^0)\,,\end{aligned} \tag{3.92}$$

where we used the value of $V(0)$ in (3.74). The result is indeed in agreement with the direct evaluation (3.91).

3.3.2 Hybrid WKB vs. real time holography

For the non-rotating BTZ black hole, we calculated the black hole retarded scalar correlator using real-time holography in section 3.2.1 as:

$$\mathcal{R}^{\rm BH} = \alpha\beta^- \,, \tag{3.93}$$

Using the fact that $(\alpha\beta^\pm)^* = \alpha\beta^\mp$, we note that:

$$\mathrm{Re}\big(\mathcal{R}^{\rm BH}\big) = \frac{1}{2}(\alpha\beta^+ + \alpha\beta^-)\,, \qquad \mathrm{Im}\big(\mathcal{R}^{\rm BH}\big) = \frac{i}{2}(\alpha\beta^+ - \alpha\beta^-)\,. \tag{3.94}$$

For the corresponding non-rotating Solodukhin wormhole, in section 3.2.2 we calculated:

$$\mathcal{R}^{\rm WH} = \frac{1}{1-\kappa^2}\alpha\beta^+ - \frac{\kappa^2}{1-\kappa^2}\alpha\beta^- = \mathrm{Re}\big(\mathcal{R}^{\rm BH}\big) - i\,\frac{1+\kappa^2}{1-\kappa^2}\mathrm{Im}\big(\mathcal{R}^{\rm BH}\big)\,, \tag{3.95}$$

where κ is given by (3.39) (and (3.18)). Noting that $|\kappa| = 1$, we can define the angle η through:

$$\kappa \equiv ie^{-i\eta}\,, \tag{3.96}$$

so that (3.95) becomes:

$$\mathcal{R}^{\rm WH} = \mathrm{Re}\big(\mathcal{R}^{\rm BH}\big) + \tan\eta\,\mathrm{Im}\big(\mathcal{R}^{\rm BH}\big)\,, \tag{3.97}$$

As an aside, we note that, curiously, there is a simple way to go from the black hole to wormhole correlator in the large frequency limit: one simply does an "analytic continuation" of the inverse temperature β to the travel time Δt, where $\Delta t = 2L_\lambda$ in the wormhole. Then $e^{-\beta\omega} \to e^{-i\Delta t\omega}$, so the "information losing" factor becomes an oscillatory factor which shows the recovery of information in a time Δt.

The real-time holography result (3.97) is to be compared to the full WKB answer for the propagator (where we set $\mu = 1$), which we derived in the previous section:

$$\mathcal{R}^{\rm WH}_{\rm WKB} \approx \mathrm{Re}\left(\mathcal{R}^{\rm BH}\right) + (\mathrm{sign}(\omega)\tan\Theta)\ \mathrm{Im}\left(\mathcal{R}^{\rm BH}\right)\,, \tag{3.98}$$

where Θ is given by (3.90).

Comparison Comparing (3.98 to (3.97), we see that the WKB approximation does a good job of capturing the propagator when $\Theta \approx \eta$ (for $\omega > 0$).

In the low-frequency regime (3.41), we have:

$$\eta \approx \omega L_\lambda + \frac{\pi}{2}\,, \qquad \Theta \approx \omega L_\lambda\,, \tag{3.99}$$

so that the mismatch is maximal at low frequencies.[12] On the other hand, in the high-frequency regime (3.43), expanding upon (3.91):

$$\begin{aligned}\eta &\approx \omega L_\lambda + \frac{1}{2}\left(\frac{R^2}{r_+}\omega\right)^{-1} - \frac{5}{864}\left(\frac{R^2}{r_+}\omega\right)^{-3} + \mathcal{O}(\omega^{-5})\,,\\ \Theta &\approx \omega L_\lambda + \frac{2}{3}\left(\frac{R^2}{r_+}\omega\right)^{-3} + \mathcal{O}(\omega^{-7})\,.\end{aligned} \tag{3.100}$$

Thus, we see that the the propagators start differing in the high-frequency regime at $\mathcal{O}(\omega^{-1})$. We give an example of the difference between η and Θ in figure 3.8; for large wormhole throat lengths L_λ, we see that the (large) mismatch is only at very low frequencies so that Θ asymptotes to η rather quickly. Thus, we can conclude that the hybrid WKB approximation captures the wormhole propagator quantitatively very well.

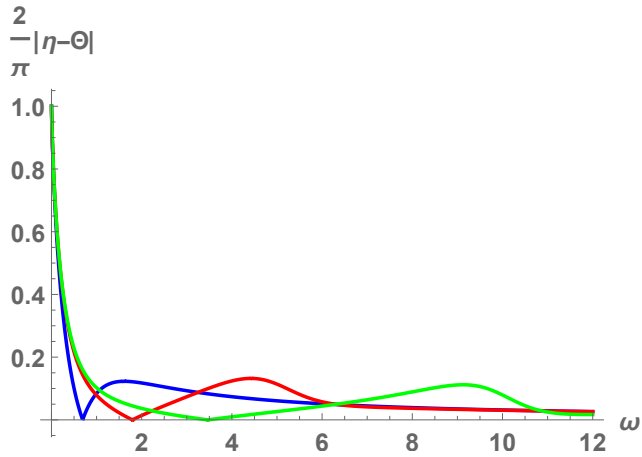


Figure 3.8: A plot of $(2/\pi)\,|(\eta - \Theta) \mod \pi|$ as a function of ω. We take $R = r_+ = 1$, and $\lambda = 10^{-20}$ ($L_\lambda \approx 94.88$). The blue, red, and green lines respectively correspond to $k = 0, 5, 10$. The mismatch starts out maximally at $\pi/2$ (see (3.99)) but asymptotes (quickly) to zero (see (3.100)).

[12] Note that we must actually take the entire WKB approximation with a grain of salt for small ω, as mentioned above around (3.76). Small frequencies should be treated separately, see [41].

3.4 Position-space correlators

In this section, we will integrate explicitly the frequency-space propagators found in section 3.2 to obtain the position-space propagators for both the (non-rotating) BTZ black hole and the corresponding Solodukhin wormhole. We will also present the position-space correlator and interpretation thereof for the "wormhole transition" correlator of section 3.2.3.

We repeat the general relation (3.65) between the frequency space retarded propagator $\mathcal{R}$ and the position-space one, valid for all of the correlators we are considering:

$$iG^R(\Delta t, \Delta\varphi) = \frac{\theta(\Delta t)}{2\pi^2 i} \sum_k \int_{\mathbb{R}+i\epsilon} \mathrm{d}\omega\, e^{-i\omega\Delta t + ik\Delta\varphi} \mathcal{R}(\omega, k)\,. \tag{3.101}$$

Note that compared to (3.35) or (3.50), we have set $\Delta t = t - t'$ and $\Delta\varphi = \varphi - \varphi'$.

3.4.1 Black hole correlator

To calculate the position-space retarded propagator for the BTZ black hole, we need to consider the contributions from G^{LL} and G^{RR} separately. We refer to appendix A of [66] for details of this calculation; here, we review this derivation briefly.

Starting with G^{LL} in (3.34), we take $t > t'$ and thus close the ω integral in the lower half plane. The functions α and β^+ have no poles here, while we pick up the residues of the poles $\omega^-_{nk\pm}$ given in (3.20) of β^-. Note that $n_\omega = (e^{\beta\omega} - 1)^{-1}$ also has (purely imaginary) poles at $\omega = 2\pi\beta^{-1} in$ for $n \in \mathbb{Z}$ (depicted by circles on figure 3.3). As discussed in [66], in principle one needs to take the residues of these poles into account as well, but since they end up giving a zero contribution in the final result, we will omit them here. Then we get:

$$iG^{LL}(\Delta t, \Delta\varphi) = -\frac{2}{\pi i}\frac{r_+}{R^2} \sum_{k\in\mathbb{Z}} \sum_{n=1}^{\infty} \sum_{\pm} e^{ik(\Delta\varphi \mp \frac{\Delta t}{R})} e^{-2\frac{r_+}{R^2} n\Delta t} \alpha(\omega^-_{nk\pm}) \frac{e^{\beta\omega^-_{nk\pm}}}{e^{\beta\omega^-_{nk\pm}} - 1}\,. \tag{3.102}$$

To evaluate the k sum, we use the Poisson resummation formula:[13]

$$\sum_k f(k) = \sum_m \int dk f(k) e^{2\pi k m i}\,, \tag{3.106}$$

[13]For a periodic function $\tilde{f}(x) = \tilde{f}(x + 2\pi n)$, we can write the two expansions:

$$\tilde{f}(x) = \sum_{n\in\mathbb{Z}} C_n e^{inx}, \qquad \tilde{f}(x) = \frac{1}{2\pi}\int dk f(k) e^{ikx}\,, \tag{3.103}$$

to rewrite the sum over k in (3.102) as an integral over k and a "sum over images" m:

$$iG^{LL}(\Delta t,\Delta\varphi)=-\frac{2}{\pi i}\frac{r_+}{R^2}\sum_{m\in\mathbb{Z}}\sum_{n=1}^{\infty}\sum_{\pm}\int dk\, e^{ik(\Delta\varphi\mp\frac{\Delta t}{R}+2\pi m)}e^{-2\frac{r_+}{R^2}n\Delta t}\times$$

$$\alpha(\omega^-_{nk\pm})\frac{e^{\pm 2\pi\frac{R}{r_+}k}}{e^{\pm 2\pi\frac{R}{r_+}k}-1}\,, \tag{3.107}$$

where we used $\beta=2\pi R^2/r_+$. To regulate this integral as $k\to\pm\infty$, we must send $\Delta t\to\Delta t(1-i\epsilon)$ with $\epsilon>0$; this regulates both ends of the integral for both the terms with $\pm$ in (3.107). Then, for $\Delta\varphi\mp\Delta t/R<0$, we can close this k integral in the lower half plane. Only the factors $(e^{\pm 2\pi R/r_+k}-1)^{-1}$ have poles (when $k=-i\,l\,r_+/R$ for $l\in\mathbb{Z}$), and so we pick up the residus:

$$iG^{LL}(\Delta t,\Delta\varphi)=\frac{2}{\pi}\frac{r_+^2}{R^3}\sum_{m\in\mathbb{Z}}\sum_{n=1}^{\infty}\sum_{l=1}^{\infty}\sum_{\pm}\pm\, e^{l\frac{r_+}{R}(\Delta\varphi\mp\frac{\Delta t}{R}(1-i\epsilon)+2\pi m)}\times$$

$$e^{-2\frac{r_+}{R^2}n\Delta t(1-i\epsilon)}n(n\pm l)\,. \tag{3.108}$$

We can explicitly perform the sum over the two terms with $\pm$ as well as the infinite sums over n,l, resulting in:

$$iG^{LL}(\Delta t,\Delta\varphi)=\frac{1}{2\pi}\frac{r_+^2}{R^3}\sum_{m\in\mathbb{Z}}\frac{1}{\left(\cosh\left[\frac{r_+}{R^2}\Delta t(1-i\epsilon)\right]-\cosh\left[\frac{r_+}{R}(\Delta\varphi+2m\pi)\right]\right)^2}\,, \tag{3.109}$$

which agrees with [66]. Even though (3.109) was derived for $\Delta\varphi\mp\Delta t/R<0$, it can be analytically continued outside of this region.

To calculate G^{RR}, we again start with (3.34) and proceed analogously. The only difference is that to regulate the resulting k integral, we will need to send $\Delta t\to\Delta t(1+i\epsilon)$.[14] Thus, we indeed find $iG^{RR}=[iG^{LL}]^*$. The retarded

and one finds the relation between the two expansions:

$$f(k)=\int dx\tilde{f}(x)e^{-ikx}=\sum_n C_n\delta(n-k)\,, \tag{3.104}$$

so that, using $\sum_k\delta(k-n)=\sum_m e^{2\pi mni}$:

$$\sum_k f(k)=\sum_n C_n\sum_m e^{2\pi mni}=\sum_m\tilde{f}(2\pi m)=\sum_m\int dk' f(k')e^{2\pi kmi}\,. \tag{3.105}$$

[14]The origin of this difference in regulator is that in G^{RR} in (3.34), β^- is multiplied by n instead of $(n+1)$ as it is in G^{LL}.

propagator is then given by (3.35), i.e.:

$$iG^R_{\rm BH}(\Delta t,\Delta\varphi)=\frac{\theta(\Delta t)}{2\pi}\frac{r_+^2}{R^3}\sum_{m\in\mathbb{Z}}\left[\frac{1}{\left(\cosh\left[\frac{r_+}{R^2}\Delta t(1-i\epsilon)\right]-\cosh\left[\frac{r_+}{R}(\Delta\varphi+2m\pi)\right]\right)^2}\right.$$
$$\left.-\frac{1}{\left(\cosh\left[\frac{r_+}{R^2}\Delta t(1+i\epsilon)\right]-\cosh\left[\frac{r_+}{R}(\Delta\varphi+2m\pi)\right]\right)^2}\right]. \qquad (3.110)$$

A plot of this correlator is given in figure 3.9.

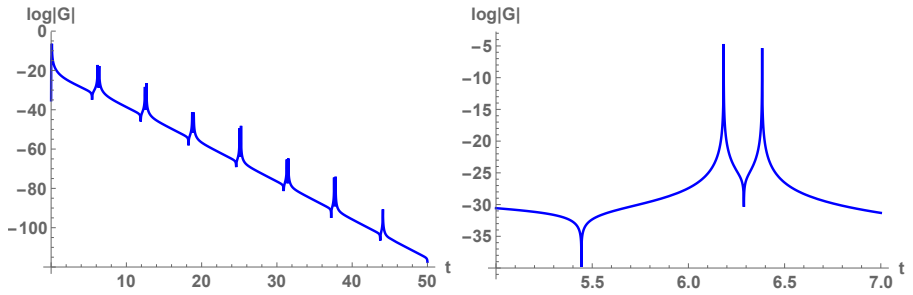


Figure 3.9: The black hole correlator $G^R_{\rm BH}(\Delta t,\Delta\varphi=0.1)$ as given in (3.110). We take $R=r_+=1$ and $\epsilon=10^{-10}$. The correlator decays exponentially for $t>0$; note that each subsequent (small) peak at $t>0$ come from the contribution of an "image" $m>0$. The "double-peak" structure (apparent from the close-up on the right) is typical for $\Delta\varphi\neq 0$.

3.4.2 Three ways to the wormhole correlator

For the wormhole position-space propagator (3.97), we will first illustrate its basic properties using a quick and dirty, "naive" calculation. We will show the expressions for the actual wormhole propagator and attempt a numerical evaluation of this. Finally, we will simplify the wormhole by altering its matching condition to be frequency-dependent, which will allow us to integrate the propagator analytically.

Naive high-frequency calculation

In the high-frequency limit (3.100), $\eta\approx\omega L_\lambda$ thus the correlator (3.97) simplifies to:

$$\mathcal{R}^{\rm WH}\approx{\rm Re}\big(\mathcal{R}^{\rm BH}\big)+\tan(\omega L_\lambda){\rm Im}\big(\mathcal{R}^{\rm BH}\big)\,, \qquad (3.111)$$

Note that the poles of $\tan \omega L_\lambda$ indeed correspond to the normal modes (3.44) in this regime.[15]

A naive way to evaluate the wormhole propagator approximately would then be to use the distributional identity:

$$\tan x = \sum_{n=1}^{\infty} 2(-1)^{n-1} \sin(2nx)\,, \tag{3.112}$$

and its Fourier transform:

$$\begin{aligned}\mathcal{F}(t) &\equiv \frac{1}{2\pi}\int d\omega e^{-i\omega t}\tan \omega L_\lambda \\ &= i\sum_{n=1}^{\infty}(-1)^{n-1}\left(\delta(t+2nL_\lambda)-\delta(t-2nL_\lambda)\right)\,,\end{aligned} \tag{3.113}$$

Then, using the convolution theorem for Fourier transforms on the high-frequency retarded propagator (3.111):

$$G^R_{\rm WH}(\Delta t,\Delta\varphi) \approx G^0(\Delta t,\Delta\varphi) + (G^1 * \mathcal{F})(\Delta t,\Delta\varphi)\,, \tag{3.114}$$

$$G^0(\Delta x) \equiv -\frac{\theta(\Delta t)}{2\pi^2}\sum_k e^{ik\Delta\varphi}\int d\omega e^{-i\omega\Delta t}{\rm Re}(\mathcal{R}^{\rm BH})\,,$$

$$G^1(\Delta x) \equiv -\frac{\theta(\Delta t)}{2\pi^2}\sum_k e^{ik\Delta\varphi}\int d\omega e^{-i\omega\Delta t}{\rm Im}(\mathcal{R}^{\rm BH})\,,$$

so that $G^R_{\rm BH}(\Delta t,\Delta\varphi) = G^0(\Delta t,\Delta\varphi) + iG^1(\Delta t,\Delta\varphi)$, and the convolution gives:

$$\begin{aligned}(G^1 * \mathcal{F})(\Delta t,\Delta\varphi) &= i\sum_{n=1}^{\infty}(-1)^{n-1}\int dt' G^1(\Delta t - t',\Delta\varphi)\left(\delta(t'+2nL_\lambda)-\delta(t'-2nL_\lambda)\right) \\ &= i\sum_{n=1}^{\infty}(-1)^{n-1}\left(G^1(\Delta t+2nL_\lambda)-G^1(\Delta t-2nL_\lambda)\right)\,,\end{aligned} \tag{3.115}$$

[15] Note that if one tries to calculate the position-space retarded propagator using (3.101) and (3.111), in addition to the contributions from residus around the (approximated) normal modes of the wormhole coming from the poles of $\tan(\omega L_\lambda)$, there are also contributions from the residus of poles of $\alpha\beta^-$ (i.e. the quasinormal modes of the original BTZ black hole). This is an artifact of the approximation used to obtain (3.111), which is only valid in a particular regime for *real* ω. The exact result (3.97) does not have any poles off the real axis; (3.111) is not valid in the entire complex plane.

so that we have the relation:

$$G^R_{\rm WH}(\Delta t, \Delta\varphi) \approx G^0(\Delta t, \Delta\varphi) + i\sum_{n\in\mathbb{Z}}(-1)^n \mathrm{sgn}(n) G^1(\Delta t - 2nL_\lambda)\,, \quad (3.116)$$

where we define the $n = 0$ term of the sum to be $G^1(\Delta t)$ — although note that the Fourier transform of the tan, as naively calculated above, does not contain this $n = 0$ term.

From the expression (3.116), we can clearly see the appearance of "echoes" in the propagator, i.e. recurrences at periodic intervals $2L_\lambda$ of the correlator. Thus, at early times $0 < \Delta t \ll L_\lambda$, the propagator will mimic the BTZ one (3.110) and decay exponentially; only at a time $\Delta t \sim L_\lambda$ will the propagator start to differ qualitatively from the black hole one due to the appearance of the first echo. This is the most important property of the wormhole propagator that we wish to highlight; we will confirm this qualitative echo behavior of (3.116) below in a (numerical) calculation of the full propagator (3.97), and also (analytically) in a frequency-dependent wormhole alteration.

Full propagator

The derivation of (3.116) was rather imprecise; for example, we did not take care of the correct contour for the ω integration in (3.101), and we resorted to the approximation of the full propagator (3.97) by the high-frequency regime expression (3.111).

Calculating the full retarded propagator (3.97) is difficult as we do not have an analytic expression for the propagator's poles. As discussed in section 3.3.2, these poles are only located on the real axis (i.e. they are normal modes) and are given at the location where $\kappa = \pm 1$ with κ given in (3.39) and (3.18). Note that κ satisfies the following properties:

$$|\kappa| = 1\,, \qquad [\kappa(\omega, k)]^* = \kappa(-\omega, k)\,, \qquad \kappa(\omega, k) = \kappa(\omega, -k)\,. \quad (3.117)$$

For a fixed $k \in \mathbb{Z}$, we can denote the positive normal modes as ω^+_{nk} with $n = 1, 2, \cdots$ and $n = 1$ corresponding to the first (strictly) positive normal mode. Similarly, ω^-_{nk} are the negative normal modes. From the properties (3.117), it follows that $\omega^-_{nk} = -\omega^+_{nk}$ and also $\omega^\pm_{n(-k)} = \omega^\pm_{nk}$, for any n, k. Therefore, we can choose to express everything in terms of $k \geq 0$ and ω^+_{nk}.

Evaluating the ω integral by closing in the lower half plane then gives:

$$iG^R_{\rm WH}(\Delta t,\Delta\varphi)=\frac{\theta(\Delta t)}{2\pi^2 i}\Bigg[\tag{3.118}$$
$$\sum_{k=0}^{\infty}\sum_{n=1}^{\infty}e^{-i\omega^+_{nk}\Delta t+ik\Delta\varphi}\mathcal{G}(k,\omega^+_{kn})-\sum_{k=0}^{\infty}\sum_{n=1}^{\infty}e^{+i\omega^+_{nk}\Delta t+ik\Delta\varphi}\mathcal{G}(k,\omega^+_{kn})$$
$$+\sum_{k=1}^{\infty}\sum_{n=1}^{\infty}e^{-i\omega^+_{nk}\Delta t-ik\Delta\varphi}\mathcal{G}(k,\omega^+_{kn})-\sum_{k=1}^{\infty}\sum_{n=1}^{\infty}e^{+i\omega^+_{nk}\Delta t-ik\Delta\varphi}\mathcal{G}(k,\omega^+_{kn})\Bigg],$$

with

$$\mathcal{G}(k,\omega)\equiv\frac{i\pi^2}{2r_+}\frac{(k^2-R^2\omega^2)\sum_\pm\pm\coth\left(\pi\frac{R}{2r_+}(k\pm R\omega)\right)}{\sum_\pm\left[-2\psi\left(\pm i\frac{R^2}{r_+}\omega\right)+\psi\left(i\frac{R}{2r_+}(k\pm R\omega)\right)+\psi\left(i\frac{R}{2r_+}(-k\pm R\omega)\right)\right]}, \tag{3.119}$$

where we used that $\mathcal{G}(k,\omega)=\mathcal{G}(-k,\omega)=-\mathcal{G}(k,-\omega)$. We split the k,n sums (each) into positive and negative frequency parts. Then, to evaluate these four sums directly, we put regulators by changing:

$$e^{\mp i\omega^+_{nk}\Delta t}\to e^{\mp i\omega^+_{nk}\Delta t(1\mp i\epsilon)}\,,\qquad e^{\pm ik\Delta\varphi}\to e^{\pm ik\Delta\varphi(1\pm i\epsilon)}\,, \tag{3.120}$$

which gives the correct regulation of all four sums for $\Delta t,\Delta\varphi>0$. Then, we can numerically evaluate the four sums in (3.118) to a given cut-off value n_{max},k_{max}, see figure 3.10. Although the result clearly suffers from numerical noise (brought on by incomplete sums),[16] we can already clearly see the recurrences or "echoes" in the correlator occurring at $\Delta t\approx 2nL_\lambda$.

Low- and high-frequency approximation

The main obstacle to being able to explicitly find the wormhole correlator, and in particular evaluate the infinite sums in (3.118), is that we do not have an analytic expression for the normal modes $\omega^\pm_{nk}$. These normal modes are solutions to the transcendental equation $\kappa^2=1$ with κ given by (3.39).

However, in the low- and high-frequency limits (see (3.41) and (3.43)), κ simplifies considerably and we can find the normal modes explicitly. Therefore, let us consider replacing κ entirely by either its low- or high-frequency limit:

$$\tilde\kappa^{(\rm low)}=\exp\left(-iL_\lambda\omega\right),\qquad \tilde\kappa^{(\rm high)}=\exp\left(-iL_\lambda\omega+i\frac{\pi}{2}\right), \tag{3.121}$$

[16] For example, note that we do not see images appearing, nor the "double-peak" structure, as was obtained for the black hole correlator (see figure 3.9).

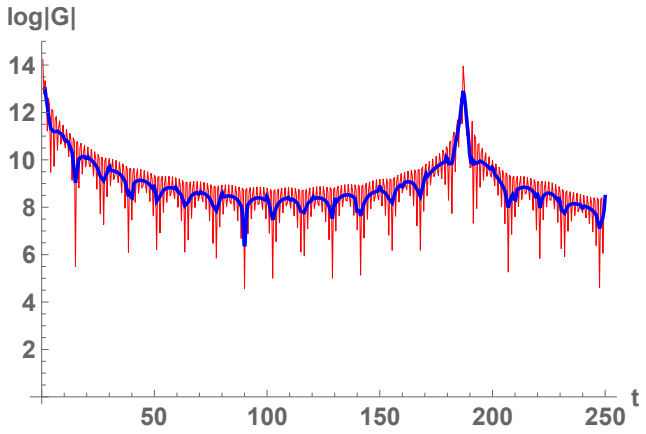


Figure 3.10: The wormhole correlator $G^R_{\text{WH}}(\Delta t, \Delta\varphi = 0.1)$ as given in (3.118). We take $R = r_+ = 1$, $\lambda = 2 \cdot 10^{-20}$ and $\epsilon = 10^{-1}$, and evaluate each of the four sums in (3.118) up to $n_{max} = 500, k_{max} = 50$. The red line is the computed value and the blue line is a smoothed out average. We can clearly see the first recurrence or "echo", which occur at $\Delta t \approx 2nL_\lambda \approx 186.98n$.

Physically, we can interpret replacing κ by one of the $\tilde{\kappa}$'s as introducing a frequency-dependent boundary condition at the middle of the wormhole throat (replacing (3.11)).

Replacing κ by either one of the $\tilde{\kappa}$'s in the wormhole modes f^λ given in (3.39), it is immediately clear that the normal modes of this altered wormhole satisfy $\tilde{\kappa}^2 = 1$ and are thus now given by:

$$\tilde{\omega}_n^{(\text{low})} = n\frac{\pi}{L_\lambda}, \qquad \tilde{\omega}_n^{(\text{high})} = \left(n + \frac{1}{2}\right)\frac{\pi}{L_\lambda}, \tag{3.122}$$

with $n \in \mathbb{Z}$. We will choose to work with the low-frequency limit in the rest of this section (as opposed to the high-frequency limit that we chose in section 3.4.2); the high-frequency case proceeds entirely analogously and moreover gives very similar end-results (such as figure 3.11).

We consider the retarded propagator (3.50) and close the ω integral in the lower half plane:

$$iG^R_{\widetilde{\mathrm{WH}}_{(\mathrm{low})}}(\Delta t,\Delta\varphi)=\frac{R^2\theta(\Delta t)}{8L_\lambda^3 r_+^2}\sum_{k\in\mathbb{Z}}\sum_{n\in\mathbb{Z}}\sum_{\pm} \tag{3.123}$$

$$e^{ik\Delta\varphi-i\frac{n\pi}{L_\lambda}\Delta t}(n^2\pi^2R^2-k^2L_\lambda^2)\coth\left(\frac{n\pi^2R^2}{2r_+L_\lambda}\pm\frac{\pi R}{2r_+}k\right).$$

We use the same Poisson resummation trick as we in the calculation of the black hole propagator, which converts the sum over k into an integral and a sum over images, introducing a factor $e^{i2\pi km}$, with $m\in\mathbb{Z}$:

$$iG^R_{\widetilde{\mathrm{WH}}_{(\mathrm{low})}}(\Delta t,\Delta\varphi)=\frac{R^2\theta(\Delta t)}{8L_\lambda^3 r_+^2}\sum_{m\in\mathbb{Z}}\sum_{n\in\mathbb{Z}}\sum_{\pm}$$

$$\int dk\, e^{ik(\Delta\varphi+2\pi m)-i\frac{n\pi}{L_\lambda}\Delta t}(n^2\pi^2R^2-k^2L_\lambda^2)$$

$$\times\coth\left(\frac{n\pi^2R^2}{2r_+L_\lambda}\pm\frac{\pi R}{2r_+}k\right). \tag{3.124}$$

For $\Delta\varphi>0$, we can close the k contour in the upper half plane; note that the integrand is already well-behaved as $k\to\pm\infty$ so there is no need for introducing an extra regulator (as there was in the black hole case). The coth factors have poles when:

$$k=\pm\frac{n\pi R}{L_\lambda}+2il\frac{r_+}{R}, \tag{3.125}$$

for $l\in\mathbb{Z}$, so we obtain:

$$iG^R_{\widetilde{\mathrm{WH}}_{(\mathrm{low})}}(\Delta t,\Delta\varphi)=-\frac{2\theta(\Delta t)}{RL_\lambda^2}\sum_{m\in\mathbb{Z}}\sum_{n\in\mathbb{Z}}\sum_{l=1}^{\infty}\sum_{\pm}l(n\pi R^2\pm ilL_\lambda r_+) \tag{3.126}$$

$$\times\exp\left(-2l\frac{r_+}{R}(\Delta\varphi+2m\pi)+in\pi\left(\pm\frac{R}{L_\lambda}(\Delta\varphi+2m\pi)-\frac{t}{L_\lambda}\right)\right).$$

We can now perform the sums over l and n explicitly; just as for the empty AdS correlator (see (A.45)), we need to regulate the sum over negative n by taking $\Delta t\to\Delta t(1+i\epsilon)$ and the sum over positive n by taking $\Delta t\to\Delta t(1-i\epsilon)$. Using the shorthand notation:

$$\tilde{t}_\epsilon\equiv\frac{\pi}{L_\lambda}\Delta t(1+i\epsilon),\qquad \tilde{\varphi}_m\equiv\frac{\pi R}{L_\lambda}\left(\Delta\varphi+2\pi m\right), \tag{3.127}$$

we can express the final result as:

$$iG^{R}_{\widetilde{\mathrm{WH}}_{(\mathrm{low})}}(\Delta t,\Delta\varphi)=\frac{\theta(\Delta t)}{2RL_\lambda^2}\sum_{m\in\mathbb{Z}}\left(\tilde{\mathcal{G}}(\tilde{t}_\epsilon,\tilde{\varphi}_m)-\tilde{\mathcal{G}}(\tilde{t}_{-\epsilon},\tilde{\varphi}_m)\right), \tag{3.128}$$

$$\tilde{\mathcal{G}}(\tilde{t}_\epsilon,\tilde{\varphi}_m)\equiv\frac{\pi R^2\left(\cos\tilde{t}_\epsilon\cos\tilde{\varphi}_m-1\right)+L_\lambda r_+\sin\tilde{\varphi}_m\coth\frac{r_+L_\lambda\tilde{\varphi}_m}{\pi R^2}\left(\cos\tilde{\varphi}_m-\cos\tilde{t}_\epsilon\right)}{\sinh^2\frac{r_+L_\lambda\tilde{\varphi}_m}{\pi R^2}\left(\cos\tilde{t}_\epsilon-\cos\tilde{\varphi}_m\right)^2}.$$

From the final correlator expression (3.128), it is immediately clear that:

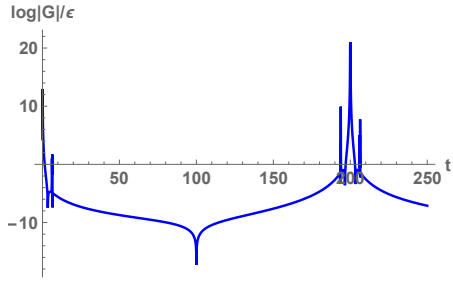
$$G^{R}_{\widetilde{\mathrm{WH}}_{(\mathrm{low})}}(\Delta t+2nL_\lambda,\Delta\varphi)=G^{R}_{\widetilde{\mathrm{WH}}_{(\mathrm{low})}}(\Delta t,\Delta\varphi), \tag{3.129}$$

for any $n\in\mathbb{Z}$;, so that this correlator has exact, periodic echoes (as anticipated above in section 3.4.2). We plot this correlator in figure 3.11; we can clearly see the the first echo at $\Delta t=2L_\lambda$. Note that there is also a "dip" in the correlator at $\Delta t=L_\lambda$. It is interesting to note that, as opposed to the black hole correlator (see figure 3.9), the contribution from the images $m\geq 2$ is exponentially suppressed compared to the $m=0$ term as we can see figure 3.11d (i.e. the red line for $m=0$ is above the $m>2$ peaks). Another difference with the black hole correlator is that this correlator does not die off (exponentially) as fast as the black hole one; note additionally that the $L_\lambda\to\infty$ limit does not reproduce the black hole correlator. These differences with the black hole correlator are artifacts of extrapolating the low-frequency limit of the original wormhole to all frequencies, which (as mentioned above) can be interpreted as a frequency-dependent modification of the wormhole boundary condition. In particular, the normal modes $\tilde{\omega}_n^{(\mathrm{low})}$ in (3.122) differ significantly from the actual normal modes of the original wormhole at high frequencies (3.44); of course, the original wormhole has a correlator that (by construction) must have the correct exponential fall-off for $0<\Delta t\ll L_\lambda$.[17]

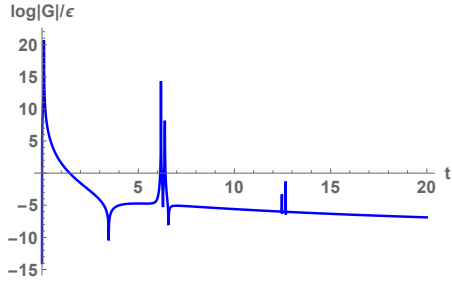
3.4.3 Wormhole transition Feynman correlator

We would like to calculate the position-space correlator for the "off-diagonal" Feynman correlator $\langle\lambda|\mathcal{O}\mathcal{O}|\lambda'\rangle$ in (3.64) that we discussed in section 3.2.3. The calculation of this correlator suffers from the same problems we encountered in section 3.4.2, namely that we cannot explicitly perform the relevant infinite sums over normal modes as we do not have an analytic expression for these

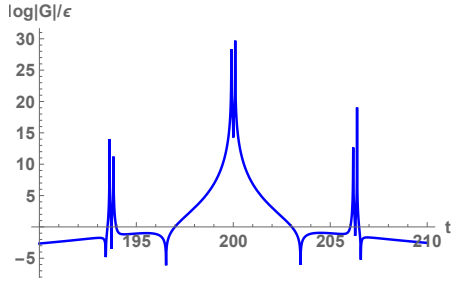
[17] Note that the result for the correlator is very similar if we had selected instead the high-frequency limit $\kappa^{(\mathrm{high})}$ in (3.121) as basis for our calculation. This is somewhat curious, since in this case it is of course at *low* frequencies where this approximation and extrapolation diverges from the actual wormhole results.



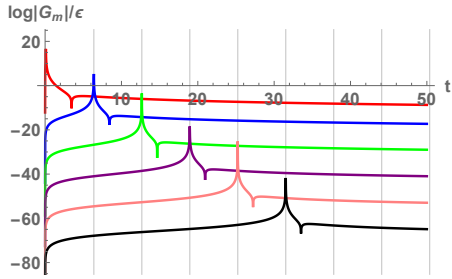
(a) The wormhole correlator



(b) The wormhole correlator around $\Delta t = 0$



(c) The wormhole correlator around $\Delta t = 2L_\lambda$



(d) The $m = 0, \cdots, 5$ terms in (3.128) separately

Figure 3.11: The altered wormhole correlator $G^R_{\widetilde{\mathrm{WH}}_{(\mathrm{low})}}(\Delta t, \Delta\varphi = 0.1)$ as given in (3.128). We take $R = r_+ = 1$, $\epsilon = 10^{-10}$, and $L_\lambda = 100$. We see the clear onset of the first echo at $\Delta t = 2L_\lambda$.

modes. Instead, we will calculate the off-diagonal correlator given by (3.64) in the low-frequency approximation introduced above in section 3.4.2, which we will be able to find analytically.[18]

Recall that the low-frequency approximation of section 3.4.2 is obtained by replacing κ in the scalar wave solutions (3.39) by $\tilde{\kappa}^{(\mathrm{low})}$ given in (3.121). The normal modes are then given by $\tilde{\omega}_n^{(\mathrm{low})}$ in (3.122), which are the solutions to $(\tilde{\kappa}^{(\mathrm{low})})^2 = 1$. It is then a straightforward exercise to calculate the residus of $(1 - (\tilde{\kappa}^{(\mathrm{low})})^2)^{-1}$ and $(1 - (\tilde{\kappa}^{(\mathrm{low})})^2)^{-2}$ at these normal modes, to find the

[18] Just as for the diagonal correlator discussed in section 3.4.2, the calculation for the off-diagonal correlator using instead the high-frequency approximation $\tilde{\kappa}^{(\mathrm{high})}$ is completely analogous, and gives qualitatively the same result as the low-frequency approximation described here.

modified expressions that replace q, A in (3.59). We find the simple expressions:

$$\tilde{q} = 2L_\lambda, \qquad \tilde{A} = 1. \tag{3.130}$$

The off-diagonal Feynman correlator then follows from (3.64), after replacing the normal modes $\omega_{nk}^{\pm}$ by their modified versions $\tilde{\omega}_n^{(\text{low})}$ and replacing the functions A, q by $\tilde{A}, \tilde{q}$. Note that we can also replace $\delta\lambda$ by δL_λ using the following relation:

$$\delta L_\lambda = -2\frac{R^2}{r_+}\frac{\delta\lambda}{\lambda}. \tag{3.131}$$

The actual calculation of the Feynman correlator proceeds precisely analogously as in section 3.4.2 for the diagonal (retarded) correlator, although we note that the sum over n is only over the *negative* poles ($n < 0$) as indicated in (3.64). As usual, we trade the sum over k for an integral over k and sum over images m; after performing the integrals over ω and k, we obtain (using $\Delta t = t - t'$, $\Delta\varphi = \varphi - \varphi'$ and assuming $t' > t_0 > t$):

$$iG^F_{\widetilde{\text{WH}}_{(\text{low})},\lambda\to\lambda'}(\Delta t, \Delta\varphi) = -\frac{2}{RL_\lambda^2}\sum_{m\in\mathbb{Z}}\sum_{n<0}\sum_{l=1}^{\infty}\sum_{\pm} l(n\pi R^2 \pm ilL_\lambda r_+) \times \left(1 - 2n\pi i\frac{\delta L_\lambda}{L_\lambda}\right)$$

$$\times \exp\left(-2l\frac{r_+}{R}(\Delta\varphi + 2m\pi) + in\pi\left(\pm\frac{R}{L_\lambda}(\Delta\varphi + 2m\pi) - \frac{\Delta t}{L_\lambda}\right)\right). \tag{3.132}$$

This is the analogue of (3.126); note that compared to (3.126), the only difference in the expression to be summed over is in the last factor on the first line. We can then again perform the l, n sums explicitly, obtaining:

$$iG^F_{\widetilde{\text{WH}}_{(\text{low})},\lambda\to\lambda'}(\Delta t, \Delta\varphi) = \frac{1}{2RL_\lambda^2}\sum_{m\in\mathbb{Z}}\left(\tilde{\mathcal{G}}(\tilde{t}_\epsilon, \tilde{\varphi}_m) + \frac{\pi\delta L_\lambda}{L_\lambda}\Delta\tilde{\mathcal{G}}(\tilde{t}_\epsilon, \tilde{\varphi}_m)\right),$$

$$\Delta\tilde{\mathcal{G}}(\tilde{t}_\epsilon, \tilde{\varphi}_m) \equiv \sin\tilde{t}_\epsilon \times$$

$$(\pi R^2\left(-3 + 2\cos\tilde{\varphi}_m\cos\tilde{t}_\epsilon + \cos 2\tilde{\varphi}_m\right) + 2L_\lambda r_+ \coth\frac{r_+ L_\lambda\tilde{\varphi}_m}{\pi R^2}\sin\tilde{\varphi}_m\left(\cos\tilde{\varphi}_m - \cos\tilde{t}_\epsilon\right))/$$

$$(\sinh^2\frac{r_+ L_\lambda\tilde{\varphi}_m}{\pi R^2}\left(\cos\tilde{t}_\epsilon - \cos\tilde{\varphi}_m\right)^3), \tag{3.133}$$

and $\tilde{\mathcal{G}}(\tilde{t}_\epsilon, \tilde{\varphi}_m)$ is the expression from the original (diagonal) correlator we found in (3.128).

We plot the correlator (3.133) and compare it to the diagonal correlator (when $\delta L_\lambda = 0$) in figure 3.12. We can clearly see that the off-diagonal correlator has a wider echo peak than the diagonal correlator, suggesting that sharp

features of the (diagonal) correlators (like the echoes at $\Delta t \sim 2nL_\lambda$) become less pronounced in off-diagonal correlators. Note that in obtaining the off-diagonal correlator (3.133), we have integrated over all modes ω, including those that do not satisfy $\omega \ll (\delta L_\lambda)^{-1}$; for such high-frequency modes, it can easily be seen that the expansion (3.58) (with κ replaced by $\tilde{\kappa}^{(\text{low})}$) breaks down. Therefore, the obtained correlator (and in particular any spurious short-time behaviour) should be taken with a grain of salt.

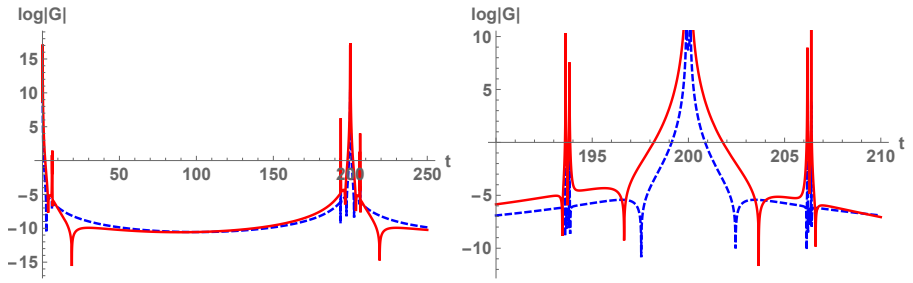


Figure 3.12: The altered, off-diagonal wormhole correlator $G^F_{\widetilde{\text{WH}}_{(\text{low}),\lambda\to\lambda'}}(\Delta t, \Delta\varphi = 0.1)$ (in red) from (3.133) together with the diagonal correlator $G^F_{\widetilde{\text{WH}}_{(\text{low}),\lambda\to\lambda}}(\Delta t, \Delta\varphi = 0.1)$ (in blue, dashed) (which is (3.133) with $\delta L_\lambda = 0$). We take $R = r_+ = 1$, $\epsilon = 10^{-10}$, $L_\lambda = 100$ and $\delta L_\lambda = 5$.

Chapter 4

Wrapped M5-branes at leading order in large-N

String and M-theory provide a consistent framework to describe the quantum physics of black holes in terms of microscopic ingredients such as strings and branes. The AdS/CFT correspondence gives an additional vantage point on this venerable research endeavor. Asymptotically AdS black holes can be viewed through the prism of holography and their properties can in principle be delineated using the quantum dynamics of a dual CFT. This is best understood when the AdS black hole solution is constructed in a consistent supergravity theory that arises as a low-energy limit of string or M-theory. This allows to understand the black hole solution in terms of its microscopic ingredients, identify its dual CFT, and then harness the power of holography to study the black hole itself. Supersymmetry can be a very useful crutch in this enterprise. It is often technically easier to construct explicit supersymmetric AdS black hole solutions in supergravity and explore their properties. Moreover, the recent advances in supersymmetric localization allow for the explicit calculation of the path integral of holographic SCFTs, which in turn provides a host of information about the physics of the black hole. Indeed, recently there has been a flurry of activity using these methods to study the thermodynamic and microscopic properties of supersymmetric AdS black holes and their dual QFT description, see [211] and references therein for a review.

Our goal in this chapter is to contribute to these developments by studying supersymmetric AdS_5 black holes in M-theory that arise from the backreaction of M5-branes wrapped on a compact Riemann surface, $\Sigma_{\mathfrak{g}}$, of genus $\mathfrak{g}$. The supergravity solutions describing this system of branes can be constructed in a

two-step procedure that involves supergravity consistent truncations. As shown in [168], reducing 11d supergravity on S^4 leads to the maximal 7d $SO(5)$ gauged supergravity of [176]. This theory admits an infinite family of supersymmetric AdS_5 vacua first explored in the seminal work of Maldacena-Núñez [158] and then generalized in [18, 19]. In addition to the number of M5-branes, N, these AdS_5 solutions are characterized by the genus of the Riemann surface, $\mathfrak{g}$, and a rational number z. We show that for each value of $(\mathfrak{g}, z)$ the 7d gauged supergravity theory admits a consistent truncation to 5d $\mathcal{N} = 2$ minimal gauged supergravity. This type of consistent truncations were studied previously in the literature, see [121, 200, 164, 84, 116, 85, 159, 144], and our analysis adds several technical details to these constructions including explicit formulae that allow to uplift any solution of the 5d supergravity theory to 11d.

It is well-known that 5d $\mathcal{N} = 2$ minimal gauged supergravity admits supersymmetric asymptotically AdS_5 black hole solutions with one electric charge and two independent angular momenta [132, 99]. The sequence of consistent truncations described above provides an embedding of these supersymmetric black holes in M-theory and associates a family of black hole solutions to each of the supersymmetric AdS_5 vacua found in [18, 19]. As emphasized and carefully studied in [72, 88], the thermodynamic properties of these black holes are somewhat subtle to study since they have finite entropy and on-shell action even in the zero temperature supersymmetric limit. We build on these results and show how the entropy, on-shell action, and charges of the black hole solution can be expressed in terms of the microscopic parameters $(N, \mathfrak{g}, z)$ that define the underlying M5-brane system. The black hole solutions admit a somewhat subtle analytic continuation to Euclidean signature which allows for rigorous calculations of their properties using the tools of holographic renormalization which we discuss in some detail. The asymptotic boundary of these Euclidean saddles points of the gravitational path integral has $S^1 \times S^3$ topology and points to a description of this system in terms of the superconformal index of a dual 4d $\mathcal{N} = 1$ SCFT.

Indeed, we show that these supersymmetric gravitational solutions can be described by the large N limit of the 4d $\mathcal{N} = 1$ class $\mathcal{S}$ SCFTs constructed in [120, 55, 18, 19]. The different values of z that label these theories correspond to the family of topological twists of the 6d $\mathcal{N} = (2, 0)$ SCFT living on the worldvolume of the M5-branes that preserve 4d $\mathcal{N} = 1$ supersymmetry. The superconformal index of the class $\mathcal{S}$ theories can be studied at low values of N using the results in [33, 118, 119, 182], however we are not aware of a detailed study of the index at large N using these methods. Fortunately we can bypass this impasse. It was realized recently that the superconformal index of general 4d $\mathcal{N} = 1$ SCFTs exhibits universal properties that prove very useful in a holographic setup like ours. In particular, it was shown in [86], see also [128],

that carefully treating the superconformal index as a complex function of its fugacities leads to a simple universal formula for it in the so-called Cardy-like limit where the radius of the S^1 is much smaller than that of S^3. This universal expression for the superconformal index is entirely controlled by the 't Hooft anomalies of the 4d $\mathcal{N}=1$ SCFT and as discussed recently in [63, 89] can be reproduced by a similarly universal supergravity on-shell action for large N holographic SCFTs.[1] These results have important implications for our wrapped M5-brane setup. We use the 't Hooft anomalies of the 4d $\mathcal{N}=1$ class $\mathcal{S}$ SCFTs derived in [120, 55, 18, 19] to write the leading N^3 term of the superconformal index on "the second sheet" in terms of the microscopic parameters $(N, \mathfrak{g}, z)$. This expression then exactly agrees with the on-shell action of the supersymmetric CCLP solution computed via holographic renormalization. An appropriate Legendre transformation of this index then yields an expression for the microscopic entropy of the dual black hole which perfectly agrees with the Bekenstein-Hawking entropy formula.

The rest of this chapter is organized as follows. In Section 4.1 we summarize some results on the dimensional reduction and consistent truncation from 11d supergravity to 7d gauged supergravity. In Section 4.2 we derive a family of dimensional reductions on $\Sigma_{\mathfrak{g}}$ from this 7d theory to 5d $\mathcal{N}=2$ minimal gauged supergravity. Further details on the reduction of the supergravity action and BPS equations are given in Appendix A.3. In Section 4.3, supplemented by Appendix A.4, we provide some details on mostly known results regarding the thermodynamics of the most general known rotating black hole solution of the 5d gauged supergravity theory and the calculation of its on-shell action. Section 4.4 is devoted to the holographic interpretation of these results and their connection to the superconformal index of the 4d $\mathcal{N}=1$ class $\mathcal{S}$ SCFTs. In Section 4.5 we provide some concluding comments, while in Appendix A.5 we summarize our conventions.

4.1 7d gauged supergravity from 11d

The bosonic sector of the 11d supergravity contains the metric with line element $\mathrm{d}s_{11}^2$ and a three-form $\mathcal{A}$. The bosonic action of the theory is given by

$$I_{11} = \frac{1}{16\pi G_{11}} \int \left(\star_{11} R - \frac{1}{2} \mathcal{F} \wedge \star_{11} \mathcal{F} + \frac{1}{6} \mathcal{F} \wedge \mathcal{F} \wedge \mathcal{A} \right), \tag{4.1}$$

[1] As discussed below, it is not clear to us why the large N and Cardy-like limit have an overlapping regime of validity but the results we present here, as well as the ones in [63, 89], point to a more general regime of validity of the "second sheet" formula for the index derived in [86].

where $\mathcal{F} = \mathrm{d}\mathcal{A}$. As shown in [168], see also [112] for some more details, a reduction of 11d supergravity on S^4 results in a consistent truncation to the 7d, $\mathcal{N} = 4$, $SO(5)$ gauged supergravity of [176]. The 7d gauged supergravity can be further consistently truncated to its $U(1) \times U(1)$ invariant sector as described in [151]. The bosonic field content of this 7d theory, which plays an important role below, consists of the metric with line element $\mathrm{d}s_7^2$, together with a three-form, two Abelian one-forms and two scalars: (S, A_1, A_2, λ_1, λ_2).

We now provide some more details on how this sequence of consistent truncations works. We parametrize the S^4 by the four angles: (α, β, ϕ_1, ϕ_2), as

$$\mathrm{d}s_4^2 = \frac{1}{\mu^2}\big(e^{-2\lambda_1}\big[\mathrm{d}\nu_1{}^2 + \nu_1^2(D\phi_1)^2\big] + e^{-2\lambda_2}\big[\mathrm{d}\nu_2{}^2 + \nu_2^2(D\phi_2)^2\big] + e^{4\lambda_1+4\lambda_2}\,\mathrm{d}\nu_3{}^2\big)\,, \tag{4.2}$$

where μ is an inverse length scale, $\nu_{1,2,3}$ are alternative (constrained) coordinates for the two angles (α, β):

$$\nu_1 = \sin\alpha\cos\beta\,, \quad \nu_2 = \sin\alpha\sin\beta\,, \quad \nu_3 = \cos\alpha\,; \qquad \nu_1^2 + \nu_2^3 + \nu_3^2 = 1\,, \tag{4.3}$$

and $D\phi_{1,2} = \mathrm{d}\phi_{1,2} + \mu A_{1,2}$. The coordinates $\phi_{1,2}$ parametrize the $U(1) \times U(1)$ isometry directions. The 11d fields are expressed in terms of the 7d fields as

$$
\begin{aligned}
\mathrm{d}s_{11}^2 &= \Delta^{1/3}\,\mathrm{d}s_7^2 + \Delta^{-2/3}\,\mathrm{d}s_4^2\,,\\
\mathcal{F} &= -e^{-4\lambda_1-4\lambda_2}\nu_3 \star_7 S + \frac{1}{\mu} S\wedge \mathrm{d}\nu_3\\
&\quad + \frac{1}{\Delta\mu^2}\Big[- e^{2\lambda_1}\nu_1^2\, D\phi_1\wedge F_2\wedge \mathrm{d}\nu_3 - e^{2\lambda_2}\nu_2^2\, D\phi_2\wedge F_1\wedge \mathrm{d}\nu_3\\
&\qquad + e^{-4\lambda_1-4\lambda_2}\nu_1\nu_3\, D\phi_1\wedge F_2\wedge \mathrm{d}\nu_1 + e^{-4\lambda_1-4\lambda_2}\nu_2\nu_3\, D\phi_2\wedge F_1\wedge \mathrm{d}\nu_2\Big]\\
&\quad + \frac{U\nu_1\nu_2}{\Delta^2\mu^3}\Big[\nu_1\, D\phi_1\wedge D\phi_2\wedge \mathrm{d}\nu_2\wedge \mathrm{d}\nu_3 + \nu_2\, D\phi_2\wedge D\phi_1\wedge \mathrm{d}\nu_1\wedge \mathrm{d}\nu_3\\
&\qquad + \nu_3\, D\phi_1\wedge D\phi_2\wedge \mathrm{d}\nu_1\wedge \mathrm{d}\nu_2\Big]\\
&\quad + \frac{\nu_1\nu_2}{\Delta^2\mu^3}\Big[2e^{2\lambda_1+2\lambda_2}\nu_1\nu_2\, D\phi_1\wedge D\phi_2\wedge \mathrm{d}(\lambda_1-\lambda_2)\wedge \mathrm{d}\nu_3\\
&\qquad + 2e^{-2\lambda_1-4\lambda_2}\nu_1\nu_3\, D\phi_1\wedge D\phi_2\wedge \mathrm{d}(3\lambda_1-2\lambda_2)\wedge \mathrm{d}\nu_2\\
&\qquad + 2e^{-4\lambda_1-2\lambda_2}\nu_2\nu_3\, D\phi_1\wedge D\phi_2\wedge \mathrm{d}(3\lambda_1+2\lambda_2)\wedge \mathrm{d}\nu_1\Big]\,,
\end{aligned}
\tag{4.4}
$$

where $F_{1,2} = \mathrm{d}A_{1,2}$ and (Δ, U) are functions given by

$$
\begin{aligned}
\Delta &= e^{2\lambda_1}\nu_1^2 + e^{2\lambda_2}\nu_2^2 + e^{-4\lambda_1-4\lambda_2}\nu_3^2\,,\\
U &= -\big(2e^{2\lambda_1+2\lambda_2} + e^{-2\lambda_1-4\lambda_2}\big)\nu_1^2 - (2e^{2\lambda_1+2\lambda_2} + e^{-4\lambda_1-2\lambda_2})\nu_2^2\\
&\quad + \big(e^{-8\lambda_1-8\lambda_2} - 2e^{-2\lambda_1-4\lambda_2} - 2e^{-4\lambda_1-2\lambda_2}\big)\nu_3^2\,.
\end{aligned}
\tag{4.5}
$$

The resulting 7d theory has the following bosonic action

$$I_7 = \frac{1}{16\pi G_7}\int\Big[\star_7\,(R-V) - 5\,\mathrm{d}\lambda_+\wedge\star_7\,\mathrm{d}\lambda_+ - \mathrm{d}\lambda_-\wedge\star_7\,\mathrm{d}\lambda_- - \frac{1}{2}e^{-4\lambda_1}F_1\wedge\star_7 F_1$$
$$-\frac{1}{2}e^{-4\lambda_2}F_2\wedge\star_7 F_2 - \frac{1}{2}e^{-4\lambda_+}S\wedge\star_7 S + \frac{1}{2\mu}\,S\wedge\mathrm{d}S$$
$$-\frac{1}{\mu}F_1\wedge F_2\wedge S + \frac{1}{4\mu}(A_1\wedge F_1\wedge F_2\wedge F_2 + A_2\wedge F_2\wedge F_1\wedge F_1)\Big], \quad (4.6)$$

where we have defined $\lambda_\pm = \lambda_1 \pm \lambda_2$ and V is the potential for the scalars, given by

$$V = \frac{\mu^2}{2}\big(e^{-8\lambda_1-8\lambda_2} - 4e^{-2\lambda_1-4\lambda_2} - 4e^{-4\lambda_1-2\lambda_2} - 8e^{2\lambda_1+2\lambda_2}\big)\,. \quad (4.7)$$

Out of this action we obtain the following equations of motion

$$\mathrm{d}S = \mu\, e^{-4\lambda_+}S + F_1\wedge F_2\,,$$
$$\mathrm{d}\big(e^{-4\lambda_{1,2}}\star_7 F_{1,2}\big) = \frac{1}{\mu}F_{1,2}\wedge F_{2,1}\wedge F_{2,1} - \frac{1}{\mu}F_{2,1}\wedge\mathrm{d}S\,,$$
$$\mathrm{d}\star_7\,\mathrm{d}(3\lambda_{1,2}+2\lambda_{2,1}) = -\frac{1}{2}e^{-4\lambda_{1,2}}F_{1,2}\wedge\star_7 F_{1,2} - \frac{1}{2}e^{-4\lambda_+}S\wedge\star_7 S + \frac{1}{4}\star_7\frac{\partial V}{\partial\lambda_{1,2}}\,,$$
$$R_{MN} = 5\partial_M\lambda_+\partial_N\lambda_- + \partial_M\lambda_-\partial_N\lambda_+ + \frac{1}{2}e^{-4\lambda_1}F^2_{1\,MN} + \frac{1}{2}e^{-4\lambda_2}F^2_{2\,MN}$$
$$+\frac{1}{4}e^{-4\lambda_+}S^2_{MN} + \frac{1}{5}g_{MN}\left[V - \frac{1}{4}e^{-4\lambda_1}F_1^2 - \frac{1}{4}e^{-4\lambda_2}F_2^2 - \frac{1}{6}e^{-4\lambda_+}S^2\right],$$

where $M,N,\ldots$ are curved 7d indices and we have defined $F^2_{1,2\,MN} = F_{1,2\,M}{}^R F_{1,2\,NR}$, $S^2_{MN} = S_M{}^{RS}S_{NRS}$, $F^2_{1,2} = F^{MN}_{1,2}F_{1,2\,MN}$, $S^2 = S^{MNR}S_{MNR}$. To ensure that a solution of the equations of motion of the $U(1)\times U(1)$ invariant truncation of the 7d supergravity theory is supersymmetric one should check that the supersymmetry variations of one spin-$\frac{3}{2}$ gravitino and two spin-$\frac{1}{2}$ dilatini, $\big(\widetilde{\psi}_M,\,\widetilde{\zeta}_1,\,\widetilde{\zeta}_2\big)$, vanish. Setting the supersymmetry variations of these fields to zero gives the following BPS equations for the 32-dimensional 7D spinor

$\widetilde{\epsilon}\otimes\mathcal{E}$, which we have split into a purely 7D part $\widetilde{\epsilon}$ and an $SO(5)$ part $\mathcal{E}$:

$$\begin{aligned}
\delta\widetilde{\psi}_M = \Bigg[&\partial_M + \frac{1}{4}\omega_{M\widehat{A}\widehat{B}}\widetilde{\gamma}^{\widehat{A}\widehat{B}}\otimes 1_4 + \frac{\mu}{2}\,1_8\otimes\big(A_{1\,M}\Gamma^{12}+A_{2\,M}\Gamma^{34}\big)\\
&+\left(\frac{\mu}{4}e^{-4\lambda_+}\widetilde{\gamma}_M+\frac{1}{2}\widetilde{\gamma}_M\widetilde{\gamma}^N\partial_N\lambda_+\right)\otimes 1_4\\
&+\frac{1}{4}\big(e^{-2\lambda_1}F_{1\,MN}\widetilde{\gamma}^N\otimes\Gamma^{12}+e^{-2\lambda_2}F_{2\,MN}\widetilde{\gamma}^N\otimes\Gamma^{34}\big)\\
&-\frac{1}{8}e^{-2\lambda_+}S_{MNP}\widetilde{\gamma}^{NP}\otimes\Gamma^5\Bigg]\widetilde{\epsilon}\otimes\mathcal{E}\,,\\
\delta\widetilde{\zeta}_{1,2} = \Bigg[&\frac{\mu}{4}\big(e^{2\lambda_{1,2}}-e^{-4\lambda_+}\big)-\frac{1}{4}\widetilde{\gamma}^M\partial_M(3\lambda_{1,2}+2\lambda_{2,1})\otimes 1_4\\
&-\frac{1}{16}e^{-2\lambda_{1,2}}F_{1,2\,MN}\widetilde{\gamma}^{MN}\otimes\Gamma^{12}\\
&+\frac{1}{48}e^{-2\lambda_+}S_{MNP}\widetilde{\gamma}^{MNP}\otimes\Gamma^5\Bigg]\widetilde{\epsilon}\otimes\mathcal{E}\,.
\end{aligned}\tag{4.8}$$

Here $\widetilde{\gamma}^M$ is an 8×8 curved 7d spacetime gamma matrix, $\widetilde{\gamma}^{\widehat{A}}$ is a flat 7d Lorentz gamma matrix, $\omega_{M\widehat{A}\widehat{B}}$ is the 7d spin connection, Γ^i, with $i=1,\ldots,5$, is a 4×4 flat internal $SO(5)$ gamma matrix, and finally 1_n is an $n\times n$ identity matrix.

4.2 Dimensional reduction to 5d $\mathcal{N}=2$ minimal gauged supergravity

As shown in [158, 18, 19] the 7d $U(1)\times U(1)$ invariant truncation discussed above admits an infinite family of supersymmetric AdS_5 vacua. This suggests that there is a further consistent truncation of this model to 5d $\mathcal{N}=2$ minimal gauged supergravity. Indeed, it is possible to construct such a consistent truncation for each of the supersymmetric vacua studied in [18, 19]. This type of consistent truncations arising from wrapped M5-branes have been discussed in various level of detail in [121, 200, 164, 84, 116, 85, 159, 144]. Our goal here is to rederive some of these results in a way tailored to our goal of discussing asymptotically AdS_5 black hole solutions and where needed fill in small gaps in the literature.

More concretely, our aim is to reduce the 7d $U(1) \times U(1)$ gauged supergravity truncation on a smooth Riemann surface $\Sigma_{\mathfrak{g}}$ with genus $\mathfrak{g}$ to arrive at 5d $\mathcal{N} = 2$ minimal gauged supergravity, with bosonic field content given by the metric with line element $\mathrm{d}s_5^2$ and a single one-form gauge field A. For concreteness, we take the Riemann surface to be hyperbolic, i.e. $\mathfrak{g} > 1$,[2] and parametrize it with coordinates (x_1, x_2) as:[3]

$$\mathrm{d}s_2^2 = \left(\mathrm{d}{x_1}^2 + \mathrm{d}{x_2}^2\right)/x_2^2 \,. \tag{4.9}$$

We also define the one-form $\omega = \mathrm{d}x_1 \, / x_2$, such that the volume form on $\Sigma_{\mathfrak{g}}$ is given by $\mathrm{d}\omega$. We take the 7d scalars to assume constant values $\lambda_{1,2} = \Lambda_{1,2}$ as dictated by the AdS_5 vacua of [18, 19] and define two new constants, (g_0, f_0), in terms of them

$$\begin{aligned}
\Lambda_1 &= \frac{1}{10} \ln \left(\frac{1 + 7z + 7z^2 + 33z^3 - (1 + 4z + 19z^2)\sqrt{1 + 3z^2}}{4z(1-z)^2} \right) , \\
\Lambda_2 &= \Lambda_1 - \frac{1}{2} \ln \left(\frac{1+z}{2z + \sqrt{1+3z^2}} \right) , \\
f_0 &= 4\Lambda_+ \,, \\
g_0 &= \frac{1}{2} \ln \left(\frac{1}{8} e^{2\Lambda_+} \left[(1-z) e^{2\Lambda_1} + (1+z) e^{2\Lambda_2} \right] \right) ,
\end{aligned} \tag{4.10}$$

where $\Lambda_\pm = \Lambda_1 \pm \Lambda_2$ and z is a rational number obeying $z(\mathfrak{g} - 1) \in \mathbb{Z}$. In this way we will obtain a family of dimensional reductions labelled by $(z, \mathfrak{g})$. For the remaining 7d fields we take the following reduction Ansatz

$$\begin{aligned}
\mathrm{d}s_7^2 &= e^{2f_0} \, \mathrm{d}s_5^2 + e^{2g_0} L^2 \, \mathrm{d}s_2^2 \,, \\
S &= \mathfrak{c} \, e^{f_0 + 2g_0 + 2\Lambda_+} L^2 \, \star_7 \left(F \wedge \mathrm{d}\omega \right) , \\
A_{1,2} &= \mathfrak{a} \, (1 \pm z) L \, \omega + \mathfrak{b} \, e^{f_0 + 2\Lambda_{1,2}} \, A \,,
\end{aligned} \tag{4.11}$$

where $F = \mathrm{d}A$, $L = 2/\mu$ is the AdS_5 radius, and $(\mathfrak{a}, \mathfrak{b}, \mathfrak{c})$ are z-independent constants that we will fix below. We present the details of the dimensional reduction based on this Ansatz in Appendix A.3.1. The upshot is that to have a 5d theory with z-independent cosmological constant one has to fix $\mathfrak{a} = \pm 1/4$.

[2] Our results can be adapted to the AdS_5 vacua of [18, 19] with $\mathfrak{g} = 0, 1$ in a straightforward way.

[3] To have a compact Riemann surface we have to mod out the upper half plane with an appropriate discrete group. From now on we will assume that this discrete identification has been performed and will work with local coordinates on the Riemann surface.

To retain the normalization of the 5d Maxwell field such that $F = \mathrm{d}A$ we need to take $c = \mathfrak{b}$ and we also found it convenient to rescale $\mathfrak{b}$ as $\mathfrak{b} = \chi/\sqrt{3}$. As shown in Appendix A.3.1, integrating over the Riemann surface we obtain the bosonic action of 5d $\mathcal{N}=2$ minimal gauged supergravity

$$I_5 = \frac{1}{16\pi G_5}\int\left[\star_5\left(R+\frac{12}{L^2}\right) - \frac{\chi^2}{2}\,F\wedge\star_5 F + \frac{\chi^3}{3\sqrt{3}}A\wedge F\wedge F\right], \qquad (4.12)$$

where χ can be viewed as a normalization constant associated with the freedom[4] to rescale the gauge filed A. Importantly, the 5d Newton constant is given in terms of the 7d one by

$$\boxed{G_7 = e^{3f_0+2g_0}L^2\,4\pi(\mathfrak{g}-1)\,G_5}\,. \qquad (4.13)$$

The equations of motion of the 5d supergravity can be derived from the action above and read

$$\begin{aligned}\mathrm{d}\star_5 F &= \frac{\chi}{\sqrt{3}}F\wedge F\,,\\ R_{\mu\nu} &= -\frac{4}{L^2}g_{\mu\nu} + \frac{\chi^2}{2}F_\mu{}^\alpha F_{\nu\alpha} - \frac{\chi^2}{12}g_{\mu\nu}F^{\alpha\beta}F_{\alpha\beta}\,,\end{aligned} \qquad (4.14)$$

where we have denoted the 5d curved indices with Greek letters. The only fermionic field in the 5d supergravity theory is the spin-$\frac{3}{2}$ gravitino ψ_μ. Setting its supersymmetry variation to zero we obtain the following BPS equation for the 4-dimensional 5d spinor ϵ:

$$\begin{aligned}\delta\psi_\mu = \Bigg[&\partial_\mu + \frac{1}{4}\omega_{\mu\widehat{\alpha}\widehat{\beta}}\gamma^{\widehat{\alpha}\widehat{\beta}} - \frac{\mathrm{i}\,\chi}{8\sqrt{3}}\big(\gamma_{\mu\alpha\beta}F^{\alpha\beta} - 4F_{\mu\alpha}\gamma^\alpha\big)\\ &- \frac{1}{2L}\Big(\gamma_\mu + \mathrm{i}\sqrt{3}\,\chi A_\mu\Big)\Bigg]\epsilon\,,\end{aligned} \qquad (4.15)$$

where γ^μ is a 4×4 curved 5d spacetime gamma matrix, $\gamma^{\widehat{\alpha}}$ is a flat 5d Lorentz gamma matrix and $\omega_{\mu\widehat{\alpha}\widehat{\beta}}$ is the 5d spin connection. In Appendix A.3.2 we show that the three 7d supersymmetry variations in (4.8) reduce to (4.15) provided we identify

$$\begin{aligned}&\widetilde{\gamma}_\mu = -\chi_7\,\gamma_\mu\otimes\sigma_1\,, \quad \widetilde{\gamma}_{\widehat{x}_1} = \chi_7\,1_4\otimes\sigma_2\,,\\ &\widetilde{\gamma}_{\widehat{x}_2} = \chi_7\,1_4\otimes\sigma_3\,, \quad \widetilde{\epsilon} = \epsilon\otimes\begin{pmatrix}1\\ \chi_7\end{pmatrix},\end{aligned} \qquad (4.16)$$

[4]Some common choices include: [99, 87]: $\chi=1$, [132]: $\chi=-2$, [72]: $\chi = 2/(\sqrt{3}\,g)$.

which in turn also implies that $\widetilde{\gamma}_{\widehat{x}_1\widehat{x}_2} = \mathrm{i}\, 1_4 \otimes \sigma_1$, use the projectors

$$\Big(\widetilde{\gamma}_{\widehat{x}_1\widehat{x}_2} \otimes \Gamma^{12}\Big)(\widetilde{\epsilon} \otimes \mathcal{E}) = \chi_7\, \widetilde{\epsilon} \otimes \mathcal{E}\,, \qquad \big(1_8 \otimes \Gamma^5\big)(\widetilde{\epsilon} \otimes \mathcal{E}) = \widetilde{\epsilon} \otimes \mathcal{E}\,, \tag{4.17}$$

and set

$$\mathfrak{a} = -\frac{\chi_7}{4}\,, \quad \mathfrak{c} = \mathfrak{b} = \frac{\mathfrak{x}}{\sqrt{3}}\,, \quad \partial_{x_1}(\widetilde{\epsilon} \otimes \mathcal{E}) = \partial_{x_2}(\widetilde{\epsilon} \otimes \mathcal{E}) = 0\,, \tag{4.18}$$

where $\chi_7 = \pm 1$ is the chirality of the highest rank 7d Clifford algebra element. Note that the choice of sign leftover in $\mathfrak{a}$ from reducing the action is dictating which of the two inequivalent representation of the 7d Clifford algebra one should use.

4.3 Thermodynamics of the 5d black hole

After showing that to each of the supersymmetric AdS_5 vacua constructed in [18, 19] one can associate a distinct truncation of 11d supergravity to 5d $\mathcal{N} = 2$ minimal gauged supergravity we now proceed to discuss a family of rotating asymptotically AdS_5 black hole solutions of this theory. Although our discussion will be in five dimensions we stress that these solutions can be explicitly uplifted to 11d using the formulae in Section 4.1 and Section 4.2 above. Many of the results presented below have appeared before in the literature, in particular in [99, 169, 72, 88]. Our goal is to collect them here for completeness and clarify some aspects of the calculations.[5]

4.3.1 CCLP solution

The 5d $\mathcal{N} = 2$ gauged supergravity with bosonic action (4.12) admits a general non-supersymmetric black hole solution found in [99] which we will refer to as CCLP. The solution is specified by four real parameters (a, b, q, m) which determine its two angular momentum, electric charge and mass. For the Lorentzian black hole solutions these parameters are further constrained as

$$-1 < ag < 1\,, \quad -1 < bg < 1\,, \quad 0 \leq q \leq \frac{m}{1 + ag + bg}\,, \tag{4.19}$$

where $g = 1/L$ is the inverse of the AdS scale. The first two conditions arise from requiring that the black hole is not over-rotating and the last condition

[5] Most of the supergravity, holographic renormalization, and black hole thermodynamics calculations were performed with the help of a new `Mathematica` package we developed which is based on `xAct` and can be found at `https://github.com/waskou/SolutionsX`.

constitutes the BPS bound. The solution is specified by the following metric and gauge field

$$\begin{aligned} \mathrm{d}s^2_{\mathrm{CCLP}} &= -\frac{\Delta_\eta[(1+g^2r^2)\rho^2\,\mathrm{d}t + 2q\nu]\,\mathrm{d}t}{\Xi_a\Xi_b\rho^2} + \frac{2q\nu\omega}{\rho^2} + \frac{f}{\rho^4}\left(\frac{\Delta_\eta\,\mathrm{d}t}{\Xi_a\Xi_b} - \omega\right)^2 \\ &\quad + \frac{\rho^2\,\mathrm{d}r^2}{\Delta_r} + \frac{\rho^2\,\mathrm{d}\eta^2}{\Delta_\eta} + \frac{r^2+a^2}{\Xi_a}\sin^2\eta\,\mathrm{d}{\xi_1}^2 + \frac{r^2+b^2}{\Xi_b}\cos^2\eta\,\mathrm{d}{\xi_2}^2\,, \end{aligned} \tag{4.20}$$

$$A_{\mathrm{CCLP}} = \frac{\sqrt{3}\,q}{\varkappa\rho^2}\left(\frac{\Delta_\eta\,\mathrm{d}t}{\Xi_a\Xi_b} - \omega\right) + \alpha\,\mathrm{d}t\,,$$

where we have defined the one-forms

$$\nu = b\,\sin^2\eta\,\mathrm{d}\xi_1 + a\,\cos^2\eta\,\mathrm{d}\xi_2\,, \quad \omega = \frac{a\,\sin^2\eta}{\Xi_a}\,\mathrm{d}\xi_1 + \frac{b\,\cos^2\eta}{\Xi_b}\,\mathrm{d}\xi_2\,, \tag{4.21}$$

the functions

$$\begin{aligned} \Delta_r(r) &= \frac{(r^2+a^2)(r^2+b^2)(1+g^2r^2)+q^2+2abq}{r^2} - 2m\,, \\ \Delta_\eta(\eta) &= 1 - a^2g^2\cos^2\eta - b^2g^2\sin^2\eta\,, \\ \rho^2(r,\eta) &= r^2 + a^2\cos^2\eta + b^2\sin^2\eta\,, \\ f(r,\eta) &= 2\big(m + abqg^2\big)\rho^2(r,\eta) - q^2\,, \end{aligned} \tag{4.22}$$

and the constants

$$\Xi_a = 1 - a^2g^2\,, \quad \Xi_b = 1 - b^2g^2\,. \tag{4.23}$$

We have also included a pure gauge term, $\alpha\,\mathrm{d}t$, in A_{CCLP}, which is important to guarantee regularity of $A^\mu A_\mu$ on the horizon. These coordinates cover the region outside of the black hole and have the following ranges and identifications

$$-\infty < t < \infty\,, \quad r_+ < r < \infty\,, \quad 0 < \eta < \frac{\pi}{2}\,, \quad \xi_1 \sim \xi_1 + 2\pi\,, \quad \xi_2 \sim \xi_2 + 2\pi\,, \tag{4.24}$$

where r_+ is the largest positive root of $\Delta_r(r)$. The surface $r = r_+$ is the event horizon of the Lorentzian black hole, see Appendix A.4.4 for further details. Sometimes, it will be convenient to trade the parameter m for r_+. The explicit relation, which is obtained by solving $\Delta_r(r_+) = 0$, reads

$$m = \frac{(r_+^2+a^2)(r_+^2+b^2)(1+g^2r_+^2)+q^2+2abq}{2r_+^2}\,. \tag{4.25}$$

As emphasized in [72] the Lorentzian CCLP black hole can be analytically continued to a Euclidean "black saddle", which solves the equations of motion of the Euclidean theory (A.80)[6]. The Euclidean metric and gauge field are given by

$$\mathrm{d}s^2_{\mathrm{CCLP},\mathcal{E}} = \mathrm{d}s^2_{\mathrm{CCLP}}\Big|_{t\to -\mathrm{i}\,\tau}\,, \quad A_{\mathrm{CCLP},\mathcal{E}} = A_{\mathrm{CCLP}}\Big|_{t\to -\mathrm{i}\,\tau}\,. \tag{4.26}$$

Note that these metric and gauge field are both complex. One might want to work with a real Euclidean section by, in addition to Wick rotation, also analytically continuing the rotation parameters as: $a \to \mathrm{i}\,a, b \to \mathrm{i}\,b$. Once this is done the Euclidean metric is purely real and the Euclidean gauge field is purely imaginary. In the context of evaluating the on-shell action of this solution it is useful to work with this real Euclidean section. To interpret the result holographically as a Lorentzian partition function the rotation parameters have to be analytically continued back to their original values: $a \to -\mathrm{i}\,a, b \to -\mathrm{i}\,b$. It turns out that this procedure gives the same final answer as simply working with the complex Wick rotated metric and gauge field (4.26), without continuing the rotation parameters back and forth.

In the holographic context it will be useful also to work with the conformally rescaled boundary metric

$$\begin{aligned}\mathrm{d}s^2_{\mathrm{CCLP},\mathcal{B}} &= \lim_{r\to\infty} g^{-2} r^{-2}\, \mathrm{d}s^2_{\mathrm{CCLP}} \\ &= -\frac{\Delta_\eta}{\Xi_a \Xi_b}\,\mathrm{d}t^2 + \frac{1}{g^2\Delta_\eta}\,\mathrm{d}\eta^2 + \frac{\sin^2\eta}{g^2\Xi_a}\,\mathrm{d}{\xi_1}^2 + \frac{\cos^2\eta}{g^2\Xi_b}\,\mathrm{d}{\xi_2}^2\,.\end{aligned} \tag{4.27}$$

This metric, with certain identifications of the coordinates that are discussed in detail in [72], determines the background on which the 4d $\mathcal{N}=1$ dual SCFT is placed.

[6]The term "black saddle" was coined in [62] and refers to the fact that, in general, there exist Euclidean saddle points of the supergravity path integral that do not admit analytic continuation to sensible Lorentzian field configurations. The CCLP black saddle is an example of an Euclidean solution that does admit continuation to the Lorentzian black hole of [99] for some values of the parameters. We refer to this black saddle also as CCLP and the meaning is to be inferred from the context.

4.3.2 Thermodynamic properties CCLP

In Appendix A.4.4 we show that to the CCLP black hole we can associate the following thermodynamic potentials:

$$\beta = \frac{2\pi r_+\big[(r_+^2+a^2)(r_+^2+b^2)+abq\big]}{r_+^4\big[1+g^2(2r_+^2+a^2+b^2)\big]-(ab+q)^2}\,,$$

$$\Omega_1 = \frac{a(r_+^2+b^2)(1+g^2r_+^2)+bq}{(r_+^2+a^2)(r_+^2+b^2)+abq}\,,\quad \Omega_2 = \frac{b(r_+^2+a^2)(1+g^2r_+^2)+aq}{(r_+^2+a^2)(r_+^2+b^2)+abq}\,, \tag{4.28}$$

$$\Phi = \frac{\sqrt{3}qr_+^2}{\varkappa\big[(r_+^2+a^2)(r_+^2+b^2)+abq\big]}\,,$$

physically corresponding to: inverse temperature, angular velocities measured in a non-rotating frame at infinity, and electrostatic potential. To obtain the entropy, via the Bekenstein-Hawking area formula $S = \text{Area}/4G_5$, one has to integrate the square root determinant, $\sqrt{g_{\mathcal{H}}}$, of the induced metric on the horizon, which has topology of S^3 and metric given by

$$\mathrm{d}s^2_{\mathcal{H}} = \mathrm{d}s^2_{\text{CCLP}}\Big|_{\mathrm{d}t\to 0,\,\mathrm{d}r\to 0,\,r\to r_+}\,. \tag{4.29}$$

Performing this integral we obtain

$$S = \frac{\pi^2\big[(r_+^2+a^2)(r_+^2+b^2)+abq\big]}{2\Xi_a\Xi_b r_+ G_5}\,. \tag{4.30}$$

In Appendices A.4.5 and A.4.7 we calculate the following charges of the CCLP black hole

$$E = \Big(E_{\text{AdS}} - \widetilde{\zeta}'\Big) + \frac{m\pi(2\Xi_a+2\Xi_b-\Xi_a\Xi_b)+2abq^2\pi(\Xi_a+\Xi_b)}{4\Xi_a^2\Xi_b^2 G_5}\,,$$

$$J_1 = \frac{\pi\big[2am+bq(1+a^2g^2)\big]}{4\Xi_a^2\Xi_b G_5}\,,\quad J_2 = \frac{\pi\big[2bm+aq(1+b^2g^2)\big]}{4\Xi_a\Xi_b^2 G_5}\,, \tag{4.31}$$

$$Q = \frac{\varkappa\sqrt{3}\pi q}{4\Xi_a\Xi_b G_5}\,,$$

physically corresponding to: energy, angular momenta and electric charge. Above we have defined the constants

$$E_{\text{AdS}} = \frac{3\pi}{32g^2G_5}\left(1+\frac{(\Xi_a-\Xi_b)^2}{9\Xi_a\Xi_b}\right),\quad \widetilde{\zeta}' = \frac{9g\pi\beta\big(\Xi_a^2-\Xi_a\Xi_b+\Xi_b^2\big)}{\Xi_a\Xi_b G_5}\zeta'\,, \tag{4.32}$$

where ζ' is the coefficient of a certain finite counterterm that we introduce to the boundary action in the process of holographic renormalization, see Appendix A.4.6. In a similar calculation [169] obtains the energy of the Kerr-AdS$_5$ black hole — the special case $q = 0$, in a renormalization scheme where $\widetilde{\zeta}' = 0$. For the quantity $E_{\rm AdS}$, which physically corresponds to the Casimir energy of empty AdS$_5$, we find agreement with [169]. The Euclidean on-shell action is obtained by evaluating (A.79), on-shell, on a surface $r = R_0$, where $R_0 \gg r_+$. Naively, one obtains divergences, scaling as R_0^4 and R_0^2. They can be cancelled by subtracting the on-shell action of AdS$_5$, written in suitable coordinates, in a background subtraction procedure. The final answer reads

$$\mathcal{I}_{\rm bs} = \frac{\pi\beta}{4\Xi_a\Xi_b G_5}\left[m - g^2(a^2+r_+^2)(b^2+r_+^2) - \frac{q^2 r_+^2}{(a^2+r_+^2)(b^2+r_+^2)+abq}\right]. \tag{4.33}$$

To obtain this answer, crucially, one has to include the gauge parameter α in (4.20) and then set it to $-\Phi$ to ensure that the gauge field is regular on the horizon. This important aspect of the calculation was not explicitly stated in the original derivation presented in [96]. Alternatively, in Appendix A.4.6 we employ holographic renormalization to obtain the following Euclidean on-shell action

$$\mathcal{I} = \beta\Big(E_{\rm AdS} - \widetilde{\zeta}'\Big) + \mathcal{I}_{\rm bs}\,, \tag{4.34}$$

where precisely the constants (4.32) appear. We can interpret this discrepancy between the two on-shell action results as follows. In a non-supersymmetric setting there is no preferred mechanism to fix the coefficient ζ' of the finite counterterm, i.e. the value of the constant $\widetilde{\zeta}'$ defines a choice of renormalization scheme. In particular, the "background subtraction renormalization scheme" corresponds to setting $\widetilde{\zeta}' = E_{\rm AdS}$. In a different scheme the energy acquires an additive constant factor and the on-shell action acquires the same additive factor times β.

Having collected the potentials, charges, entropy and on-shell action of CCLP we have verified explicitly that, in any renormalization scheme, the quantum statistical relation holds

$$\mathcal{I} = \beta E - S - \beta\Omega_1 J_1 - \beta\Omega_2 J_2 - \beta\Phi Q\,. \tag{4.35}$$

Naively, the first law of thermodynamics

$$\mathrm{d}E = \frac{1}{\beta}\,\mathrm{d}S + \Omega_1\,\mathrm{d}J_1 + \Omega_2\,\mathrm{d}J_2 + \Phi\,\mathrm{d}Q\,, \tag{4.36}$$

where the variations are taken with respect to the "bare" black hole parameters $(a,\, b,\, r_+,\, q)$, is only satisfied in the renormalization scheme $\widetilde{\zeta}' = E_{\rm AdS}$. Insisting on using the "bare" parameters, it was argued in [169] that in a renormalization scheme where $\widetilde{\zeta}' \neq E_{\rm AdS}$ one should use the following generalized first law

$$\mathrm{d}E = \delta_\sigma E + \frac{1}{\beta}\,\mathrm{d}S + \Omega_1\,\mathrm{d}J_1 + \Omega_2\,\mathrm{d}J_2 + \Phi\,\mathrm{d}Q\ , \tag{4.37}$$

where $\delta_\sigma E$ is the variation of the energy with respect to a Weyl transformation that keeps representative of the conformal class of boundary metrics fixed. They go further to prove that the variation of the on-shell action under this Weyl transformation is[7]

$$\delta_\sigma \mathcal{I} = \beta\,\mathrm{d}\Big(E_{\rm AdS} - \widetilde{\zeta}'\Big) = \beta\,\delta_\sigma E\,. \tag{4.38}$$

Using this result, we see that the generalized first law takes the form

$$\mathrm{d}\Big(E - \Big(E_{\rm AdS} - \widetilde{\zeta}'\Big)\Big) = \frac{1}{\beta}\,\mathrm{d}S + \Omega_1\,\mathrm{d}J_1 + \Omega_2\,\mathrm{d}J_2 + \Phi\,\mathrm{d}Q\ , \tag{4.39}$$

which is now trivially satisfied in any renormalization scheme, when the variation is taken with respect to the parameters (a, b, r_+, q).

The Euclidean on-shell action can be though of as minus the logarithm of the grand canonical partition function

$$\mathcal{I}(\beta, \Omega_1, \Omega_2, \Phi) = -\log \mathcal{Z}(\beta, \Omega_1, \Omega_2, \Phi)\,, \tag{4.40}$$

where the grand canonical ensemble is the one in which the thermodynamic potentials $(\beta,\, \Omega_1,\, \Omega_2,\, \Phi)$ are held fixed, while the charges are allowed to fluctuate. In this setup each state is assigned a probability

$$P_i = \frac{1}{\mathcal{Z}} e^{-\beta(E_i - \Omega_1 J_{1,i} - \Omega_2 J_{2,i} - \Phi Q_i)}\,, \quad \mathcal{Z} = \sum_i e^{-\beta(E_i - \Omega_1 J_{1,i} - \Omega_2 J_{2,i} - \Phi Q_i)}\,. \tag{4.41}$$

Then the average charges are given by

$$\begin{aligned} E &= \sum_i P_i E_i = \frac{\partial \mathcal{I}}{\partial \beta} + \Omega_1 J_1 + \Omega_2 J_2 + \Phi Q\,, \\ J_1 &= \sum_i P_i J_{1,i} = -\frac{1}{\beta}\frac{\partial \mathcal{I}}{\partial \Omega_1}\,, \quad J_2 = \sum_i P_i J_{2,i} = -\frac{1}{\beta}\frac{\partial \mathcal{I}}{\partial \Omega_2}\,, \\ Q &= \sum_i P_i Q_i = -\frac{1}{\beta}\frac{\partial \mathcal{I}}{\partial \Phi}\,. \end{aligned} \tag{4.42}$$

[7]Technically, they only prove this in the renormalization scheme $\widetilde{\zeta}' = 0$, but their result trivially generalizes.

The above relations can be readily seen from the quantum statistical relation (4.35) and indicate that the potentials $(\beta,\, \Omega_1,\, \Omega_2,\, \Phi)$ are conjugate to the charges $(E,\, J_1,\, J_2,\, Q)$, respectively. We can verify these relations on the CCLP solution as follows. First, we express the Euclidean on-shell action and the potentials solely in terms of the black hole parameters $(a,\, b,\, r_+,\, q)$. Then we solve the following system of four equations

$$\begin{aligned}\frac{\partial \mathcal{I}}{\partial(a,b,r_+,q)} &= \frac{\partial \mathcal{I}}{\partial \beta}\frac{\partial \beta}{\partial(a,b,r_+,q)} + \frac{\partial \mathcal{I}}{\partial \Omega_1}\frac{\partial \Omega_1}{\partial(a,b,r_+,q)} \\ &\quad + \frac{\partial \mathcal{I}}{\partial \Omega_2}\frac{\partial \Omega_2}{\partial(a,b,r_+,q)} + \frac{\partial \mathcal{I}}{\partial \Phi}\frac{\partial \Phi}{\partial(a,b,r_+,q)}\end{aligned} \tag{4.43}$$

for the four unknowns $\left(\frac{\partial \mathcal{I}}{\partial \beta},\, \frac{\partial \mathcal{I}}{\partial \Omega_1},\, \frac{\partial \mathcal{I}}{\partial \Omega_2},\, \frac{\partial \mathcal{I}}{\partial \Phi}\right)$. Plugging the results in (4.42) we get perfect agreement with the charges obtained in Appendices A.4.5 and A.4.7 via holographic renormalization and Komar integrals. Finally, one can view the entropy as a function of the charges $(E,\, J_1,\, J_2,\, Q)$ and write the quantum statistical relation as

$$S(E,J_1,J_2,Q) = \beta E - \beta\Omega_1 J_1 - \beta\Omega_2 J_2 - \beta\Phi Q - \mathcal{I}(\beta,\Omega_1,\Omega_2,\Phi)\,, \tag{4.44}$$

where the following relations should hold

$$\beta = \frac{\partial S}{\partial E}\,, \quad \Omega_1 = -\frac{1}{\beta}\frac{\partial S}{\partial J_1}\,, \quad \Omega_2 = -\frac{1}{\beta}\frac{\partial S}{\partial J_2}\,, \quad \Phi = -\frac{1}{\beta}\frac{\partial S}{\partial Q}\,. \tag{4.45}$$

Again, we establish their validity on the CCLP solution by solving the following system of four equations

$$\begin{aligned}\frac{\partial S}{\partial(a,b,r_+,q)} &= \frac{\partial S}{\partial E}\frac{\partial E}{\partial(a,b,r_+,q)} + \frac{\partial S}{\partial J_1}\frac{\partial J_1}{\partial(a,b,r_+,q)} \\ &\quad + \frac{\partial S}{\partial J_2}\frac{\partial J_2}{\partial(a,b,r_+,q)} + \frac{\partial S}{\partial Q}\frac{\partial Q}{\partial(a,b,r_+,q)}\,,\end{aligned} \tag{4.46}$$

for the four unknowns $\left(\frac{\partial S}{\partial E},\, \frac{\partial S}{\partial J_1},\, \frac{\partial S}{\partial J_2},\, \frac{\partial S}{\partial Q}\right)$ and plugging the results in (4.45). This analysis shows that the entropy is the Legendre transform of the Euclidean on-shell action, in which the charges $(E,\, J_1,\, J_2,\, Q)$ replace the potentials $(\beta,\, \Omega_1, \Omega_2, \Phi)$ as independent variables.

4.3.3 Thermodynamics in the supersymmetric and BPS limits of CCLP

One can make the CCLP solution supersymmetric by saturating the BPS bound

$$q = \frac{m}{1 + ag + bg} \,. \tag{4.47}$$

In what follows it is convenient to also exchange the parameter m for

$$\widetilde{m} = \frac{mg}{(a+b)(1+ag)(1+bg)(1+ag+bg)} - 1 \,. \tag{4.48}$$

We show that the resulting three-parameter family of solutions, i.e. $(a,\, b,\, \widetilde{m})$, is supersymmetric in Appendix A.4.8 by explicitly solving the Killing spinor equations. This three parameter family of Euclidean supersymmetric solutions can be analytically continued to Lorentzian signature resulting in a family of supersymmetric black holes. These black hole solutions are however not regular and causal outside their horizon which is manifested by the generically complex roots of $\Delta_r(r) = 0$. Setting $\widetilde{m} = 0$ one obtains a two-parameter family, i.e. $(a,\, b)$, of supersymmetric and extremal black holes that do not suffer from such problems and have vanishing temperature, i.e. $\beta \to \infty$. This was called the BPS limit in [72] and one can show that in this BPS limit $\Delta_r(r) = 0$ has a real double root given by

$$r_*^2 = \frac{1}{g}(a + b + abg) \,, \tag{4.49}$$

and the surface $r = r_*$ constitutes the event horizon of the BPS black hole.

To have better control over the IR divergence associated with the fact that $\beta \to \infty$ in the BPS limit, we provide an alternative description of the supersymmetric black hole. Using (5.7) and (4.25), the supersymmetry condition (5.6) can be rewritten as

$$q = -ab + r_+^2(1 + ag + bg) \pm \sqrt{-r_+^2(r_*^2 - r_+^2)} \,. \tag{4.50}$$

Insisting that q is real, we see that we are forced to take the extremal limit $r_+ \to r_*$ alongside the supersymmetric limit. In general however q is complex

and leads to the following (complex) supersymmetric thermodynamic quantities

$$\beta = -\frac{2\pi(a-\mathrm{i}r_+)(b-\mathrm{i}r_+)(gr_*^2+\mathrm{i}r_+)}{g(r_*^2-r_+^2)\big[2r_+(1+ag+bg)+\mathrm{i}g(r_*^2-3r_+^2)\big]}\,,$$

$$\Omega_1 = \frac{g(r_*^2+\mathrm{i}ar_+)(1-\mathrm{i}gr_+)}{(gr_*^2+\mathrm{i}r_+)(a-\mathrm{i}r_+)}\,,\quad \Omega_2 = \Omega_1\Big|_{a\leftrightarrow b}\,,$$

$$\Phi = \frac{\sqrt{3}\,\mathrm{i}r_+(1-\mathrm{i}gr_+)}{\varkappa(gr_*^2+\mathrm{i}r_+)}\,,$$

$$\widetilde{E} = \frac{\pi\big[3-g^2\big(a^2(1+bg)+b^2(1+ag)-ab\big)\big]\big[-ab+r_+^2(1+ag+bg)+\mathrm{i}gr_+\big(r_*^2-r_+^2\big)\big]}{4\Xi_a\Xi_b(1-ag)(1-bg)G_5}\,,$$

$$J_1 = \frac{\pi[2a+b(1+ag)]\big[-ab+r_+^2(1+ag+bg)+\mathrm{i}gr_+\big(r_*^2-r_+^2\big)\big]}{4\Xi_a\Xi_b(1-ag)G_5}\,,\quad J_2 = J_1\Big|_{a\leftrightarrow b}\,,$$

$$Q = \frac{\varkappa\sqrt{3}\,\pi\big[-ab+r_+^2(1+ag+bg)+\mathrm{i}gr_+\big(r_*^2-r_+^2\big)\big]}{4\Xi_a\Xi_bG_5}\,,$$

$$S = \frac{\pi^2\big[r_+\big(r_+^2+a^2(1+bg)+b^2(1+ag)+ab\big)+\mathrm{i}abg(r_*^2-r_+^2)\big]}{2\Xi_a\Xi_bG_5}$$

$$\widetilde{\mathcal{I}} = \frac{\pi^2(a-\mathrm{i}r_+)^2(b-\mathrm{i}r_+)^2(1+g^2r_*^2)}{2\Xi_a\Xi_b\big[2r_+(1+ag+bg)+\mathrm{i}g(r_*-3r_+^2)\big]G_5}\,, \tag{4.51}$$

where we have defined $\widetilde{E} = E - \Big(E_{\mathrm{AdS}} - \widetilde{\zeta}'\Big)$ and $\widetilde{\mathcal{I}} = \mathcal{I} - \beta\Big(E_{\mathrm{AdS}} - \widetilde{\zeta}'\Big)$. As expected, the quantum statistical relation (4.35) and the generalized first law (4.39) continue to hold in the supersymmetric limit. We also find that the charges obey the following linear relation

$$E - gJ_1 - gJ_2 - \frac{\sqrt{3}}{\varkappa}Q = E_{\mathrm{AdS}} - \widetilde{\zeta}'\,. \tag{4.52}$$

If the right hand side of this equation vanishes it will look like the familiar BPS constraint of the charges obeyed by supersymmetric black holes. As explained in Appendix A.4 the parameter $\widetilde{\zeta}'$ is the coefficient of a finite counterterm in the holographic renormalization procedure used to compute the gravitational charges. We can therefore make the right hand side of (4.52) vanish if we choose a scheme in which $\widetilde{\zeta}' = E_{\mathrm{AdS}}$. This choice is implemented by the background subtraction scheme discussed above (4.33). We note that since there is no preferred holographic renormalization scheme for 5d minimal gauged supergravity that is compatible with covariance, gauge invariance, and

supersymmetry, see for example [51], one is in principle free to choose any other value of the finite counterterm coefficient $\widetilde{\zeta}'$. From now on we will work in the $\widetilde{\zeta}' = E_{\rm AdS}$ scheme which implies that $E = \widetilde{E}$ and $\mathcal{I} = \widetilde{\mathcal{I}}$.

In addition to the linear relation in (4.52), supersymmetry implies a linear relation between the corresponding potentials that reads

$$\beta\Big(g + \Omega_1 + \Omega_2 - g\chi\sqrt{3}\,\Phi\Big) = 2\pi\mathrm{i}\,. \tag{4.53}$$

In Appendix A.4.8 we show how this constraint arises from a periodicity condition on the Killing spinor on the horizon. It is useful to define new chemical potentials which are convenient for taking the $\beta \to \infty$ supersymmetric black hole limit

$$\omega_1 = \beta(\Omega_1 - g)\,, \quad \omega_2 = \beta(\Omega_2 - g)\,, \quad \varphi = \beta\left(\Phi - \frac{\sqrt{3}}{\chi}\right). \tag{4.54}$$

In terms of them the supersymmetric Euclidean on-shell action takes the remarkably simple form

$$\mathcal{I} = \frac{\pi\chi^3}{12\sqrt{3}\,G_5}\frac{\varphi^3}{\omega_1\omega_2}\,. \tag{4.55}$$

The quantum statistical relation (4.35) and the linear constraint (4.53) can also be written in a manifestly β-independent way

$$\mathcal{I} = -S - \omega_1 J_1 - \omega_2 J_2 - \varphi Q\,; \quad \omega_1 + \omega_2 - g\chi\sqrt{3}\,\varphi = 2\pi\mathrm{i}\,, \tag{4.56}$$

where the energy has been eliminated using (4.52).

This presentation of the supersymmetric CCLP black hole is adapted to taking the limit to extremality: $r_+ \to r_*$. Even though β diverges in this limit, the newly defined chemical potentials assume the following finite (and complex) BPS values

$$\begin{aligned}
\boldsymbol{\omega}_1 &= -\frac{\pi(1-ag)(b-\mathrm{i}\,r_*)}{r_*[1+g(a+b-\mathrm{i}\,r_*)]}\,, \quad \boldsymbol{\omega}_2 = \omega_1\Big|_{a\leftrightarrow b}\,, \\
\boldsymbol{\varphi} &= \frac{\sqrt{3}\,\pi(a-\mathrm{i}\,r_*)(b-\mathrm{i}\,r_*)}{\chi\, r_*[1+g(a+b-\mathrm{i}\,r_*)]}\,,
\end{aligned} \tag{4.57}$$

where we adopted the convention to denote BPS quantities in the $\beta \to \infty$ limit with bold letters. The BPS charges and the entropy become real in this limit

and read

$$\begin{aligned}
\boldsymbol{E} &= \frac{\pi(a+b)\big[3-g^2\big(a^2(1+bg)+b^2(1+ag)-ab\big)\big]}{4g(1-ag)^2(1-bg)^2G_5}\,,\\
\boldsymbol{Q} &= \frac{\mathrm{i}\sqrt{3}\,\pi(a+b)}{4(1-ag)(1-bg)G_5}\,,\\
\boldsymbol{J}_1 &= \frac{\pi(a+b)[2a+b(1+ag)]}{4g(1-ag)^2(1-bg)G_5}\,,\quad \boldsymbol{J}_2 = \boldsymbol{J}_1\Big|_{a\leftrightarrow b}\,,\\
\boldsymbol{S} &= \frac{\pi^2(a+b)r_*}{2g(1-ag)(1-bg)G_5}\,,
\end{aligned} \tag{4.58}$$

while the BPS Euclidean on-shell action remains complex and is naturally expressed in terms of the new BPS potentials

$$\boldsymbol{\mathcal{I}} = \mu\frac{\boldsymbol{\varphi}^3}{\boldsymbol{\omega}_1\boldsymbol{\omega}_2}\,, \tag{4.59}$$

where we have extracted the constant pre-factor $\mu = \pi\mathrm{i}^3/(12\sqrt{3}G_5)$. The quantum statistical relation and linear constraint between the potentials take precisely the same form as in the supersymmetric case

$$\boldsymbol{\mathcal{I}} = -\boldsymbol{S} - \boldsymbol{\omega}_1\boldsymbol{J}_1 - \boldsymbol{\omega}_2\boldsymbol{J}_2 - \boldsymbol{\varphi}\boldsymbol{Q}\,;\quad \boldsymbol{\omega}_1+\boldsymbol{\omega}_2-\nu\boldsymbol{\varphi} = 2\pi\mathrm{i}\,, \tag{4.60}$$

where we have defined $\nu = g\mathrm{i}\sqrt{3}$. We again work in the grand canonical ensemble where the potentials are held fixed and the charges allowed to fluctuate and write the entropy as

$$\begin{aligned}
\boldsymbol{S}(\boldsymbol{J}_1,\boldsymbol{J}_2,\boldsymbol{Q}) = -\boldsymbol{\mathcal{I}}(\boldsymbol{\omega}_1,\boldsymbol{\omega}_2,\boldsymbol{\varphi}) - \boldsymbol{\omega}_1\boldsymbol{J}_1 - \boldsymbol{\omega}_2\boldsymbol{J}_2 - \boldsymbol{\varphi}\boldsymbol{Q}\\
- \lambda(\boldsymbol{\omega}_1+\boldsymbol{\omega}_2-\nu\boldsymbol{\varphi}-2\pi\mathrm{i})\,,
\end{aligned} \tag{4.61}$$

where we have included a Lagrange multiplier λ multiplying the linear constraint. Taking partial derivatives of the above with respect to the potentials one obtains three extremization equations

$$\begin{gathered}
-\frac{\partial\boldsymbol{\mathcal{I}}}{\partial\boldsymbol{\omega}_1} = \boldsymbol{J}_1+\lambda\,,\quad -\frac{\partial\boldsymbol{\mathcal{I}}}{\partial\boldsymbol{\omega}_2} = \boldsymbol{J}_2+\lambda\,,\quad -\frac{\partial\boldsymbol{\mathcal{I}}}{\partial\boldsymbol{\varphi}} = \boldsymbol{Q}-\nu\lambda\\
\Downarrow\\
\mu\frac{\boldsymbol{\varphi}^3}{\boldsymbol{\omega}_1^2\boldsymbol{\omega}_2} = \boldsymbol{J}_1+\lambda\,,\quad \mu\frac{\boldsymbol{\varphi}^3}{\boldsymbol{\omega}_1\boldsymbol{\omega}_2^2} = \boldsymbol{J}_2+\lambda\,,\quad -\mu\frac{3\boldsymbol{\varphi}^2}{\boldsymbol{\omega}_1\boldsymbol{\omega}_2^2} = \boldsymbol{Q}-\nu\lambda\,.
\end{gathered} \tag{4.62}$$

In principle, to perform the Legendre transform one has to invert the bottom line above (together with the linear constraint) to express $(\boldsymbol{\omega}_1, \boldsymbol{\omega}_2, \boldsymbol{\varphi}, \lambda)$ in terms of the charges $(\boldsymbol{J}_1, \boldsymbol{J}_2, \boldsymbol{Q})$ and then plug the results in (4.61) to obtain the entropy. However, due to $\boldsymbol{\mathcal{I}}$ being a homogeneous function of degree 1, from Euler's theorem one has $\boldsymbol{\mathcal{I}} = \boldsymbol{\omega}_1 \partial_{\boldsymbol{\omega}_1} \boldsymbol{\mathcal{I}} + \boldsymbol{\omega}_2 \partial_{\boldsymbol{\omega}_2} \boldsymbol{\mathcal{I}} + \boldsymbol{\varphi} \partial_{\boldsymbol{\varphi}} \boldsymbol{\mathcal{I}}$, and the expression for the entropy simplifies to

$$\boldsymbol{S} = 2\pi \mathrm{i} \lambda \,. \tag{4.63}$$

This provides the following shortcut to obtaining the entropy. By inspection we see that

$$0 = \frac{1}{\nu^3} \left[\left(\frac{\partial \boldsymbol{\mathcal{I}}}{\partial \boldsymbol{\varphi}} \right)^3 - 27\mu \frac{\partial \boldsymbol{\mathcal{I}}}{\partial \boldsymbol{\omega}_1} \frac{\partial \boldsymbol{\mathcal{I}}}{\partial \boldsymbol{\omega}_2} \right] \implies 0 = p_0 + p_1 \lambda + p_2 \lambda^2 + \lambda^3 \,, \tag{4.64}$$

where after the implies sign we have used the extremization equations and extracted the coefficients in front of the λ terms

$$\begin{aligned} p_0 &= -\frac{1}{\nu^3} \boldsymbol{Q}^3 - \frac{27\mu}{\nu^3} \boldsymbol{J}_1 \boldsymbol{J}_2 \,, \\ p_1 &= \frac{3}{\nu^2} \boldsymbol{Q}^2 - \frac{27\mu}{\nu^3} (\boldsymbol{J}_1 + \boldsymbol{J}_2) \,, \\ p_2 &= -\frac{3}{\nu} \boldsymbol{Q} - \frac{27\mu}{\nu^3} \,. \end{aligned} \tag{4.65}$$

We seek a purely real entropy in the BPS limit, so we should have a purely imaginary root of the cubic (4.64). This is possible if $p_0 = p_1 p_2$, which translates to the following non-linear relation between the BPS charges:

$$\left(\frac{2}{g\varkappa\sqrt{3}} \boldsymbol{Q} \right)^3 + \frac{2\pi}{g^3 G_5} \boldsymbol{J}_1 \boldsymbol{J}_2 = \left(\frac{2\sqrt{3}}{g\varkappa} \boldsymbol{Q} + \frac{\pi}{2g^3 G_5} \right) \left[\left(\frac{2}{g\varkappa} \boldsymbol{Q} \right)^2 - \frac{\pi}{g^3 G_5} (\boldsymbol{J}_1 + \boldsymbol{J}_2) \right] . \tag{4.66}$$

Then the purely imaginary roots are $\lambda = \pm \mathrm{i} \sqrt{p_1}$. Picking the minus sign in order to have positive entropy we obtain

$$\boldsymbol{S} = \frac{\pi}{g} \sqrt{\frac{4}{\varkappa^2} \boldsymbol{Q}^2 - \frac{\pi}{g G_5} (\boldsymbol{J}_1 + \boldsymbol{J}_2)} \,. \tag{4.67}$$

While we have shown how to obtain the supersymmetric black hole entropy as a Legendre transformation of the on-shell action it is also possible to verify the validity of (4.67) and (4.66) using the explicit expression of the BPS charges and entropy in terms of the black hole parameters given in (4.58).

4.4 Holography and the superconformal index

The results for the on-shell action and entropy of the supersymmetric CCLP solution presented above can be understood from a holographic viewpoint in terms of an appropriate supersymmetric partition function on $S^1 \times S^3$ called the superconformal index $\mathcal{I}_{\rm QFT}$, see [183] for a review. Here we discuss how this can be done in some detail.

4.4.1 Anomalies and the index on the second sheet

The superconformal index of class $\mathcal{S}$ SCFTs has been studied for low values of N in [33, 118, 119, 182]. We are not aware of an extension of these results valid in the large N limit relevant to our holographic setup. Recently, building on previous results in [138, 72], it was shown in [86], see also [128], that the superconformal index of general 4d $\mathcal{N}=1$ SCFTs is given by the following compact expression

$$\log \mathcal{I}_{\rm QFT} = \frac{\varphi_R^3}{48\omega_1\omega_2} k_{RRR} - \frac{\varphi_R(\omega_1^2+\omega_2^2-4\pi^2)}{48\omega_1\omega_2} k_R + \log|G| \,, \tag{4.68}$$

where, $\omega_{1,2}$ are the fugacities for the two angular momenta on S^3, φ_R is the $U(1)$ R-symmetry fugacity, G is the order of the Abelian 1-form symmetry in the theory (if any), and (k_{RRR}, k_R) are the cubic and linear 't Hooft anomalies. Supersymmetry imposes the following linear relation between the fugacities

$$\varphi_R = (\omega_1 + \omega_2 + 2\pi \mathrm{i} n_0) \,, \tag{4.69}$$

and the expression in (5.1) is valid for $n_0 = \pm 1$, i.e. on the "second sheet" of the complexified fugacities. This result for the index includes the contribution from the supersymmetric Casimir energy [59, 12] and is valid up to exponentially suppressed terms of the form $e^{-\ell_3/\beta}$ where ℓ^3 is the radius of the S^3 and β is the circumference of the S^1. It is not immediately clear that this Cardy-like limit of the index is useful for studying its large N properties. However, it was shown in [138, 72, 63, 89] that the k_{RRR} and k_R terms in (5.1) are in perfect agreement with the regularized on-shell action of the supersymmetric CCLP solution in 5d $\mathcal{N}=2$ minimal gauged supergravity and its four-derivative extension. This in turn implies that the on-shell action and entropy of the wrapped M5-brane black holes we constructed above can be reproduced by using the index in (5.1). This is indeed possible as we show below.

To use the expression in (5.1) we need the 't Hooft anomalies for the R-symmetry of the SCFT at hand. The 4d $\mathcal{N}=1$ class $\mathcal{S}$ SCFTs of interest here have a $U(1)_F$ flavor symmetry in addition to the $U(1)_R$ R-symmetry. The 't Hooft

anomalies for these global symmetries can be computed as in [120, 55, 10, 18, 19] either with field theory methods or by integrating the anomaly polynomial of the 6d $\mathcal{N} = (2, 0)$ SCFT over $\Sigma_{\mathfrak{g}}$. For concreteness here we focus on the type A_{N-1} class $\mathcal{S}$ theories and take $\mathfrak{g} > 1$[8] for which the 't Hooft anomalies read

$$\begin{aligned} k_{RRR} &= \frac{2(\mathfrak{g}-1)}{27z^2}\left[9z^2 - 1 + (3z^2+1)^{\frac{3}{2}}\right] N^3\,, \quad k_{RRF} = \frac{(\mathfrak{g}-1)}{9}\, z\, N\,, \\ k_{RFF} &= -\frac{(\mathfrak{g}-1)}{3}\sqrt{3z^2+1}N^3\,, \qquad\qquad k_{FFF} = (\mathfrak{g}-1)\, z\, N^3\,, \\ k_R &= \frac{\mathfrak{g}-1}{3}\left[4 - \sqrt{3z^2+1}\right] N\,, \qquad\qquad k_F = (\mathfrak{g}-1)\, z\, N\,. \end{aligned} \tag{4.70}$$

We have presented the results for the leading term in the large N expansion of the anomalies which is all we need for our holographic discussion. The exact finite N values can be easily found using the results in [18, 19]. To obtain these results for the 't Hooft anomalies, as explained in [18, 19], one has to employ a-maximization [141]. As expected from a-maximization we find that k_{RFF} is negative and that the superconformal Ward identity $k_F = 9k_{RRF}$ is obeyed. In addition, one can use superconformal Ward identities to find the following conformal anomalies

$$\begin{aligned} a &= \frac{1}{32}(9k_{RRR} - 3k_R) = (\mathfrak{g}-1)\frac{\left(9z^2 - 1 + (1+3z^2)^{\frac{3}{2}}\right)}{48z^2}N^3\,, \\ c &= \frac{1}{32}(9k_{RRR} - 5k_R) = (\mathfrak{g}-1)\frac{\left(9z^2 - 1 + (1+3z^2)^{\frac{3}{2}}\right)}{48z^2}N^3\,. \end{aligned} \tag{4.71}$$

Again we have presented the conformal anomalies only to leading order in the large N limit and as expected for a holographic SCFT we find that $a = c$ to this order.

Plugging the results for k_{RRR} and k_R presented above in the formula for the superconformal index (5.1) we obtain an explicit expression for $\mathcal{I}_{\rm QFT}$ valid in the Cardy-like limit and to leading order in the large N limit. To compare $\mathcal{I}_{\rm QFT}$ with the regularized on-shell action of the supersymmetric CCLP solution we need to employ the holographic dictionary. As shown in [65, 63] the cubic 't Hooft anomaly is related to the 5d AdS radius and Newton constant as

$$k_{RRR} = \frac{4\pi L^3}{9G_5}\,, \tag{4.72}$$

[8]The results below have a straightforward generalization to arbitrary genus and to the type D_N theories.

while k_R is related to the coefficients of the four-derivative corrections to the 5d supergravity theory. To relate this 5d supergravity expression for k_{RRR} to the microscopic parameters $(N, \mathfrak{g}, z)$ one should use the relation between the 5d and 7d Newton constants in (4.13), the expressions that define the AdS_5 supersymmetric vacua in (4.10), as well as the uplift of this solution to 11d using the formulae in Section 4.1. As shown in [65, 63], and can be checked explicitly using the formulae above, this supergravity calculation leads to exactly the same result for k_{RRR} as the one in (4.70).

Another entry from the holographic dictionary we need is the relation between the fugacities specifying the index and the gravitational potentials of the CCLP solution. This was also discussed in some detail recently in [63] where it was shown that the supergravity BPS potentials in (4.57) can be related to the field theory fugacities as follows

$$\omega_{1,2} \longleftrightarrow \boldsymbol{\omega}_{1,2}\,, \qquad\qquad \varphi_R \longleftrightarrow \frac{\mathfrak{x}\sqrt{3}}{L}\boldsymbol{\varphi}\,. \tag{4.73}$$

Comparing the supergravity BPS relation in (4.60) with the field theory one in (4.69) we see that we must set $n_0 = -1$ in order to find agreement. This choice for the sign of n_0 is related to a conventional choice in the sign of the electric field in the CCLP solution.

Combining all these ingredients together we find that regularized supergravity on-shell action $\boldsymbol{\mathcal{I}}$ in (4.59) precisely agrees with the k_{RRR} term in the logarithm of the superconformal index $\log \mathcal{I}_{\rm QFT}$ in (5.1). If one would like to obtain the entropy of the supersymmetric CCLP black hole in (4.67) one can simply take $\log \mathcal{I}_{\rm QFT}$ and repeat the Legendre transformation procedure discussed above (4.67). These results constitute a precision test of holography for the wrapped M5-brane black holes we constructed above and a microscopic understanding of their Bekenstein-Hawking entropy in terms of the superconformal index of the dual 4d $\mathcal{N} = 1$ class $\mathcal{S}$ SCFTs.

4.4.2 More general black holes?

The 4d $\mathcal{N} = 1$ SCFTs in [18, 19] have a $U(1)_F$ flavor symmetry in addition to the $U(1)_R$ R-symmetry. This means that the superconformal index can be additionally refined with a flavor fugacity φ_F. The explicit form of this refined index in the Cardy-like or large N limit has not been studied in the literature. From the supergravity point of view the $U(1)_F \times U(1)_R$ global symmetry is realized by the two Killing vectors in the 11d metric in (4.2) or alternatively by the two Abelian gauge fields in the 7d gauged supergravity (4.6). The asymptotically AdS_5 black hole solutions we studied above have only

one electric charge associated with the $U(1)_R$ gauge field. Both the QFT and supergravity setups therefore suggest that there may be more general black hole solutions with two electric charges and two angular momenta with entropy and on-shell action that can be accounted for by the large N limit of the refined superconformal index. While we have not calculated the refined index or constructed these supergravity solutions we present some speculations and educated guesses about their properties.

We begin with the following proposal for the generalized version of the "second sheet" formula for the index of a general 4d $\mathcal{N}=1$ SCFT with a $U(1)$ flavor symmetry

$$\log \mathcal{I}_{\rm QFT} = \frac{k_{RRR}\,\varphi_R^3 + k_{RRF}\,\varphi_R^2\varphi_F + k_{RFF}\,\varphi_R\varphi_F^2 + k_{FFF}\,\varphi_F^3}{48\omega_1\omega_2}\,, \tag{4.74}$$

where φ_R obeys the linear constraint (4.69) and we have only presented terms that involve the cubic 't Hooft anomalies since these should be the leading contributions to the large N limit of the index of a holographic SCFT. This proposed formula for the index is based on the form of the supersymmetric Casimir energy for general 4d $\mathcal{N}=1$ SCFTs in [59] as well as the holographic results for the index of $\mathcal{N}=4$ SYM in [138].

Then, we propose the following identification between the field theory fugacities and the supergravity BPS potentials

$$\omega_{1,2} \longleftrightarrow \boldsymbol{\omega}_{1,2}\,, \quad \varphi_R \longleftrightarrow \nu\boldsymbol{\varphi}_R\,, \quad \varphi_F \longleftrightarrow \rho\boldsymbol{\varphi}_F\,, \tag{4.75}$$

where, the constants ν and ρ should be determined by using the holographic dictionary using the explicit putative black hole solutions.To be consistent with the form of the on-shell action in (4.59) we expect that $\nu = \chi\sqrt{3}\,g$, such that $\boldsymbol{\varphi} \equiv \boldsymbol{\varphi}_R$.

In the dual supergravity there should be a supersymmetric Euclidean solution with two angular momenta and two electric charges that has the following on-shell action

$$\boldsymbol{\mathcal{I}} = \frac{\mu_1\,\boldsymbol{\varphi}_R^3 + \mu_2\,\boldsymbol{\varphi}_R^2\boldsymbol{\varphi}_F + \mu_3\,\boldsymbol{\varphi}_R\boldsymbol{\varphi}_F^2 + \mu_4\,\boldsymbol{\varphi}_F^3}{\boldsymbol{\omega}_1\boldsymbol{\omega}_2}\,, \tag{4.76}$$

where the real parameters $\mu_{1,2,3,4}$ should be determined by the coupling constants of the particular supergravity theory hosting the proposed new black hole. One should then derive, via the holographic dictionary, explicitly how they are related to the 't Hooft anomalies $k_{RRR}, k_{RRF}, k_{RFF}$ and k_{FFF}. In order to have a holographic match between $\boldsymbol{\mathcal{I}}$ and $\log\mathcal{I}_{\rm QFT}$ we need the following relations to hold

$$\mu_1 = \frac{k_{RRR}\nu^3}{48}\,, \quad \mu_2 = \frac{k_{RRF}\nu^2\rho}{48}\,, \quad \mu_3 = \frac{k_{RFF}\nu\rho^2}{48}\,, \quad \mu_4 = \frac{k_{FFF}\rho^3}{48}\,, \tag{4.77}$$

Establishing this equivalence is of course non-trivial and hinges on the explicit construction of the black hole solution with two electric charges, the details of the holographic map, and the validity of the formula for the index in (4.74).

If all our educated guesses (4.74)-(4.77) are correct and such a non-trivial agreement can indeed be established one can try to proceed and perform a Legendre transform of the on-shell action, or equivalently the large N index in order to derive the entropy of the black hole. This proves to be a non-trivial calculation as we now outline. First let us rewrite the on-shell action as

$$\boldsymbol{\mathcal{I}} = \frac{\pi}{24\boldsymbol{\omega}_1\boldsymbol{\omega}_2}\kappa_{IJK}\boldsymbol{\varphi}^I\boldsymbol{\varphi}^J\boldsymbol{\varphi}^K\,, \tag{4.78}$$

where κ_{IJK} is totally symmetric with its independent components given by

$$\kappa_{111} = \frac{24\mu_1}{\pi}\,, \quad \kappa_{112} = \frac{8\mu_2}{\pi}\,, \quad \kappa_{122} = \frac{8\mu_3}{\pi}\,, \quad \kappa_{222} = \frac{24\mu_4}{\pi}\,, \tag{4.79}$$

and $\boldsymbol{\varphi}^I = (\boldsymbol{\varphi}_R, \boldsymbol{\varphi}_F)$. This rewriting of the on-shell action is inspired by the on-shell action of supersymmetric black holes in 5d gauged supergravity coupled to two vector multiplets studied in [88]. The only difference here is that we use a basis of supergravity BPS potentials that explicitly singles out the superconformal R-symmetry. To find the entropy we now follow the familiar procedure of extremizing

$$\boldsymbol{S} = -\boldsymbol{\mathcal{I}} - \boldsymbol{\varphi}^I\boldsymbol{Q}_I - \boldsymbol{\omega}_1\boldsymbol{J}_1 - \boldsymbol{\omega}_2\boldsymbol{J}_2 - \lambda(\boldsymbol{\omega}_1 + \boldsymbol{\omega}_2 - \nu\boldsymbol{\varphi}_R - 2\pi\mathrm{i})\,, \tag{4.80}$$

where $\boldsymbol{Q}_I = (\boldsymbol{Q}_R, \boldsymbol{Q}_F)$ and, crucially, only $\boldsymbol{\varphi}_R$ is on the "second sheet". The extremization equations read

$$-\frac{\partial\boldsymbol{\mathcal{I}}}{\partial\boldsymbol{\omega}_1} = \boldsymbol{J}_1 + \lambda\,, \quad -\frac{\partial\boldsymbol{\mathcal{I}}}{\partial\boldsymbol{\omega}_2} = \boldsymbol{J}_2 + \lambda\,, \quad -\frac{\partial\boldsymbol{\mathcal{I}}}{\partial\boldsymbol{\varphi}_R} = \boldsymbol{Q}_R - \nu\lambda\,, \quad -\frac{\partial\boldsymbol{\mathcal{I}}}{\partial\boldsymbol{\varphi}_F} = \boldsymbol{Q}_F\,. \tag{4.81}$$

Together with the linear constraint $\boldsymbol{\omega}_1 + \boldsymbol{\omega}_2 - \nu\boldsymbol{\varphi}_R = 2\pi\mathrm{i}$, this amounts to a system of 5 non-linear equations that need to be solved for $(\boldsymbol{\omega}_1, \boldsymbol{\omega}_2, \boldsymbol{\varphi}_R, \boldsymbol{\varphi}_F, \lambda)$ in terms of the charges $(\boldsymbol{J}_1, \boldsymbol{J}_2, \boldsymbol{Q}_R, \boldsymbol{Q}_F)$. We have not been able to solve this system of equations analytically and have only found numerical solutions. To proceed further we resort to the shortcut outlined in Section 4.3.3. We note that $\boldsymbol{\mathcal{I}}$ is again homogeneous of degree 1 and the extremized entropy is therefore given by $\boldsymbol{S} = 2\pi\mathrm{i}\lambda$.

We note that the relation

$$0 = \frac{1}{6}\kappa^{IJK}\frac{\partial\boldsymbol{\mathcal{I}}}{\partial\boldsymbol{\varphi}^I}\frac{\partial\boldsymbol{\mathcal{I}}}{\partial\boldsymbol{\varphi}^J}\frac{\partial\boldsymbol{\mathcal{I}}}{\partial\boldsymbol{\varphi}^K} - \frac{\pi}{4}\frac{\partial\boldsymbol{\mathcal{I}}}{\partial\boldsymbol{\omega}_1}\frac{\partial\boldsymbol{\mathcal{I}}}{\partial\boldsymbol{\omega}_2}\,, \tag{4.82}$$

holds provided that κ_{IJK} obeys

$$\kappa_{IJK}\kappa_{J'(LM}\kappa_{PQ)K'}g^{JJ'}g^{KK'} = \frac{4}{3}g_{I(L}\kappa_{MPQ)}\,, \tag{4.83}$$

where the metric and the inverse metric read

$$g_{IJ} = 6\left(\frac{\pi}{2\mu_1}\right)^{-2/3}\delta_{IJ}\,, \quad g^{IJ} = \frac{1}{6}\left(\frac{\pi}{2\mu_1}\right)^{2/3}\delta^{IJ}\,, \tag{4.84}$$

and consequently, the non-zero components of κ^{IJK} are given by

$$\kappa^{111} = \frac{\pi}{18\mu_1}\,, \quad \kappa^{112} = \frac{\pi\mu_2}{54\mu_1^2}\,, \quad \kappa^{122} = \frac{\pi\mu_3}{54\mu_1^2}\,, \quad \kappa^{222} = \frac{\pi\mu_4}{18\mu_1^2}\,. \tag{4.85}$$

In the symmetric fugacity basis used in the supergravity analysis in [88] the relation (4.83) holds since it ensures that the scalars residing in the two vector multiplets parametrize a symmetric coset space. If we take this requirement imposed by gauged supergravity as a given and use the extremization equations (4.81) together with (4.82) we find that λ has to obey the following cubic equation:

$$\begin{aligned}
0 &= p_0 + p_1\lambda + p_2\lambda^2 + \lambda^3\,,\\
p_0 &= -\frac{1}{\nu^3}\boldsymbol{Q}_R^3 - \frac{27\mu_1}{\nu^3}\boldsymbol{J}_1\boldsymbol{J}_2 - \frac{\mu_2}{\mu_1\nu^3}\boldsymbol{Q}_R^2\boldsymbol{Q}_F - \frac{\mu_4}{\mu_1\nu^3}\boldsymbol{Q}_F^3\,,\\
p_1 &= -\frac{27\mu_1}{\nu^3}(\boldsymbol{J}_1+\boldsymbol{J}_2) + \frac{3}{\nu^2}\boldsymbol{Q}_R^2 + \frac{2\mu_2}{\mu_1\nu^2}\boldsymbol{Q}_R\boldsymbol{Q}_F + \frac{\mu_3}{\mu_1\nu^2}\boldsymbol{Q}_F^2\,,\\
p_2 &= -\frac{27\mu_1}{\nu^3} - \frac{3}{\nu}\boldsymbol{Q}_R - \frac{\mu_2}{\mu_1\nu}\boldsymbol{Q}_F\,.
\end{aligned} \tag{4.86}$$

Then the non-linear relation between the charges and the entropy read

$$p_0 = p_1p_2\,, \quad \boldsymbol{S} = 2\pi\sqrt{p_1}\,. \tag{4.87}$$

Note that these expression nicely reduce to our results in Section 4.3.3 when $\boldsymbol{Q}_F = 0$ and

$$\mu_1 = \frac{k_{RRR}\nu^3}{48} = \frac{1}{48}\frac{4\pi L^3}{9G_5}\left(\frac{\mathfrak{r}\sqrt{3}}{L}\right)^3 = \frac{\pi\mathfrak{r}^3}{12\sqrt{3}G_5} = \mu\,, \tag{4.88}$$

where we have used our educated guess for the relation between the supergravity constant μ_1 and the SCFT anomaly k_{RRR}. More importantly, this expression for the entropy and the non-linear constraint between the black hole charges are only valid when (4.83) is satisfied. From the point of view of the dual SCFT

the origin of this relation is far from clear. We assume that μ_2 is subleading in large N, which is indeed realized by the concrete example of the class $\mathcal{S}$ theories studied above, see (4.77) and (4.70) where ρ is assumed not to scale with N. Using this we find that the only way to satisfy the constraint in (4.83) is if the following relations hold

$$\mu_3 = -\frac{3}{2}\mu_1\,, \quad \mu_4 = \frac{1}{\sqrt{2}}\mu_1\,. \tag{4.89}$$

We are not aware of any QFT reason why such a relation should be obeyed by the supergravity constants μ_1, μ_3 and μ_4. Indeed, using our educated guess (4.77), in terms of the QFT anomalies these relations read

$$k_{RFF}\rho^2 = -\frac{3}{2}k_{RRR}\nu^2\,, \quad k_{FFF}\rho^3 = \frac{1}{\sqrt{2}}k_{RRR}\nu^3 \tag{4.90}$$

Clearly, these relations cannot hold for the explicit anomalies (4.70) for any value of ρ , even if we allow it to be z-dependent.

Based on the discussion above we conclude that for general holographic SCFTs with a $U(1)_F$ flavor symmetry, including the particular example of the $\mathcal{S}$ SCFTs discussed above, one cannot find a simple compact expression for the black hole entropy in terms of the two electric charges and two angular momenta. This points to the fact that perhaps the sought more general wrapped M5-brane black holes with an additional flavor electric charge cannot be constructed using a 5d $\mathcal{N} = 2$ gauged supergravity theory coupled to a finite number of vector multiplets. Indeed, based on the consistent truncation classification results in [85, 144] there are no candidates for such a gauged supergravity theory.

The situation is different for $\mathcal{N} = 4$ SYM. One can show that for this theory the 't Hooft anomalies for the $U(1)^3$ Cartan subalgebra of the $SO(6)$ global symmetry obey the constraints in (4.89) and indeed, as shown in [147], there is a simple compact expression for the entropy of the supersymmetric black hole with two angular momenta and three electric charges constructed in [149] using the STU model of 5d $\mathcal{N} = 2$ gauged supergravity.

4.5 Discussion

The results presented above leave several open questions and interesting possibilities for generalizations. Here we discuss some of them.

- As discussed in Section 4.4.2 it is very likely that there are more general supersymmetric black holes with an additional electric charge

corresponding to the $U(1)_F$ flavor symmetry of the class $\mathcal{S}$ SCFTs. It will be very interesting to construct these solutions, either by using an appropriate 5d matter-coupled supergravity theory arising as a consistent truncation of 11d supergravity, or by a judicious Ansatz for the fields of the 7d maximal gauged supergravity. Of course it should in principle be possible to construct such solutions directly in 11d supergravity but we expect that to be prohibitively difficult since the corresponding BPS equations should reduce to a system of coupled nonlinear PDEs.

- There are two other generalizations of the black hole solutions discussed above that one can contemplate. For concreteness here we have focused the discussion on the class $\mathcal{S}$ SCFTs associated to the 6d $\mathcal{N} = (2, 0)$ SCFT of type A_{N-1} compactified on a smooth $\Sigma_{\mathfrak{g}}$ with $\mathfrak{g} > 1$. Using the results in [18, 19] it is straightforward to generalize this setup to the D_N type class $\mathcal{S}$ SCFTs and to $\mathfrak{g} = 0, 1$. On the supergravity side this corresponds to modifying the 11d supergravity solutions discussed above to have an internal $\mathbb{RP}^4$ space instead of the S^4 used in (4.2) and to modify the metric in (4.9) to that of the torus or the two-sphere. More non-trivially, one can attempt to find a larger class of black hole solutions arising from wrapped branes on punctured Riemann surfaces. While it is known how to construct such AdS_5 vacua with $\mathcal{N} = 2$ and $\mathcal{N} = 1$ supersymmetry, see [120, 16, 17], it is not entirely clear how to generalize these supergravity solutions to include a black hole. Perhaps the 7d gauged supergravity method developed in [58] to treat some special punctures on the Riemann surface will prove useful in this regard.

- As already emphasized in Section 4.4.1 it is not entirely clear to us why the Cardy-like limit of the index used to derive the "second sheet" formula for the index in [86] has a larger regime of validity that captures the behavior of the large N limit of the index relevant for holography. It will be most interesting to understand this better and also to generalize the "second sheet" formula for the index to include fugacities associated with flavor symmetries. We have proposed such a generalization in (4.74) and it will be interesting to check our educated guess more rigorously. Finally, it is important to study $\log N$ corrections to the large N class $\mathcal{S}$ superconformal index which should correspond to the 1-loop contributions to the gravitational path integral of the KK modes of 11d supergravity around the AdS_5 black hole solutions. Establishing this relation rigorously will provide a stringent precision test of holography. We also note in passing that subleading terms in the large N power law expansion of the superconformal index are also captured by "second sheet" formula. These correspond to higher-derivative corrections to the CCLP solution in gauged supergravity. This was studied recently in [63, 89] where a precise

agreement between the holographic and QFT results was established. In particular a discussion on higher-derivative corrections to AdS_5 black holes arising from wrapped branes was presented in [63] based on the assumptions that such solutions indeed exist. Our results here indeed show that this is true.

- The superconformal index for the class $\mathcal{S}$ SCFTs discussed above was studied in [33] for low values of N. It will be most interesting to understand how to extend the results of this work to larger values of N. For gauge theories coupled to matter a useful approach to studying the large N limit of the index is to employ the Bethe Ansatz re-formulation, see [53, 54]. If such a formulation is possible for class $\mathcal{S}$ SCFTs it will provide a concrete calculational tool to gain valuable insights into the quantum gravity corrections to the properties of the black holes constructed in this work.

Chapter 5

Wrapped M5-branes including subleading large-N effects

Exploring the AdS/CFT correspondence beyond the classical two-derivative supergravity approximation is a challenging endeavor that is bound to lead to important insights into quantum gravity. Supersymmetry is an invaluable tool that allows for quantitative access to physical observables on both sides of the duality. There have been recent important advances in this context using supersymmetric localization for 3d $\mathcal{N} = 2$ SCFTs and higher-derivative corrections in 4d supergravity. In particular, supersymmetric localization allows for the systematic calculation of the path integral of the SCFT on compact Euclidean manifolds order by order in the $1/N$ expansion, see [177] for a review. For SCFTs arising from M2-branes, the leading and subleading terms at large N can be reproduced using holography by studying the four-derivative corrections to 4d gauged supergravity [211, 52, 60, 61]. Our goal in this work is to extend this success to 5d gauged supergravity and the dual 4d $\mathcal{N} = 1$ SCFTs.

The QFT observable of interest here is the superconformal index which can be defined for any 4d $\mathcal{N} = 1$ SCFT as the path integral of the theory on $S^1 \times S^3$ with appropriate supersymmetric periodicity conditions [185, 148, 183]. The large N limit of the superconformal index for holographic SCFTs is subtle and it was recently understood that one needs to consider the analyticity properties of the index on the complex fugacity plane in order to find non-trivial large N scaling indicative of a weakly coupled holographic bulk dual, see [138, 72, 54, 97] and references thereof. While the superconformal index contains detailed information about the spectrum of BPS states in the 4d $\mathcal{N} = 1$ SCFT, it simplifies drastically in the large N limit when one takes the fugacities to be

on the "second sheet" [86]. It was argued in [86, 128], that the superconformal index on the second sheet, $\mathcal{I}$, takes the following form

$$\log \mathcal{I} = \frac{(\omega_1+\omega_2+2\pi \mathrm{i} n_0)^3}{48\omega_1\omega_2}\mathrm{Tr}R^3 \tag{5.1}$$
$$- \frac{(\omega_1+\omega_2+2\pi \mathrm{i} n_0)(\omega_1^2+\omega_2^2-4\pi^2)}{48\omega_1\omega_2}\mathrm{Tr}R + \log|G|\,,$$

where $\omega_{1,2}$ are the two angular momentum fugacities, $\mathrm{Tr}R^3$ and $\mathrm{Tr}R$ are the cubic and linear 't Hooft anomalies for $\mathrm{U}(1)_\mathrm{R}$, the supersymmetry constraint that fixes the R-symmetry fugacity has already been implemented with $n_0 = \pm 1$, and $|G|$ is the order of the Abelian one-form symmetry in the theory (if any). This result is valid up to terms of order $e^{-\ell_3/\beta}$ in the small β limit, where β is the circumference of S^1 and ℓ_3 is the radius of the S^3, and includes the contribution from the supersymmetric Casimir energy [12, 59]. Our main result in this chapter is a supergravity calculation that reproduces the first two terms on the RHS of (5.1). This constitutes a non-trivial precision test of holography and provides strong independent evidence for the validity of the results in [86, 128].

For holographic SCFTs with a weakly coupled supergravity dual, $\mathrm{Tr}R^3$ is the leading term in the large N expansion and is proportional to the dimensionless ratio L^3/G_5 between the scale L of AdS_5 and the 5d Newton constant. Indeed, it was shown in [72] how the first term on the RHS of (5.1) can be obtained holographically by calculating the regularized on-shell action of a class of supersymmetric Euclidean solutions of 5d minimal $\mathcal{N}=2$ gauged supergravity with an $S^1 \times S^3$ boundary derived in [98, 99]. In SCFTs with an appropriate large N scaling the $\mathrm{Tr}R$ term in (5.1) should be captured by including four-derivative corrections to the supergravity theory. Recently the full 5d minimal $\mathcal{N}=2$ gauged supergravity action including the two possible four-derivative terms was derived in [65], see also [152]. We show that evaluating the regularized four-derivative on-shell action for the CCLP solution of [98, 99] in this four-derivative theory yields precise agreement with the $\mathrm{Tr}R^3$ and $\mathrm{Tr}R$ terms in (5.1). We then employ this result and the first law of thermodynamics to calculate the Wald entropy of the Lorentzian AdS_5 black hole obtained by analytic continuation of the CCLP solution and comment on its relation to the superconformal index

5.1 The Euclidean CCLP solution

In this section we remind the reader of the relevant equations for the Wick-rotated CCLP black hole on the 2∂ level. This material can also be found in chapter 4. Here we emphasize on the Euclidean properties of the solution. It was shown in [98, 99] that the following background, which we will refer to as the CCLP solution, solves the equations of motion of the two-derivative 5d minimal $\mathcal{N}=2$ gauged supergravity

$$\begin{aligned} ds^2 =& \frac{\Delta_\eta \left[\left(1+\frac{r^2}{L^2}\right)\rho^2\, d\tau + 2\mathrm{i}q\nu\right] d\tau}{\Xi_a\Xi_b\rho^2} + \frac{2q\nu\omega}{\rho^2} + \frac{f}{\rho^4}\left(\frac{\mathrm{i}\Delta_\eta\, d\tau}{\Xi_a\Xi_b}+\omega\right)^2 \\ &+ \frac{\rho^2 dr^2}{\Delta_r} + \frac{\rho^2 d\eta^2}{\Delta_\eta} + \frac{r^2+a^2}{\Xi_a}\sin^2\eta\, d\xi_1^2 + \frac{r^2+b^2}{\Xi_b}\cos^2\eta\, d\xi_2^2\,, \qquad (5.2) \\ A =& -\frac{\sqrt{3}q}{\rho^2}\left(\frac{\mathrm{i}\Delta_\eta d\tau}{\Xi_a\Xi_b}+\omega\right) - \mathrm{i}\alpha\, d\tau, \end{aligned}$$

where we have defined

$$\begin{aligned} \nu &= b\sin^2\eta\, d\xi_1 + a\cos^2\eta\, d\xi_2\,, \\ \Delta_r &= \frac{(r^2+a^2)(r^2+b^2)\left(1+\frac{r^2}{L^2}\right)+q^2+2abq-2mr^2}{r^2}\,, \\ \omega &= \frac{a}{\Xi_a}\sin^2\eta\, d\xi_1 + \frac{b}{\Xi_b}\cos^2\eta\, d\xi_2\,, \qquad (5.3) \\ \Delta_\eta &= 1-\frac{a^2}{L^2}\cos^2\eta - \frac{b^2}{L^2}\sin^2\eta\,, \\ \rho^2 &= r^2 + a^2\cos^2\eta + b^2\sin^2\eta\,, \\ f &= 2m\rho^2 - q^2 + \frac{2abq\rho^2}{L^2}\,,\quad \Xi_a = 1-\frac{a^2}{L^2}\,,\quad \Xi_b = 1-\frac{b^2}{L^2}\,. \end{aligned}$$

We present the solution in Euclidean signature and do not assume any reality properties of the four parameters (m,q,a,b). The solution in Lorentzian signature can be obtained from the expressions above by the replacement $\tau \to it$ and describes a black hole in AdS_5 with one electric charge and two independent angular momenta.

We are interested in studying the effects of the four-derivative corrections to 5d $\mathcal{N}=2$ gauged supergravity on the on-shell action and thermodynamic

properties of this solution. These four-derivative corrections were studied recently in [65] where it was shown that they are controlled by two constant coefficients $c_{1,2}$, see (5.11) for the full bosonic Lagrangian of the supergravity theory. As discussed in [184, 166], see also [131, 73] for earlier observations to this effect, if one is interested in corrections linear in $c_{1,2}$ it is not necessary to correct the two-derivative solution but it is sufficient to consider only the effects due to the corrected action. It is expected on very general grounds that $c_{1,2}$ are parametrically small corrections to the two-derivative action [74]. We will therefore use the results in [184, 166] as our starting point and work with the two-derivative CCLP solution [1].

The Euclidean solution caps off at the location of the outer black hole horizon obtained by solving $\Delta_r(r_+) = 0$. The length β of the Euclidean time circle is determined by requiring regularity of the metric in the limit $r \to r_+$ and reads

$$\beta = \frac{2\pi r_+[(r_+^2 + a^2)(r_+^2 + b^2) + abq]}{r_+^4[1 + g^2(2r_+^2 + a^2 + b^2)] - (ab + q)^2}\,, \tag{5.4}$$

where $g = 1/L$ and the coordinate ranges of the Euclidean solution are

$$\tau \in [0, \beta)\,,\ r \in [r_+, \infty)\,,\ \eta \in [0, \tfrac{\pi}{2})\,,\ \xi_{1,2} \in [0, 2\pi)\,. \tag{5.5}$$

The Euclidean CCLP solution is supersymmetric if one constrains the parameters as

$$q = \frac{m}{1 + ag + bg}\,. \tag{5.6}$$

It is important to stress that this supersymmetric Euclidean solution does not in general admit a Lorentzian continuation to a supersymmetric and causal black hole solution, see [72] for a more detailed discussion. To obtain the BPS Lorentzian black hole found in [132, 98, 99] one has to impose the additional relation

$$\frac{mg}{(a + b)(1 + ag)(1 + bg)(1 + ag + bg)} = 1\,, \tag{5.7}$$

together with the inequality $a + b + abg > 0$.

To properly understand the four-derivative corrections to the thermodynamic properties of this gravitational solution one needs to carefully compute the conserved charge, angular momentum, and entropy. We will discuss some aspects of these calculations below. For the chemical potentials dual to these

[1] Note that the logic here is different from the one used in [60, 61] where it was shown that every solution of the two-derivative minimal 4d $\mathcal{N} = 2$ gauged supergravity also solves the equations of motion of the four-derivative theory without assuming that the coefficients $c_{1,2}$ are small.

thermodynamic variables one can simply employ the fact that we are working with an uncorrected two-derivative solution and use the temperature $T = 1/\beta$, with β in (5.4), as well as the following angular and electric chemical potentials [72]

$$\begin{aligned} \Omega_1 &= \frac{a(r_+^2+b^2)(1+g^2r_+^2)+bq}{(r_+^2+a^2)(r_+^2+b^2)+abq}\,, \quad \Omega_2 = \frac{b(r_+^2+a^2)(1+g^2r_+^2)+aq}{(r_+^2+a^2)(r_+^2+b^2)+abq}\,, \\ \Phi &= \frac{\sqrt{3}qr_+^2}{(r_+^2+a^2)(r_+^2+b^2)+abq}\,. \end{aligned} \tag{5.8}$$

It is important to stress that imposing regularity of the gauge field at $r = r_+$, i.e. demanding that $A_\mu A^\mu$ is finite, fixes the pure gauge constant α in (5.2) as $\alpha = -\Phi$.

Studying thermodynamics for supersymmetric black holes is subtle due to their finite entropy and vanishing temperature. Here we will follow the approach of [72], see also [62], and use the supersymmetric Euclidean solution as a crutch to calculate finite gravitational observables in the supersymmetric limit. This means that we will study the two-parameter family of supersymmetric Euclidean solutions obtained by imposing the constraint (5.6). The supersymmetric temperature and chemical potentials are then obtained from (5.4) and (5.8) by imposing the constraint (5.6) and will be denoted by a superscript s, while the relevant quantities for the supersymmetric Lorentzian black hole solution will be denoted by a $*$ superscript and are obtained by additionally imposing (5.7). To make a connection with the fugacities in the $S^1 \times S^3$ supersymmetric partition function of the dual SCFT it was shown in [72] that it is useful to define the following angular and electric gravitational fugacities

$$\begin{aligned} \omega_1^s &\equiv \beta^s(\Omega_1^s - \Omega_1^*) = \frac{\pi(ag-1)(b-\mathrm{i}r_+)}{\Xi}\,, \\ \omega_2^s &\equiv \beta^s(\Omega_2^s - \Omega_2^*) = \frac{\pi(bg-1)(a-\mathrm{i}r_+)}{\Xi}\,, \\ \varphi^s &\equiv \beta^s(\Phi^s - \Phi^*) = \frac{\sqrt{3}\,\pi(a-\mathrm{i}r_+)(b-\mathrm{i}r_+)}{\Xi}\,, \end{aligned} \tag{5.9}$$

where $\Xi \equiv r_+(1+ag+bg) + \frac{\mathrm{i}g}{2}(r_*^2 - 3r_+^2)$ and r_* is the value of r_+ when both constraints in (5.6) and (5.7) are imposed. These new chemical potentials satisfy the linear constraint

$$\omega_1^s + \omega_2^s - \frac{\sqrt{3}}{L}\,\varphi^s = 2\pi\mathrm{i}\,, \tag{5.10}$$

which is the supergravity analog of the linear relation between the SCFT fugacities that is already implemented in (5.1). The fact that the supergravity fugacities add up to an imaginary number reflects the analytic continuation to the second sheet used in [86].

5.2 HD corrections and the on-shell action

According to the standard holographic dictionary the supergravity dual of the logarithm of the superconformal index in (5.1) should be equal to the regularized on-shell action of the CCLP solution. To compute this action we use the four-derivative Lagrangian of 5d minimal $\mathcal{N}=2$ gauged supergravity, as derived in [65]

$$
\begin{aligned}
e^{-1}\mathcal{L}_{4\partial} = & -\Big[\frac{1}{\kappa^2}+\frac{(5\,c_1+24\,c_2)g^2}{2\sqrt{3}}\Big]R+\Big[\frac{1}{4\kappa^2}+\frac{7(5\,c_1-12\,c_2)g^2}{24\sqrt{3}}\Big]F_{ab}^2 \\
& -\Big[\frac{12g^2}{\kappa^2}+\frac{1}{\sqrt{3}}\,(25\,c_1+156\,c_2)\,g^4\Big]-\frac{\mathrm{i}}{12\sqrt{3}}\Big[\frac{1}{\kappa^2}-\frac{3\sqrt{3}(c_1+6\,c_2)}{2}g^2\Big]e^{-1}\varepsilon^{\mu\nu\rho\sigma\tau}A_\mu F_{\nu\rho}F_{\sigma\tau} \\
& -\frac{\mathrm{i}c_1}{16}e^{-1}\varepsilon^{\mu\nu\rho\sigma\tau}A_\mu R_{\nu\rho}{}^{\lambda\epsilon}R_{\sigma\tau\lambda\epsilon}-\frac{(2\,c_1-3\,c_2)}{24\sqrt{3}}R\,F_{ab}^2+\frac{5c_1}{4\sqrt{3}}R^{ab}F_{ac}F_b{}^c \\
& -\frac{\sqrt{3}c_1}{16}R_{abcd}F^{ab}F^{cd}-\frac{(c_1+6\,c_2)}{8\sqrt{3}}\,R^2+\frac{c_1}{2\sqrt{3}}R_{ab}^2-\frac{\sqrt{3}c_1}{8}(R_{abcd})^2 \\
& -\frac{5\sqrt{3}}{64}\,c_1\,F^{ab}F_a{}^cF_b{}^dF_{cd}+\frac{(61\,c_1-6\,c_2)}{1152\sqrt{3}}F_{ab}^2\,F_{cd}^2+\frac{\sqrt{3}c_1}{2}(\nabla_aF_{bc})(\nabla^{[a}F^{b]c}) \\
& +\frac{\sqrt{3}c_1}{2}F_{ab}\nabla^b\nabla_cF^{ac}-\frac{\mathrm{i}c_1}{8}e^{-1}\varepsilon^{\mu\nu\rho\sigma\tau}F_\mu{}^\lambda F_{\sigma\tau}\Big(\frac{3}{2}\,\nabla_\nu F_{\lambda\rho}-\nabla_\lambda F_{\nu\rho}\Big) \\
& -\frac{3\mathrm{i}c_1}{32}e^{-1}\varepsilon^{\mu\nu\rho\sigma\tau}F_{\mu\nu}F_{\rho\sigma}\nabla^\lambda F_{\lambda\tau}+\mathcal{O}(c_i^2)\,. \qquad (5.11)
\end{aligned}
$$

We have written the Lagrangian in Euclidean signature, used e to denote the square root of the determinant of the metric, and have defined the ε symbol as $\varepsilon^{01234}=\varepsilon_{01234}=1$. In addition to the metric, the only bosonic field in the theory is the U(1) gauge field A_μ with field strength $F_{\mu\nu}$ and we use conventions where $\kappa^2=16\pi G_5$ and the supergravity gauge coupling is related to the AdS_5 scale L used in (5.2), (5.3) as $g=1/L$. We emphasize that (5.11) was derived by working to linear order in the small parameters $c_{1,2}$ determining the four-derivative invariants. When the couplings $c_{1,2}$ vanish, the Lagrangian

above reduces to the one for the two-derivative 5d minimal $\mathcal{N}=2$ gauged supergravity. In computing the on-shell action from (5.11) we regulate the UV divergences by employing background subtraction. More specifically, we calculate the difference between the on-shell action of the CCLP solution for general values of the parameters (using the coordinate ranges in (5.5)) and the on-shell action of empty AdS_5 in global coordinates. We note that the same holographic regularization scheme was used in the two-derivative on-shell action analysis in [96, 72]. The on-shell action calculation is arduous and was performed with the help of `Mathematica` [2]. The final result for the regularized four-derivative on-shell action however is compact and simple and reads

$$I_{\rm reg} = \frac{(\varphi^s)^3}{\omega_1^s\omega_2^s}\left[\frac{\pi}{12\sqrt{3}G_5} - \frac{2\pi^2(c_1+6c_2)}{L^2}\right] + \frac{\varphi^s[(\omega_1^s)^2+(\omega_2^s)^2-4\pi^2]}{\omega_1^s\omega_2^s}2\pi^2 c_1 . \tag{5.12}$$

To compare this calculation with the field theory result in (5.1) we need to invoke the holographic map between field theory and gravitational quantities. The relation between the supergravity parameters and the 't Hooft anomaly coefficients in the dual SCFT was worked out in [65, 15] and reads [3]

$$\begin{aligned} \mathrm{Tr}\, R^3 &= \frac{16(5\mathfrak{a}-3\mathfrak{c})}{9} = \frac{4\pi L^3}{9G_5} - \frac{32\sqrt{3}\pi^2}{3}L(c_1+6c_2)\,, \\ \mathrm{Tr}\, R &= 16(\mathfrak{a}-\mathfrak{c}) = -32\sqrt{3}\pi^2 L c_1\,. \end{aligned} \tag{5.13}$$

As discussed in [72], the supersymmetric angular fugacities $\omega_{1,2}^s$ in (5.9) should be identified with $\omega_{1,2}$ in (5.1). Using all this, together with the relation between the supergravity fugacities in (5.10), we find a perfect agreement between the four-derivative regularized on-shell action in (5.12) and the first two terms on the RHS of (5.1) for $n_0=-1$ [4]. This agreement constitutes a precision test of holography beyond the two-derivative supergravity approximation.

The field theory result in (5.1) applies to all 4d $\mathcal{N}=1$ SCFTs. Similarly, the four-derivative 5d supergravity on-shell action in (5.12) is universal and should apply to all holographic SCFTs with a weakly coupled bulk dual. It is important however to keep in mind that not all holographic SCFTs have an appropriate large N scaling of $\mathrm{Tr}\, R$ which ensures that the four-derivative

[2] Our code for the calculations that lead to the results presented in this chapter is based on the `xAct` package and can be found at `https://github.com/waskou/SolutionsX`.

[3] The parameter L we use in this work is related to the ℓ used in (2.54) of [65] by $L=\ell+16\pi\sqrt{3}G_5c_2/\ell$.

[4] The fact that our supergravity result yields $n_0=-1$ has to do with the choice of conventions for the sign of the electric charge of the CCLP solution.

supergravity couplings $c_{1,2}$ do not vanish. For instance, as discussed in [65], in $\mathcal{N}=4$ SYM one has $\mathrm{Tr}\, R=0$, while in the well-known $Y^{(p,q)}$ quiver gauge theories $\mathrm{Tr}\, R\sim N^0$ and thus we find that $c_{1,2}$ vanish in these models. As a result, one probably needs to study loop effects in supergravity to capture the $\mathrm{Tr}\, R=0$ term in (5.1). Two notable examples where the 5d Lagrangian in (5.11) captures the effects of $\mathrm{Tr}R$ are the 4d $\mathcal{N}=2$ F-theory models discussed in [7, 9] and the 4d $\mathcal{N}=1$ class $\mathcal{S}$ SCFTs that arise from M5-branes wrapped on a Riemann surface [158, 120, 18, 19]. In both of these examples $\mathrm{Tr}R$ scales as N and, as shown in [65], $c_{1,2}$ do not vanish.

To be concrete, the $\mathrm{U}(1)_{\mathrm{R}}$ 't Hooft anomalies for the 4d $\mathcal{N}=2$ SCFTs arising from D3-branes at F-theory singularities are [7, 9]

$$\begin{aligned}\mathrm{Tr}\, R^3 &= \frac{8\Delta}{9}N^2+\frac{4(\Delta-1)}{9}N+\frac{2}{27}\,,\\ \mathrm{Tr}\, R &= 4(1-\Delta)N+\frac{2}{3}\,,\end{aligned}\tag{5.14}$$

where N is the number of D3-branes and the rational number Δ specifies the global flavor symmetry of the SCFT and is related to the number of D7-branes, n_7, used in the construction. It is given by $\Delta=\frac{12}{12-n_7}$ with n_7 taking values in the set $\{2,3,4,6,8,9,10\}$.

For the theories arising from wrapped M5-branes on a smooth compact Riemann surface $\Sigma_{\mathfrak{g}}$ of genus $\mathfrak{g}>1$ the 't Hooft anomalies were computed in [18, 19] and the result to leading and subleading order at large N reads

$$\begin{aligned}\mathrm{Tr}\, R^3 &= \frac{2(\mathfrak{g}-1)}{27z^2}\left[9z^2-1+(3z^2+1)^{\frac{3}{2}}\right]N^3\\ &\quad-\frac{\mathfrak{g}-1}{9z^2}\left[(\sqrt{3z^2+1}-1)(2+3z^2)-3z^2\right]N+\dots\,,\\ \mathrm{Tr}\, R &= \frac{\mathfrak{g}-1}{3}\left[4-\sqrt{3z^2+1}\right]N+\dots\,.\end{aligned}\tag{5.15}$$

Here N is the number of M5-branes and the rational parameter z specifies the choice of partial topological twist on $\Sigma_{\mathfrak{g}}$ for the theory on the worldvolume of the M5-branes. We can use the anomalies (5.14) and (5.15), together with the supergravity relation in (5.13), to find the large N behavior of the superconformal index in these two classes of models. We emphasize that for these models the large N behavior of the superconformal index has not been studied by "standard methods" and the only available large N results are the application of the universal QFT formula in (5.1) and the supergravity results presented above.

5.3 Wald entropy

In a higher-derivative diffeomorphism covariant theory of gravity the entropy of a black hole solution can be computed using Wald's formalism [207]. Given the Lagrangian density of the d-dimensional theory, $\mathcal{L}$, the Wald entropy can be found through the following integral

$$S_{\rm W} = -2\pi \int_\Sigma d^{d-2}x\sqrt{\gamma}\,\frac{\delta\mathcal{L}}{\delta R_{\mu\nu\rho\sigma}}\,\epsilon_{\mu\nu}\epsilon_{\rho\sigma}\,, \tag{5.16}$$

where Σ is a bifurcate Killing horizon with induced metric $\gamma_{\mu\nu}$, $\epsilon_{\mu\nu}$ is the binormal to Σ defined as $\kappa\,\epsilon_{\mu\nu} = \nabla_\mu V_\nu$ with V^μ the null Killing vector generating the horizon and κ the surface gravity. As emphasized in [202], the Wald procedure has to be modified in the presence of gravitational Chern-Simons terms. Applying the results of [202] to the $A\wedge R\wedge R$ term in the four-derivative Lagrangian (5.11) we find the following additional contribution to the Wald entropy

$$S_{\rm W}^{\rm CS} = -2\pi \int_\Sigma d^3x\,\varepsilon^{\mu\nu\rho}\,\epsilon^\sigma{}_\lambda\,\Gamma^\lambda{}_{\sigma\mu}\,F_{\nu\rho}\,. \tag{5.17}$$

Using (5.16) and (5.17) and the Lagrangian in (5.11) we find that the Wald entropy of any black hole solution in the four-derivative 5d $\mathcal{N}=2$ minimal supergravity can be found by computing the integral

$$\begin{aligned} S_{\rm W} = -2\pi \int_\Sigma d^3x\sqrt{\gamma}\Bigg[&\Big(\frac{1}{\kappa^2} + \frac{5c_1+24c_2}{2\sqrt{3}}g^2 + \frac{2c_1-3c_2}{24\sqrt{3}}F_{ab}^2 + \frac{c_1+6c_2}{4\sqrt{3}}R\Big)\eta^{[a[c}\eta^{d]b]} \\ &- \frac{c_1}{4\sqrt{3}}\Big(5F^{eg}F^f{}_g + 4R^{ef}\Big)\eta^{[a[c}\eta^{d]}{}_e\eta^{b]}{}_f + \frac{\sqrt{3}\,c_1}{16}\Big(F^{ab}F^{cd} + 4R^{abcd}\Big)\Bigg]\epsilon_{ab}\,\epsilon_{cd} \\ &- \frac{c_1\pi}{2}\int_\Sigma d^3x\,\varepsilon^{\mu\nu\rho}\,\epsilon^\sigma{}_\lambda\,\Gamma^\lambda{}_{\sigma\mu}F_{\nu\rho}\,. \end{aligned} \tag{5.18}$$

The last term on the RHS of (5.18) is the contribution from the $A\wedge R\wedge R$ term in the supergravity action. It is straightforward but quite tedious to evaluate the Wald entropy for the general non-supersymmetric two-derivative CCLP black hole solution in (5.2), (5.3). We performed the calculation using `Mathematica` and found explicitly the Wald entropy for the uncorrected black hole solution. Unfortunately this result for the Wald entropy does not agree with the entropy computed using the first law of thermodynamics and presented in (5.19). This implies that in order to find the correct Wald entropy one needs to find the correction to the CCLP solution due to the presence of the four-derivative terms in the supergravity action.

In the absence of the explicit corrections to the CCLP background, one can use the four-derivative gravitational on-shell action and the first law of thermodynamics as a shortcut to obtain the entropy of the corrected black hole solution as follows. Choosing an ensemble where the fugacities $\{\beta, \Phi, \Omega_{1,2}\}$ are kept fixed, varying the on-shell action with respect to the quantities in (5.4) and (5.8) yields the corrected angular momenta $J_{1,2} = -\frac{1}{\beta}\frac{\partial I}{\partial \Omega_{1,2}}$, electric charge $Q = -\frac{2L}{\sqrt{3}\beta}\frac{\partial I}{\partial \Phi}$ and energy $E = \frac{\partial I}{\partial \beta} + \Omega_1 J_1 + \Omega_2 J_2 + \frac{\sqrt{3}}{2L}\Phi Q$. The normalization of Q is chosen for later convenience. In the BPS limit, these conserved quantities obey the linear relation $2LE = 2(J_1 + J_2) + 3Q$. Using this and the first law of thermodynamics, the entropy of the four-derivative BPS black hole reads:

$$S_{\rm W}^{\rm BPS} = \pi\sqrt{3Q^2 - 8\mathfrak{a}(J_1 + J_2) - \frac{16\mathfrak{a}(\mathfrak{a} - \mathfrak{c})(J_1 - J_2)^2}{Q^2 - 2\mathfrak{a}(J_1 + J_2)}}\,. \tag{5.19}$$

We write this formula as a non-linear expression in terms of the black hole charges and the conformal anomalies of the dual SCFT. This is inspired by the two-derivative result in [147] but is somewhat misleading. All quantities in (5.19) should be linearized in the HD parameters $c_{1,2}$ to obtain the four-derivative black hole entropy in terms of the parameters of the CCLP solution. The explicit expressions for the charges and black hole entropy to linear order in $c_{1,2}$ are unwieldy and can be found at `https://github.com/waskou/SolutionsX`. We have also checked that the linearized form of (5.19) follows from a Legendre transform of the on-shell action in (5.12) with respect to $\{\varphi^s, \omega^s_{1,2}\}$ subject to the constraint in (5.10), and then taking the BPS limit.

5.4 Discussion

In this chapter we established a precise agreement between the leading and first subleading correction in the large N limit of the superconformal index of a holographic 4d $\mathcal{N} = 1$ SCFT and the on-shell action of the dual CCLP supergravity solution evaluated in the four-derivative 5d $\mathcal{N} = 2$ minimal gauged supergravity. Importantly, for the subleading correction to be non-vanishing in supergravity we need an appropriate large N scaling of the linear and cubic 't Hooft anomalies. In particular, our results imply that in [166] no correction to the black hole entropy was observed simply because $\mathrm{Tr}R = 0$ in $\mathcal{N} = 4$ SYM and thus $c_{1,2}$ vanish.

Our results also point to a number of important open questions. It is desirable to put on a more solid footing the thermodynamic properties of the CCLP solution in the four-derivative theory of interest here. As discussed above, the chemical potentials remain the same as their two-derivative values and we have

calculated the four-derivative corrections to the on-shell action. Calculating the corrections to the entropy, charge, mass, and angular momentum is however non-trivial since it involves finding the corrections to the CCLP solution due to the four-derivative terms in the action as well as a proper treatment of holographic renormalization in the presence of higher-derivative terms. It will certainly be most interesting to compute these quantities explicitly and in particular check the validity of the quantum statistical relation and the first law of black hole thermodynamics [122, 123], which we have assumed to be valid when computing the black hole entropy in (5.19). By the time of completing this thesis the explicit computation of the black hole charges was performed in [90], in the BPS limit, where the near-horizon of the corrected CCLP solution can be derived with relative ease. Then, the authors employed Page's formalism to calculate the asymptotic charges using only the corrected near-horizon limit. In this broad context, it is also desirable to understand how to use supergravity or string theory to account for the higher order terms in the $1/N$ expansion of the superconformal index as well as for the exponentially suppressed corrections. We hope that our results here are a useful step in that direction.

Chapter 6

Conclusion

In this thesis we have explored various quantum properties of black holes beyond the semi-classical approximation, where the standard black hole thermodynamics was established in the 70's.

Conclusion for chapters 2 and 3 In chapters 2 and 3 we consider the fuzzball proposal: a radical deviation from the GR description of the black hole interior. Namely, that some of the microstates that make up the black hole entropy can be described as smooth, horizonless solitonic solutions of an Einstein + matter theory, dubbed microstate geometries. Each microstate geometry can be viewed as a coherent state in the full quantum gravity formulation. For a certain supersymmetric (zero temperature, but finite entropy) black hole the construction of these microstate geometries within supergravity and their string theory origin is well understood. There are two fundamental questions:

(1) What is the linear response of such a coherent state, when it is explored with a low-energy observable?

(2) How does the system dynamically explore the phase space of microstate geometries and what are the implications for low-energy observations?

The first question was answered in [41] using the there-developed hybrid-WKB approximation: a low-energy scalar probe returns a clear echo after traveling twice the optical length of the geometry. Subsequently, in [161] it was shown that if the probe is a closed string, due to large tidal forces experienced as it travels down the throat of the geometry, its higher energy vibrational modes get

excited and it builds up mass: the probe is effectively trapped for a substantially larger time. The second question is much harder to answer, since a mechanism to trigger a dynamical tunneling between microstates is not established, largely because it is hard to construct non-supersymmetric microstates or microstate geometries.

To make qualitative statements regarding these questions we consider a simplified toy model of the phase space of microstates of a non-supersymmetric black hole. As microstates we take a set of e^S traversable wormholes each having slightly different optical length. Probing one of these wormholes with a low-energy scalar, we find qualitative agreement with the results of [41]: a return of a clear echo after traveling twice the optical length. The new feature is that we are able to obtain this result in two independent ways: using the hybrid-WKB approximation, and using real time holography which involves solving the full wave equation in a mixed signature (Lorentzian and Euclidean) background. This is possible due to the simplicity of our toy model. Thus, we pinpoint in a simple setup the precise regime of validity of the hybrid-WKB method. Within our toy model we also explore for the first time the effects of a microstate tunnelling on the linear response of a scalar probe: the echo broadens and becomes less pronounced. This calculation is performed using the real time holography method as the hybrid-WKB method is not directly applicable to such a scenario. We remain agnostic of the mechanism that triggers the tunnelling between the coherent states.

Extrapolating our results beyond the toy model should be done cautiously. One clear drawback is that the simple traversable wormhole does not produce tidal forces, so our toy model does not capture the trapping of a stringy probe in a full fledged microstate geometry. Taking the most conservative viewpoint, we have provided an independent test of the validity of the hybrid-WKB approximation method. From a broader perspective, we find that studying both Lorentzian and Euclidean microstate geometries is beneficial for exploring dynamical properties of the phase space of black hole microstates. It will be most interesting to pursue a line of research where Euclidean versions of the known microstate geometries are constructed. Then a suitable combination of the real time holography mixed signature method and the hybrid-WKB method might be useful for studying the linear response of a tunnelling scenario in a more trustworthy setup.

Conclusion for chapters 4 and 5 The "unreasonable effectiveness" of supergravity higher derivative corrections in capturing subleading terms to the string/M-theory path integral was first noticed in [60] in the context of the AdS_4/CFT_3 correspondence. The obvious procedure is to derive the UV fixed coefficients of the higher derivative corrections directly in M-theory or

IIA/B string theory and follow the chain of dimensional reductions of their low energy limits down to the effective 4d supergravity, such that the coefficients of the HD terms in 4d are fixed from the UV completion of the theory. One can imagine how complicated this task is. Instead, in [60, 61], supersymmetry was used to restrict the allowed HD terms directly in the 4d effective theory and reduce the unknown UV input to only two constants (c_1 and c_2). As in holography bulk correlation functions are anchored at the boundary, knowledge of the boundary correlation functions in the dual CFT_3 (for example in terms of anomalies) can be used to UV fix the coefficients c_1 and c_2, thus the usage of the phrase "unreasonable effectiveness". This allows for a highly non-trivial test of the AdS/CFT master formula

$$\mathcal{Z}_{\text{string/M}} \approx e^{-I_{\text{on-shell}}} \approx \mathcal{Z}_{\text{CFT}}\,, \tag{6.1}$$

beyond leading order in large-N, where the $\approx$ signs signify that the further subleading KK modes, supergavity loops effects and subdominant saddles are not captured. In string theory the vanishing of the worldsheet β-function gives the equations of motion of the low-energy supergravity theory and HD corrections can in principle be derived from expanding the β-function to higher orders in α'. In M-theory, however, one lacks such a precise UV formulation in the bulk, making this holographic fixing of the coefficients of the HD terms all the more valuable. Once the partition function in the bulk is reliably HD corrected and holographically tested, one can proceed and study HD thermodynamics. For example, the entropy of the asymptotically AdS black hole can be obtained in two ways: first by taking the Legendre transform of $I_{\text{on-shell}}$, and second by using the Wald formula in the near-horizon region.

One can view our work in chapters 4 and 5 as an extension of this procedure to a particular $\text{AdS}_5/\text{CFT}_4$ realizations of holography. In chapter 4 we work out the thermodynamics of the dominant AdS_5 saddle (the Wick rotated CCLP black hole) on the two-derivative level. This has been done previously in [72], but in our work we emphasize the significance of finite counterterms in the process of holographic renormalization, in particular in relation to taking the supersymmetric limit. More importantly, we show explicitly how to embed the CCLP black hole in M-theory. In chapter 5 we include the HD corrections, calculate the corrected on-shell action and perform the Legendre transform to obtain the corrected entropy. The rest of the HD corrected thermodynamics was subsequently worked out in [90].

It will be highly interesting to repeat the procedure in other dimensions. From a broader perspective, again, we emphasize that the HD approach advertized here only captures the leading and subleading in large-N terms in the partition function. Further subleading terms include a complicated interplay between loops in supergravity, KK modes (when there is no scale

separation), subdominant saddles and HD corrections beyond four derivatives. It will be immensely interesting to find a trackable example where these effects can be studied. We hope that our work provides first steps in understanding the string/M-theory path integral. Especially in the case of M-theory (where there is no worldsheet formulation) reformulating everything in terms of the boundary theory degrees of freedom, might be our best bet to understand the M-theory partition function.

Appendix A

Appendix

A.1 Schwinger-Keldysh formalism in field theory

In this appendix, we briefly review the Schwinger-Keldysh formalism [186, 20, 21, 146] for d-dimensional QFTs in Lorentzian signature. This formalism was developed for cases where the in state and the out state are not *both* eigenstates of the Hamiltonian and as such it is particularly useful for studying non-equilibrium phenomena. It provides a natural definition of the various two-point correlation functions in Lorentzian signature (Feynman, anti-Feynman, retarded, advanced, etc.) in a pure or a thermal state, which is relevant for the discussions in this paper. We begin by defining a Keldysh contour, γ, in the complex time plane $\theta = t - i\tau$. Without loss of generality, we can take γ to consist of three Euclidean segments γ_I, where $I = \{a, b, c\}$, and two Lorentzian segments γ_i, where $i = \{1, 2\}$, whose complex times run as (see figure A.1)[1]

$$\begin{aligned} \gamma_a: &\quad \theta \in [-T + i\sigma_a, -T]\,, \\ \gamma_b: &\quad \theta \in [T, T - i\sigma_b]\,, \\ \gamma_c: &\quad \theta \in [-T - i\sigma_b, -T - i\sigma_c]\,, \end{aligned} \qquad \begin{aligned} \gamma_1: &\quad \theta \in [-T, T]\,, \\ \gamma_2: &\quad \theta \in [-T - i\sigma_b, T - i\sigma_b]\,. \end{aligned} \tag{A.1}$$

[1]This type of Schwinger-Keldysh contour is known as an in-in contour, since the Euclidean pieces that prepare the state are both glued at Lorentzian time $t = -T$. For particle scattering problems it is customary to instead work with an in-out contour whose Euclidean pieces are glued at times $t = -T$ and $t = T$, since both the in and out states are eigenstates of the Hamiltonian. The downside of this other configuration is that it can only produce the Feynman correlator explicitly. We will work with such an in-out contour when we calculate the Feynman correlator for a time dependent geometry dual to a wormhole transitioning state in section 3.2.3.

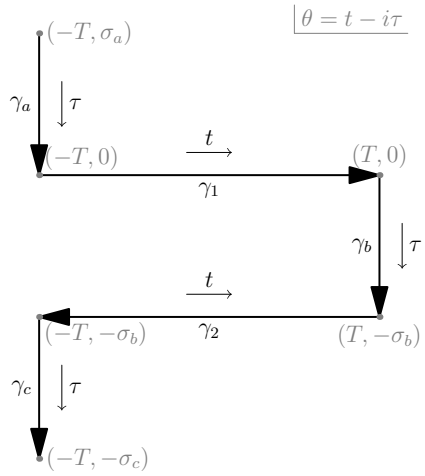


Figure A.1: General Keldysh contour given by (A.1)

The Euclidean segments prepare the state ρ. When ρ is the vacuum or some other pure state, we set $\sigma_b \to 0$ and $\sigma_a = \sigma_c \to \infty$. When ρ is a thermal state of temperature β we set $\sigma_a = \sigma_b = \sigma_c = \beta/2$ and identify the end points of the contour. The partition function, evaluated in the state ρ, in the presence of a source s coupled to some operator $\mathcal{O}$, is given by

$$Z_\rho^{\mathrm{QFT}}[s] = \int_\rho \mathcal{D}\chi \ \exp\left(i \int_\gamma \mathrm{d}\theta \int \mathrm{d}\vec{x} \, [\mathcal{L}_{\mathrm{QFT}}[\chi, \partial_\mu \chi] + s(\theta, \vec{x}) \mathcal{O}(\theta, \vec{x})] \right), \quad \text{(A.2)}$$

where χ collectively describes the QFT degrees of freedom. Omitting the spatial $\vec{x}$ integral in what follows, the source term in the partition function reads

$$\begin{aligned}
\int_\gamma \mathrm{d}\theta \, s(\theta)\mathcal{O}(\theta) = & \int_{-\sigma_a}^{0} \mathrm{d}\tau \, s(-T - i\tau)\mathcal{O}(-T - i\tau) + i \int_{-T}^{T} \mathrm{d}t \, s(t)\mathcal{O}(t) \\
& + \int_0^{\sigma_b} \mathrm{d}\tau \, s(T - i\tau)\mathcal{O}(T - i\tau) + i \int_T^{-T} \mathrm{d}t \, s(t - i\sigma_b)\mathcal{O}(t - i\sigma_b) \\
& + \int_{\sigma_b}^{\sigma_c} \mathrm{d}\tau \, s(-T - i\tau)\mathcal{O}(-T - i\tau) \\
\equiv & \int_{-\sigma_a}^{0} \mathrm{d}\tau \, s_a(\tau)\mathcal{O}_a(\tau) + i \int_{-T}^{T} \mathrm{d}t \, s_1(t)\mathcal{O}_1(t) + \int_0^{\sigma_b} \mathrm{d}\tau \, s_b(\tau)\mathcal{O}_b(\tau) \\
& - i \int_{-T}^{T} \mathrm{d}t \, s_2(t)\mathcal{O}_2(t) + \int_{\sigma_b}^{\sigma_c} \mathrm{d}\tau \, s_c(\tau)\mathcal{O}_c(\tau) \,, \qquad \text{(A.3)}
\end{aligned}$$

where we have defined

$$\begin{aligned} s_a(\tau) &= s(-T - i\tau)\,, \qquad \tau \in [-\sigma_a, 0]\,, \\ s_b(\tau) &= s(T - i\tau)\,, \qquad \tau \in [0, \sigma_b]\,, \\ s_c(\tau) &= s(-T - i\tau)\,, \qquad \tau \in [\sigma_b, \sigma_c]\,, \end{aligned} \qquad \begin{aligned} s_1(t) &= s(t)\,, \qquad t \in [-T, T]\,, \\ s_2(t) &= s(t - i\sigma_b)\,, \quad t \in [-T, T]\,, \end{aligned} \tag{A.4}$$

and analogously for $\mathcal{O}_i$ and $\mathcal{O}_I$. The vev of $\mathcal{O}_i$, in the state ρ, and in the presence of the source s, is given by

$$\langle \mathcal{O}_i(x) \rangle_{\rho,s} = \frac{(-1)^{\delta_{i2}}}{i} \frac{\delta \ln Z_\rho^{\rm CFT}[s]}{\delta s_i(x)}\,, \tag{A.5}$$

where $x = (t, \vec{x})$. The Keldysh propagator, in the state ρ, is

$$iG_\rho^{ij}(x, x') = \frac{(-1)^{\delta_{ij} - \delta_{i2} + 1}}{i} \frac{\delta \langle \mathcal{O}_i(x) \rangle_{\rho,s}}{\delta s_j(x')}\bigg|_{s=0} = \langle T_\gamma \mathcal{O}_i(x) \mathcal{O}_j(x') \rangle_\rho\,, \tag{A.6}$$

where T_γ stands for time ordering along the Keldysh contour. In our conventions the Feynman (iG_ρ^F), Wightman ($iG_\rho^>$), anti-Wightman ($iG_\rho^<$), and anti-Feynman ($iG_\rho^{\overline{F}}$) correlators are defined as

$$\begin{aligned} \langle T_\gamma \mathcal{O}_1(x) \mathcal{O}_1(x') \rangle_\rho &\equiv \langle T\mathcal{O}(x)\mathcal{O}(x') \rangle_\rho = iG_\rho^F(x, x')\,, \\ \langle T_\gamma \mathcal{O}_1(x) \mathcal{O}_2(x') \rangle_\rho &\equiv \langle \mathcal{O}(x')\mathcal{O}(x) \rangle_\rho = iG_\rho^<(x, x')\,, \\ \langle T_\gamma \mathcal{O}_2(x) \mathcal{O}_1(x') \rangle_\rho &\equiv \langle \mathcal{O}(x)\mathcal{O}(x') \rangle_\rho = iG_\rho^>(x, x')\,, \\ \langle T_\gamma \mathcal{O}_2(x) \mathcal{O}_2(x') \rangle_\rho &\equiv \langle \overline{T}\mathcal{O}(x)\mathcal{O}(x') \rangle_\rho = iG_\rho^{\overline{F}}(x, x')\,, \end{aligned} \tag{A.7}$$

where the equivalences stem from the fact that any operator that appears on the backwards piece, γ_2, by construction has larger Keldysh time than any operator appearing on the forwards contour, γ_1, and we have dropped the subscripts $(1, 2)$ from the operators. It is easy to see that

$$\begin{aligned} iG^>(x, x') &= \theta(t - t')iG^F(x, x') + \theta(t' - t)iG^{\overline{F}}(x, x')\,, \\ iG^<(x, x') &= \theta(t' - t)iG^F(x, x') + \theta(t - t')iG^{\overline{F}}(x, x')\,. \end{aligned} \tag{A.8}$$

Out of the components of the Keldysh propagator one can build the retarded (iG^R_ρ) and advanced (iG^A_ρ) propagators

$$iG^R_\rho(x,x') = iG^F_\rho(x,x') - iG^<_\rho(x,x') = \theta(t-t')\Big[iG^F_\rho(x,x') - iG^{\overline{F}}_\rho(x,x')\Big]\,,$$
$$iG^A_\rho(x,x') = iG^F_\rho(x,x') - iG^>_\rho(x,x') = -\theta(t'-t)\Big[iG^F_\rho(x,x') - iG^{\overline{F}}_\rho(x,x')\Big]\,. \tag{A.9}$$

Of particular physical interest is the retarded correlator; this appears as the causal linear response of the system due to external perturbations. We can see this when calculating the variation of the one-point function on γ_1, in state ρ and in the presence of the *same* external source $s_1 = s_2$ on γ_1 and γ_2:

$$\begin{aligned}\delta\left\langle \mathcal{O}_1(x')\right\rangle_{\rho,s} &= \int \mathrm{d}x\left[\delta s_1(x)\frac{\delta\left\langle \mathcal{O}_1(x')\right\rangle_{\rho,s}}{\delta s_1(x)} + \delta s_2(x)\frac{\delta\left\langle \mathcal{O}_1(x')\right\rangle_{\rho,s}}{\delta s_{1'}(x)}\right]\\ &= i\int \mathrm{d}x\,\delta s_1(x)\Big[\left\langle T\mathcal{O}(x)\mathcal{O}(x')\right\rangle_\rho - \left\langle \mathcal{O}(x)\mathcal{O}(x')\right\rangle_\rho\Big]\\ &= -\int \mathrm{d}x\,\delta s_1(x) G^R_\rho(x,x')\,.\end{aligned} \tag{A.10}$$

A good consistency check is that the correlators we obtain should obey the identities:

$$\begin{gathered}\left[iG^>(x,x')\right]^* = iG^<(x,x')\,,\quad \left[iG^F(x,x')\right]^* = iG^{\overline{F}}(x,x')\,,\\ iG^>(x',x) = iG^<(x,x')\,,\qquad iG^{F,\overline{F}}(x',x) = iG^{F,\overline{F}}(x,x')\,.\end{gathered} \tag{A.11}$$

A.2 Skenderis-van Rees real time holography

In this appendix, we briefly review the parts of the Skenderis-van Rees formalism for real-time $\mathrm{AdS}_{d+1}/\mathrm{CFT}_d$ holography [193, 194] which are most relevant for our discussion in section 3.2, see [194] for a much more complete discussion and derivation. The Skenderis-van Rees formalism can be seen as the holographic dual of the Schwinger-Keldysh formalism in field theory, which we briefly review in appendix A.1.

We will focus on a scalar field $\Phi(\theta,\vec{x},r)$ with mass m dual to the operator $\mathcal{O}(\theta,\vec{x})$ of conformal dimension Δ, which satisfies:

$$R^2m^2 = \Delta(\Delta-d)\,, \tag{A.12}$$

using R as the AdS scale. The bulk dual to a field theory state ρ can be prepared by allowing Φ to fluctuate on top of a mixed-signature spacetime $\mathcal{M}$ with fixed background metric $g^{E,L}_{\mu\nu}$, which is Euclidean or Lorentzian depending on the segment. The bulk partition function, as a functional of the boundary value of the field[2] $\Phi\big|_{\partial\mathcal{M}}(\theta,\vec{x}) \equiv s(\theta,\vec{x})$, is given by

$$Z^{\rm bulk}_{g_{\mu\nu}}[s] = \int_{\Phi\big|_{\partial\mathcal{M}}=s} \mathcal{D}\Phi\; e^{iS_{\rm bulk}[\Phi]} \approx e^{iS^{\text{on-shell}}_{\rm bulk}[s]}\,. \tag{A.13}$$

The bulk action along the contour γ is

$$\begin{aligned} iS_{\rm bulk}[\Phi] = \int_\gamma \mathrm{d}\theta\, L(\theta) &= \int_{-\sigma_a}^{0} \mathrm{d}\tau\, L(-T-i\tau) + i\int_{-T}^{T} \mathrm{d}t\, L(t) + \int_0^{\sigma_b} \mathrm{d}\tau\, L(T-i\tau) \\ &\quad + i\int_{T}^{-T} \mathrm{d}t\, L(t-i\sigma_b) + \int_{\sigma_b}^{\sigma_c} \mathrm{d}\tau\, L(-T-i\tau) \\ &\equiv -\int_{-\sigma_a}^{0} \mathrm{d}\tau\, L^E_a(\tau) + i\int_{-T}^{T} \mathrm{d}t\, L^L_1(t) - \int_0^{\sigma_b} \mathrm{d}\tau\, L^E_b(\tau) \\ &\quad - i\int_{-T}^{T} \mathrm{d}t\, L^L_2(t) - \int_{\sigma_b}^{\sigma_c} \mathrm{d}\tau\, L^E_c(\tau)\,, \end{aligned} \tag{A.14}$$

where the Lorentzian and Euclidean Lagrangians are given by

$$\begin{aligned} L^L_i(t) &= \frac{1}{2}\int \mathrm{d}\vec{x}\,\mathrm{d}r\,\sqrt{-g^L}\big[-g^{L,\mu\nu}\partial_\mu\Phi_i(t,\vec{x},r)\partial_\nu\Phi_i(t,\vec{x},r) - m^2\Phi_i^2(t,\vec{x},r)\big]\,, \\ L^E_I(\tau) &= \frac{1}{2}\int \mathrm{d}\vec{x}\,\mathrm{d}r\,\sqrt{g^E}\big[g^{E,\mu\nu}\partial_\mu\Phi_I(\tau,\vec{x},r)\partial_\nu\Phi_I(\tau,\vec{x},r) + m^2\Phi_I^2(\tau,\vec{x},r)\big]\,, \end{aligned} \tag{A.15}$$

and the fields Φ_i and Φ_I are defined analogously to (A.4). Further, in (A.13) we have approximated the path integral using the saddle point approximation around the mixed-signature classical solution $\Phi^{\rm cl}(\theta,\vec{x},r)$. We build this by first solving for the two Lorentzian $(\Phi^{\rm cl}_i(t,\vec{x},r))$ and the three Euclidean pieces $(\Phi^{\rm cl}_I(\tau,\vec{x},r))$ separately, which satisfy the respective equations of motion

$$\begin{aligned} \frac{1}{\sqrt{-g^L}}\partial_\mu\Big(\sqrt{-g^L}g^{L,\mu\nu}\partial_\nu\Phi^{\rm cl}_i\Big) - m^2\Phi^{\rm cl}_i = 0\,, \\ \frac{1}{\sqrt{g^E}}\partial_\mu\Big(\sqrt{g^E}g^{E,\mu\nu}\partial_\nu\Phi^{\rm cl}_I\Big) - m^2\Phi^{\rm cl}_I = 0\,. \end{aligned} \tag{A.16}$$

[2]Here, we do not yet specify the precise meaning of $\Phi\big|_{\partial\mathcal{M}}$; the correct interpretation of this equation can be found in (A.21).

Then, the properly extremized mixed-signature classical solution is such that, at the spatial hypersurfaces where Euclidean and Lorentzian segments meet, the piecewise fields obey the matching conditions[3]

$$\Phi_i^{\rm cl} = \Phi_I^{\rm cl}\,, \qquad -i\partial_t \Phi_i^{\rm cl} = \partial_\tau \Phi_I^{\rm cl}\,. \tag{A.17}$$

The classical solution puts the bulk action on-shell: $iS_{\rm bulk}\big[\Phi^{\rm cl}\big] = iS_{\rm bulk}^{\text{on-shell}}[s]$, and renders it a functional of the boundary value of the field $\Phi\big|_{\partial\mathcal{M}}(\theta,\vec{x}) \equiv s(\theta,\vec{x})$. We assume we can solve the Lorentzian and Euclidean equations of motion by separation of variables:

$$\begin{aligned}\Phi_i^{\rm cl} &= \sum_{l,\vec{m}} \int d\omega e^{-i\omega t} Y_{l\vec{m}}(\vec{x}) f_i(\omega, l, \vec{m}, r)\,,\\ \Phi_I^{\rm cl} &= \sum_{l,\vec{m}} \int d\omega e^{-\omega\tau} Y_{l\vec{m}}(\vec{x}) f_I(\omega, l, \vec{m}, r)\,.\end{aligned} \tag{A.18}$$

The radial parts f_i, f_I then obey the same second-order ODE,[4] which needs to be supplied with two boundary conditions. If the geometry in question has only one boundary (e.g. empty AdS), then one boundary condition comes from demanding regularity in the IR (e.g. at the origin of AdS) and another from demanding that the field asymptotes to the source in the UV (e.g. at the boundary of AdS). If the geometry has two boundaries (e.g. the the eternal black hole, then we have two UV boundary conditions. To implement UV boundary condition(s), we expand the fields in powers of r near the boundary[5]

$$\Phi_{i,I}^{\rm cl}(x,r) = \left(\frac{a}{r}\right)^{d-\Delta} \phi_{i,I}^{(d-\Delta)}(x) + \ldots + \left(\frac{a}{r}\right)^{\Delta}\left(\phi_{i,I}^{(\Delta)}(x) + \psi_{i,I}^{(\Delta)}(x)\log\frac{a^2}{r^2}\right) + \ldots\,, \tag{A.20}$$

where $x = (t,\vec{x})$ or $x = (\tau,\vec{x})$ depending on whether we are on an Euclidean or a Lorentzian segment, and a is some distance scale of the geometry in question.

[3] In equation (4.1.15) of [194], the matching conditions have different signs. The difference stems from the fact that they parametrize the time on γ_2 to run in the opposite direction. In our convention the minus appearing in front of the action on γ_2 cancels with the minus coming from the fact that the derivation $-\partial_\tau$ on γ_b runs in the opposite direction compared to the derivation $i\partial_t$ on γ_2, thus (A.17) applies universally at all meeting hypersurfaces.

[4] A Euclidean mode will satisfy exactly the same radial equation as a Lorentzian one, since e.g. $e^{i\omega t} g^{L,tt} \partial_t^2 e^{-i\omega t} = e^{\omega\tau} g^{E,\tau\tau} \partial_\tau^2 e^{-\omega\tau}$ (similar relations hold involving off-diagonal time-space components of the metric). As such, there is no need to distinguish between the Lorentzian and Euclidean radial functions.

[5] We use coordinates where the boundary is at $r \to \infty$ and looks like:

$$ds^2|_{r\to\infty} = \frac{r^2}{R^2}\left(-d\theta^2 + d\vec{x}^2\right) + \frac{R^2}{r^2} dr^2\,, \tag{A.19}$$

where $d\theta^2 = dt^2$ or $d\theta^2 = -d\tau^2$, depending on if we are in Lorentzian or Euclidean signature.

The first set of dots in (A.20) contains terms between orders $d-\Delta+2$ and $\Delta-2$, while the second set of dots contains terms of orders beyond Δ, which all might have log pieces to them. These log pieces only appear when d is even *and* when $\Delta \in \mathbb{Z}$, and are related to the conformal anomaly in the CFT. From these expansions, we read off the sources as:

$$s_{i,I}(x) = \lim_{r\to\infty} \left(\frac{r}{a}\right)^{d-\Delta} \Phi_{i,I}(x,r) \equiv \phi_{i,I}^{(d-\Delta)}(x)\,. \tag{A.21}$$

We can also define the Fourier transformed sources $\tilde{s}_{i,I}$ through:

$$\begin{aligned} s_i(x) &= \sum_{l,\vec{m}} \int d\omega e^{-i\omega t} Y_{l\vec{m}}(\vec{x}) \tilde{s}_i(\omega,l,\vec{m}) f(\omega,l,\vec{m},r)\,, \\ s_I(x) &= \sum_{l,\vec{m}} \int d\omega e^{-\omega\tau} Y_{l\vec{m}}(\vec{x}) \tilde{s}_I(\omega,l,\vec{m}) f(\omega,l,\vec{m},r)\,, \end{aligned} \tag{A.22}$$

which can alternatively be seen as fixing the normalization of the radial functions f. Having obtained the piecewise bulk fields $\Phi_{i,I}$ that solve the equations of motion with the correct boundary conditions and obey the matching conditions, we build up the mixed-signature bulk field Φ using the analogous expression to (A.4) and express the on-shell action as

$$iS_{\text{bulk}}^{\text{on-shell}}[s] = \lim_{r\to\infty} \frac{i}{2}\left(\frac{r}{a}\right)^{\Delta} \int_\gamma \mathrm{d}\theta \int \mathrm{d}\vec{x}\, s(\theta,\vec{x}) r\partial_r \Phi(\theta,\vec{x},r). \tag{A.23}$$

It is clear that all terms beyond order Δ in (A.20) decay when the limit is taken, while all terms between orders $d-\Delta$ and $\Delta-2$ diverge. We can cancel these divergences with appropriate counterterms; this procedure is called holographic renormalization [191]. The final, renormalized result is:

$$iS_{\text{bulk}}^{\text{on-shell}}[s] = i(2\Delta-d)\int_\gamma \mathrm{d}\theta \int \mathrm{d}\vec{x}\, s(\theta,\vec{x})\phi^{(\Delta)}(\theta,\vec{x})\,. \tag{A.24}$$

With this setup one can extend the Gubser-Klebanov-Polyakov-Witten dictionary [210, 130], originally developed only for Euclidean AdS/CFT, to these mixed-signature bulks and boundaries. The dictionary states that the boundary value of the field, $\Phi\big|_{\partial\mathcal{M}}$, acts as a source for the operator $\mathcal{O}$. Further the boundary partition function in the state ρ is equivalent to the bulk partition function on the background $g_{\mu\nu}$, which in the large N limit can be approximated by the classical on-shell action

$$Z_\rho^{\text{CFT}}[s] = Z_{g_{\mu\nu}}^{\text{bulk}}[s] \approx e^{iS_{\text{bulk}}^{\text{on-shell}}[s]}\,. \tag{A.25}$$

Thus, in the large N limit, we can compute correlation functions holographically as

$$\begin{aligned}\langle \mathcal{O}_i(x)\rangle_{\rho,s} &= \frac{(-1)^{\delta_{i2}}}{i}\frac{\delta i S^{\text{on-shell}}_{\text{bulk}}[s]}{\delta s_i(x)} = (2\Delta - d)\phi_i^{(\Delta)}(x)\,,\\ iG^{ij}_{\rho}(x,x') &= \frac{(-1)^{\delta_{ij}-\delta_{i2}+1}}{i}\frac{\delta\langle \mathcal{O}_i(x)\rangle_{\rho,s}}{\delta s_j(x')}\bigg|_{s=0}\\ &= \frac{(-1)^{\delta_{ij}-\delta_{i2}+1}(2\Delta-d)}{i}\frac{\delta\phi_i^{(\Delta)}(x)}{\delta s_j(x')}\bigg|_{s=0}\,.\end{aligned} \tag{A.26}$$

A.2.1 Correlators of empty AdS

In this section, we briefly review the real-time holography calculation that obtains the two-point function of a minimally coupled scalar field in empty AdS_3. This calculation can be found in section 4.1 of [194].

The metric of global (Lorentzian) AdS_3 is:

$$\mathrm{d}s^2 = -\left(1+\frac{r^2}{R^2}\right)\mathrm{d}t^2 + \left(1+\frac{r^2}{R^2}\right)^{-1}\mathrm{d}r^2 + r^2\,\mathrm{d}\varphi^2\,, \tag{A.27}$$

where the coordinate ranges are $t\in(-\infty,\infty)$, $r\in[0,\infty)$, $\varphi\in[0,2\pi)$. The Euclidean metric is obtained by taking $t\to i\tau$. A conformal diagram of empty AdS_3 is given in figure A.2.

Schwinger-Keldysh contour We take the following Schwinger-Keldysh consisting of two Euclidean (γ_I, $I=a,b$) and two Lorentzian (γ_i, $i=1,2$) segments, whose Keldysh time $\theta = t - i\tau$ runs as

$$\begin{aligned}\gamma_a:&\quad \theta\in[-T+i\infty,-T]\,, &\qquad \gamma_1:&\quad \theta\in[-T,T]\,,\\ \gamma_b:&\quad \theta\in[T,T-i\infty]\,, &\qquad \gamma_2:&\quad \theta\in[-T,T]\,.\end{aligned} \tag{A.28}$$

The bulk dual to this contour is made out of two Lorentzian pieces and one Euclidean piece, which is split in two at $t=0$. The two Euclidean sub-pieces are then glued to the Lorentzian pieces as depicted in figure 3.4. Note that the boundary contours of empty AdS and the Solodukhin wormhole are the same; however, the blue line in the bulk contour has a different interpretation: for the wormhole, it is the center of the wormhole throat, whereas for empty AdS it is

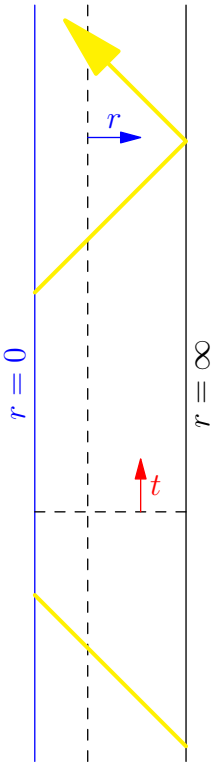


Figure A.2: Empty AdS_3 with a radial light ray (depicted in yellow). The light ray appears discontinuous on the diagram because we have suppressed the angle φ: after reaching the center of AdS the light ray continues propagating in the antipodal part of the spacetime, reflects from the antipodal point on the boundary and re-emerges at $r = 0$ after time πR.

the center of AdS at $r = 0$. These gluings dictate the matching conditions that the piecewise bulk fields obey[6]

$$\begin{aligned}
&\Phi_a(0,\varphi,r) = \Phi_1(-T,\varphi,r)\,, \quad \partial_\tau \Phi_a(0,\varphi,r) = -i\partial_t \Phi_1(-T,\phi,r)\,,\\
&\Phi_1(T,\varphi,r) = \Phi_2(T,\varphi,r)\,, \qquad \partial_t \Phi_1(T,\varphi,r) = \partial_t \Phi_2(T,\varphi,r)\,,\\
&\Phi_b(0,\varphi,r) = \Phi_2(-T,\varphi,r)\,, \quad \partial_\tau \Phi_b(0,\varphi,r) = -i\partial_t \Phi_2(-T,\varphi,r)\,.
\end{aligned} \tag{A.29}$$

[6]The matching condition between the two Lorentzian fields is the $\sigma_b \to 0$ limit of the matching conditions of the general contour (A.1) in appendix A.1.

Scalar wave solutions We can use separation of variables as in (3.7) to solve the equations of motion for the minimally coupled scalar on the different pieces of the Schwinger-Keldysh contour:

$$\Phi_i = e^{-i\omega t}e^{ik\varphi}\tilde{s}_i(\omega,k)f(\omega,k,r)\,, \qquad \Phi_I = e^{-\omega\tau}e^{ik\varphi}\tilde{s}_I(\omega,k)f(\omega,k,r)\,, \tag{A.30}$$

with $i=\{1,2\}$ for the Lorentzian segments and $I=\{a,b\}$ for the Euclidean segments. The solutions to the wave equation (3.8) for the AdS metric (A.27) are

$$f^{\pm}(\omega,k,r) = \left(\frac{r}{R}\right)^{\pm k}\left(1+\frac{r^2}{R^2}\right)^{\frac{R\omega}{2}}{}_2F_1\left(\frac{1}{2}(R\omega\pm k),1+\frac{1}{2}(R\omega\pm k);1\pm k;-\frac{r^2}{R^2}\right). \tag{A.31}$$

Demanding regularity in the IR (near the origin $r=0$) necessitates that the only allowed solution is the linear combination:

$$f(\omega,k,r) = \mathcal{N}_{\omega k}\big[\theta(k)f^+(\omega,k,r)+\theta(-k)f^-(\omega,k,r)\big] = \mathcal{N}_{\omega k}f^+(\omega,|k|,r)\,, \tag{A.32}$$

where $\mathcal{N}_{\omega k}$ is a constant of normalization

$$\mathcal{N}_{\omega k} = \frac{\Gamma\big(1+\frac{1}{2}(R\omega+|k|)\big)\Gamma\big(1-\frac{1}{2}(R\omega-|k|)\big)}{\Gamma(1+|k|)}\,, \tag{A.33}$$

which is chosen such that the leading behavior at the UV (near the boundary $r=\infty$) is normalized to unity. Then the asymptotic expansion of the modes near the boundary is:

$$f(\omega,k,r) = 1+\frac{R^2}{r^2}\alpha(\omega,k)\left(\beta(\omega,k)+\log\frac{R^2}{r^2}\right)+\dots\,, \tag{A.34}$$

$$\alpha(\omega,k) = -\frac{1}{4}\Big(R^2\omega^2-|k|^2\Big)\,,$$

$$\beta(\omega,k) = \psi\left(1-\frac{1}{2}(R\omega-|k|)\right)+\psi\left(1+\frac{1}{2}(R\omega+|k|)\right)+\frac{2(R\omega+|k|)}{R^2\omega^2-|k|^2}\,,$$

where $\psi(\cdot)=\Gamma'(\cdot)/\Gamma(\cdot)$ is the diagamma function and we have given $\beta(\omega,k)$ modulo constants which do not affect the poles of $\alpha\beta$. The poles of f are given by

$$R\omega^{\pm}_{nk} = \pm(2n+|k|)\,, \qquad n=1,2,\dots\,, \quad k\in\mathbb{Z}\,. \tag{A.35}$$

These (real) poles constitute the normal modes of empty AdS.

Construction of the piecewise bulk fields Our next task is to construct the piecewise bulk fields. A generic Lorentzian field is expanded as

$$\begin{aligned}\Phi_i &= \sum_k e^{ik\varphi} \int_{\mathcal{C}_i} \mathrm{d}\omega\, e^{-i\omega t} f \delta_{ij} \tilde{s}_j \\ &= \sum_k e^{ik\varphi} \left[\int_{\mathcal{F}} \mathrm{d}\omega\, e^{-i\omega t} f \delta_{ij} \tilde{s}_j + \int_{\mathcal{W}^<} \mathrm{d}\omega\, e^{-i\omega t} f V_{ij} \tilde{s}_j + \int_{\mathcal{W}^>} \mathrm{d}\omega\, e^{-i\omega t} f W_{ij} \tilde{s}_j \right],\end{aligned} \tag{A.36}$$

where in the first line $\mathcal{C}_i$ is an arbitrary contour that avoids the poles of f. In the second line we have parametrized the freedom in choosing the contour $\mathcal{C}_i$ by taking a Feynman contour and adding "contour-correcting" functions V_{ij} and W_{ij} to it. These contours are depicted in figure 3.3. The Feynman contour corresponds to the non-normalizable modes while the Wightman contours pick up normalizable mode contributions. Note that our ansatz has the correct UV asymptotics since:

$$\lim_{r\to\infty} \Phi_i = \sum_k e^{ik\varphi} \int_{\mathbb{R}} \mathrm{d}\omega\, e^{-i\omega t} \delta_{ij} \tilde{s}_j = s_i\,. \tag{A.37}$$

We do not allow sources on the Euclidean pieces as we are preparing empty AdS without excitations, so the Euclidean fields are composed of normalizable pieces alone:[7]

$$\Phi_I = \sum_k e^{ik\varphi} \left[\int_{\mathcal{W}^<} \mathrm{d}\omega\, e^{-\omega\tau} f V_{Ij} \tilde{s}_j + \int_{\mathcal{W}^>} \mathrm{d}\omega\, e^{-\omega\tau} f W_{Ij} \tilde{s}_j \right]. \tag{A.38}$$

Regularity imposes a further restriction on the allowed Euclidean pieces. On γ_a, $\tau < 0$ so regularity as $\omega \to +\infty$ demands that $W_{aj} = 0$. Similarly, regularity for $\tau > 0$ on γ_b as $\omega \to -\infty$ is enforced by $V_{bj} = 0$.

Applying matching conditions Now, we wish to apply the matching conditions (A.29). First of all, the Fourier transform of $\tilde{s}_i$ in (A.36) is given by (A.37). Noting that the source must only have support for $-T < t' < T$, at $t \sim -T$, the factor $e^{-i\omega(t-t')} = e^{i\omega|t-t'|}$ blows up in the lower half plane so that we must close the Feynman integral in (A.36) in the upper half plane. Similarly, when $t \sim T$, we close the $\mathcal{F}$ integral in the lower half plane. This results in the

[7] Note that we have already assumed no sources on the Euclidean segments when we constrained the generic linear combinations of the sources $V_{ij}\tilde{s}_j$ and $W_{ij}\tilde{s}_j$ to run only along the Lorentzian sources.

expressions:

$$\Phi_i(t\sim -T)=\sum_k e^{ik\varphi}\left[\int_{\mathcal{W}^<}\mathrm{d}\omega\, e^{-i\omega t}f(\delta_{ij}+V_{ij})\tilde{s}_j+\int_{\mathcal{W}^>}\mathrm{d}\omega\, e^{-i\omega t}fW_{ij}\tilde{s}_j\right],$$
$$\Phi_i(t\sim T)=\sum_k e^{ik\varphi}\left[\int_{\mathcal{W}^<}\mathrm{d}\omega\, e^{-i\omega t}fV_{ij}\tilde{s}_j+\int_{\mathcal{W}^>}\mathrm{d}\omega\, e^{-i\omega t}f(\delta_{ij}+W_{ij})\tilde{s}_j\right]. \tag{A.39}$$

Now, we can apply the matching conditions (A.29); since each pole is independent we must apply them separately to the $\mathcal{W}^<$ and $\mathcal{W}^>$ integrals:

$$\begin{aligned}\mathcal{W}^<:\quad V_{aj}e^{-i\omega T}&=\delta_{1j}+V_{1j}\,, & \mathcal{W}^>:\qquad 0&=W_{1j}\,,\\ V_{1j}&=V_{2j}\,, & \delta_{1j}+W_{1j}&=\delta_{2j}+W_{2j}\,,\\ 0&=\delta_{2j}+V_{2j}\,, & W_{bj}e^{-i\omega T}&=W_{2j}\,.\end{aligned} \tag{A.40}$$

The solution to these matching conditions is given by:

$$\begin{aligned}V_{ij}&=\begin{pmatrix}0&-1\\0&-1\end{pmatrix}_{ij}, & W_{ij}&=\begin{pmatrix}0&0\\1&-1\end{pmatrix}_{ij},\\ V_{aj}&=\begin{pmatrix}1&-1\end{pmatrix}_j e^{i\omega T}, & W_{bj}&=\begin{pmatrix}1&-1\end{pmatrix}_j e^{i\omega T},\end{aligned} \tag{A.41}$$

so that the Euclidean and Lorentzian fields are now completely determined in terms of the sources $\tilde{s}_i$.

Extracting the correlators Finally, having solved the bulk fields entirely, we can extract the correlation functions from them. For this, we extract the r_+^2/r^2 term in the expansion of the Lorentzian fields (see appendix A.2):

$$\begin{aligned}\phi_i^{(2)}=\sum_k e^{ik\varphi}\Bigg[&\int_{\mathcal{F}}\mathrm{d}\omega\, e^{-i\omega t}(\alpha\beta)\delta_{ij}\tilde{s}_j+\int_{\mathcal{W}^<}\mathrm{d}\omega\, e^{-i\omega t}(\alpha\beta)V_{ij}\tilde{s}_j\\ &+\int_{\mathcal{W}^>}\mathrm{d}\omega\, e^{-i\omega t}(\alpha\beta)W_{ij}\tilde{s}_j\Bigg].\end{aligned} \tag{A.42}$$

Then, we use the Fourier transform $s(t,\varphi)$ of $\tilde{s}_j(\omega,k)$ defined in (A.37) and perform functional derivatives with respect to $s_j(t',\varphi')$ to obtain the correlators:

$$\begin{aligned} iG^{ij}_{\rm AdS}(x,x') &= \frac{2(-1)^{\delta_{ij}-\delta_{i2}+1}}{i}\,\frac{\delta\phi_i^{(2)}(x)}{\delta s_j(x')}\bigg|_{s_i=0} \\ &= \frac{(-1)^{\delta_{ij}-\delta_{i2}+1}}{2\pi^2 i}\sum_k e^{ik(\varphi-\varphi')}\bigg[\int_{\mathcal{F}} {\rm d}\omega\, e^{-i\omega(t-t')}\delta_{ij}\alpha\beta \\ &\quad + \int_{\mathcal{W}^<} {\rm d}\omega\, e^{-i\omega(t-t')}V_{ij}\alpha\beta + \int_{\mathcal{W}^>} {\rm d}\omega\, e^{-i\omega(t-t')}W_{ij}\alpha\beta\bigg]\,. \end{aligned} \tag{A.43}$$

For example, the retarded correlator is given by:

$$\begin{aligned} iG^R_{\rm AdS}(x,x') &= \theta(t-t')\Big[iG^F_{\rm AdS}(x,x') - iG^{\overline{F}}_{\rm AdS}(x,x')\Big] \\ &= \theta(t-t')\big[iG^{11}_{\rm AdS}(x,x') - iG^{22}_{\rm AdS}(x,x')\big] \\ &= \frac{\theta(t-t')}{2\pi^2 i}\sum_k e^{ik(\varphi-\varphi')}\int_{\mathcal{F}-\overline{\mathcal{F}}} {\rm d}\omega\, e^{-i\omega(t-t')}\alpha\beta \\ &= \frac{\theta(t-t')}{2\pi^2 i}\sum_k e^{ik(\varphi-\varphi')}\int_{\mathbb{R}+i\epsilon} {\rm d}\omega\, e^{-i\omega(t-t')}\alpha\beta \\ &= \frac{\theta(t-t')}{2\pi^2 i}\sum_k e^{ik(\varphi-\varphi')}\int_{\mathcal{W}^>-\mathcal{W}^<} {\rm d}\omega\, e^{-i\omega(t-t')}\alpha\beta\,, \end{aligned} \tag{A.44}$$

where we have used the relation $\overline{\mathcal{F}} = -\mathcal{F}+\mathcal{W}^>+\mathcal{W}^<$, as well as $\mathcal{F}-\overline{\mathcal{F}} = \mathbb{R}+i\epsilon$ with ϵ a small positive number. In the last line we have employed the fact that the $\theta(t-t')$ function demands to close $\mathbb{R}+i\epsilon$ in the lower half plane, see figure 3.5 (where now the crosses should be considered to be poles of the empty AdS mode f). Finally, we compute this integral as a sum over the residues of β. We obtain (with $\Delta t = t-t'$ and $\Delta\varphi = \varphi-\varphi'$):

$$\begin{aligned} iG^R_{\rm AdS}(x,x') &= \frac{2\theta(\Delta t)}{\pi R}\left[\sum_{n,k} e^{-i\omega^+_{nk}\Delta t+ik\Delta\varphi}\alpha(\omega^+_{nk}) - \sum_{n,k} e^{-i\omega^-_{nk}\Delta t+ik\Delta\varphi}\alpha(\omega^-_{nk})\right] \\ &= -\frac{\theta(\Delta t)}{2\pi R}\left[\frac{1}{\left(\cos\left(\frac{\Delta t(1-i\epsilon)}{R}\right)-\cos(\Delta\varphi)\right)^2} - \frac{1}{\left(\cos\left(\frac{\Delta t(1+i\epsilon)}{R}\right)-\cos(\Delta\varphi)\right)^2}\right], \end{aligned} \tag{A.45}$$

where the $i\epsilon$ prescription appears with a minus sign to regulate the ω_{nk}^{+} sum and with a plus sign to regulate the ω_{nk}^{-} sum.

A.3 Details on the dimensional reduction from 7d to 5d

A.3.1 Reducing the action

We begin with the 7d action (4.6) and set the parameter $\mu = 2/L$, where L is eventually going to be the AdS_5 radius. We define the respective volume forms

$$\varepsilon_{(7)} = \star_7 1\,, \quad \varepsilon_{(5)} = \star_5 1\,, \quad \varepsilon_{(2)} = \star_2 1 = \mathrm{d}\omega\ , \tag{A.46}$$

and use the Ansatz in (4.11) to calculate

$$\varepsilon_{(7)} = e^{5f_0+2g_0} L^2\, \varepsilon_{(5)} \wedge \mathrm{d}\omega\ . \tag{A.47}$$

Then we express the constituents of the 7d action purely in terms of the 5d fields and 5d Hodge star

$$\begin{aligned} S &= \mathfrak{c}\, e^{2f_0+2\Lambda_+} \star_5 F\,, \\ \star_7 S &= -\mathfrak{c}\, e^{f_0+2g_0+2\Lambda_+} L^2\, F \wedge \mathrm{d}\omega\ , \\ F_{1,2} &= \mathfrak{a}\,(1 \pm z) L\ \mathrm{d}\omega + \mathfrak{b}\, e^{f_0+2\Lambda_{1,2}}\, F\,, \\ \star_7 F_{1,2} &= \mathfrak{a}\, e^{5f_0-2g_0}(1 \pm z) L^{-1}\, \varepsilon_{(5)} + \mathfrak{b}\, e^{2f_0+2g_0+2\Lambda_{1,2}} L^2\ \star_5 F \wedge \mathrm{d}\omega\ . \end{aligned} \tag{A.48}$$

Finally, we evaluate the 7d Ricci scalar in terms of the 5d Ricci scalar

$$R_{(7)} = e^{-2f_0} R_{(5)} + e^{-2g_0} L^{-2} R_{(2)}\,, \quad R_{(2)} = -2\,. \tag{A.49}$$

These expressions allow us to write down all the terms in the 7d action as

$$\begin{aligned}
\star_7 R &= -2\, e^{5f_0}\, \varepsilon_{(5)} \wedge \mathrm{d}\omega + L_0^2\, \star_5 R \wedge \mathrm{d}\omega \ , \\
-\star_7 V &= -e^{5f_0+2g_0} L^2\, V\, \varepsilon_{(5)} \wedge \mathrm{d}\omega \ , \\
-\frac{1}{2} e^{-4\Lambda_{1,2}} F_{1,2} \wedge \star_7 F_{1,2} &= -\frac{a^2}{2}\, e^{5f_0-2g_0-4\Lambda_{1,2}} (1 \pm z)^2\, \varepsilon_{(5)} \wedge \mathrm{d}\omega \\
&\quad - \frac{b^2}{2}\, L_0^2\, F \wedge \star_5 F \wedge \mathrm{d}\omega \ , \\
-\frac{1}{2} e^{-4\Lambda_+} S \wedge \star_7 S &= \frac{c^2}{2}\, L_0^2\, F \wedge \star_5 F \wedge \mathrm{d}\omega \ , \\
\frac{L}{4} S \wedge \mathrm{d}S &= 0 \, , \\
-\frac{L}{2} F_1 \wedge F_2 \wedge S &= -4abc\, L_0^2\, F \wedge \star_5 F \wedge \mathrm{d}\omega \ , \\
\frac{L}{8} [A_1 \wedge F_1 \wedge F_2 \wedge F_2 + (1 \leftrightarrow 2)] &= 4ab^3\, L_0^2\, A \wedge F \wedge F \wedge \mathrm{d}\omega \ .
\end{aligned}$$

Here we have defined $L_0^2 \equiv e^{3f_0+2g_0} L^2$ and in the last expression we integrated by parts. The terms on the right hand side proportional to $L_0^2\, \varepsilon_{(5)} \wedge \mathrm{d}\omega$ sum to

$$-\frac{1}{2L^2} e^{2f_0-2g_0-2\Lambda_+} \big(2e^{2g_0+4\Lambda_+} \big(2 + e^{2g_0} L^2 V\big) + a^2 \big(e^{4\Lambda_1} (1-z)^2 + e^{4\Lambda_2} (1+z)^2\big)\big) \, , \tag{A.50}$$

where V is the scalar potential (4.7) evaluated on the constant scalars $\lambda_{1,2} = \Lambda_{1,2}$, and all the constants are given in terms of z as in (4.10). This combination should evaluate to $12 L_0^2/L^2$ if one is to find the expected z-independent 5D cosmological constant term with the correct coefficient relative to R. Remarkably, setting

$$a = \pm \frac{1}{4} \tag{A.51}$$

achieves precisely that, where the leftover sign choice will be important later on when we dimensionally reduce the BPS equations. Then the 7d action simplifies to

$$I_7 = \frac{L_0^2}{16\pi G_7} \int \left[\star_5 \left(R + \frac{12}{L^2} \right) - \frac{1}{2} \big(2b^2 + 2bc - c^2\big) F \wedge \star_5 F + b^3 A \wedge F \wedge F \right] \wedge \mathrm{d}\omega \ . \tag{A.52}$$

To retain $F = \mathrm{d}A$ when the 5d equation of motion for F is derived we demand $\left(2\mathfrak{b}^2 + 2\mathfrak{b}\mathfrak{c} - \mathfrak{c}^2\right) = 3\mathfrak{b}^2$, which fixes $\mathfrak{c} = \mathfrak{b}$. We integrate over $\Sigma_\mathfrak{g}$: $\int \mathrm{d}\omega = 4\pi(\mathfrak{g}-1)$, and rescale the last remaining constant to $\mathfrak{b} = \chi/\sqrt{3}$. Then expressions (4.12) and (4.13) readily follow.

A.3.2 Reducing the BPS equations

In this section we dimensionally reduce the 7d BPS equations (4.8) to the 5d BPS equation (4.15). We introduce the following notation: 7d curved indices are labelled by $M, N, \ldots$, 5d curved indices are labelled by $\mu, \nu, \ldots$, 2d curved indices (on the Riemann surface) are labelled by $m, n, \cdots = x_1, x_2$, and flat indices in any dimension carry hats. The 7d metric decomposes as

$$g_{MN} = e^{2f_0}\, g_{\mu\nu} \oplus e^{2g_0} L^{-2}\, g_{mn}\,, \tag{A.53}$$

where $g_{\mu\nu}$ and g_{mn} are the metrics originating from $\mathrm{d}s_5^2$ and $\mathrm{d}s_2^2$ respectively (without the scaling factors). Then the 7D vielbeins decompose as

$$e_M{}^{\widehat{M}} = e^{f_0}\, e_\mu{}^{\widehat{\mu}} \oplus e^{g_0} L\, e_m{}^{\widehat{m}}\,. \tag{A.54}$$

From the reduction ansatz (4.11) we see that the 7D gauge fields decompose as

$$\begin{aligned} S_{MNR} &= \mathfrak{c}\, e^{2f_0+2\Lambda_+}\, \frac{1}{2!} F^{\alpha\beta} \varepsilon_{\alpha\beta\mu\nu\rho}\,, \\ F_{1,2MN} &= \mathfrak{b}\, e^{f_0+2\Lambda_{1,2}}\, F_{\mu\nu} \oplus \mathfrak{a}\,(1 \pm z) L\, (\mathrm{d}\omega)_{mn}\,, \\ A_{1,2M} &= \mathfrak{b}\, e^{f_0+2\Lambda_{1,2}}\, A_\mu \oplus \mathfrak{a}\,(1 \pm z) L\, \omega_m\,. \end{aligned} \tag{A.55}$$

The 7d gamma matrices decompose as

$$\widetilde{\gamma}^{MN} = e^{-2f_0}\, \widetilde{\gamma}^{\mu\nu} \oplus e^{-2g_0} L^{-2}\, \widetilde{\gamma}^{mn}\,, \qquad \widetilde{\gamma}^{M} = e^{-f_0}\, \widetilde{\gamma}^{\mu} \oplus e^{-g_0} L^{-1}\, \widetilde{\gamma}^{m}\,. \tag{A.56}$$

The 7d spin connection decomposes trivially

$$\omega_{M\widehat{A}\widehat{B}} = \omega_{\mu\widehat{\alpha}\widehat{\beta}} \oplus \omega_{m\widehat{a}\widehat{b}}, \tag{A.57}$$

and we note that the 2d spin connection has only one non-zero component given by

$$\omega_{x_1\widehat{x}_1\widehat{x}_2} = -x_2^{-1}\,. \tag{A.58}$$

We also need the following relations between 7d gamma matrices

$$\widetilde{\gamma}^{MNR} = \chi_7\, \frac{1}{4!} \varepsilon^{MNRABCD} \widetilde{\gamma}_{ABCD}\,, \quad \widetilde{\gamma}^{MN} = \chi_7\, \frac{1}{5!} \varepsilon^{MNABCDE} \widetilde{\gamma}_{ABCDE} \tag{A.59}$$

where $\chi_7 = \pm 1$ dictates which of the two conventions one uses for the 1-index 7d gamma matrices, where the sign choice appears in the relation $\widetilde{\gamma}^6 = \chi_7 \widetilde{\gamma}^0 \widetilde{\gamma}^1 \dots \widetilde{\gamma}^5$. Using our metric Ansatz we obtain

$$\widetilde{\gamma}^{\mu\nu\rho} = \chi_7 \frac{1}{2!} e^{-3f_0} \varepsilon^{\mu\nu\rho\alpha\beta} \widetilde{\gamma}_{\alpha\beta} \widetilde{\gamma}_{\widehat{x_1}\widehat{x_2}} \,, \quad \widetilde{\gamma}^{\mu\nu} = \chi_7 \frac{1}{3!} e^{-2f_0} \varepsilon^{\mu\nu\alpha\beta\gamma} \widetilde{\gamma}_{\alpha\beta\gamma} \widetilde{\gamma}_{\widehat{x_1}\widehat{x_2}} \,. \tag{A.60}$$

Finally, we note that $\mathrm{d}\omega$, being the volume form on the Riemann surface, acts to lower 7d gamma matrix index, restricted to the Riemann surface, as

$$\widetilde{\gamma}^m (\mathrm{d}\omega)_{mn} = -\widetilde{\gamma}_n \widetilde{\gamma}_{x_1 x_2} \,. \tag{A.61}$$

With this setup in mind, in (4.8) we set $\mu = 2/L$ and take constant scalars: $\lambda_{1,2} = \Lambda_{1,2}$. Then, the first dilatini variation reduces to

$$\begin{aligned} \delta\widetilde{\zeta}_1 = \frac{L^{-1}}{2} \Big[\big(e^{2\Lambda_1} - e^{-4\Lambda_+} \big) - \frac{\mathfrak{a}}{4} (1+z) e^{-2g_0 - 2\Lambda_1} \, \widetilde{\gamma}_{\widehat{x_1}\widehat{x_2}} \otimes \Gamma^{12} \Big] \widetilde{\epsilon} \otimes \mathcal{E} \\ - \frac{e^{-f_0}}{16} \widetilde{\gamma}^{\mu\nu} F_{\mu\nu} \Big[\mathfrak{b} \, 1_8 \otimes \Gamma^{12} + \chi_7 \, \mathfrak{c} \, \widetilde{\gamma}_{\widehat{x_1}\widehat{x_2}} \otimes \Gamma^5 \Big] \widetilde{\epsilon} \otimes \mathcal{E} \,. \end{aligned} \tag{A.62}$$

We find that the following projectors:

$$\Big(\widetilde{\gamma}_{\widehat{x_1}\widehat{x_2}} \otimes 1_4 \Big) (\widetilde{\epsilon} \otimes \mathcal{E}) = p_2 \, \big(1_8 \otimes \Gamma^{12} \big) (\widetilde{\epsilon} \otimes \mathcal{E}) \,, \qquad \big(1_8 \otimes \Gamma^5 \big) (\widetilde{\epsilon} \otimes \mathcal{E}) = p_5 \, \widetilde{\epsilon} \otimes \mathcal{E} \,, \tag{A.63}$$

together with the identities $\Big(\widetilde{\gamma}_{\widehat{x_1}\widehat{x_2}} \Big)^2 = -1_8$ and $\big(\Gamma^{12} \big)^2 = -1_4$, imply that the two brackets in (A.62) vanish when:

$$p_2 = s_a \,, \quad p_5 = -\chi_7 \, s_a \,; \qquad \mathfrak{a} = \frac{s_a}{4} \,, \quad \mathfrak{c} = \mathfrak{b} = \frac{\varkappa}{\sqrt{3}} \,, \tag{A.64}$$

where $s_a = \pm 1$ and the latter two conditions come from consistency of the reduced action as discussed around (A.52). The second dilatini variation automatically vanishes upon using (A.63) and (A.64) giving no new constraints. Next, we manipulate the gravitini variation when $M = m$, keeping in mind that $\big(1_8 \otimes \Gamma^5 \big) (\widetilde{\epsilon} \otimes \mathcal{E}) = p_5 \, \widetilde{\epsilon} \otimes \mathcal{E} \implies \big(1_8 \otimes \Gamma^{34} \big) (\widetilde{\epsilon} \otimes \mathcal{E}) = p_5 \big(1_8 \otimes \Gamma^{12} \big) (\widetilde{\epsilon} \otimes \mathcal{E})$:

$$\begin{aligned} \delta\widetilde{\psi}_m \overset{p_5 = 1}{=} \Bigg[\partial_m - \frac{1}{2} x_2^{-1} \delta_{m x_1} \Big(\widetilde{\gamma}_{\widehat{x_1}\widehat{x_2}} \otimes 1_4 - 4\mathfrak{a} \, 1_8 \otimes \Gamma^{12} \Big) \\ + \frac{1}{2} e^{-f_0 + g_0} \widetilde{\gamma}_m \Big(1_8 \otimes 1_4 + 4\mathfrak{a} \, \widetilde{\gamma}_{\widehat{x_1}\widehat{x_2}} \otimes \Gamma^{12} \Big) \Bigg] \widetilde{\epsilon} \otimes \mathcal{E} \,, \end{aligned} \tag{A.65}$$

where we have set $p_5 = 1$, since otherwise the terms in the bracket are z-dependent, and no projector can make them vanish. Upon using (A.63) and (A.64), with $p_5 = 1$, the two brackets above vanish. For the whole equation to vanish we find that the spinor should be independent of the Riemann surface coordinates. We thus find the following constraints between the constants defined above

$$p_2 = -\chi_7\,, \quad p_5 = 1\,; \qquad a = -\frac{\chi_7}{4}\,, \quad c = b = \frac{\varkappa}{\sqrt{3}}\,; \qquad \partial_m(\widetilde{\epsilon}\otimes\mathcal{E}) = 0\,. \tag{A.66}$$

Finally, we manipulate the gravitini variation for $M = \mu$ to find:

$$\delta\widetilde{\psi}_\mu = \Bigg(\Bigg[\partial_\mu + \frac{1}{4}\omega_{\mu\widehat{\alpha}\widehat{\beta}}\widetilde{\gamma}^{\widehat{\alpha}\widehat{\beta}} + \chi_7\frac{\varkappa}{8\sqrt{3}}\big(\widetilde{\gamma}_{\mu\alpha\beta}F^{\alpha\beta} - 4\,F_{\mu\alpha}\widetilde{\gamma}^{\alpha}\big)\widetilde{\gamma}_{\widehat{x}_1\widehat{x}_2}$$

$$+ \frac{1}{2L}\Big(\widetilde{\gamma}_\mu - \chi_7\,\sqrt{3}\,\varkappa\,A_\mu\widetilde{\gamma}_{\widehat{x}_1\widehat{x}_2}\Big)\Bigg]\widetilde{\epsilon}\Bigg)\otimes\mathcal{E}\,,$$

where we have already imposed (A.63) and (A.66). To complete the reduction we further split the 7d gamma matrices and spinor as

$$\widetilde{\gamma}_\mu = \gamma_\mu\otimes g_1\,, \quad \widetilde{\gamma}_{\widehat{x}_1\widehat{x}_2} = 1_4\otimes g_2\,, \quad \widetilde{\epsilon} = \epsilon\otimes\eta\,, \tag{A.67}$$

where γ_μ and ϵ are 5d gamma matrices and spinor, η is a 2d spinor and $(g_1,\, g_2)$ are (yet undetermined) matrices in the 2d Clifford algebra. Then the round bracket in the gravitini variation above becomes

$$\Bigg[\partial_\mu + \frac{1}{4}\omega_{\mu\widehat{\alpha}\widehat{\beta}}\gamma^{\widehat{\alpha}\widehat{\beta}}\otimes g_1^2 + \chi_7\frac{\varkappa}{8\sqrt{3}}\big(\gamma_{\mu\alpha\beta}F^{\alpha\beta}\otimes g_1^3 g_2 - 4\,F_{\mu\alpha}\gamma^{\alpha}\otimes g_1 g_2\big)$$

$$- \frac{1}{2L}\Big(-\gamma_\mu\otimes g_1 + \chi_7\,\sqrt{3}\,\varkappa\,A_\mu\,1_4\otimes g_2\Big)\Bigg]\epsilon\otimes\eta\,.$$

This equation reduces to (4.15) if we are able to find matrices $(g_1,\, g_2)$ in the 2d Clifford algebra that satisfy

$$g_1\eta = -\eta\,, \quad g_2\eta = \mathrm{i}\,\chi_7\,\eta\,. \tag{A.68}$$

Upon using (A.66), we find consistency of (A.68) with the projectors (A.63) if

$$\Gamma^{12}\mathcal{E} = -\mathrm{i}\,\mathcal{E}\,, \quad \Gamma^5\mathcal{E} = \mathcal{E}\,: \quad \Longrightarrow \quad \mathcal{E}_1 = \mathcal{E}_2 = \mathcal{E}_3 = 0\,. \tag{A.69}$$

In turn, upon using the projectors again, the latter condition demands $\eta \propto (1,\, c_7)^T$. Thus, we fix the matrices $(g_1,\, g_2)$ as

$$g_1 = -\chi_7\,\sigma_1\,, \quad g_2 = \mathrm{i}\,\sigma_1\,. \tag{A.70}$$

This completes the reduction of the 7d supersymmetry variations to the 5d ones.

A.4 Details on the analysis of the 5d CCLP solution

Here we collect some calculational details related to the analysis of the 5d CCLP solution discussed in Section 4.3.

A.4.1 Derivation of the Euclidean 5d action

We define the ε-pseudo-tensor as

$$\varepsilon_{01234} = \sqrt{-g}\,, \quad \varepsilon^{01234} = \frac{s}{\sqrt{-g}}\,, \tag{A.71}$$

where $s = -1$ denotes the signature of the Lorentzian spacetime and $g = \det(g_{\mu\nu})$ (not to be confused with the inverse AdS scale parameter g used in Section 4.3). In our conventions, described in Appendix A.5, we write the action (4.12) in component form as

$$I = \frac{1}{16\pi G_5}\int \mathrm{d}^5x\,\sqrt{-g}\Big(R + \frac{12}{L^2} - \frac{\varkappa^2}{4}F^{\mu\nu}F_{\mu\nu} + \frac{s\varkappa^3}{12\sqrt{3}}\varepsilon^{\nu\alpha\beta\gamma\delta}A_\nu F_{\alpha\beta}F_{\gamma\delta}\Big)\,, \tag{A.72}$$

The Euclidean theory is obtained from the Lorentzian one by performing Wick rotation

$$t \to -\mathrm{i}\,\tau\,. \tag{A.73}$$

Under Wick rotation the components of a generic tensor transform as

$$T_{0ij\ldots} \to \mathrm{i}\,T_{0ij\ldots}\,, \quad T^{0ij\ldots} \to -\mathrm{i}\,T^{0ij\ldots}\,, \tag{A.74}$$

where $i, j, \cdots = 1, 2, \ldots$ label coordinates distinct from t or τ, in the respective coordinates systems. In particular, we have

$$\mathrm{d}^5x \to -\mathrm{i}\,\mathrm{d}^5x\,, \quad \sqrt{-g} \to \sqrt{g}\,, \quad R \to R\,, \quad F^{\mu\nu}F_{\mu\nu} \to F^{\mu\nu}F_{\mu\nu}\,. \tag{A.75}$$

The components of a pseudo-tensor transform involving also the sign of the coordinate transformation. In particular, the ε-pseudo-tensor transforms as

$$\varepsilon_{0ijkl} \to (-\mathrm{i})\cdot\mathrm{i}\,\varepsilon_{0ijkl} = \varepsilon_{0ijkl}\,, \quad \varepsilon^{0ijkl} \to \mathrm{i}\cdot(-\mathrm{i})\cdot s\,\varepsilon^{0ijkl} = s\,\varepsilon^{0ijkl}\,, \tag{A.76}$$

where we have included a factor of $s = -1$ in the upper components to ensure that the Euclidean ε-pseudo-tensor is adapted to the positive Euclidean signature

$$\varepsilon_{01234} = \sqrt{g}\,, \quad \varepsilon^{01234} = \frac{1}{\sqrt{g}}\,. \tag{A.77}$$

Thus, the Chern-Simons term transforms as

$$\begin{aligned}\varepsilon^{\nu\alpha\beta\gamma\delta}A_\nu F_{\alpha\beta}F_{\gamma\delta} &= \big(\varepsilon^{0ijkl}A_0F_{ij}F_{kl} - \varepsilon^{0ijkl}A_iF_{0j}F_{kl} + \dots\big)\\ &\to \mathrm{i}\,s\big(\varepsilon^{0ijkl}A_0F_{ij}F_{kl} - \varepsilon^{0ijkl}A_iF_{0j}F_{kl} + \dots\big)\\ &= \mathrm{i}\,s\,\varepsilon^{\nu\alpha\beta\gamma\delta}A_\nu F_{\alpha\beta}F_{\gamma\delta}\,,\end{aligned} \tag{A.78}$$

and the Euclidean action takes the form

$$I_{\mathrm{E}} = -\frac{1}{16\pi G_5}\int \mathrm{d}^5x\,\sqrt{g}\bigg(R + \frac{12}{L^2} - \frac{\varkappa^2}{4}F^{\mu\nu}F_{\mu\nu} + \frac{\mathrm{i}\,\varkappa^3}{12\sqrt{3}}\varepsilon^{\nu\alpha\beta\gamma\delta}A_\nu F_{\alpha\beta}F_{\gamma\delta}\bigg)\,, \tag{A.79}$$

Using this action one can derive the following Euclidean equations of motion

$$\begin{aligned}R_{\mu\nu} + \frac{4}{L^2}g_{\mu\nu} - \frac{\varkappa^2}{2}F_\mu{}^\alpha F_{\nu\alpha} + \frac{\varkappa^2}{12}g_{\mu\nu}F^{\alpha\beta}F_{\alpha\beta} = 0\,,\\ \nabla_\mu F^{\mu\nu} + \frac{\mathrm{i}\,\varkappa}{4\sqrt{3}}\varepsilon^{\nu\alpha\beta\gamma\delta}F_{\alpha\beta}F_{\gamma\delta} = 0\,.\end{aligned} \tag{A.80}$$

A.4.2 Near-horizon Lorentzian geometry

In the near-horizon region we first perform the coordinate transformation

$$r = r_+ + \varrho^2\,, \tag{A.81}$$

then we expand the Lorentzian metric (4.20) for small ϱ to obtain

$$\mathrm{d}s^2_{\mathrm{CCLP},\mathcal{H}} = \widetilde{g}_{\varrho\varrho}\bigg(\mathrm{d}\varrho^2 - \bigg(\frac{2\pi}{\beta^{\mathcal{H}}}\bigg)^2\varrho^2\,\mathrm{d}t^2\bigg) + \widetilde{g}_{\eta\eta}\,\mathrm{d}\eta^2 + 2\,\widetilde{g}_{12}\big(\mathrm{d}\xi_1 - \Omega_1^{\mathcal{H}}\,\mathrm{d}t\big)\big(\mathrm{d}\xi_2 - \Omega_2^{\mathcal{H}}\,\mathrm{d}t\big)$$

$$+\,\widetilde{g}_{11}\big(\mathrm{d}\xi_1 - \Omega_1^{\mathcal{H}}\,\mathrm{d}t\big)^2 + \widetilde{g}_{22}\big(\mathrm{d}\xi_2 - \Omega_2^{\mathcal{H}}\,\mathrm{d}t\big)^2\,. \tag{A.82}$$

Here we defined the constants

$$\begin{aligned}\beta^{\mathcal{H}} &= \frac{2\pi r_+\big[(r_+^2+a^2)(r_+^2+b^2)+abq\big]}{r_+^4\big[1+g^2(2r_+^2+a^2+b^2)\big]-(ab+q)^2}\,,\\ \Omega_1^{\mathcal{H}} &= \frac{a(r_+^2+b^2)(1+g^2r_+^2)+bq}{(r_+^2+a^2)(r_+^2+b^2)+abq}\,,\quad \Omega_2^{\mathcal{H}} = \Omega_1^{\mathcal{H}}\Big|_{a\leftrightarrow b}\,,\end{aligned} \tag{A.83}$$

and $(\widetilde{g}_{\varrho\varrho}, \widetilde{g}_{\eta\eta}, \widetilde{g}_{11}, \widetilde{g}_{22}, \widetilde{g}_{12})$ are functions of (ϱ, η) expanded to the relevant orders in the small variable ϱ:

$$\begin{aligned}
\widetilde{g}_{\varrho\varrho} &= \frac{4\rho_+^2}{\Delta'_{r,+}}\,, \qquad \widetilde{g}_{\eta\eta} = \frac{\rho_+^2}{\Delta_\eta}\,,\\
\frac{\widetilde{g}_{11}}{\mathcal{S}_\eta^2} &= -\frac{(\Delta_\eta-\Xi_a)\big(a^2 f_+ + 2abq\Xi_a\rho_+^2\big) - (a^2+r_+^2)\Xi_a(\Xi_a-\Xi_b)\rho_+^4}{\Xi_a^2(\Xi_a-\Xi_b)\rho_+^4}\\
&\quad - \frac{(\Delta_\eta-\Xi_a)\Big[a^2 f'_+\rho_+^2 - 2a\big(af_+ + bq\Xi_a\rho_+^2\big)\big(\rho_+^2\big)'\Big] - 2r_+\Xi_a(\Xi_a-\Xi_b)\rho_+^6}{\Xi_a^2(\Xi_a-\Xi_b)\rho_+^6}\varrho^2\,,\\
\frac{\widetilde{g}_{12}}{\mathcal{S}_\eta^2\mathcal{C}_\eta^2} &= \frac{abf_+ + (b^2\Xi_a + a^2\Xi_b)q\rho_+^2}{\Xi_a\Xi_b\rho_+^4}\\
&\quad + \frac{ab\Big[f'_+\rho_+^2 - 2f_+\big(\rho_+^2\big)'\Big] - (b^2\Xi_a + a^2\Xi_b)\rho_+^2\big(\rho_+^2\big)'}{\Xi_a\Xi_b\rho_+^6}\varrho^2\,,\\
\frac{\widetilde{g}_{22}}{\mathcal{C}_\eta^2} &= \frac{(\Delta_\eta-\Xi_b)\big(b^2 f_+ + 2abq\Xi_b\rho_+^2\big) + (b^2+r_+^2)\Xi_b(\Xi_a-\Xi_b)\rho_+^4}{\Xi_b^2(\Xi_a-\Xi_b)\rho_+^4}\\
&\quad + \frac{(\Delta_\eta-\Xi_b)\Big[b^2 f'_+\rho_+^2 - 2b\big(bf_+ + aq\Xi_b\rho_+^2\big)\big(\rho_+^2\big)'\Big] + 2r_+\Xi_b(\Xi_a-\Xi_b)\rho_+^6}{\Xi_b^2(\Xi_a-\Xi_b)\rho_+^6}\varrho^2\,,
\end{aligned} \tag{A.84}$$

where we have defined the shorthands

$$\begin{aligned}
&f_+ = f(r_+,\eta)\,, \quad \rho_+^2 = \rho^2(r_+,\eta)\,, \quad \mathcal{S}_\eta = \sin\eta\,, \quad \mathcal{C}_\eta = \cos\eta\,,\\
&f'_+ = \frac{\partial f}{\partial r}(r_+,\eta)\,, \quad \big(\rho_+^2\big)' = \frac{\partial\rho^2}{\partial r}(r_+,\eta)\,, \quad \Delta'_{r,+} = \frac{\partial\Delta_r}{\partial r}(r_+)\,.
\end{aligned}$$

A.4.3 Asymptotic Lorentzian geometry

To obtain the Lorentzian metric in the asymptotic region we perform the coordinate transformation

$$r = \widehat{r}\left(1 + \frac{1}{\widehat{r}^2}f_1(\widehat{\eta}) + \frac{1}{\widehat{r}^4}f_2(\widehat{\eta})\right), \quad \eta = \widehat{\eta} + \frac{1}{\widehat{r}^4}h_1(\widehat{\eta}) + \frac{1}{\widehat{r}^6}h_2(\widehat{\eta})\,, \tag{A.85}$$

where $(f_{1,2},\ h_{1,2})$ are functions of $\widehat{\eta}$ that will be fixed by demanding that the asymptotic metric takes the Fefferman-Graham form. We expand the

components of the transformed metric to (and including) the following orders:

$$\begin{array}{cccccccccc} \widehat{g}_{tt} & & \widehat{g}_{t1} & & \widehat{g}_{t2} & & \widehat{g}_{\widehat{r}\widehat{r}} & \widehat{g}_{\widehat{r}\widehat{\eta}} & \widehat{g}_{\widehat{\eta}\widehat{\eta}} & \widehat{g}_{11} & \widehat{g}_{12} & \widehat{g}_{22} \\ O\big(\widehat{r}^{-2}\big) & & O\big(\widehat{r}^{-2}\big) & & O\big(\widehat{r}^{-2}\big) & & O\big(\widehat{r}^{-6}\big) & O\big(\widehat{r}^{-5}\big) & O\big(\widehat{r}^{-2}\big) & O\big(\widehat{r}^{-2}\big) & O\big(\widehat{r}^{-2}\big) & O\big(\widehat{r}^{-2}\big) \end{array}.$$

Putting the metric in Fefferman-Graham form amounts to having $\widehat{g}_{\widehat{r}\widehat{r}} = g^{-2}\widehat{r}^{-2}$ and $\widehat{g}_{\widehat{r}\widehat{\eta}} = 0$. Demanding that the $O\big(\widehat{r}^{-4}\big)$ and $O\big(\widehat{r}^{-6}\big)$ terms of $\widehat{g}_{\widehat{r}\widehat{r}}$ and the $O\big(\widehat{r}^{-3}\big)$ and $O\big(\widehat{r}^{-5}\big)$ terms of $\widehat{g}_{\widehat{r}\widehat{\eta}}$ vanish achieves that and uniquely fixes

$$f_1(\widehat{\eta}) = -\frac{1}{4g^2}\left[2 - \Xi_a - \Xi_b + \Delta_\eta(\widehat{\eta})\right],$$

$$f_2(\widehat{\eta}) = \frac{1}{8g^4}\Big[1 - 2g^2 m - \Xi_a \sin^2\widehat{\eta} - \Xi_b \cos^2\widehat{\eta} - \cos^2\widehat{\eta}\sin^2\widehat{\eta}(\Xi_a - \Xi_b)^2\Big],$$

$$h_1(\widehat{\eta}) = -\frac{\Xi_a - \Xi_b}{8g^4}\cos\widehat{\eta}\sin^2\widehat{\eta}\,\Delta_\eta(\widehat{\eta}),$$

$$h_2(\widehat{\eta}) = -\frac{\Xi_a - \Xi_b}{16g^6}\cos\widehat{\eta}\sin^2\widehat{\eta}\big[2\Xi_a^2\cos^2\widehat{\eta} - \Xi_a\Xi_b + 2\Xi_b^2\sin^2\widehat{\eta} - 3\cos^2\widehat{\eta}\sin^2\widehat{\eta}(\Xi_a - \Xi_b)^2\big].$$

The resulting Fefferman-Graham asymptotic Lorentzian metric reads

$$\begin{aligned} \mathrm{d}s^2_{\mathrm{CCLP},\mathcal{A}} = \frac{1}{g^2\widehat{r}^2}\,\mathrm{d}\widehat{r}^2 + \widehat{g}_{tt}\,\mathrm{d}t^2 + 2\,\widehat{g}_{t1}\,\mathrm{d}t\,\mathrm{d}\xi_1 + 2\,\widehat{g}_{t2}\,\mathrm{d}t\,\mathrm{d}\xi_2 + \widehat{g}_{\widehat{\eta}\widehat{\eta}}\mathrm{d}\widehat{\eta}^2 \\ + \widehat{g}_{11}\,\mathrm{d}{\xi_1}^2 + 2\,\widehat{g}_{12}\,\mathrm{d}\xi_1\,\mathrm{d}\xi_2 + \widehat{g}_{22}\,\mathrm{d}{\xi_2}^2\,. \end{aligned} \tag{A.86}$$

In the equation above $(\widehat{g}_{tt}, \widehat{g}_{t1}, \widehat{g}_{t2}, \widehat{g}_{\widehat{\eta}\widehat{\eta}}, \widehat{g}_{11}, \widehat{g}_{12}, g_{22})$ are function of $(\widehat{r}, \widehat{\eta})$, expanded to the relevant orders in the large variable $\widehat{r}$:

$$
\begin{aligned}
\widehat{g}_{tt} &= -\frac{g^2\widehat{\Delta}_\eta\,\widehat{r}^2}{\Xi_a\Xi_b} - \frac{\widehat{\Delta}_\eta\left(\Xi_a+\Xi_b-\widehat{\Delta}_\eta\right)}{2\Xi_a\Xi_b} \\
&\quad + \frac{2\widehat{\Delta}_\eta^2\left(abg^2q+m\right) - \frac{\Xi_a\Xi_b\widehat{\Delta}_\eta\left(-2\widehat{\Delta}_\eta(\Xi_a+\Xi_b)+(\Xi_a+\Xi_b)^2+\widehat{\Delta}_\eta^2+8g^2m\right)}{16g^2}}{\Xi_a^2\Xi_b^2\,\widehat{r}^2}\,, \\
\frac{\widehat{g}_{t1}}{\widehat{\mathcal{S}}_\eta^2} &= -\frac{\widehat{\Delta}_\eta\left(a^2bg^2q+2am+bq\right)}{\Xi_a^2\Xi_b\,\widehat{r}^2}\,, \\
\frac{\widehat{g}_{t2}}{\widehat{\mathcal{C}}_\eta^2} &= -\frac{\widehat{\Delta}_\eta\left(ab^2g^2q+aq+2bm\right)}{\Xi_a\Xi_b^2\,\widehat{r}^2}\,, \\
\widehat{g}_{\widehat{\eta}\widehat{\eta}} &= \frac{\widehat{r}^2}{\widehat{\Delta}_\eta} + \frac{\Xi_a+\Xi_b-3\widehat{\Delta}_\eta}{2g^2\widehat{\Delta}_\eta} + \frac{-6\widehat{\Delta}_\eta\left(\Xi_a+\Xi_b\right)+\left(\Xi_a+\Xi_b\right)^2+9\widehat{\Delta}_\eta^2+8g^2m}{16g^4\widehat{\Delta}_\eta\,\widehat{r}^2}\,, \\
\frac{\widehat{g}_{11}}{\widehat{\mathcal{S}}_\eta^2} &= \frac{\widehat{r}^2}{\Xi_a} - \frac{\Xi_a-\Xi_b+\widehat{\Delta}_\eta}{2g^2\Xi_a} \\
&\quad - \frac{\frac{8g^2\left(4a^2g^2m\widehat{\Delta}_\eta+4abg^2q\left(\widehat{\Delta}_\eta-\Xi_a\right)+m\Xi_a(3\Xi_a+\Xi_b-4)\right)}{\Xi_a-\Xi_b} - \Xi_a\left(\Xi_a-\Xi_b+\widehat{\Delta}_\eta\right)^2}{16g^4\Xi_a^2\,\widehat{r}^2}\,, \\
\frac{\widehat{g}_{12}}{\widehat{\mathcal{S}}_\eta^2\widehat{\mathcal{C}}_\eta^2} &= \frac{a^2q+2abm+b^2q}{\Xi_a\Xi_b\,\widehat{r}^2}\,, \\
\frac{\widehat{g}_{22}}{\widehat{\mathcal{C}}_\eta^2} &= \frac{\widehat{r}^2}{\Xi_b} + \frac{\Xi_a-\Xi_b-\widehat{\Delta}_\eta}{2g^2\Xi_b} \\
&\quad + \frac{\frac{8g^2\left(4b^2g^2m\widehat{\Delta}_\eta+4abg^2q\left(\widehat{\Delta}_\eta-\Xi_b\right)+m\Xi_b(\Xi_a+3\Xi_b-4)\right)}{\Xi_a-\Xi_b} + \Xi_b\left(-\Xi_a+\Xi_b+\widehat{\Delta}_\eta\right)^2}{16g^4\Xi_b^2\,\widehat{r}^2}\,,
\end{aligned}
\tag{A.87}
$$

where we have defined the shorthands

$$
\widehat{\Delta}_\eta \equiv \Delta_\eta(\widehat{\eta})\,, \quad \widehat{\mathcal{S}}_\eta = \sin\widehat{\eta}\,, \quad \widehat{\mathcal{C}}_\eta = \cos\widehat{\eta}\,.
$$

A.4.4 Potentials: $(\Omega_1,\, \Omega_2,\, \beta,\, \Phi)$

The thermodynamic potentials associated with the two angular momentum parameters of the CCLP black hole are defined as

$$\Omega_i = \Omega_i^{\mathcal{H}} - \Omega_i^{\mathcal{B}}\,, \quad \Omega_i^{\mathcal{H}} = \left.\frac{\mathrm{d}\xi_i}{\mathrm{d}t}\right|_{r\to r_+}\,, \quad \Omega_i^{\mathcal{B}} = \left.\frac{\mathrm{d}\xi_i}{\mathrm{d}t}\right|_{r\to\infty}\,, \quad i=1,2\,. \tag{A.88}$$

From (A.82) and (4.27) it is easy to see that $\Omega_i^{\mathcal{H}} = \Omega_i^{\mathcal{H}}$ and $\Omega_i^{\mathcal{B}} = 0$, or explicitly

$$\Omega_1 = \frac{a(r_+^2+b^2)(1+g^2r_+^2)+bq}{(r_+^2+a^2)(r_+^2+b^2)+abq}\,, \quad \Omega_2 = \frac{b(r_+^2+a^2)(1+g^2r_+^2)+aq}{(r_+^2+a^2)(r_+^2+b^2)+abq}\,. \tag{A.89}$$

The inverse temperature of the CCLP black hole can be obtained from the Wick rotated near-horizon metric

$$\begin{aligned}\mathrm{d}s^2_{\mathrm{CCLP},\mathcal{H},\mathcal{E}} = \widetilde{g}_{\varrho\varrho}\left(\mathrm{d}\varrho^2 + \left(\frac{2\pi}{\beta^{\mathcal{H}}}\right)^2\varrho^2\,\mathrm{d}\tau^2\right) + \widetilde{g}_{\eta\eta}\,\mathrm{d}\eta^2 \\ + 2\,\widetilde{g}_{12}(\mathrm{d}\xi_1 + \mathrm{i}\,\Omega_1\,\mathrm{d}\tau)(\mathrm{d}\xi_2 + \mathrm{i}\,\Omega_2\,\mathrm{d}\tau) \\ + \widetilde{g}_{11}(\mathrm{d}\xi_1 + \mathrm{i}\,\Omega_1\,\mathrm{d}\tau)^2 + \widetilde{g}_{22}(\mathrm{d}\xi_2 + \mathrm{i}\,\Omega_2\,\mathrm{d}\tau)^2\,,\end{aligned} \tag{A.90}$$

where we have already implemented the relations $\Omega_i^{\mathcal{H}} = \Omega_i$. The above metric is a warped fibration of S^3 over $\mathbb{R}^2$. Demanding absence of conical singularity at the origin of the $\mathbb{R}^2$ fixes

$$\tau \sim \tau + \beta^{\mathcal{H}}\,. \tag{A.91}$$

Demanding that the S^3 fibration is also well defined at the origin of the $\mathbb{R}^2$ shows that going around the Euclidean time circle once should be accompanied by the identifications

$$(\tau,\, \xi_1,\, \xi_2) \sim \left(\tau + \beta^{\mathcal{H}},\, \xi_1 - \mathrm{i}\,\Omega_1\beta^{\mathcal{H}},\, \xi_2 - \mathrm{i}\,\Omega_2\beta^{\mathcal{H}}\right). \tag{A.92}$$

From (4.27) we see that the Wick rotated conformal boundary metric is regular for any length of the Euclidean time circle (also regular for non-compact τ for that matter). For consistency, we translate the IR imposed periodicity on τ to the boundary. Back in the Lorentzian picture, the periodicity in the Euclidean time has the interpretation of inverse temperature so we define $\beta = \beta^{\mathcal{H}}$, or explicitly

$$\beta = \frac{2\pi r_+\left[(r_+^2+a^2)(r_+^2+b^2)+abq\right]}{r_+^4\left[1+g^2(2r_+^2+a^2+b^2)\right]-(ab+q)^2}\,. \tag{A.93}$$

The inverse temperature can also be obtained directly from the Lorentzian description as follows. First, note the surface $r = r_+$ is an event horizon as it is generated by a Killing vector

$$V = V^\mu \partial_\mu = \frac{\partial}{\partial t} + \Omega_1 \frac{\partial}{\partial \xi_1} + \Omega_2 \frac{\partial}{\partial \xi_2}; \quad \nabla_\mu V_\nu + \nabla_\nu V_\mu = 0\,, \tag{A.94}$$

that becomes null on that surface

$$V_\mu V^\mu \Big|_{r=r_+} = 0\,. \tag{A.95}$$

Note that contrary to the familiar similar expressions from spacetimes with flat asymptotics, $V_\mu V^\mu$ is not normalized to unity at infinity. Using this Killing vector we calculate the surface gravity on the horizon from

$$\kappa_{\mathcal{H}} = \sqrt{-\frac{1}{2}\nabla^\mu V^\nu \nabla_\mu V_\nu}\Big|_{r\to r_+}\,. \tag{A.96}$$

The inverse temperature is then given by $\beta = 2\pi/\kappa_{\mathcal{H}}$. Simplifying this expression we obtain precisely (A.93). The electrostatic potential is defined as

$$\Phi = V^\mu A_\mu \Big|_{r=r_+} - V^\mu A_\mu \Big|_{r\to\infty}\,. \tag{A.97}$$

It is instructive to look at the above terms separately:

$$V^\mu A_\mu \Big|_{r=r_+} = \frac{\sqrt{3} q r_+^2}{\varkappa\big[(r_+^2+a^2)(r_+^2+b^2)+abq\big]} + \alpha\,, \qquad V^\mu A_\mu \Big|_{r\to\infty} = \alpha\,. \tag{A.98}$$

We see that the definition of Φ given above is independent of the choice of gauge parameter α. The final expression reads

$$\Phi = \frac{\sqrt{3} q r_+^2}{\varkappa\big[(r_+^2+a^2)(r_+^2+b^2)+abq\big]}\,. \tag{A.99}$$

For consistency, one needs to ensure that $A^\mu A_\mu$ is regular on the horizon. However, $A^\mu A_\mu\big|_{r=r_+}$ diverges as $O\big((r-r_+)^{-1}\big)$. Demanding that the coefficient of the divergent term vanishes fixes the gauge parameter α to

$$\alpha = -\Phi\,. \tag{A.100}$$

With this at hand we find that the following relations hold

$$A^\mu A_\mu \Big|_{r=r_+} = 0\,, \quad V^\mu A_\mu \Big|_{r=r_+} = 0\,. \tag{A.101}$$

A.4.5 Charges: (J_1, J_2, Q), via boundary integrals

To obtain the two conserved angular momenta (J_1, J_2) we first note that the boundary metric (4.27) has three independent Killing vectors

$$K_{(t)} = \frac{\partial}{\partial t}\,, \quad K_{(\xi_1)} = \frac{\partial}{\partial \xi_1}\,, \quad K_{(\xi_2)} = \frac{\partial}{\partial \xi_2}\,. \tag{A.102}$$

To each of them we associate a Killing form as

$$\widetilde{K}_{(\cdot)} = K^{\mu}_{(\cdot)} g_{\mu\nu}\, \mathrm{d}x^{\nu}\ . \tag{A.103}$$

Then, the angular momenta of the black hole are defined via the following Komar integrals

$$J_i = \lim_{r\to\infty} \frac{1}{16\pi G_5} \int_{S^3} \star_5\, \mathrm{d}\widetilde{K}_{(\xi_i)}\ , \quad i = 1, 2\,. \tag{A.104}$$

The final results read

$$J_1 = \frac{\pi\big[2am + bq(1+a^2g^2)\big]}{4\Xi_a^2\Xi_b G_5}\,, \quad J_2 = \frac{\pi\big[2bm + aq(1+b^2g^2)\big]}{4\Xi_a\Xi_b^2 G_5}\,. \tag{A.105}$$

To calculate the electric charge Q one needs a conserved current arising from the Maxwell equation. The following manipulation identifies such current

$$0 = \sigma\left[\mathrm{d}\star_5 F - \frac{1}{\sqrt{3}} F\wedge F\right] = \sigma\left[\mathrm{d}\star_5 F - \frac{1}{\sqrt{3}}\,\mathrm{d}(F\wedge A)\right] = \mathrm{d}\left[\sigma\left(\star_5 F - \frac{1}{\sqrt{3}} F\wedge A\right)\right]\,,$$

where we have included an arbitrary multiplicative parameter σ. The asymptotic electric charge is then given by

$$Q = \lim_{r\to\infty} \frac{\sigma}{16\pi G_5} \int_{S^3} \left(\star_5 F - \frac{1}{\sqrt{3}} F\wedge A\right) = -\frac{\sigma\sqrt{3}\pi q}{4\chi\Xi_a\Xi_b G_5}\,. \tag{A.106}$$

Consistency with the quantum statistical relation (4.35) fixes $\sigma = -\chi^2$. Thus, the electric charge is given by

$$Q = \frac{\chi\sqrt{3}\pi q}{4\Xi_a\Xi_b G_5}\,. \tag{A.107}$$

A.4.6 Euclidean on-shell action

The on-shell action can be calculated using holographic renormalization. In the Lorentzian setting one begins by augmenting the action (A.72) with the

following boundary terms

$$I_{\rm GH} = \frac{1}{8\pi G_5}\int \mathrm{d}^4x\,\sqrt{-\gamma}\,K\,,$$
$$I_{\rm ct} = \frac{1}{8\pi G_5}\int \mathrm{d}^4x\,\sqrt{-\gamma}\left(-3g-\frac{1}{4g}\mathcal{R}\right), \tag{A.108}$$
$$I_{\rm fct} = \frac{1}{8\pi G_5}\int \mathrm{d}^4x\,\sqrt{-\gamma}\left(\zeta'\mathcal{R}^2-\zeta''F_{ij}F^{ij}\right),$$

where the integrations are most easily performed over a spacelike hypersurface $\widehat{r}=\widehat{R}_0$ in Fefferman-Graham coordinates $(t,\widehat{r},\widehat{\eta},\xi_1,\xi_2)$. The induced metric on this hypersurface is obtained from (A.86). We denote it by γ_{ij} with indices $i,j=t,\widehat{\eta},\xi_1,\xi_2$ running over the boundary coordinates. The extrinsic curvature and its trace are given, in Fefferman-Graham coordinates, by

$$K_{ij} = \frac{g\widehat{r}}{2}\frac{\partial}{\partial\widehat{r}}\gamma_{ij}\,,\quad K=\gamma^{ij}K_{ij}\,. \tag{A.109}$$

Finally, $\mathcal{R}$ is the Ricci scalar calculated from the induced metric γ_{ij}. The meaning of these boundary terms is as follows: $I_{\rm GH}$ is the usual Gibbons-Hawking boundary term, $I_{\rm ct}$ includes the counterterms needed to cancel the divergences of the bulk on-shell action[8], $I_{\rm fct}$ includes the allowed diffeomorphism invariant finite counterterms with arbitrary coefficients ζ' and ζ''. In 5d one also needs to include a non-diffeomorphism invariant conformal anomaly term given by

$$I_{\rm an} = \frac{1}{8\pi G_5}\int \mathrm{d}^4x\,\sqrt{-\gamma}\,\frac{1}{16g^3}\left(\mathcal{R}_{ij}\mathcal{R}^{ij}-\frac{1}{3}\mathcal{R}^2-4F_{ij}F^{ij}\right)\log e^{-2\widehat{R}_0}\,. \tag{A.110}$$

If the integrated conformal anomaly is non-vanishing, generically there is a logarithmic divergence left over that cannot be cancelled. However, on the CCLP solution it is easy to see that, although the un-integrated anomaly does not vanish, its integral does, so $I_{\rm an}$ does not contribute at all. Overall, the holographically renormalized Euclidean on-shell action is given by

$$\mathcal{I}_{\rm hr} = I_{\mathcal{E}} + I^{\mathcal{E}}_{\rm GH} + I^{\mathcal{E}}_{\rm ct} + I^{\mathcal{E}}_{\rm fct}\,, \tag{A.111}$$

where $I_{\mathcal{E}}$ is given by (A.79) and the superscripts $\mathcal{E}$ on the boundary terms signify that we are working with the Euclideanized versions of (A.108). Performing the above integrals is arduous and was done with the help of Mathematica. The final answer for the Euclidean on-shell action is given in (4.34).

[8]Strictly speaking the quoted coefficients of the g and $\mathcal{R}$ terms are only valid in Fefferman-Graham coordinates, in other coordinate systems these coefficients might change.

A.4.7 Charges: $(E,\, J_1,\, J_2)$, via holographic renormalization

In the Lorentzian description, we can harness holographic renormalization, see [191] for a review, to obtain the energy of the CCLP black hole. First, we construct the renormalized holographic stress energy tensor as, see [169] for more details,

$$\begin{aligned} T_{ij} &= -\frac{2}{\sqrt{-\gamma}}\frac{\delta}{\delta\gamma^{ij}}(\mathcal{L}_{\rm GH}+\mathcal{L}_{\rm ct}+\mathcal{L}_{\rm fct}) \\ &= \frac{1}{8\pi G_5}\bigg[K_{ij}-\gamma_{ij}K+3g\gamma_{ij}-\frac{1}{2g}\mathcal{R}_{ij}+\frac{1}{4g}\mathcal{R}\gamma_{ij} \\ &\qquad +4\zeta'\bigg(\mathcal{R}_{ij}\mathcal{R}-\frac{1}{4}\gamma_{ij}\mathcal{R}^2-\nabla_i\nabla_j\mathcal{R}+\gamma_{ij}\nabla_k\nabla^k\mathcal{R}\bigg)\bigg]\,, \end{aligned} \tag{A.112}$$

where we have already set the ζ'' contribution to zero since $F_{ij}F^{ij}$ vanishes sufficiently fast near the boundary of the CCLP solution. Then, the conserved charge associated to a boundary conformal Killing vector K can be obtained from

$$\mathcal{Q}[K]=\int_0^{2\pi}\mathrm{d}\xi_1\int_0^{2\pi}\mathrm{d}\xi_2\int_0^{\pi/2}\mathrm{d}\widehat{\eta}\,\sqrt{-\gamma}\,T^i{}_j\,K^j\,. \tag{A.113}$$

In particular, for the two angular momenta we obtain

$$J_1=\mathcal{Q}[\partial_{\xi_1}]=\frac{\pi\big(2am+bq(1+a^2g^2)\big)}{4\Xi_a^2\Xi_bG_5}\,,\quad J_2=\mathcal{Q}[\partial_{\xi_2}]=J_1\Big|_{b\leftrightarrow a} \tag{A.114}$$

in agreement with our previous Komar integral results (A.105). For the energy we obtain

$$\begin{aligned} E=\mathcal{Q}[\partial_t] &= \Big(E_{\rm AdS}-\widetilde{\zeta}'\Big) \\ &\quad +\frac{m\pi(2\Xi_a+2\Xi_b-\Xi_a\Xi_b)+2abq^2\pi(\Xi_a+\Xi_b)}{4\Xi_a^2\Xi_b^2G_5}\,, \end{aligned} \tag{A.115}$$

where $E_{\rm AdS}$ and $\widetilde{\zeta}'$ are the constants given in (4.32).

A.4.8 Killing spinor and frame in suitable coordinates

Here we show that the three parameter, i.e. $(a,\, b,\, \widetilde{m})$, CCLP solution, described in Section 4.3.3, is supersymmetric by explicitly verifying that the following

spinor

$$\epsilon = \exp\left\{\frac{\mathrm{i}}{2}\Big[g\Big(1+\sqrt{3}\chi\alpha\Big)t+\xi_1+\xi_2\Big]\right\}\times$$
$$\frac{1}{\rho}\big[\widetilde{m}\rho^2-(1+\widetilde{m})\big(r^2-r_*^2\big)\big]^{1/2}\,\epsilon_0\,, \tag{A.116}$$

solves (4.15). Here ϵ_0 is a constant spinor that satisfies the projection condition

$$\frac{\mathrm{i}}{2}\big(\gamma^{12}-\gamma^{34}\big)\epsilon_0=\epsilon_0\,, \tag{A.117}$$

which reduces the number of independent (complex) spinor components from four to one. We use the explicit realization of the Clifford algebra described in [117] and the following frames

$$\begin{aligned}
e^0 &= -\frac{g^2\Delta_\eta}{\Xi_a\Xi_b}\left[\frac{(a+b)(1+\widetilde{m})(1+g^2r_*^2)}{g^3\rho^2}-\big(g^{-2}+r_*^2\big)-\frac{\rho^2}{1+\widetilde{m}}\left(1-\frac{\widetilde{m}\rho}{h}\right)\right]\mathrm{d}t\\
&\quad+\frac{g\sin^2\eta}{\Xi_a}\left[\frac{a(a+b)(1+\widetilde{m})(1+g^2r_*^2)}{g^2\rho^2}-\big(a^2+r_*^2\big)-\frac{\rho^2}{1+\widetilde{m}}\left(1-\frac{\widetilde{m}\rho}{h}\right)\right]\mathrm{d}\xi_1\\
&\quad+\frac{g\cos^2\eta}{\Xi_b}\left[\frac{b(a+b)(1+\widetilde{m})(1+g^2r_*^2)}{g^2\rho^2}-\big(b^2+r_*^2\big)-\frac{\rho^2}{1+\widetilde{m}}\left(1-\frac{\widetilde{m}\rho}{h}\right)\right]\mathrm{d}\xi_1\,,\\
e^1 &= \sqrt{\frac{\rho^2}{\Delta_r}}\,\mathrm{d}r\,,\\
e^2 &= \frac{r\sqrt{\Delta_r\rho^2}}{h}\left(-\frac{g\Delta_\eta}{\Xi_a\Xi_b}\,\mathrm{d}t+\frac{\sin^2\eta}{\Xi_a}\,\mathrm{d}\xi_2+\frac{\cos^2\eta}{\Xi_b}\,\mathrm{d}\xi_1\right),\\
e^3 &= -\sqrt{\frac{\rho^2}{\Delta_\eta}}\,\mathrm{d}\eta\,,\\
e^4 &= \frac{\sin\eta\cos\eta\sqrt{\Delta_\eta\rho^2}}{h}\left\{-\frac{g(\Xi_a-\Xi_b)}{\Xi_a\Xi_b}\big(g^{-2}+(1+\widetilde{m})r_*^2-r^2\big)\,\mathrm{d}t\right.\\
&\quad\left.+\frac{1}{\Xi_a}(a^2+(1+\widetilde{m})r_*^2-r^2)\,\mathrm{d}\xi_1+\frac{1}{\Xi_b}(b^2+(1+\widetilde{m})r_*^2-r^2)\,\mathrm{d}\xi_2\right\}.
\end{aligned} \tag{A.118}$$

In [72] a much simpler expressions for the frames in the so called orthotoric coordinates were presented. Our expressions are merely coordinate transformed

versions of their (A.4). In these orthotoric coordinates the frame is degenerate in the interesting limits to extremality, $\widetilde{m} \to 0$, and equal rotation parameters, $b \to a$. In [87] it was explained how to take these limits sensibly by performing accompanying field redefinitions. The benefit of working directly coordinates presented here is that the frame is perfectly valid in both the extremal and the equal-rotation-parameters limits. One can use the explicit expressions for the spinor and frame to understand the linear constraint (4.53). It arises from evaluating the Lie derivative along the Killing vector V, described in Appendix A.4.5, on ϵ, at the horizon

$$\begin{aligned}\mathcal{L}_V\epsilon &= V^\mu\big(\partial_\mu\epsilon + \omega_{\mu ab}\gamma^{ab}\epsilon\big) - \frac{1}{4}\nabla_\mu V_\nu\gamma^{\mu\nu}\epsilon \\ &= \frac{\mathrm{i}}{2}\left(g + \Omega_1 + \Omega_2 + g\chi\sqrt{3}\,\alpha + 2\,V^\mu A_\mu\Big|_{r=r_+}\right)\epsilon\,. \end{aligned} \tag{A.119}$$

We implement the regularity condition $A^\mu A_\mu < \infty$, by setting $\alpha = -\Phi$. This removes the $V^\mu A_\mu\big|_{r=r_+}$ term. Now we want to ensure that

$$\mathcal{L}_V\epsilon = \frac{\pi}{\beta}\epsilon \implies e^{t\mathcal{L}_V}\epsilon\Big|_{t=t_0}^{t=t_0-\mathrm{i}\beta} = e^{-\mathrm{i}\beta\mathcal{L}_V}\epsilon = -\epsilon\,, \tag{A.120}$$

which implies that the Killing spinor has the correct antiperiodic behavior in the vicinity of the horizon. This is compatible with the Lorentzian signature identification in (A.92). This results in precisely the linear constraint (4.53) between the potentials $(\beta, \Omega_1, \Omega_2, \Phi)$, where Φ appears through $-\alpha$.

A.5 Conventions

We define forms with explicit factorial factors, for example a p-form ω reads

$$\omega = \frac{1}{p!}\omega_{\mu_1\ldots\mu_p}\,\mathrm{d}x^{\mu_1}\wedge\cdots\wedge\mathrm{d}x^{\mu_p}\ . \tag{A.121}$$

In particular, we have

$$A = A_\mu\,\mathrm{d}x^\mu\ , \quad F = \frac{1}{2!}F_{\mu\nu}\,\mathrm{d}x^\mu\wedge\mathrm{d}x^\nu\ , \quad F = \mathrm{d}A = \partial_{[\mu}A_{\nu]}\,\mathrm{d}x^\mu\wedge\mathrm{d}x^\nu\ ,$$

where antisymmetrization is also defined with explicit factorial factors as

$$T_{[\mu_1\ldots\mu_p]} = \frac{1}{p!}\sum_{\sigma\in S_p}\mathrm{sign}(\sigma)T_{\mu_{\sigma(1)}\ldots\mu_{\sigma(p)}}\,. \tag{A.122}$$

Thus, the components of the field strength are

$$F_{\mu\nu} = 2!\partial_{[\mu}A_{\nu]} = \partial_\mu A_\nu - \partial_\nu A_\mu \,. \tag{A.123}$$

The Hodge star in our conventions is defined to act on a p-form ω as

$$\star\omega = \frac{1}{p!(D-p)!}\omega_{\mu_1\ldots\mu_p}\varepsilon^{\mu_1\ldots\mu_p}{}_{\nu_1\ldots\nu_{D-p}}\,\mathrm{d}x^{\nu_1}\wedge\cdots\wedge\mathrm{d}x^{\nu_{D-p}}\,, \tag{A.124}$$

where ε is the epsilon pseudo tensor, related to the totally antisymmetric symbol η as

$$\varepsilon_{\mu_1\ldots\mu_D} = \sqrt{|g|}\,\eta_{\mu_1\ldots\mu_D}\,, \quad \varepsilon^{\mu_1\ldots\mu_D} = \frac{\mathrm{sgn}(g)}{\sqrt{|g|}}\eta^{\mu_1\ldots\mu_D}\,. \tag{A.125}$$

We define the Riemann curvature tensor as

$$R_{\mu\nu}{}^{\rho}{}_{\sigma} = \partial_\mu\Gamma^{\rho}{}_{\nu\sigma} - \partial_\nu\Gamma^{\rho}{}_{\mu\sigma} + \Gamma^{\rho}{}_{\mu\lambda}\Gamma^{\lambda}{}_{\nu\sigma} - \Gamma^{\rho}{}_{\nu\lambda}\Gamma^{\lambda}{}_{\mu\sigma}\,, \tag{A.126}$$

and the Ricci tensor and Ricci scalar as

$$R_{\mu\nu} = R_{\mu}{}^{\rho}{}_{\nu\rho} = R^{\rho}{}_{\mu\rho\nu}\,, \quad R = R^{\mu}{}_{\mu}\,. \tag{A.127}$$

For the gamma matrices in arbitrary dimensions we use the conventions of [117], in particular, for the S^4 and $\Sigma_{\mathfrak{g}}$, described in the main text, we use Euclidean gamma matrices, while for the 7d and the 5d spacetimes we use the Lorentzian ones.

Bibliography

[1] Abedi, J., and Afshordi, N. Echoes from the Abyss: A highly spinning black hole remnant for the binary neutron star merger GW170817. *JCAP 11* (2019), 010.

[2] Abedi, J., and Afshordi, N. Echoes from the Abyss: A Status Update.

[3] Abedi, J., Dykaar, H., and Afshordi, N. Echoes from the Abyss: Tentative evidence for Planck-scale structure at black hole horizons. *Phys. Rev. D 96*, 8 (2017), 082004.

[4] Abedi, J., Dykaar, H., and Afshordi, N. Echoes from the Abyss: The Holiday Edition!

[5] Abedi, J., Dykaar, H., and Afshordi, N. Comment on: "Low significance of evidence for black hole echoes in gravitational wave data".

[6] Aharony, O., Benini, F., Mamroud, O., and Milan, E. A gravity interpretation for the Bethe Ansatz expansion of the $\mathcal{N} = 4$ SYM index. *Phys. Rev. D 104* (2021), 086026.

[7] Aharony, O., Fayyazuddin, A., and Maldacena, J. M. The Large N limit of N=2, N=1 field theories from three-branes in F theory. *JHEP 07* (1998), 013.

[8] Aharony, O., Gubser, S. S., Maldacena, J. M., Ooguri, H., and Oz, Y. Large N field theories, string theory and gravity. *Phys. Rept. 323* (2000), 183–386.

[9] Aharony, O., and Tachikawa, Y. A Holographic computation of the central charges of d=4, N=2 SCFTs. *JHEP 01* (2008), 037.

[10] Alday, L. F., Benini, F., and Tachikawa, Y. Liouville/Toda central charges from M5-branes. *Phys. Rev. Lett. 105* (2010), 141601.

[11] Ashton, G., Birnholtz, O., Cabero, M., Capano, C., Dent, T., Krishnan, B., Meadors, G. D., Nielsen, A. B., Nitz, A., and Westerweck, J. Comments on: "Echoes from the abyss: Evidence for Planck-scale structure at black hole horizons".

[12] Assel, B., Cassani, D., Di Pietro, L., Komargodski, Z., Lorenzen, J., and Martelli, D. The Casimir Energy in Curved Space and its Supersymmetric Counterpart. *JHEP 07* (2015), 043.

[13] Avery, S. G., Chowdhury, B. D., and Mathur, S. D. Emission from the D1D5 CFT. *JHEP 10* (2009), 065.

[14] Baggio, M., de Boer, J., Jottar, J. I., and Mayerson, D. R. Conformal Symmetry for Black Holes in Four Dimensions and Irrelevant Deformations. *JHEP 04* (2013), 084.

[15] Baggio, M., Halmagyi, N., Mayerson, D. R., Robbins, D., and Wecht, B. Higher Derivative Corrections and Central Charges from Wrapped M5-branes. *JHEP 12* (2014), 042.

[16] Bah, I. Quarter-BPS AdS_5 solutions in M-theory with a T^2 bundle over a Riemann surface. *JHEP 08* (2013), 137.

[17] Bah, I. AdS5 solutions from M5-branes on Riemann surface and D6-branes sources. *JHEP 09* (2015), 163.

[18] Bah, I., Beem, C., Bobev, N., and Wecht, B. AdS/CFT Dual Pairs from M5-Branes on Riemann Surfaces. *Phys. Rev. D 85* (2012), 121901.

[19] Bah, I., Beem, C., Bobev, N., and Wecht, B. Four-Dimensional SCFTs from M5-Branes. *JHEP 06* (2012), 005.

[20] Bakshi, P. M., and Mahanthappa, K. T. Expectation value formalism in quantum field theory. 1. *J. Math. Phys. 4* (1963), 1–11.

[21] Bakshi, P. M., and Mahanthappa, K. T. Expectation value formalism in quantum field theory. 2. *J. Math. Phys. 4* (1963), 12–16.

[22] Balasubramanian, V., Czech, B., Hubeny, V. E., Larjo, K., Rangamani, M., and Simon, J. Typicality versus thermality: An Analytic distinction. *Gen. Rel. Grav. 40* (2008), 1863–1890.

[23] Balasubramanian, V., de Boer, J., El-Showk, S., and Messamah, I. Black Holes as Effective Geometries. *Class. Quant. Grav. 25* (2008), 214004.

[24] Balasubramanian, V., and Kraus, P. A Stress tensor for Anti-de Sitter gravity. *Commun. Math. Phys. 208* (1999), 413–428.

[25] Balasubramanian, V., Kraus, P., and Shigemori, M. Massless black holes and black rings as effective geometries of the D1-D5 system. *Class. Quant. Grav. 22* (2005), 4803–4838.

[26] Banados, M., Henneaux, M., Teitelboim, C., and Zanelli, J. Geometry of the (2+1) black hole. *Phys. Rev. D 48* (1993), 1506–1525. [Erratum: Phys.Rev.D 88, 069902 (2013)].

[27] Banados, M., Teitelboim, C., and Zanelli, J. The Black hole in three-dimensional space-time. *Phys. Rev. Lett. 69* (1992), 1849–1851.

[28] Banerjee, S., Bryan, J.-W., Papadodimas, K., and Raju, S. A toy model of black hole complementarity. *JHEP 05* (2016), 004.

[29] Barack, L., et al. Black holes, gravitational waves and fundamental physics: a roadmap. *Class. Quant. Grav. 36*, 14 (2019), 143001.

[30] Barbon, J. L. F., and Rabinovici, E. Very long time scales and black hole thermal equilibrium. *JHEP 11* (2003), 047.

[31] Bardeen, J. M., Carter, B., and Hawking, S. W. The Four laws of black hole mechanics. *Commun. Math. Phys. 31* (1973), 161–170.

[32] Becker, K., Becker, M., and Schwarz, J. H. *String theory and M-theory: A modern introduction*. Cambridge University Press, 12 2006.

[33] Beem, C., and Gadde, A. The $N = 1$ superconformal index for class S fixed points. *JHEP 04* (2014), 036.

[34] Bekenstein, J. D. Black holes and entropy. *Phys. Rev. D 7* (1973), 2333–2346.

[35] Bena, I., Bossard, G., Katmadas, S., and Turton, D. Non-BPS multi-bubble microstate geometries. *JHEP 02* (2016), 073.

[36] Bena, I., Eperon, F., Heidmann, P., and Warner, N. P. The Great Escape: Tunneling out of Microstate Geometries. *JHEP 04* (2021), 112.

[37] Bena, I., Giusto, S., Martinec, E. J., Russo, R., Shigemori, M., Turton, D., and Warner, N. P. Smooth horizonless geometries deep inside the black-hole regime. *Phys. Rev. Lett. 117*, 20 (2016), 201601.

[38] Bena, I., Giusto, S., Martinec, E. J., Russo, R., Shigemori, M., Turton, D., and Warner, N. P. Asymptotically-flat supergravity solutions deep inside the black-hole regime. *JHEP 02* (2018), 014.

[39] Bena, I., Giusto, S., Russo, R., Shigemori, M., and Warner, N. P. Habemus Superstratum! A constructive proof of the existence of superstrata. *JHEP 05* (2015), 110.

[40] Bena, I., Guica, M., and Song, W. Un-twisting the NHEK with spectral flows. *JHEP 03* (2013), 028.

[41] Bena, I., Heidmann, P., Monten, R., and Warner, N. P. Thermal Decay without Information Loss in Horizonless Microstate Geometries. *SciPost Phys. 7*, 5 (2019), 063.

[42] Bena, I., Heidmann, P., and Turton, D. AdS_2 holography: mind the cap. *JHEP 12* (2018), 028.

[43] Bena, I., Heurtier, L., and Puhm, A. AdS_3: the NHEK generation. *JHEP 05* (2016), 120.

[44] Bena, I., Houppe, A., and Warner, N. P. Delaying the Inevitable: Tidal Disruption in Microstate Geometries. *JHEP 02* (2021), 103.

[45] Bena, I., Mayerson, D. R., Puhm, A., and Vercnocke, B. Tunneling into Microstate Geometries: Quantum Effects Stop Gravitational Collapse. *JHEP 07* (2016), 031.

[46] Bena, I., Turton, D., Walker, R., and Warner, N. P. Integrability and Black-Hole Microstate Geometries. *JHEP 11* (2017), 021.

[47] Bena, I., Wang, C.-W., and Warner, N. P. Mergers and typical black hole microstates. *JHEP 11* (2006), 042.

[48] Bena, I., Wang, C.-W., and Warner, N. P. Plumbing the Abyss: Black ring microstates. *JHEP 07* (2008), 019.

[49] Bena, I., and Warner, N. P. Black holes, black rings and their microstates. *Lect. Notes Phys. 755* (2008), 1–92.

[50] Bena, I., and Warner, N. P. Resolving the Structure of Black Holes: Philosophizing with a Hammer.

[51] Benetti Genolini, P., Cassani, D., Martelli, D., and Sparks, J. Holographic renormalization and supersymmetry. *JHEP 02* (2017), 132.

[52] Benini, F., Hristov, K., and Zaffaroni, A. Black hole microstates in AdS_4 from supersymmetric localization. *JHEP 05* (2016), 054.

[53] Benini, F., and Milan, E. A Bethe Ansatz type formula for the superconformal index. *Commun. Math. Phys. 376*, 2 (2020), 1413–1440.

[54] Benini, F., and Milan, E. Black Holes in 4D $\mathcal{N}$=4 Super-Yang-Mills Field Theory. *Phys. Rev. X 10*, 2 (2020), 021037.

[55] Benini, F., Tachikawa, Y., and Wecht, B. Sicilian gauge theories and N=1 dualities. *JHEP 01* (2010), 088.

[56] Berti, E., Cardoso, V., and Starinets, A. O. Quasinormal modes of black holes and black branes. *Class. Quant. Grav. 26* (2009), 163001.

[57] Birmingham, D., Sachs, I., and Solodukhin, S. N. Conformal field theory interpretation of black hole quasinormal modes. *Phys. Rev. Lett. 88* (2002), 151301.

[58] Bobev, N., Bomans, P., and Gautason, F. F. Wrapped Branes and Punctured Horizons. *JHEP 06* (2020), 011.

[59] Bobev, N., Bullimore, M., and Kim, H.-C. Supersymmetric Casimir Energy and the Anomaly Polynomial. *JHEP 09* (2015), 142.

[60] Bobev, N., Charles, A. M., Hristov, K., and Reys, V. The Unreasonable Effectiveness of Higher-Derivative Supergravity in AdS_4 Holography. *Phys. Rev. Lett. 125*, 13 (2020), 131601.

[61] Bobev, N., Charles, A. M., Hristov, K., and Reys, V. Higher-derivative supergravity, AdS_4 holography, and black holes. *JHEP 08* (2021), 173.

[62] Bobev, N., Charles, A. M., and Min, V. S. Euclidean black saddles and AdS_4 black holes. *JHEP 10* (2020), 073.

[63] Bobev, N., Dimitrov, V., Reys, V., and Vekemans, A. Higher-Derivative Corrections and AdS_5 Black Holes.

[64] Bobev, N., Dimitrov, V., and Vekemans, A. Wrapped M5-branes and AdS_5 black holes. *JHEP 05* (2023), 012.

[65] Bobev, N., Hristov, K., and Reys, V. AdS_5 holography and higher-derivative supergravity. *JHEP 04* (2022), 088.

[66] Botta-Cantcheff, M., Martínez, P. J., and Silva, G. A. The Gravity Dual of Real-Time CFT at Finite Temperature. *JHEP 11* (2018), 129.

[67] Botta-Cantcheff, M., Martínez, P. J., and Silva, G. A. Holographic excited states in AdS Black Holes. *JHEP 04* (2019), 028.

[68] Breckenridge, J. C., Lowe, D. A., Myers, R. C., Peet, A. W., Strominger, A., and Vafa, C. Macroscopic and microscopic entropy of near extremal spinning black holes. *Phys. Lett. B 381* (1996), 423–426.

[69] Breckenridge, J. C., Myers, R. C., Peet, A. W., and Vafa, C. D-branes and spinning black holes. *Phys. Lett. B 391* (1997), 93–98.

[70] Brehm, E. M., Das, D., and Datta, S. Probing thermality beyond the diagonal. *Phys. Rev. D 98*, 12 (2018), 126015.

[71] Bueno, P., Cano, P. A., Goelen, F., Hertog, T., and Vercnocke, B. Echoes of Kerr-like wormholes. *Phys. Rev. D 97*, 2 (2018), 024040.

[72] Cabo-Bizet, A., Cassani, D., Martelli, D., and Murthy, S. Microscopic origin of the Bekenstein-Hawking entropy of supersymmetric AdS_5 black holes. *JHEP 10* (2019), 062.

[73] Caldarelli, M. M., and Klemm, D. M theory and stringy corrections to Anti-de Sitter black holes and conformal field theories. *Nucl. Phys. B 555* (1999), 157–182.

[74] Camanho, X. O., Edelstein, J. D., Maldacena, J., and Zhiboedov, A. Causality Constraints on Corrections to the Graviton Three-Point Coupling. *JHEP 02* (2016), 020.

[75] Carballo-Rubio, R., Di Filippo, F., Liberati, S., and Visser, M. Phenomenological aspects of black holes beyond general relativity. *Phys. Rev. D 98*, 12 (2018), 124009.

[76] Cardoso, V., del Rio, A., and Kimura, M. Distinguishing black holes from horizonless objects through the excitation of resonances during inspiral. *Phys. Rev. D 100* (2019), 084046. [Erratum: Phys.Rev.D 101, 069902 (2020)].

[77] Cardoso, V., Dias, O. J. C., Hovdebo, J. L., and Myers, R. C. Instability of non-supersymmetric smooth geometries. *Phys. Rev. D 73* (2006), 064031.

[78] Cardoso, V., Franzin, E., and Pani, P. Is the gravitational-wave ringdown a probe of the event horizon? *Phys. Rev. Lett. 116*, 17 (2016), 171101. [Erratum: Phys.Rev.Lett. 117, 089902 (2016)].

[79] Cardoso, V., Hopper, S., Macedo, C. F. B., Palenzuela, C., and Pani, P. Gravitational-wave signatures of exotic compact objects and of quantum corrections at the horizon scale. *Phys. Rev. D 94*, 8 (2016), 084031.

[80] Cardoso, V., and Lemos, J. P. S. Scalar, electromagnetic and Weyl perturbations of BTZ black holes: Quasinormal modes. *Phys. Rev. D 63* (2001), 124015.

[81] Cardoso, V., and Pani, P. Tests for the existence of black holes through gravitational wave echoes. *Nature Astron. 1*, 9 (2017), 586–591.

[82] Cardoso, V., and Pani, P. The observational evidence for horizons: from echoes to precision gravitational-wave physics.

[83] Cardoso, V., and Pani, P. Testing the nature of dark compact objects: a status report. *Living Rev. Rel. 22*, 1 (2019), 4.

[84] Cassani, D., Josse, G., Petrini, M., and Waldram, D. Systematics of consistent truncations from generalised geometry. *JHEP 11* (2019), 017.

[85] Cassani, D., Josse, G., Petrini, M., and Waldram, D. $\mathcal{N} = 2$ consistent truncations from wrapped M5-branes. *JHEP 02* (2021), 232.

[86] Cassani, D., and Komargodski, Z. EFT and the SUSY Index on the 2nd Sheet. *SciPost Phys. 11* (2021), 004.

[87] Cassani, D., Lorenzen, J., and Martelli, D. Comments on supersymmetric solutions of minimal gauged supergravity in five dimensions. *Class. Quant. Grav. 33*, 11 (2016), 115013.

[88] Cassani, D., and Papini, L. The BPS limit of rotating AdS black hole thermodynamics. *JHEP 09* (2019), 079.

[89] Cassani, D., Ruipérez, A., and Turetta, E. Corrections to AdS_5 black hole thermodynamics from higher-derivative supergravity. *JHEP 11* (2022), 059.

[90] Cassani, D., Ruipérez, A., and Turetta, E. Boundary terms and conserved charges in higher-derivative gauged supergravity.

[91] Chakrabarty, B., Ghosh, D., and Virmani, A. Quasinormal modes of supersymmetric microstate geometries from the D1-D5 CFT. *JHEP 10* (2019), 072.

[92] Chakrabarty, B., Turton, D., and Virmani, A. Holographic description of non-supersymmetric orbifolded D1-D5-P solutions. *JHEP 11* (2015), 063.

[93] Charles, A. M., and Mayerson, D. R. Probing Black Hole Microstate Evolution with Networks and Random Walks. *SciPost Phys. 8*, 5 (2020), 077.

[94] Chen, B., and Long, J. Hidden Conformal Symmetry and Quasi-normal Modes. *Phys. Rev. D 82* (2010), 126013.

[95] Chen, B., and Zhang, J.-j. Quasi-normal Modes of Extremal Black Holes from Hidden Conformal Symmetry. *Phys. Lett. B 699* (2011), 204–210.

[96] Chen, W., Lu, H., and Pope, C. N. Mass of rotating black holes in gauged supergravities. *Phys. Rev. D 73* (2006), 104036.

[97] Choi, S., Kim, J., Kim, S., and Nahmgoong, J. Large AdS black holes from QFT.

[98] Chong, Z. W., Cvetic, M., Lu, H., and Pope, C. N. Five-dimensional gauged supergravity black holes with independent rotation parameters. *Phys. Rev. D 72* (2005), 041901.

[99] Chong, Z. W., Cvetic, M., Lu, H., and Pope, C. N. General non-extremal rotating black holes in minimal five-dimensional gauged supergravity. *Phys. Rev. Lett. 95* (2005), 161301.

[100] Chowdhury, B. D., and Mathur, S. D. Radiation from the non-extremal fuzzball. *Class. Quant. Grav. 25* (2008), 135005.

[101] Conklin, R. S., Holdom, B., and Ren, J. Gravitational wave echoes through new windows. *Phys. Rev. D 98*, 4 (2018), 044021.

[102] Cremonesi, S. An Introduction to Localisation and Supersymmetry in Curved Space. *PoS Modave2013* (2013), 002.

[103] Cvetic, M., and Larsen, F. General rotating black holes in string theory: Grey body factors and event horizons. *Phys. Rev. D 56* (1997), 4994–5007.

[104] Cvetic, M., and Larsen, F. Grey body factors for rotating black holes in four-dimensions. *Nucl. Phys. B 506* (1997), 107–120.

[105] Damour, T., and Solodukhin, S. N. Wormholes as black hole foils. *Phys. Rev. D 76* (2007), 024016.

[106] de Boer, J., Heller, M. P., and Pinzani-Fokeeva, N. Holographic Schwinger-Keldysh effective field theories. *JHEP 05* (2019), 188.

[107] De Boer, J., Van Breukelen, R., Lokhande, S. F., Papadodimas, K., and Verlinde, E. Probing typical black hole microstates. *JHEP 01* (2020), 062.

[108] D'Hoker, E., and Freedman, D. Z. Supersymmetric gauge theories and the AdS / CFT correspondence. In *Theoretical Advanced Study Institute in Elementary Particle Physics (TASI 2001): Strings, Branes and EXTRA Dimensions* (1 2002), pp. 3–158.

[109] Dias, O. J. C., Emparan, R., and Maccarrone, A. Microscopic theory of black hole superradiance. *Phys. Rev. D 77* (2008), 064018.

[110] Dimitrov, V., Lemmens, T., Mayerson, D. R., Min, V. S., and Vercnocke, B. Gravitational Waves, Holography, and Black Hole Microstates.

[111] Dimitrov, V., Mayerson, D. R., and Min, V. Real-time holography and hybrid WKB for BTZ wormholes. *JHEP 06* (2022), 076.

[112] Donos, A., Gauntlett, J. P., Kim, N., and Varela, O. Wrapped M5-branes, consistent truncations and AdS/CMT. *JHEP 12* (2010), 003.

[113] Emparan, R., and Reall, H. S. Black Rings. *Class. Quant. Grav. 23* (2006), R169.

[114] Eperon, F. C. Geodesics in supersymmetric microstate geometries. *Class. Quant. Grav. 34*, 16 (2017), 165003.

[115] Eperon, F. C., Reall, H. S., and Santos, J. E. Instability of supersymmetric microstate geometries. *JHEP 10* (2016), 031.

[116] Faedo, A. F., Nunez, C., and Rosen, C. Consistent truncations of supergravity and $\frac{1}{2}$-BPS RG flows in 4*d* SCFTs. *JHEP 03* (2020), 080.

[117] Freedman, D. Z., and Van Proeyen, A. *Supergravity*. Cambridge Univ. Press, Cambridge, UK, 5 2012.

[118] Gadde, A., Pomoni, E., Rastelli, L., and Razamat, S. S. S-duality and 2d Topological QFT. *JHEP 03* (2010), 032.

[119] Gadde, A., Rastelli, L., Razamat, S. S., and Yan, W. The 4d Superconformal Index from q-deformed 2d Yang-Mills. *Phys. Rev. Lett. 106* (2011), 241602.

[120] Gaiotto, D., and Maldacena, J. The Gravity duals of N=2 superconformal field theories. *JHEP 10* (2012), 189.

[121] Gauntlett, J. P., and Varela, O. D=5 SU(2) x U(1) Gauged Supergravity from D=11 Supergravity. *JHEP 02* (2008), 083.

[122] Gibbons, G., and Hawking, S. Action Integrals and Partition Functions in Quantum Gravity. *Phys. Rev. D 15* (1977), 2752–2756.

[123] Gibbons, G., Perry, M., and Pope, C. The First law of thermodynamics for Kerr-anti-de Sitter black holes. *Class. Quant. Grav. 22* (2005), 1503–1526.

[124] Gibbons, G. W., and Warner, N. P. Global structure of five-dimensional fuzzballs. *Class. Quant. Grav. 31* (2014), 025016.

[125] Giusto, S., and Mathur, S. D. Geometry of D1-D5-P bound states. *Nucl. Phys. B 729* (2005), 203–220.

[126] Giusto, S., Mathur, S. D., and Saxena, A. Dual geometries for a set of 3-charge microstates. *Nucl. Phys. B 701* (2004), 357–379.

[127] Giusto, S., Mathur, S. D., and Saxena, A. 3-charge geometries and their CFT duals. *Nucl. Phys. B 710* (2005), 425–463.

[128] González Lezcano, A., Hong, J., Liu, J. T., and Pando Zayas, L. A. Sub-leading Structures in Superconformal Indices: Subdominant Saddles and Logarithmic Contributions. *JHEP 01* (2021), 001.

[129] Green, M. B., Schwarz, J. H., and Witten, E. *Superstring Theory Vol. 2: 25th Anniversary Edition.* Cambridge Monographs on Mathematical Physics. Cambridge University Press, 11 2012.

[130] Gubser, S. S., Klebanov, I. R., and Polyakov, A. M. Gauge theory correlators from noncritical string theory. *Phys. Lett. B 428* (1998), 105–114.

[131] Gubser, S. S., Klebanov, I. R., and Tseytlin, A. A. Coupling constant dependence in the thermodynamics of N=4 supersymmetric Yang-Mills theory. *Nucl. Phys. B 534* (1998), 202–222.

[132] Gutowski, J. B., and Reall, H. S. Supersymmetric AdS(5) black holes. *JHEP 02* (2004), 006.

[133] Hawking, S. W. Particle Creation by Black Holes. *Commun. Math. Phys. 43* (1975), 199–220. [Erratum: Commun.Math.Phys. 46, 206 (1976)].

[134] Heidmann, P. Bubbling the NHEK. *JHEP 01* (2019), 108.

[135] Heidmann, P., Mayerson, D. R., Walker, R., and Warner, N. P. Holomorphic Waves of Black Hole Microstructure. *JHEP 02* (2020), 192.

[136] Hertog, T., and Hartle, J. Observational Implications of Fuzzball Formation. *Gen. Rel. Grav. 52*, 7 (2020), 67.

[137] Herzog, C. P., and Son, D. T. Schwinger-Keldysh propagators from AdS/CFT correspondence. *JHEP 03* (2003), 046.

[138] Hosseini, S. M., Hristov, K., and Zaffaroni, A. An extremization principle for the entropy of rotating BPS black holes in AdS_5. *JHEP 07* (2017), 106.

[139] Hristov, K. Explicit black hole thermodynamics in natural variables.

[140] Hui, L., Kabat, D., and Wong, S. S. C. Quasinormal modes, echoes and the causal structure of the Green's function. *JCAP 12* (2019), 020.

[141] Intriligator, K. A., and Wecht, B. The Exact superconformal R symmetry maximizes a. *Nucl. Phys. B 667* (2003), 183–200.

[142] Israel, W. Thermo field dynamics of black holes. *Phys. Lett. A 57* (1976), 107–110.

[143] Jejjala, V., Madden, O., Ross, S. F., and Titchener, G. Non-supersymmetric smooth geometries and D1-D5-P bound states. *Phys. Rev. D 71* (2005), 124030.

[144] Josse, G., Malek, E., Petrini, M., and Waldram, D. The higher-dimensional origin of five-dimensional $\boldsymbol{\mathcal{N}=2}$ gauged supergravities.

[145] Keir, J. Evanescent ergosurface instability. *Anal. Part. Diff. Eq. 13*, 6 (2020), 1833–1896.

[146] Keldysh, L. V. Diagram technique for nonequilibrium processes. *Zh. Eksp. Teor. Fiz. 47* (1964), 1515–1527.

[147] Kim, S., and Lee, K.-M. 1/16-BPS Black Holes and Giant Gravitons in the AdS(5) X S**5 Space. *JHEP 12* (2006), 077.

[148] Kinney, J., Maldacena, J. M., Minwalla, S., and Raju, S. An Index for 4 dimensional super conformal theories. *Commun. Math. Phys. 275* (2007), 209–254.

[149] Kunduri, H. K., Lucietti, J., and Reall, H. S. Supersymmetric multi-charge AdS(5) black holes. *JHEP 04* (2006), 036.

[150] Larsen, F., and Martinec, E. J. U(1) charges and moduli in the D1 - D5 system. *JHEP 06* (1999), 019.

[151] Liu, J. T., and Minasian, R. Black holes and membranes in AdS(7). *Phys. Lett. B 457* (1999), 39–46.

[152] Liu, J. T., and Saskowski, R. J. Four-derivative corrections to minimal gauged supergravity in five dimensions. *JHEP 05* (2022), 171.

[153] Maggio, E., Testa, A., Bhagwat, S., and Pani, P. Analytical model for gravitational-wave echoes from spinning remnants. *Phys. Rev. D 100*, 6 (2019), 064056.

[154] Maldacena, J., and Susskind, L. Cool horizons for entangled black holes. *Fortsch. Phys. 61* (2013), 781–811.

[155] Maldacena, J. M. *Black holes in string theory.* PhD thesis, Princeton U., 1996.

[156] Maldacena, J. M. The Large N limit of superconformal field theories and supergravity. *Adv. Theor. Math. Phys. 2* (1998), 231–252.

[157] Maldacena, J. M. Eternal black holes in anti-de Sitter. *JHEP 04* (2003), 021.

[158] Maldacena, J. M., and Nunez, C. Supergravity description of field theories on curved manifolds and a no go theorem. *Int. J. Mod. Phys. A 16* (2001), 822–855.

[159] Malek, E., and Vall Camell, V. Consistent truncations around half-maximal AdS_5 vacua of 11-dimensional supergravity. *Class. Quant. Grav. 39*, 7 (2022), 075026.

[160] Mark, Z., Zimmerman, A., Du, S. M., and Chen, Y. A recipe for echoes from exotic compact objects. *Phys. Rev. D 96*, 8 (2017), 084002.

[161] Martinec, E. J., and Warner, N. P. The Harder They Fall, the Bigger They Become: Tidal Trapping of Strings by Microstate Geometries. *JHEP 04* (2021), 259.

[162] Mathur, S. D. The Fuzzball proposal for black holes: An Elementary review. *Fortsch. Phys. 53* (2005), 793–827.

[163] Mathur, S. D. The Information paradox: A Pedagogical introduction. *Class. Quant. Grav. 26* (2009), 224001.

[164] Matthew Cheung, K. C., Gauntlett, J. P., and Rosen, C. Consistent KK truncations for M5-branes wrapped on Riemann surfaces. *Class. Quant. Grav. 36*, 22 (2019), 225003.

[165] Mayerson, D. R., and Shigemori, M. Counting D1-D5-P microstates in supergravity. *SciPost Phys. 10*, 1 (2021), 018.

[166] Melo, J. a. F., and Santos, J. E. Stringy corrections to the entropy of electrically charged supersymmetric black holes with $AdS_5 \times S^5$ asymptotics. *Phys. Rev. D 103*, 6 (2021), 066008.

[167] Misner, C. W., Thorne, K. S., and Wheeler, J. A. *Gravitation*. W. H. Freeman, San Francisco, 1973.

[168] Nastase, H., Vaman, D., and van Nieuwenhuizen, P. Consistent nonlinear K K reduction of 11-d supergravity on AdS(7) x S(4) and selfduality in odd dimensions. *Phys. Lett. B 469* (1999), 96–102.

[169] Papadimitriou, I., and Skenderis, K. Thermodynamics of asymptotically locally AdS spacetimes. *JHEP 08* (2005), 004.

[170] Papadodimas, K., and Raju, S. An Infalling Observer in AdS/CFT. *JHEP 10* (2013), 212.

[171] Papadodimas, K., and Raju, S. The unreasonable effectiveness of exponentially suppressed corrections in preserving information. *Int. J. Mod. Phys. D 22* (2013), 1342030.

[172] Papadodimas, K., and Raju, S. Black Hole Interior in the Holographic Correspondence and the Information Paradox. *Phys. Rev. Lett. 112*, 5 (2014), 051301.

[173] Papadodimas, K., and Raju, S. State-Dependent Bulk-Boundary Maps and Black Hole Complementarity. *Phys. Rev. D 89*, 8 (2014), 086010.

[174] Papadodimas, K., and Raju, S. Remarks on the necessity and implications of state-dependence in the black hole interior. *Phys. Rev. D 93*, 8 (2016), 084049.

[175] Penrose, R. Gravitational collapse and space-time singularities. *Phys. Rev. Lett. 14* (1965), 57–59.

[176] Pernici, M., Pilch, K., and van Nieuwenhuizen, P. Gauged Maximally Extended Supergravity in Seven-dimensions. *Phys. Lett. B 143* (1984), 103–107.

[177] Pestun, V., et al. Localization techniques in quantum field theories. *J. Phys. A 50*, 44 (2017), 440301.

[178] Polchinski, J. *String theory. Vol. 1: An introduction to the bosonic string*. Cambridge Monographs on Mathematical Physics. Cambridge University Press, 12 2007.

[179] Polchinski, J. *String theory. Vol. 2: Superstring theory and beyond*. Cambridge Monographs on Mathematical Physics. Cambridge University Press, 12 2007.

[180] Price, R. H., and Khanna, G. Gravitational wave sources: reflections and echoes. *Class. Quant. Grav. 34*, 22 (2017), 225005.

[181] Raju, S., and Shrivastava, P. Critique of the fuzzball program. *Phys. Rev. D 99*, 6 (2019), 066009.

[182] Rastelli, L., and Razamat, S. S. *The Superconformal Index of Theories of Class $\mathcal{S}$*. 2016.

[183] Rastelli, L., and Razamat, S. S. The supersymmetric index in four dimensions. *J. Phys. A 50*, 44 (2017), 443013.

[184] Reall, H. S., and Santos, J. E. Higher derivative corrections to Kerr black hole thermodynamics. *JHEP 04* (2019), 021.

[185] Romelsberger, C. Counting chiral primaries in N = 1, d=4 superconformal field theories. *Nucl. Phys. B 747* (2006), 329–353.

[186] Schwinger, J. S. Brownian motion of a quantum oscillator. *J. Math. Phys. 2* (1961), 407–432.

[187] Sen, A. Logarithmic Corrections to Schwarzschild and Other Non-extremal Black Hole Entropy in Different Dimensions. *JHEP 04* (2013), 156.

[188] Shigemori, M. Counting Superstrata. *JHEP 10* (2019), 017.

[189] Shigemori, M. Superstrata. *Gen. Rel. Grav. 52*, 5 (2020), 51.

[190] Skenderis, K. Black holes and branes in string theory. *Lect. Notes Phys. 541* (2000), 325–364.

[191] Skenderis, K. Lecture notes on holographic renormalization. *Class. Quant. Grav. 19* (2002), 5849–5876.

[192] Skenderis, K., and Taylor, M. The fuzzball proposal for black holes. *Phys. Rept. 467* (2008), 117–171.

[193] Skenderis, K., and van Rees, B. C. Real-time gauge/gravity duality. *Phys. Rev. Lett. 101* (2008), 081601.

[194] Skenderis, K., and van Rees, B. C. Real-time gauge/gravity duality: Prescription, Renormalization and Examples. *JHEP 05* (2009), 085.

[195] Solodukhin, S. N. Restoring unitarity in BTZ black hole. *Phys. Rev. D 71* (2005), 064006.

[196] Son, D. T., and Starinets, A. O. Minkowski space correlators in AdS / CFT correspondence: Recipe and applications. *JHEP 09* (2002), 042.

[197] Starobinskil, A. A., and Churilov, S. M. Amplification of electromagnetic and gravitational waves scattered by a rotating "black hole". *Sov. Phys. JETP 65*, 1 (1974), 1–5.

[198] Strominger, A., and Vafa, C. Microscopic origin of the Bekenstein-Hawking entropy. *Phys. Lett. B 379* (1996), 99–104.

[199] Susskind, L. The World as a hologram. *J. Math. Phys. 36* (1995), 6377–6396.

[200] Szepietowski, P. Comments on a-maximization from gauged supergravity. *JHEP 12* (2012), 018.

[201] 't Hooft, G. Dimensional reduction in quantum gravity. *Conf. Proc. C 930308* (1993), 284–296.

[202] Tachikawa, Y. Black hole entropy in the presence of Chern-Simons terms. *Class. Quant. Grav. 24* (2007), 737–744.

[203] Taylor, M. The D1-brane D5-brane system in six-dimensions.

[204] Townsend, P. K. Black holes: Lecture notes.

[205] Tyukov, A., Walker, R., and Warner, N. P. Tidal Stresses and Energy Gaps in Microstate Geometries. *JHEP 02* (2018), 122.

[206] van Rees, B. C. Real-time gauge/gravity duality and ingoing boundary conditions. *Nucl. Phys. B Proc. Suppl. 192-193* (2009), 193–196.

[207] Wald, R. M. Black hole entropy is the Noether charge. *Phys. Rev. D 48*, 8 (1993), R3427–R3431.

[208] Wang, Y.-T., Li, Z.-P., Zhang, J., Zhou, S.-Y., and Piao, Y.-S. Are gravitational wave ringdown echoes always equal-interval? *Eur. Phys. J. C 78*, 6 (2018), 482.

[209] Wang, Y.-T., Zhang, J., Zhou, S.-Y., and Piao, Y.-S. On echo intervals in gravitational wave echo analysis. *Eur. Phys. J. C 79*, 9 (2019), 726.

[210] Witten, E. Anti-de Sitter space and holography. *Adv. Theor. Math. Phys. 2* (1998), 253–291.

[211] Zaffaroni, A. AdS black holes, holography and localization. *Living Rev. Rel. 23*, 1 (2020), 2.

[212] Zerilli, F. J. Gravitational field of a particle falling in a schwarzschild geometry analyzed in tensor harmonics. *Phys. Rev. D 2* (Nov 1970), 2141–2160.

FACULTY OF SCIENCE
DEPARTMENT OF PHYSICS AND ASTRONOMY
ITF
Celestijnenlaan 200d - box 2415
B-3001 Leuven
vasko.dimitrov@kuleuven.be
https://www.kuleuven.be/wieiswie/en/person/00124326